Dissertation

submitted to the

Combined Faculties for the Natural Sciences and for Mathematics

of the Ruperto-Carola University of Heidelberg, Germany

for the degree of

Doctor of Natural Sciences

presented by

Philipp Schult, M.Sc.

born in Hamburg

Oral examiniation: ....

Functional Dissection of the Hepatitis C Virus Non-Structural Proteins and miR-122 in Viral Replication and Translation

Referees: 1. Prof. Dr. Ralf Bartenschlager

2. PD Dr. Barbara Müller

Contents

List of Figures

List of Tables

Abstract

Hepatitis C Virus (HCV) is a positive stranded RNA virus, grouped into the family of Flaviviridae. The HCV genome encodes a single polyprotein, which is co- and post-translationally cleaved into ten structural and non-structural (NS) proteins by cellular and viral proteases. The coding sequence is flanked by 5' and 3' untranslated regions (UTRs), which contain essential cis-acting elements, regulating translation and RNA synthesis, e.g. an internal ribosome entry site (IRES) for cap-independent translation. HCV RNA replication involves the synthesis of a negative strand replication intermediate, serving as a template for the generation of multiple strands of genomic RNA. This process requires a concerted action of several viral nonstructural proteins, cis-acting replication elements and host factors, and is poorly understood at the molecular level. The first part of this study aimed to characterize the viral non-structural proteins comprising the replicase complex *in vitro* and their mode of action during (-)-strand RNA synthesis. Since the natural 3'(+)-end is a poor template for the viral polymerase NS5B, supporting roles of the viral protease/helicase NS3 and the phosphoprotein NS5A were hypothesized. Optimal conditions for NS3 activity were established by an *in vitro* helicase assay. By combining the individual proteins with different RNA templates, it was observed that initiation and processivity of NS5B were stimulated by active NS3, but not by inactive mutants. Inhibition of NS3 helicase activity did not impair the stimulatory effect on NS5B, but led to an altered mode of initiation. Addition of purified NS5A further augmented the effect of NS3. In conclusion, this work demonstrates that NS3 and NS5A can improve RNA dependent RNA polymerase activity on a natural template, thereby providing an experimental model to study the molecular mechanisms governing initiation of RNA synthesis.

Liver -specific microRNA (miR)-122 is an important host factor of HCV replication, and recognizes two conserved target sites within the first 45 nt of the HCV 5' UTR, close to the IRES. Previous studies suggested a role of miR-122 in RNA stability, translation, and RNA synthesis. The mechanisms, by which miR-122 exerts these functions, remain enigmatic. Insertion of a heterologous IRES element, allowing for miR-independent translation of the non-structural proteins, was sufficient to enable replication in miR-122-deficient Hep3B cells, suggesting a substantial role of miR-122 in IRES-dependent translation. The miR-122 binding region is engaged in a strong secondary in the complementary negative strand. Additionally, we found that a similar structure was predicted in

the positive strand, which would interfere with IRES formation. We therefore hypothesized that miR-122 binding in this region might prevent such alternative structures, thereby facilitating IRES-mediated translation.

Indeed, mutations in the miR-122 binding region, but not the IRES sequence, which were designed to stabilize or destabilize the IRES, enhanced or decreased initial translation, respectively, independent of miR-122. Translation enhancement was independent from RNA stability, but short-lived, suggesting additional roles of miR-122, e.g. recruitment of host proteins facilitating steady state translation. Moreover, structural analysis suggested that the HCV IRES folds into a number of conformers in solution, which can be modified by miR-122 under certain conditions.

Apart from the 5' UTR, HCV also contains several seed-matches for miR-122 in the coding sequence of NS5B, and the 3' UTR, with unknown functional significance. Two novel sites were identified to be conserved over a number of genotypes. The functional characterization of these miR-122 binding sites was evaluated by insertion of point mutations, abrogating miR-122 binding to single and multiple sites, revealing a previously unappreciated role in virion assembly or release. However, assembly of the mutants could not be rescued by a corresponding mutant miR, suggesting a specific need for wild type miR-122.

Conclusively, this study provides evidence for miR-122 involvement in almost every intracellular stage of HCV infection, and defines translation enhancement by suppression of RNA structures interfering with IRES activity as a key function of miR-122.

Zusammenfassung

Das Hepatitis C Virus (HCV) ist ein positiv (+)-Strang RNA Virus, welches zur Familie der Flaviviridae gezählt wird. Das HCV Genom kodiert für ein einziges Polyprotein, das co- und post-translational mit Hilfe viraler und zellulärer Proteasen in zehn Struktur- und Nichtstrukturproteine (NS) gespalten wird. Der offene Leserahmen wird am 5' und 3' Ende von nicht-translatierten Regionen (NTR) flankiert, welche essentielle Signale für Translation und Replikation enthalten, wie z.B. eine interne ribosomale Eintrittsstelle (IRES), welche *cap*-unabhängige Translation ermöglicht. Während der Replikation der HCV RNA entsteht ein negativ-Strang Intermediat, welches als Matrize für die Produktion weiterer positiv-Stränge dient. Zudem ist eine konzertierte Interaktion viraler NS-Proteine, verschiedener RNA Elemente und Wirtsproteine nötig, welche auf der molekularen Ebene noch weitestgehend unverstanden ist. Der erste Teil dieser Arbeit hatte die Charakterisierung der NS-Proteine *in vitro*, sowie die Untersuchung ihrer Funktion während der RNA Synthese zum Ziel. Da das natürliche Ende des (+)-Stranges keine effiziente Initiation der viralen Polymerase NS5B erlaubt, war eine zentrale Hypothese, dass die Protease/Helikase NS3, sowie das Phosphoprotein NS5A diesen Vorgang unterstützen könnten. Mittels einem *in vitro* Helikase Assay wurden zunächst die optimalen Bedingungen für dieses Enzym getestet. Durch die Kombination verschiedener NS-Proteine konnte gezeigt werden, dass die aktive Helikase sowohl die Initiation, als auch die enzymatische Aktivität der Polymerase steigern konnte, während katalytisch inaktive Mutanten hierzu nicht in der Lage waren. Die chemische Inhibition der Helikase hatte keinen Einfluss auf die Steigerung der Prozessivität von NS5B, führte jedoch zu einem veränderten Initiationsverhalten. Hinzugabe von NS5A konnte den NS3 vermittelten Effekt noch verstärken. Somit konnte gezeigt werden, dass NS3 und NS5A die Polymeraseaktivität auf einem natürlichen Template steigern können. Zudem stellt diese Methode auch ein experimentelles Modell für weitere Untersuchungen der Prozesse während der Initiation der (-)-Strang Synthese dar.

Die leberspezifische mikroRNA (miR)-122 ist ein wichtiger Wirtsfaktor für HCV Replikation und erkennt zwei Zielsequenzen in den ersten 45 nt der HCV 5' NTR, direkt vor der IRES. Vorhergehende Studien konnten bereits zeigen, dass die miR-122 RNA Stabilität, Translation und Replikation positiv beeinflusst. Die Mechanismen dieser Funktionen sind jedoch noch ungeklärt. Die Einführung einer fremden IRES, welche

die Translation miR-122 unabhängig macht, ermöglichte die Etablierung von Replikation in miR-122-defizienten Hep3B Zellen. Daraus ließ sich eine substantielle Rolle der miR-122 in der IRES-abhängigen Translation ableiten. Die miR-Binderegion ist im komplementären 3'(-) Ende in einen stabile Sekundärstruktur eingebunden. *In silico* Analysen zeigten die Ausbildung einer ähnlichen Konformation im positiv Strang, welche die Ausbildung der IRES stören würde. Daher wurde angenommen, dass die Bindung der miR-122 diese Strukturen unterdrücken, und dadurch die IRES Aktivität stimulieren könnte. Tatsächlich konnten Mutationen in der miR-Binderegion, welche die IRES Konformation stabilisieren oder destabilisieren, die initiale IRES Aktivität unabhängig von miR-122 erhöhen oder erniedrigen. Die Steigerung der Translation war in diesem Fall nicht abhängig von der RNA Stabilität, ließ jedoch sehr schnell nach, weshalb weitere Funktionen der miR-122, wie z.B. Rekrutierung von Wirtsfaktoren eine zusätzliche Rolle spielen könnten. Zudem ergab die experimentelle untersuchung der RNA Struktur, dass die HCV IRES in Lösung ein Ensemble von Konformeren ausbildet, welches unter bestimmten Bedingungen von miR-122 beeinflusst werden kann.

Neben den beiden Bindestellen in der 5' NTR existieren noch weitere in der kodierenden Region und der 3' NTR, deren Funktion unbekannt ist. Außerdem wurden noch zwei zusätzliche Bindestellen im offenen Leserahmen identifiziert, welche in vielen Genotypen konserviert sind. Die funktionelle Relevanz wurde durch Einführung von Punktmutationen in den Bindestellen untersucht, welche die Assoziation der miR-122 verhindern. Dies führte zu der Beobachtung, dass diese Bindestellen wichtig für Virusassemblierung oder Egress sind. Überraschender Weise konnte die korrespondierende miR-Mutante diese Funktion nicht wiederherstellen. Dies könnte für eine miR-122 Wildtyp-spezifische Rolle sprechen.

Zusammenfassend konnte diese Studie zeigen, dass miR-122 in jedem intrazellulären Schritt der HCV Infektion eine wichtige Rolle spielt. Weiterhin konnte die Steigerung der Translation, durch die Unterdrückung interferierender Strukturen, als Schlüsselfunktion der miR-122 identifiziert werden.

1. Introduction

1.1. The Hepatitis C Virus

The existence of hepatitis C virus (HCV) was first anticipated in 1975, when Feinstone et al.[1] proposed an infectious agent, which, despite causing similar symptoms in some cases, showed no reactivity with Hepatitis A nor B antibodies (accordingly termed non-A non-B hepatitis). Hence, it was suspected to be a new type of viral hepatitis. Additionally, one report suggested person-to-person transmission without the necessity of blood transfusion[2]. In 1978, studies in chimpanzees demonstrated that the disease was indeed caused by a transmissible agent. However, its identity remained enigmatic for more than a decade, until the identification of the viral genome was published in 1989[3].

1.2. Incidence and Associated Diseases

Presently, over 170 million people (or 3% of the world's population) are estimated to carry the pathogen[4]. The virus owes much of its success to its extreme inherent variability, accounting for the emergence of seven currently known genotypes (gt), and a vast number of subtypes. Significant disparities between geographical regions in incidence and genotype prevalence (**fig. 1.1**) can be observed. The routes of infection range from sexual contact over direct blood-to-blood (needle-sharing/reuse, nocosomial, blood-transfusion) to graft-derived transmission (organ transplantation), or contaminated medical products (shistosomatosis prophylaxis)[5]. Hence, high-risk individuals are men who have sex with men, injecting drug users, and patients in hospitals with poor hygienic standards. Potentially due to the wide overlap of risk groups, co-infection with HIV is rather common[6]. Only 20 - 30% of acute infections can be cleared spontaneously. Acute hepatitis C rarely involves any severe symptoms in immunocompetent persons[7]. However, in up to 80% of patients the infection progresses to a persistent state, which makes HCV the leading etiologic agent for chronic liver disease. Quasispecies emerge shortly after infection, rapidly adapting to the host's immune response[8]. Viral persis-
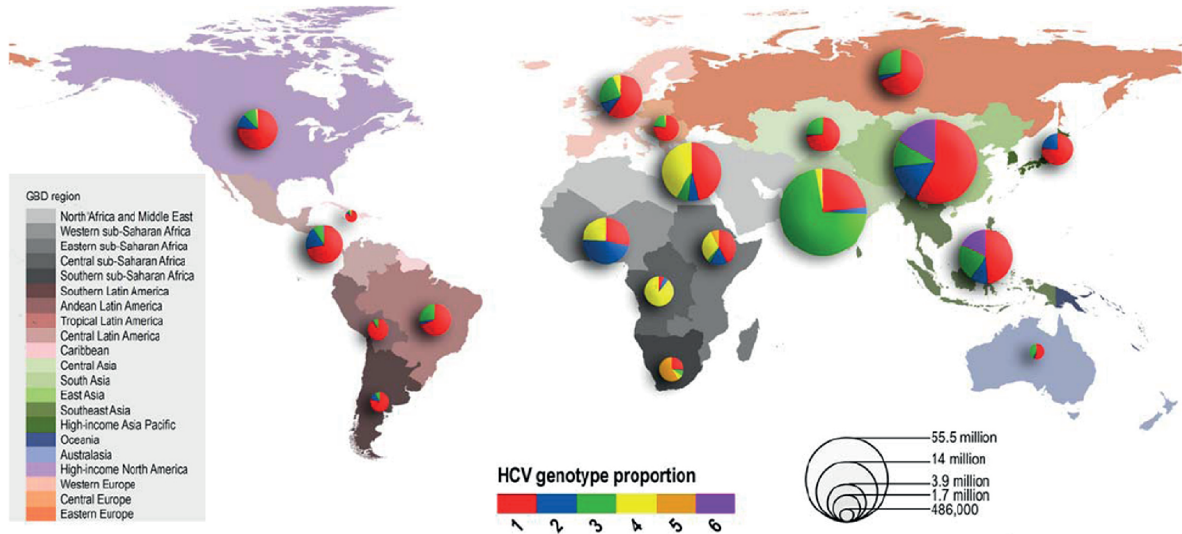
Figure 1.1.: Incidence of HCV infections in different geographical regions. HCV is distributed throughout the world. The most prevalent genotypes in America, Europe, Russia and China are 1 and 2. In contrast, genotype 4 is most common in Africa and the middle eastern regions. Genotype 4 is most often found in the Indian population. Representation based on data from Messina et al. [4]

tence can induce severe fibrosis and cirrhosis of the liver in 20% of the cases. This condition is frequently accompanied by steatosis (fatty liver disease), particularly in patients with genotype 3[9]. Eventually, the infection can culminate in hepatocellular carcinoma (HCC)[10,11], in 1 - 3% of cases per year. HCC is a particularly aggressive form of liver cancer with poor survival rates. The severity of disease is strongly influenced by gender, age, and lifestyle. Moreover, there is evidence that also extra-hepatic malignancies can be HCV related, including the reported involvement of HCV in B-cell non-Hodgkin's lymphoma[12]. Each year, HCV associated diseases account for over 500,000 deaths worldwide[4].

1.3. Treatment and Vaccination

To date, there is no approved vaccine against HCV. The standard of care treatment was at first limited to long-term high doses of PEG-ylated interferon (IFN)α in combination with the guanosid-analogon ribavirin, which blocks viral replication by an unknown mechanism[13]. However, apart from severe side effects, elimination of the virus could only be achieved in less than 50% for the predominant genotype 1 (80% for genotype 2) of

chronically infected patients. In the past decade, the approval of several highly effective direct acting antivirals (DAA), such as NS3 protease (VX950[14], Boceprevir[15]), NS5A (Daclatasvir[16]) and RdRP inhibitors (Sofosbuvir[17]) , with average sustained virological response rates of nearly 100% for genotype 2, and above 95% for gt1, has significantly improved the therapeutic success[18]. Still, the high genetic variability and plasticity, resulting in the occasional appearance of resistance mutants, complicates the development of a 100% effective therapeutic for all genotypes. Importantly, the most effective novel therapies are very costly, and therefore their availability is limited, especially in less developed regions. Another promising approach is the targeting of essential host-factors. In fact, cyclophilin A inhibitors[19–21] and locked nucleic acid (LNA)-based decoys for miR-122[22–24] have progressed to phase 2 clinical studies. However, due to the success of recent DAAs, they have not advanced into clinical use, yet.

1.4. Molecular Biology of HCV

HCV belongs to the family of *Flaviviridae*, and is a member of the genus *Hepacivirus*. The recently discovered non-primate hepatitis virus (NPHV)[25] and the GBV-B (G.-Barker-Virus, named after the first patient, in which it was discovered) are the most closely related viruses in this clade. Other genera of the *Flaviviridae* are *Flavivirus* (e.g. Yellow Fever Virus), *Pegivirus* (GBV-A, GBV-C), and *Pestivirus* (e.g. Bovine Viral Diarrhea Virus). The infectious viral particle of HCV measures around 40 - 100 nm in diameter, and is surrounded by a host-derived lipid bi-layer, protruded by viral transmembrane proteins (**fig. 1.2** E1, E2). After complete assembly, ApoE and ApoB, proteins involved in VLDL-lipoprotein formation, are acquired[26]. The genome of HCV
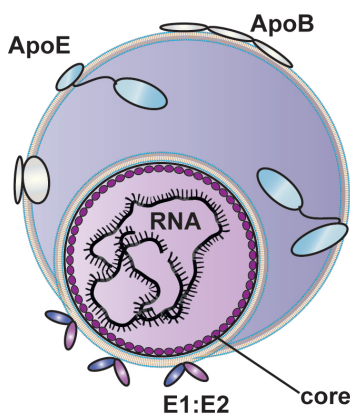
Figure 1.2.: Lipo-viral particle of HCV. In addition to the double-layer lipid envelope, HCV is associated with lipoproteins, including ApoE and B. The E1 and E2 surface proteins are responsible for host cell recognition and fusion and protrude the lipid membrane. The proteinous capsid enclosing the genomic RNA is assembled by multiple copies of the core protein.

is a positive single-stranded ((+)ss)RNA of roughly 9600 bp[3]. The genomic RNA is

protected by a capsid shell, formed by multiple copies of the viral core protein. The monocistronic transcript is translated into a polyprotein precursor of approximately 3000 aa in length[27], which is co- and post-translationally cleaved by cellular and viral endoproteases into ten individual proteins[28,29].

The structural components of the infectious virion are core, E1, and E2. p7 and the non-structural (NS) proteins NS2, 3, 4A, 4B, 5A and 5B, are likely not incorporated into the virus particle. Instead, they perform crucial activities in the viral life cycle. In fact, NS3 - 5B have been shown to be essential and sufficient for the amplification of viral RNA[29]. The uncapped genomic RNA also contains various sequence and structural features, which are critical for efficient translation, replication and assembly. A highly structured internal ribosomal entry site (IRES) of 389 nt is located at the 5' end, in the untranslated region (UTR) of the positive strand[30]. Parts of these structures interact with regulatory elements within the coding region (i.e. SL5B) to modulate the aforementioned processes (**fig. 1.3**B). Most likely, the 5' region also contains signals for the translation-replication switch, similar to the polio IRES, since translation and replication are incompatible processes[31]. Especially the first 120 nucleotides and the complementary sequence contain structures (SLII and SLIIz'), which are important for both, protein and RNA synthesis (**fig. 1.3**A,C).

1.5. The Viral Life Cycle

HCV infection relies on several membrane receptors, which are bound in a defined sequence. After penetration of the cell, the viral life cycle is completely cytoplasmic, and is accompanied by substantial membrane rearrangements in the cell, which represent the viral replication compartment.

1.5.1. Attachment and entry

Viral entry requires a concerted action of several membrane receptors. Host cell contact is initiated by capturing of cellular glycoproteins, glycosaminoglycans, and VLDL-receptors by viral E1-E2 proteins and host-acquired low-density-lipoproteins. This preliminary binding enables specific interactions of HCV with its entry-receptors. Among these are CD81 and Scavenger receptor B1 (SR-B1)[32,33]. Claudin-1 (CLDN1) and occludin (OCLN), which are exclusive to laminar tight junctions in liver tissue, are also involved in the final steps of this process[34,35](**fig. 1.4**A). Epidermal growth factor re-
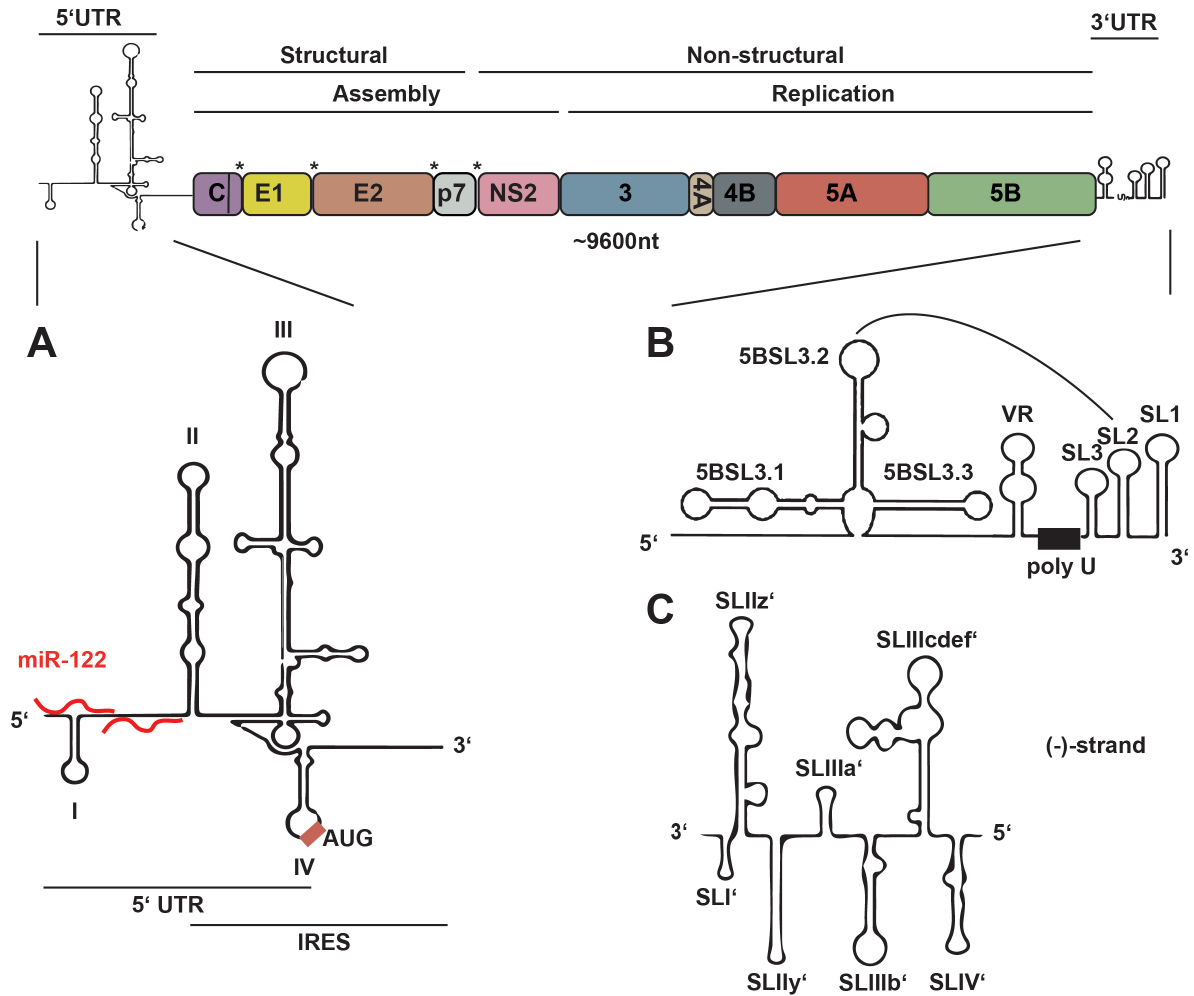
Figure 1.3.: The genome structure of HCV. The genome is a monocistronic (+)-strand RNA molecule. The 5' end encodes for the structural proteins involved in particle formation, whereas the the non-structural proteins are located at the 3' end. The replicase complex is formed by NS3-5B. **A** | The 5'UTR of HCV, containing the IRES element (domains II-IV) and two miR-122 binding sites in domain I. **B** | The 3' cis-acting elements within the coding region of NS5B (5BSL3) and the 3'UTR. VR: variable region. **C** | 3'(-) structure SLI' - SLIIy' are essential for replication.

ceptor -kinase signaling[36] induces clathrin-mediated uptake of the viral particles into endosomal vesicles[37,38]. Upon acidification of the endosomal compartment, the HCV glycoproteins undergo structural changes to promote membrane fusion[39]. This induces disassembly of the HCV core complex and liberation of the viral genome into the cytoplasm.(**fig. 1.4**B)
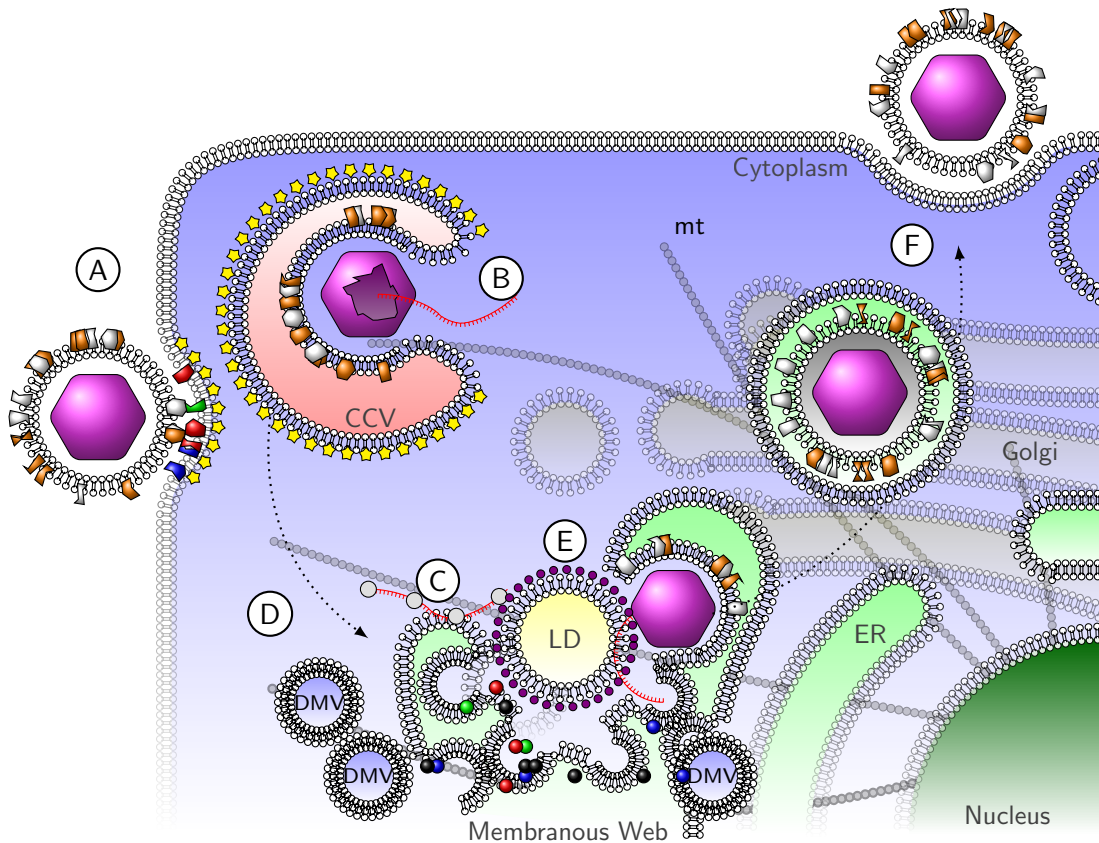
Figure 1.4.: The life cycle of HCV. A | Entry of HCV is mediated by the interaction of host cell receptors with the E1:E2 complex. **B |** After uptake of the viral particle in a clathrin-dependent manner, membrane fusion is initiated and the capsid disintegrates to release the RNA into the cytoplasm. **C |** At the ER, ribosomes are recruited by the 5' IRES, to translate the polyprotein. **D |** The mature proteins associate with the ER membrane and form the membranous web, consisting of a number of vesicular structures. Especially the DMVs are suggested to serve as platform for genome replication. Some NS5A containing vesicles of unknown function are in contact to microtubuli (mt). **E |** The transcribed RNAs are subsequently packaged into newly formed capsids. This process is in close coherence with core-beset lipid droplets. The particles then bud into the ER and follow the exocytotic pathway through the Golgi, where post-translational glycosylation of E1- E2 is carried out. **F |** The transport vesicle fuses with the plasma membrane to liberate the virion.

1.5.2. Translation and Processing of the Viral Polyprotein

The genomic RNA of HCV does not feature a 5' cap structure, which is usually needed for ribosome attachment. Instead, the virus relies on an IRES, which also eliminates the need for most canonical initiation factors and ribosomal scanning. The open reading frame encodes a polyprotein precursor, which needs to be separated during and after translation(**fig. 1.4**C). The translation product is cleaved successively by the cellular

A

B
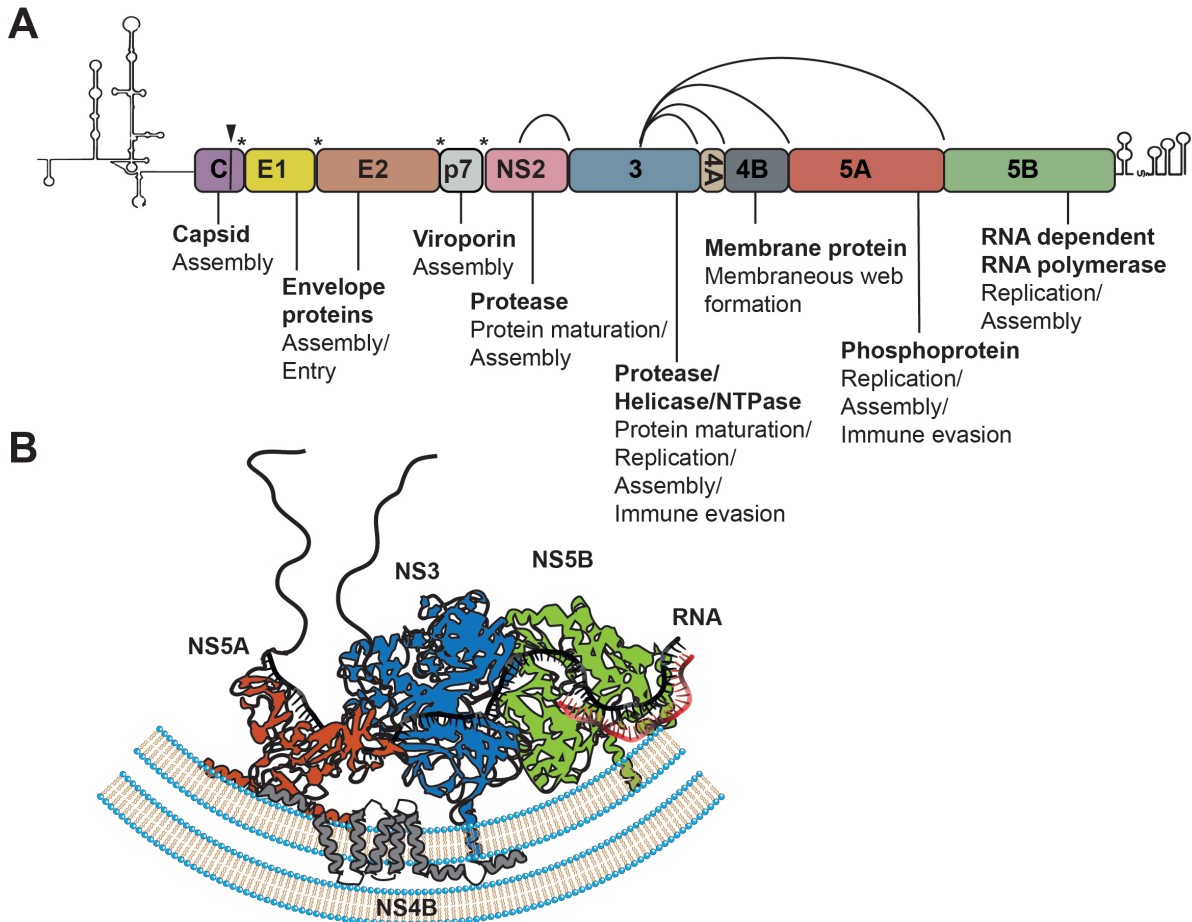
Figure 1.5.: Processing of the viral polyprotein. A | Representation of the complete HCV polyprotein. The scission of the large polyprotein is at first dependent on the host signal peptidase (asterisk), residing at the ER. After hydrolysis at the p7-NS2 junction, N2-3 is autocatalytically cleaved. All remaining proteins are released by the NS3 protease. Later, the signal-peptide peptidase catalyzes the maturation of core. **B |** The NS proteins and viral genomic RNA are recruited into DMVs, formed mainly by NS4B. NS3 might unwind secondary structures of single stranded templates or double stranded replication intermediates to facilitate polymerase initiation.

serine-protease signal peptidase, and the viral NS2/3 protease. Autocatalytic cleavage of the NS2/3 precursor ultimately activates the NS3/4A viral protease, which is responsible for the completion of polyprotein processing[40,41,29]. The 23-kDa immature form of the core protein is cleaved by the signal peptide peptidase[42] to produce the mature 21-kDa protein[43,44] (**fig. 1.5**A).

1.5.3. Membranous Web Formation and RNA Replication

After translation of the viral proteins, they induce the formation of a membrane compartment, the so-called membranous web (MW). It is composed of several types of vesicular structures. The double-membrane vesicles (DMV) are the most abundant type (**fig. 1.4**D). The non-structural proteins NS3 to NS5B, and the viral RNA are sequestered into these vesicles, which are thought to be the primary foci of replication activity[45–48]. This was convincingly shown by Paul et al.[49], since 4B-containing membrane fractions consist predominantly of DMVs and exhibit RNA amplification capacity. The exact organization of the replicase within these structures, however, is still not unequivocally shown. In all likelihood, the participating fraction of proteins and RNA are enclosed by the double membranes[45,50] (**fig. 1.5**B). The first step of RNA replication is the synthesis of a negative strand RNA replication intermediate, serving as a template for progeny positive strand genomes. However, the individual contribution of the involved proteins (and host factors), as well as the initiation mechanism of (-)-strand synthesis have yet to be clarified. Each of the involved NS proteins is thought to have multiple essential roles in initiation and continuation of RNA replication. Moreover, it becomes increasingly clear that their activities are not limited to replication[51,52]. The positive and negative strand RNA is amplified in asymmetrical quantities. While the (-)-strand synthesis is rather inefficient, the generated amount of (+)-strand is around 10-fold higher. This allows the virus to efficiently propagate its genome, while keeping double-stranded replication intermediates to a minimum, which are potent triggers for the innate immune response. The mechanistic details, as to how the amplified RNA leaves these compartments to initiate subsequent rounds of translation, or virion morphogenesis are not yet defined.

1.5.4. The Viral Replicase

The replicase of HCV consists of NS3 to NS5B and a single strand of RNA. The exact processes and interactions within the replication compartments of HCV remain elusive. However, there have been ongoing efforts to biochemically characterize the involved proteins. While many major functions have been meticulously described, especially the intermolecular interactions necessary for efficient replication initiation were difficult to address, due to the lack of appropriate model systems.

NS3/4A

NS3/4A is a multifunctional 68kDa protein. Its N-terminal serine metallo-protease domain is mainly responsible for polyprotein maturation. The protease adopts a β-barrel fold, and coordinates a stabilizing Zn^+ ion. The catalytic triad is composed of His 57, Asp 81 and Ser 139[53]. Full functionality of the protease is only achieved in presence of its co-factor NS4A, as it comprises one β-strand within the barrel, anchors the protein to the membrane and can interact with other NS proteins[54]. In addition to polyprotein processing, the enzyme exhibits a specificity for important proteins of major pathways of the antiviral recognition network, which make it a key component for immune evasion. Cleavage of the mitochondrial antiviral-signaling protein (MAVS) on mitochondria-associated membranes (MAMs) efficiently blocks signaling of the dsRNA sensor RIG-I (retinoic acid inducible gene I), and consequently detection of viral replication intermediates[55,56]. In parallel, viral RNA induced TLR3 signaling is impaired by scission of the cytoplasmic adapter protein TRIF[57]. Additionally, cell viability is enhanced via proteolytic degradation of the T-cell protein tyrosine phosphatase, which augments cytokine-independent growth signaling[58]. Importantly, the NS3/4A holo-enzyme also possesses
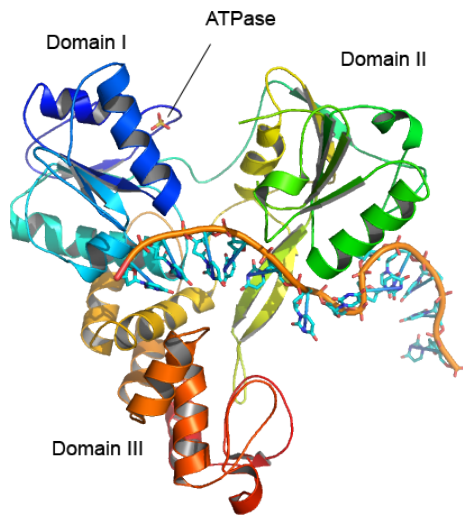
Figure 1.6.: Structural and functional features of the NS3 helicase domain. The helicase domain of NS3 $^{\triangleright 4A92}$ is comprised of 3 sub-domains. It is connected to the protease portion by an unstructured linker. The structure shows a short stretch of bound ssDNA and an ATP-analogon within the nucleotide binding site. Each step along the substrate is facilitated by a major conformational change, which is initiated by the break-down of an ATP molecule in an ATPase pocket between domains I and II.

an active NTPase and helicase domain, of the DExD-box family. It could be involved in double-strand unwinding prior to every replication cycle. Dissolution of each nucleotide bond requires the conversion of one ATP, which is processed by the intrinsic ATPase subunit. Other nucleotides can be utilized as well, albeit with lower efficiency[59]. The generated energy drives an inter-domain shift, which slides the enzyme forward on its substrate in a ratchet-like manner[60,61]. The enzyme exhibits low preference in binding-affinity to nucleic acids, and can readily unwind DNA and RNA duplexes. Accordingly,

in vitro assays have shown its capability of unwinding dsRNA and secondary structures of ssRNA molecules resembling the 3' stem-loops of the HCV genome, and indicated an essential role in HCV replication and assembly[62,59,63]. These experiments also suggest that the protease fraction enhances nucleic acid binding and helicase activity. However, functional evidence for the mode of action of the helicase in the HCV life cycle is still lacking. For HCV and the related CSFV, a role in modulating the activity of the viral polymerase has been reported based on *in vitro* experiments[64,65].

Binding of NS4A induces a structural change of the protease subunit, which is also required for optimal NS3 helicase activity[62] and vice versa[66]. Also NS5B can serve to stimulate helicase activity. The same study could also show that the active complexes are in a 1:1 stoichiometry[67]. While a role in the translation/replication switch has been proposed[68], presently no conclusive studies have been published to further elucidate the role of NS3/4A in viral RNA replication.

NS4B

NS4B is a small integral membrane protein, which is involved in different functions during viral RNA synthesis. While most of the protein is buried in the membrane, and is therefore hydrophobic, a number of defined charged residues in the terminal domains are critical for protein function[69]. NS4B is chiefly responsible for the generation of the membranous web, where replication takes place[70,71]. Its C-terminal domain is oriented towards the cytoplasm, as indicated by Proteinase K assays. The N-terminus displays a dual topology, with a considerable fraction pointing towards the luminal side of the replication vesicle[72]. Its precise function in the HCV life cycle has not been determined so far. Based on multiple interactions with other replicase members[73,74], it is assumed that the protein might serve as a hub for the assembly of the viral ribonucleic acid associated protein (RNP) complex. A nucleotide binding domain with an alleged hydrolase activity has also been detected, but its functional relevance is unclear[75]. Recently, an involvement in particle production has also been reported[76].

NS5A

NS5A is an RNA binding phospho-protein[77,78], which is tethered to the lipid membrane via an N-terminal amphiphatic helix. It consists of three domains, two of which are natively unfolded[79,80]. Only domain 1 possesses a defined tertiary fold and forms homo-dimeric or oligomeric complexes[81–83]. The protein is implicated in nearly all steps of

the intracellular life cycle of HCV, from translation[84,85] over replication[86,74] to virion assembly[51,87,88]. Moreover, due to its numerous host-interaction partners, it severely alters the cellular homeostasis[89–91]. Some studies have also established a link to immune evasion[92,93].

Due to its complex post- translational modification pattern, which is most prominently represented by a basal (p56) and a hyper-phosphorylated (p58) state[94–96], it is until now hardly possible to say how the "native" NS5A affects replication. Furthermore, both phosphorylation species apparently influence different steps in HCV infection. p56 is presumably augmenting replication, while p58 favors assembly and release[97]. Partially or abnormally phosphorylated proteins might be severely affected in its activity. So far, it is not entirely clear, which potential phosphorylation sites are actually modified in each of the two forms. It is therefore a challenging task to reproduce the native pattern in most common expression systems[98], which makes this protein particularly hard to study *in vitro*. Some of the key enzymes responsible for specific phosphorylation states have been identified. The main contribution to generate the hyper-phosphorylated form comes form the casein kinase Iα[96]. A well-described serine cluster in domain 3 seems to be the target region for the protein[97]. Moreover, the important host-factor phosphoinositol-4 kinase IIIα has been implicated to reduce hyper-phosphorylation, by a so far undefined mode of action[99]. Several other kinases have also been found to impact NS5A phosphorylation and activity, adding to the complexity of regulation[100,101,95].

NS5B

NS5B is the viral RNA-dependent RNA polymerase (RdRp) of HCV, and its catalytic site strongly resembles the respective domain of HIV reverse transcriptase[102]. Like most other proteins of the RdRP-class, it possesses a right-hand fold, with the typical finger, palm and thumb domains. The RNA template is coordinated in a narrow cleft between finger and thumb[102]. Besides those similarities, NS5B also shows some unusual features. In most cases, RdRPs can acquire two distinct conformations, open and closed, which significantly affects the size of the RNA-binding pocket. In the open conformation, RNA duplexes comprised of template and primer can efficiently be incorporated, and only this binding event induces the transition to the closed state[103]. For NS5B, there is only evidence for minor conformational changes after RNA binding, due to numerous inter-domain contacts, which restrict the flexibility of the structure. The native state of the NS5B catalytic domain is thus rather comparable to the closed conformation of model RdRPs, which only allows for binding of template RNA and a single initiating rNTP[104].

It might be attributed to this fact that *de novo* initiation is currently assumed as the main form of replication. This mode of initiation requires a di-nucleotide primer[105]. Whether NS5B generates this di-ncleotide at the site of initiation, or whether it can also use other templates, is not known. The process of incorporating the initiating nucleotide is the rate-limiting step of RNA synthesis[105]. At the C-terminus, NS5B possesses a membrane anchor and a linker, containing a β-hairpin, which can fold into the RNA-binding pocket. The function of this domain has yet to be elucidated. The anchor is essential for protein function in cell culture[48], but deletion of the 21 aa trans-membrane helix (ΔC21) (up to 60, including the linker) do not impair enzymatic activity *in vitro*, and greatly improve solubility of the protein during purification[106]. The ideal template for initiation is a stable structure, in proximity of a short single stranded 3' trailer sequence, or at least one free cytidylate[107]. These conditions are found at the 3'(-) end, allowing for efficient (+)-strand synthesis. However, the 3'(+) end is engaged in a stable stem without a single stranded region, therefore (-)-strand synthesis is significantly less efficient. In this case, the activity of the viral helicase might be needed for initiation[107]. Upon transition from initiation to processive elongation dramatic conformational changes take place, which have only recently been visualized[108]. There are marked structural differences between individual strains. These might also be indicative for the strong genotype-associated variances of *in vitro* replication capability[109,107,104,110].

1.5.5. Cis-Acting Replication Elements

Apart from the proteins composing the replicase, genome amplification is additionally governed through sequence and structural signals in the RNA template. The 3' fraction of the (+)-strand harbors various so-called cis-acting replication elements (CRE, **fig. 1.3**). These are composed of complex hairpin structures. One is located in the coding region of NS5B, called 5BSL3, and features a clover-leaf fold of three hairpins[111]. The central element, 5BSL3.2, interacts with the second of the terminal three-stem-loop structure, called the X-tail[112], and other upstream sequences[113]. It is also reported to influence IRES activity[114]. The primary sequence of the 3' X-tail is nearly 100% conserved in all known strains of HCV, and nucleotide exchanges are rarely tolerated. The kissing-loop interaction of X-tail and 5BSL3 is essential for efficient replication[112,115]. They are separated by a variable region and a PolyU/UC stretch at the start of the 3' UTR[116], which positively regulates replication, but can tolerate deletion of large patches, without a complete abolishment of infectivity[117,118]. It is a hub for viral and host protein

association[119,78,120,121], but also a strong activator of antiviral signaling[122,123].

1.5.6. Assembly and Release

Packaging of the viral RNA takes place on the surface of lipid droplets, which are covered with the capsid protein core[124]. The core protein is the only building block of the proteinacious capsid. It has RNA binding capabilities[125,126], and also interacts with the envelope glycoprotein E1:E2 heterodimer, via the cytoplasmic domain of E1[127]. Unlike the envelope proteins of other flaviviruses, they are not proteolytically processed during their passage through the secretory pathway[128]. Both proteins contain multiple glycosylation sites[129,130]. Little is known about the small p7 peptide, which can form an ion channel[131]. Apart from the fact that it is necessary for assembly[132] and can prevent degradation of the glycoprotein E2[133], the exact function of the viroporin has not been clarified. NS2 is a cysteine protease, and a part of the intermediate NS2-3 protease. It is also involved in particle production, but is not included in the mature virion[134,135].

After assembly of intact capsids, the particle enters the secretory pathway[136]. By budding of the capsid into the ER-lumen, likely mediated through interaction of core with the E1:E2 complex, the virion acquires its membrane. In the course of egress, the viral membrane picks up lipoproteins ApoE and B, and is likely associated with VLDL[137], which remain associated to the virion and are needed for the subsequent infection event. During its passage, the viral particle is packaged into a secretory vesicle, which releases the infectious virion by membrane fusion[138]. This process is, like viral entry, clathrin-dependent[137] (**fig. 1.4**F).

1.6. Cell Culture Systems for HCV Replication

The establishment of an efficient cell culture model for HCV took more than a decade after initial characterization of the virus. In those years, HCV was challenging to propagate and detect in cell culture, so most investigations relied on infected primary hepatocytes, which only survive several weeks under cultivation and detection of RNA by PCR-based methods[139,140]. Later, also susceptible cell lines were discovered, which could sustain HCV infection for prolonged periods of time[141]. The major turning point was the subgenomic replicon system, developed by Lohmann et al.[142], which is based on a truncated open reading frame, containing the replicase components NS3-5B. The core to NS2 fragment was replaced by a neomycin phosphotransferase (neo), conferring re-

sistance to the antibiotic G418, for selection in cultured cells. The first replicons were bicistronic (**fig. 1.7**B), with the selection marker under control of the HCV IRES and a second EMCV IRES element driving translation of the HCV non-structural proteins. The coding sequence was derived from a genotype 1b consensus (Con1)[142]. Modifications
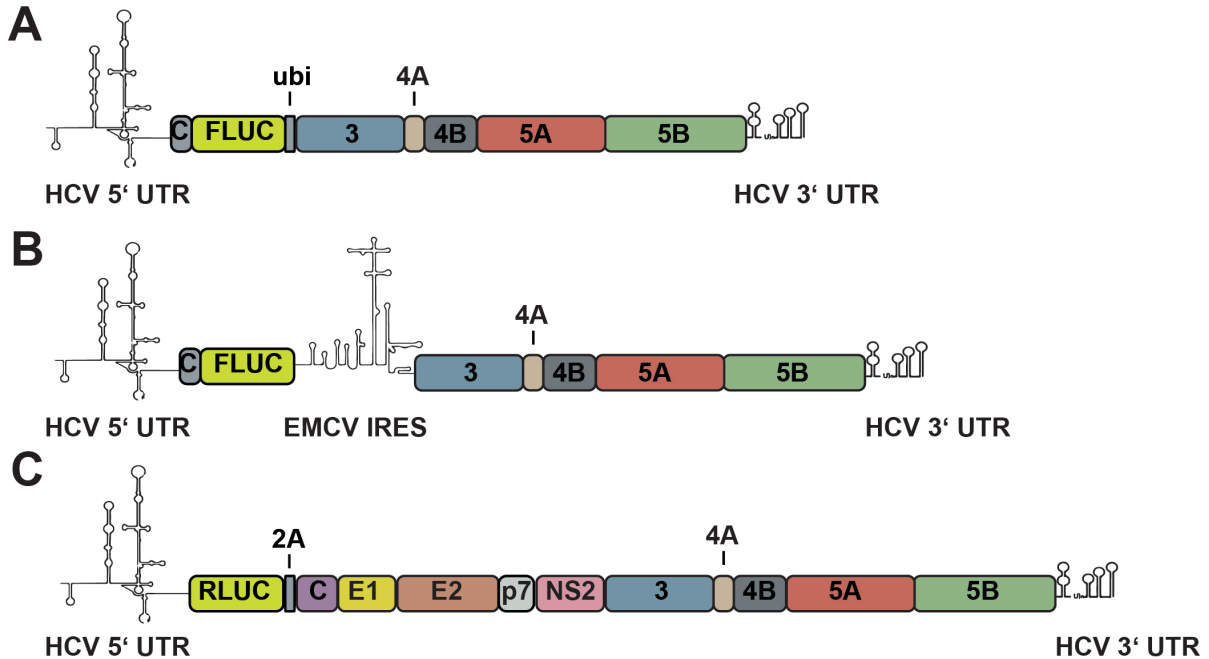
Figure 1.7.: Reporter replicons for HCV. A | Monocistronic replicon with firefly reporter. The conserved GDD motif of the polymerase is indicated. Mutation of this amino acid triplet abolished replication capacity of the replicon. **B |** Bicistronic replicon with an EMCV IRES controlling non-structural protein synthesis. **C |** Full length reporter virus (JcR2A) with a renilla luciferase gene preceding the core coding region.

of the replicon system allow insertion of a reporter (e.g. Luciferase) instead of (or in combination with) a selection marker. Additionally, the replicon system can also be used in a monocistronic context, with a recognition site for the host ubiquitin protease 3' of the reporter gene[143–145] (**fig. 1.7**A). The construct is flanked by the native non-coding regions to allow for efficient replication and translation. Usually, these sequences are *in vitro* transcribed to generate a replication competent RNA, which is then transfected into target cells by electroporation. A conserved GDD-motif in the catalytic center of the RdRP can be deleted (ΔGDD) or mutated (GND), to generate a replication deficient negative control (marked in **fig. 1.7**A). These RNAs faithfully emulate the intracellular stages of HCV replication, including membranous web formation.

Most isolates need to acquire a number of adaptive mutations to replicate efficiently

in cell culture[146]. These mutations boost replication, but completely abrogate infectious particle formation[147]. The discovery of the Japanese fulminant hepatitis (JFH)-1 strain (gt2a), which thrives in cultured cells without any need for adaptation, made it possible to generate an even more effective replicon system[148].Today, this represents one of the most frequently used model systems in HCV research, due to its high replication efficiency. Replicon systems for many other genotypes have been developed in recent years, allowing for the investigation of genotype-dependent differences[149].

Moreover, JFH-1 also produces virions in cell culture, albeit to low numbers. This was the basis for the generation of a chimeric construct (core-NS2 of the J6 strain (also gt2a)) to allow production of infectious particles in cell culture to unprecedented titers[150]. The resulting virus has been modified and a *Renilla* luciferase reporter was introduced. This construct is called JcR2A, and allows for easy detection of full-length HCV replication and infection (**fig. 1.7**C).

Selection of Con1 replicon transfected Huh-7 cells gave rise to replicon-containing clones. By curing these cells with antiviral regimens, two cell lines (Huh-7 LUNET, Huh-7.5) were obtained, which are significantly more permissive for HCV propagation than the parental cell line[151]. Apart from these highly susceptible cell lines, other liver and non-liver cells are capable of HCV replication when they are supplied with miR-122, which has been identified as a crucial host factor of HCV translation and replication[152,153]. A recently established model system are Hep3B cells. This hepatic cancer cell line has been transformed by chronic HBV infection, and lacks detectable expression of miR-122[154]. Therefore, these cells do not support efficient HCV replication natively. However, stable transduction, or transient transfection by electroporation renders these cells permissive for viral replication[155]. Similarly, HepG2 cells have been reported by one group to become permissive for HCV upon supplementation of miR-122[156]. In addition to hepatocytes, several non-hepatic cells have been coaxed into susceptibility by simple transfection of miR-122. Among them are Hec1B (ovary), 293T (fibroblast), MC-IXC (neuronal) and RERF-LC-AI (lung)[157].

1.7. miRNA in Viral Infection

Viral RNA replication is not only dependent on a number of viral, but also host factors. Apart from various protein factors, many HCV hijacks the cellular RNA interference machinery for its own propagation. Many other viral infections also modulate the host miRNA system, by targeting crucial components of the RNAi machinery (reviewed in

Skalsky and Cullen [158]). Several members of the Herpes- and Polyomavirus families even encode for their own miRNAs[159]. A relative of HCV, the Kunjin strain of West Nile Virus is currently the only RNA virus known to generate a functional miRNA from the 3' UTR of its genome[160]. Overall, the small non-coding RNA fraction is of major importance for a large number of viruses.

1.7.1. RNA interference and short non-coding RNAs

The basic process of RNA-induced inhibition of translation is called RNA interference (RNAi), and was first discovered in studies on petunia[161], and further insight was gained in Caenorhabditis elegans. It was discovered that delivery of small RNA fragments with a complementary sequence to regions of cellular mRNAs, resulted in decreased levels of the targeted transcript and the encoded protein[162]. Shortly after this revolutionary observation, the occurrence of small interfering RNAs (siRNA) in plants, shed light on possible functions of RNAi. It was observed that cauliflower mosaic virus infection is counteracted by generation of short fragments of viral RNA, which bind to their respective complements, and eventually lead to its degradation[163]. It was assumed that this ability of generating anti-viral RNAs had been lost in higher animals, until recent studies could show siRNA-mediated host defense mechanisms are existent[164]. However, the majority of cellular short RNA is generated from endogenous sources, and has important functions in cellular homeostasis. MicroRNAs are 21 - 24 nt long non-coding transcripts, which are capable of post transcriptionally regulating the translation of their target genes. MiRNAs are located either in intronic or exonic regions, as single transcripts or in clusters under a common promoter, which are transcribed to polycistronic primary miRNAs. They are usually generated by RNA polymerase II, in some cases by RNA polymerase III (PolII, PolIII). These capped and polyadenylated transcripts are several hundred base pairs in length, and form bulged, hairpin structures with a short terminal loop. These structural features are recognized by the ribonuclease III-like protein Drosha, and its co-factor DiGeorge Syndrome Critical Region Gene 8 (DGCR8), forming the microprocessor complex[165–167]. The pri-miRNA is cleaved by Drosha at around 22 nt from the terminal loop. DGCR8 functions as molecular ruler to ensure the correct length of the fragments. The resulting stem loop is now called precursor miRNA (pre-miRNA). In few cases, nuclear maturation of miRNA precursors can be Drosha/DGCR8-independent[168]. Yet, the final products of both ways have the same distinct features, most importantly a 2 nucleotide overhang at its 3' end, and a 5' phosphate. After export to the cytoplasm,

the pri-miRNA is bound by Dicer, another member of the ribonuclease III family. After binding, the terminal loop is removed[169,170]. The only known exception is pri-miR-451, which is directly processed by AGO2[171]. The resulting short RNA duplex has now 3' overhangs on both strands. Subsequently, the strand with the higher thermodynamic stability on its 5' end, or passenger strand (miR*), is released and usually degraded. The guide strand, becomes the active miR. Target specificity is primarily mediated by the 5' nucleotides 2 to 8, which compose the so-called seed region. Further pairing of the 3' nucleotides determines the stability of the hybrid. Since not all nucleotides are complementary, the miRNA:mRNA duplex has a bulged appearance. Studies have shown, that target sites are significantly over-represented in the 3' untranslated regions of cellular mRNAs. Before binding to a target mRNA, the double-stranded RNA is being incorporated into the RNA-induced silencing complex (RISC). The core proteins essential for the assembly of the initial complex are Dicer, one member of the Argonaut protein family, mostly AGO2, and TRBP[172,173]. The final RISC can be comprised of many factors, even though only AGO bound to a small RNA seems to be sufficient for functional mRNA silencing. Unlike in siRNA-mediated decay, the imperfect binding of miRNAs does usually not trigger AGO2-driven immediate destruction of the target transcript, but initially blocks translation. The definitive mechanism is not yet fully understood, but several hypotheses are discussed. One model suggests a block of ribosomal initiation, due to interference of AGO2 with eIF4F cap-binding[174], and/or recruitment of deadenylases by GW182[175], which is known to directly interact with AGO2. In addition to the translational repression or degradation of target mRNAs, miRNAs can also function via epigenetic transcription regulation in the nucleus and direct receptor binding[176–179]. In the next step, Dicer dissociates from the complex, and the residual RISC is sequestered in cytoplasmic aggregates, the processing bodies (P-body)[180]. These foci contain proteins of the degradosome, and completely lack ribosomes, thereby promoting degradation and subverting translation. The whole process is summarized in **fig. 1.8**. On the mRNA level, the overall changes are rather modest, which has lead to the term "regulatory fine-tuning"[181]. The reduction of mRNA and protein levels depends strongly on numerous factors, such as the number of binding sites, the degree of sequence complementary, potential counter regulatory events[182], and possible synergistic effects[183,184]. Many mRNAs have multiple binding sites and are targeted by more than one miRNA. By today, over 1000 human miRNAs have been discovered, and the number is rising. Estimations that up to 80% of all genes are regulated by this particular mechanism[185–187] underscore the importance of maintaining a delicate balance of proteins in the cell.
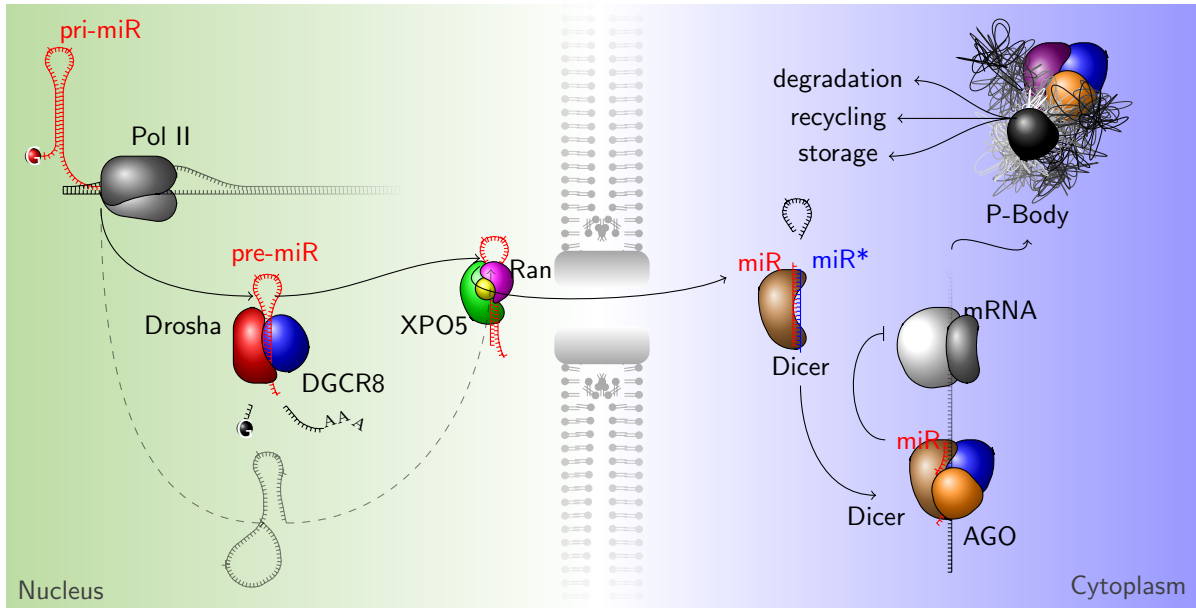
Figure 1.8.: MicroRNA biogenesis and function. In animals, PolII transcribed hairpins are cut by the nuclear microprocessor complex, comprised of Drosha and DGCR8, and transported to the cytoplasm via exportin 5/RanGTP. Dicing and unwinding is followed by embedding of the mature miRNA into the RISC, which is essential for the inhibition of translation and re-localization to P-bodies.

1.8. HCV:miR-122 interaction

miR-122 is liver specific, and with roughly 60000 copies per cell the most abundant miRNA in hepatocytes[188,189]. It is involved in a great number of cellular processes. The functional spectrum includes roles in iron and lipid metabolism[190–192], anti-tumor[193,194,192] and anti-viral[195] activities as well as immune modulation[196]. The viral genome harbors two highly conserved binding sites for the mircoRNA in the first 40 nucleotides of the 5' UTR, which have been found to be of vital importance for the virus[152]. Numerous studies have found that in cellular genes the 3' UTR show a significant enrichment of functional binding sites, and translation is reduced upon RISC binding (reviewed in Bartel[197]). In contrast, HCV translation and replication are massively increased upon miR-122 interaction[198,199]. Indeed, the miR-122 is an important dependency factor for HCV, and might be the reason for the liver tropism of the virus. So far it has been reported that most cell lines lacking miR-122 do not support replication, with few exceptions. In one study it was observed that Hec1B support low-level

replication of HCV in absence of miR-122[12], which is in line with some reports claiming extra-hepatic manifestations of the disease[200,201]. Also, Hep3B cells were shown to allow for replication of a bicistronic replicon[155]. Even though an ever growing amount of descriptive evidence for the importance of the miR-122:HCV interaction is generated, the molecular mechanisms are still elusive. A general stabilization effect of miR-122 on the HCV RNA has been described, which has been connected to host nuclease resistance. The binding model of miR-122 to the 5' portion of HCV predicts an unusual 3'-overhang of the miR, effectively masking the native 5'-terminus of the viral genome[202]. Therefore, it has been postulated, this might act as a physical shield against the recognition of 5'-3'-exonucleases. Specifically, Xrn1[203] (and recently also Xrn2[204]) were identified as likely effectors, degrading unprotected HCV RNA. The stability hypothesis is currently thought to explain most of the effects on the HCV life cycle, although there is mounting evidence that the other modes of action are at least similarly important. Especially the failure of efficient knock-down of the exonuclease Xrn1, which is thought to be the key player in HCV RNA degradation, to rescue replication in absence of miR-122 has cast some scrutiny on this view[205]. Moreover, miR-independent replication of a bicistronic construct further underscores the notion that a combination of events is necessary to fully explain the impact of miR-122 on the viral life-cycle[155]. While ongoing replication is not affected by miR-122[206], the initiation phase seems to be influenced. A recent study claimed that this might be due to displacement of translation-enhancing factors (e.g. PCBP2), leading to a greater fraction of RNA available for replication[207]. Another option that was explored in some detail, was the stimulation of protein synthesis. Reporter systems and replicon based studies, in cells or *in vitro*[208,198] have all concluded that HCV IRES-dependent protein production is increased in presence of miR-122. More specifically, the kinetics of 40S attachment are accelerated, which is a crucial step on the way to initiation complex formation[209]. The molecular basis for this effect has not yet been discovered.

1.9. Host and Viral Modes of Translation Initiation

Cellular mRNAs are commonly translated in a cap-dependent fashion. The cap structure is an important recognition site for the protein complexes that are required for ribosome attachment and translation initiation. This modification is applied to the mRNA during its nuclear maturation process. While this is the standard mechanism of translation, alternative routes exist, which rely on direct, internal ribosome recruitment

to the initiation site.

1.9.1. Cap-dependent Versus IRES-mediated Translation

The cap structure is composed of a C7-methylated guanosine (m7G) which is attached to the 5'-end via a triphosphate bridge. This is a common feature of all processed messenger RNA, which are exported from the nucleus into the cytoplasm. It protects the RNA from premature degradation, and additionally serves as a hub for protein recruitment[210]. In the nucleus, a cap-binding complex is assembled, composed of IMPα, and the cap-binding proteins CBP20 and CBP80. In addition, proteins of the spliceosome, the exon-junction complex (EJC), and polyA-binding proteins associate to the message. After translocation to the cytosol, a cascade of events is triggered, leading to the assembly of an initiation complex. First, a binary complex of the scaffolding factor eIF3 and the 40S ribosome is recruited to the cap via the CBP80/20-dependent Translation Initiation Factor (CTIF)[211,212]. At this point, the ternary complex co-associates to form a 43S pre-initiation particle[213]. Since these steps are all taking place in close proximity of the cap structure, the ribosome must be placed at the initiation codon by scanning the RNA template. For this step, the eIF4F complex is utilized, which contains the RNA helicase eIF4A[214]. Upon ATP hydrolysis, this factor moves the 43S complex along the message. Once in place, the eIFs are removed from the pre-initiation complex. This leads to the assembly of the 80S ribosome, with the help of eIF5 and 5B. The pioneer round of translation is about to begin[215]. This distinct step in the life of messenger RNAs is mainly important for quality control. Aberrantly spliced mRNAs, which contain a stop-codon in the ORF, are recognized by interaction of the SURF protein complex (**S**MG1,**U**pf1,e**RF**1+3), which associates to stalled ribosomes and a downstream EJC[216]. Then, endo- and exonucleases are recruited and degrade the faulty message, a process known as nonsense-mediated decay (NMD). If the mRNA is correctly processed, the first ribosome dislodges all EJCs in its course[217], and also a specific type of polyA-binding protein (PABPN1), which is only present during this pioneer round of translation[218]. These modifications of the mRNP are therefore referred to as translation-dependent mRNP remodeling. At the cap, a translation-independent change is mediated by IMPβ, which binds to IMPα, stably connected to the CBPs[218]. Interaction of these proteins releases the CBP complex, which is then replaced by eIF4E, also present in the eIF4F particle. The other included eIF4-protein, eIF4G, interacts with polyA-binding proteins to circularize the mRNA, and also recruits the 43S complex to initiate subsequent rounds

of translation. Now, polysome assembly and steady state translation can begin. Most DNA viruses are replicating in the nucleus, and can therefore make use of the host's capping machinery. Poxviruses are an exception, as they encode their own capping enzymes. Influenza viruses have to acquire their cap from host mRNAs employing a process termed cap-snatching. However, a large number of RNA viruses use a different strategy. Attachment of the uncapped RNA to the ribosome is in these cases mediated by an IRES. Several virus families make use of such a structured RNA element. There are currently four known types of RNA-virus IRES elements, which are grouped based on their structural properties and usage of initiation factors. Type I is present in entero-, rhino-, and polio virus[219,220]. Some members of the cardio- and apthoviruses of the *Picornavirdiae* family mediate translation from a type II IRES, sharing the archetype structure of EMCV[221]. Both of the previously mentioned IRESes rely on many canonical eukaryotic initiation factors (eIF), including eIF4A and G, but they contain distinct structural features. In contrast, HCV possesses a type III IRES, which is only dependent on eIF3 and the ternary complex (eIF2:GTP:tRNA^{met}), similar to the related GB virus-B and -C, and classical swine fever virus. Curiously, a DNA virus, Human Herpesvirus-8, also shares this type of IRES[222]. The initiation element of Cricket paralysis virus is the epitome of a type IV IRES, which is independent of initiation factors[223], including the ternary complex, and is located within an intergenic region[224].

Not only virus messages, but also some host mRNAs have been described to contain functional IRES elements in addition to the cap[225–228]. Similarly, HIV-1 produces capped mRNAs, which also harbor IRES elements. These are employed during the late stages of productive infection, when the host cell is going into translational arrest[229]. 5' UTRs with an IRES are usually longer, more structured and might contain several upstream AUGs, making them poor templates for efficient cap-dependent translation. However, both types of initiation can concur on the same message[226]. The circumstances under which either mode is used are not always clear, but for cellular genes, their regulation seems to be mostly dependent on environmental influences (e.g. starvation) or cell cycle phase. For instance, the IRES of the X-linked inhibitor of apoptosis protein evades stress-induced translation repression by using eIF5B, instead of eIF2α[230,225], a mechanism also exploited by HCV[231]. While most IRES elements are upstream of the initiator AUG, some are located in the coding region, therefore producing a shortened protein. In the case of p53, this truncated version acts as potent inhibitor of the cap-translated version, and induces cellular proliferation[232,233]. Overall, the cellular IRES still remains a mystery in many ways. In contrast to their viral counterparts, they are less structurally

stable and do not share common sequence features. One common feature is the use of specialized RNA-binding proteins, IRES-specific cellular transacting factors (ITAFs), which are non-canonical modulators of translation. These factors serve to recruit other proteins, or to structurally rearrange the RNA. Importantly, they can substitute the functions of canonical initiation factors. Almost all known IRESes circumvent the need for the cap-binding protein eIF4E[234,235]. The scanning step is also omitted in most cases, since the ribosome is assembled in close vicinity of the initiation codon. The detailed mechanisms, and whether the assembled RNP is static, or as dynamic as in cap-dependent translation remains to be investigated.

1.9.2. The HCV IRES and its Modulation by Host Factors

The HCV IRES structure is located in the 5'UTR of the viral genome, as well as a part of the core coding region[236], and is divided into three functional domains (II-IV, **fig. 1.9**A). Domain I is not included in the classical definition of the IRES, however, it is able to modulate translation. All domains feature extensive secondary structures, which are crucial for IRES function. Moreover, interactions between different parts of the IRES further increase its three dimensional complexity. The primary sequence of the IRES element is highly conserved among all genotypes. Only few positions can be exchanged without causing severe impairment of IRES activity. Genotypes 3a and 4a have exchanges at nucleotides 175 and 224, which retain the structure via non-Watson-Crick base pairing, but might impact the thermodynamic stability. For gt3a, the domain III substructures c and d are also deviating from the sequence of other genotypes. This might account for a weaker IRES activity observed for gt3 sequences, compared to 1 and 2. Reported variations in domain IV are all located in the core coding region[237].

1.9.3. Functional properties of the HCV 5' UTR and IRES domains

The role of domain I (nt1-47) has been controversially discussed. While some claimed a positive role in protein synthesis[238,239], others found it to be dispensable for IRES activity[240], or even exert repressive effects on the translation of a downstream open reading frame[241,242]. In agreement with the latter, deletion of domain I enhances translational activity not only *in vitro*, but also *in vivo*[243]. Importantly, studies on the HCV replicon system have shown that this region also harbors functional elements that facilitate replication[244]. It was later recognized that the 3' terminus of the complementary (negative) strand is responsible for this function[245]. Importantly, most assumptions on

the roles of this domain were made before the discovery of two seed-binding motifs for the liver-specific microRNA (miRNA or miR)-122[153], which can significantly increase the translation/ replication capacity of the virus by a presently undefined mode of action[246](**fig. 1.3**A). In recent years, the modulatory role of domain I in viral translation has therefore regained a lot of significance. In particular, the purportedly unstructured region separating SLI and II is in the focus of attention .

IRES domains II and III promote assembly of the 40S and 48S ribosomal complexes, respectively[247] (**fig. 1.9**A). Domain II is absolutely required for efficient IRES activity in liver cells[248,249]. Besides the primary sequence and secondary structure, also the tertiary fold is of great import. The twisted L-shaped architecture of SLII is crucial for ribosome assembly, and compounds targeting the kink region effectively abolish translation activity[250,251]. In HCV, as well as the related Classical Swine Fever Virus (CSFV), it mediates the displacement of eIF2 to facilitate attachment of the 60S ribosomal subunit[252]. Moreover, this domain is able to structurally modify the ribosome to optimize activity, stability and entry position via a GCC motive at the tip of the stem-loop[223,253,254], a feature that sets this type of IRES apart from all others. Deletion of domain II also influences the structure and ribosome binding capability of the downstream domains[255].

Domain III is mostly responsible for host factor recruitment, it comprises binding motifs for numerous ITAFs and the eIF3 complex[256], the only additional host initiation factor known to aide HCV translation, apart from the eIF2-containing ternary complex. Under stress conditions, when eIF2α is phosphorylated and thereby inactivated, eIF5B can be used as substitute. The activity of domain III depends on the formation of an internal pseudoknot at the 3' base, close to the initiation codon[30,249,236]. The structural setup confers a high binding affinity for the eIF3 N-terminal RNA binding domain[257,256,258], which allows the HCV IRES to compete with preformed eIF3:40S complexes[259]. The eIF3:40S complex is necessary for cap-dependent translation activity. The HCV IRES binds the 40S subunit independently before recruiting eIF3 and the ternary complex. Therefore, this function of the HCV IRES might also provide a means for virus-induced host cell shut off. Moreover, multiple contact sites with the 40S ribosomal subunit were identified at sub-domains IIIc and IIId by toe printing analysis, the adjacent pseudo knot, and the initiation codon by different groups[255,247] (**fig. 1.9**A).

Domain IV includes a stem containing the initiator AUG, which negatively regulates translation efficiency[260]. The domain extends into the core coding region[261]. The sequence folds into a pseudoknot element[262], which positions the ribosomal E-site directly at the start codon, without the need for a scanning step. The primary sequence seems

to be critical for 40S binding, resulting in extreme conservation among genotypes[263].
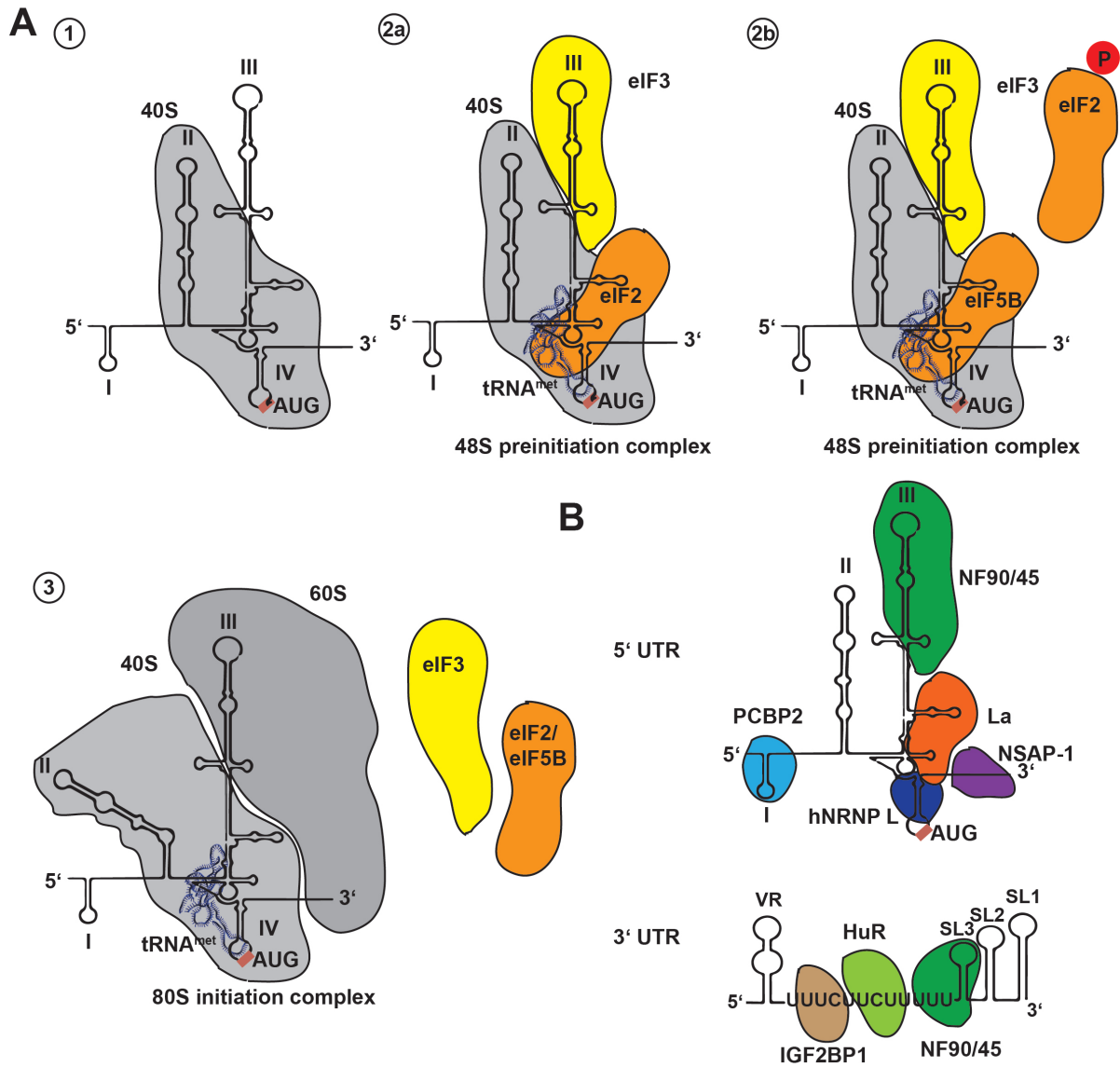
Figure 1.9.: The internal ribosomal entry site of HCV. A | Sequence of events prior to translation initiation. (1) The first step of translation initiation is the recruitment of the small subunit of the ribosome. For capped RNAs, eIF3 is needed for 40S attachment and 48S particle formation. (2a) Here it is recruited separately, together with the ternary complex, eIF2:GTP:tRNA^{met}, under normal conditions. (2b) During cell stress, eIF2α is inactivated through phosphorylation, and HCV switches to eIF5B instead. (3) 80S assembly is initiated by eIF3. Then, domain II mediates the release of initiation factors. The structure of SLII as well as of the ribosome is altered in the process, to position the ribosome correctly and activate translation. **B |** Factors that modulate HCV translation, and their respective binding position in the 5' or 3' UTR.

1.9.4. Cellular and viral proteins involved in IRES mediated translation

Several protein factors have been found to modulate HCV IRES dependent translation. As mentioned above, eIF3 and 2, and under certain circumstances eIF5B, are the only canonical initiation factors known to be associated with HCV. In contrast, the complete eIF4 complex, including the scanning factor eIF4A are thought to be dispensable for IRES activity[264]. In the 5' and 3' genome flanking regions, a number of ITAFs are bound (**fig. 1.9**B).

NSAP-1[265], La antigen[266], NFAR90/45[267,268], polycytidylic acid binding protein (PCBP)[269,270], heterogeneous ribonucleoprotein L (hnRNPL)[271,272,267,273] or UNR (upstream of N-ras)[273,274] are known interactors, which are in most cases known to enhance translational activity. Also, the polypyrimdine tract binding protein, PTB, binds to multiple sites in the viral 5' and 3' UTR[275,276,273]. The role of PTB has been subject to great controversy[277–280], but is now believed to inhibit, rather than stimulate translation, instead favoring RNA replication[281]. Of note, UNR and PTB have also been implicated in activation of a cellular IRES element in the APAF-1 message, acting as a molecular chaperone[282]. Interestingly, UNR itself can be translated via internal initiation, in this case PTB is also described as a negative regulator[283]. Also, a member of the heat-shock protein family, HSP90, has been reported to associate with eIF3 to stimulate translation[284].

While viral non-structural proteins are absent during the first round of HCV translation, at later stages of the viral life cycle it is likely that they can act as regulatory factors. Examples are NS3, which has been shown to inhibit translation and favor replication by dislodging La[68], or interaction with YB-1[285]. Additionally, some evidence has been provided that NS5A can act positively on global translation, at least in part by recruiting eIF4E[85,89,286]. Interestingly, also activation of the antiviral double stranded RNA-dependent protein kinase (PKR) and its interaction with viral NS5A seems to be beneficial for HCV translation activity under certain circumstances[287]. Concomitantly, the kinase is potently triggered by domain II-IV of the HCV IRES[84,288]. Conversely, others have found that the IRES inhibits PKR function[289], which might be due to different cell type specific modes of regulation[287]. PKR is triggered by exogenous stressors (e.g. dsRNA intermediates during viral infections), and in turn shuts off translation by phosphorylating eIF2α. Phosphorylated eIF2α cannot participate in ternary complex formation, resulting in translational arrest[290]. HCV escapes this genuinely antiviral

mechanism by usage of eIF5B, resembling a mode of translation initiation usually found in bacteria[231].

2. Aims of this study

2.1. An in vitro replication assay for HCV

To date, the mechanisms of initiation of viral RNA synthesis remain largely elusive. The vital contribution of the non-structural proteins NS3 (especially its helicase function) and NS5A to RNA replication have been described in the replicon model. However, mutations which perturb the function of a single protein are hardly interpretable in the cellular context, due to the complex network of interactions present in this setting. Hence, the isolation and reconstitution of replicase complexes *in vitro* is the method of choice in order to address the contribution of individual protein functions. Working *in vitro* systems for the HCV replicase have been established for synthetic templates, but few data are available on biologically relevant RNAs. Especially the determinants for the initiation of *de novo* (-)-strand synthesis, which is the primary step for every replication cycle, are not clear.

Therefore, the first part aimed to develop an *in vitro* assay using purified replicase proteins, to reproduce critical steps of HCV replication initiation in a test tube. This also requires a reliable expression system for the involved non-structural proteins. Initially, the focus was set on the optimization of protein expression in bacteria or mammalian cells and the characterization of protein function. In this approach, the isolated components of the viral replicase should be used to determine individual contributions of the non-structural proteins on the polymerase activity of NS5B. In particular, the functional involvement of the viral helicase NS3, but also potential activities of NS5A should be investigated.

2.2. Dissecting the roles of miR-122 in the HCV life cycle

In the second part, we were addressing the question, as to how miR-122 influences HCV at different stages of its life cycle. This issue is under vigorous debate. RNA stability, replication and translation efficiency have all been hypothesized as possible modes of action. The stability hypothesis is currently thought to explain most of the effects on the HCV life cycle, although there is mounting evidence that the other modes of action are at least similarly important. Especially the failure of efficient knock-down of the exonuclease Xrn1, which is thought to be the key player in HCV RNA degradation, to rescue replication in absence of miR-122 has cast some scrutiny on this view. Thus, this work aimed to quantify the different contributions of miR-122 to translation, RNA synthesis and RNA stability and comprehend the underlying molecular mechanisms.

One possibility under investigation was, whether binding of the RISC complex could act as an RNA chaperone to induce a structural shift in the 5' UTR of HCV, which regulates translation efficiency. The functional HCV IRES consists of three highly structured domains, II - IV, which are essential for translation[291]. We envisioned that by preventing the formation of a translation attenuating stem in domain I, miR-122 binding could create a bias towards the local structure, which is described as domain II of the HCV IRES. By means of site directed mutagenesis within the two 5' binding sites, we wanted to determine the impact of miR-122 on translation and replication. Moreover, the IRES with and without bound miR-122 was subjected to structural analysis by biochemical (SHAPE) and biophysical (NMR) methods.

Apart from the two prominent 5' miR-122 binding sequences, two more sites have already been described: one in the coding region of NS5B, and another one in the variable region of the 3' UTR. In addition, further conserved miR-122 binding sites were searched by comparing the full length RNA sequences of several genotypes. To date, the contribution of these sites to the viral life cycle has not been investigated in great detail. Therefore, this work finally aimed to interrogate the functional relevance of the additional sites in the coding region and 3' UTR.

3. Materials

3.1. Chemicals and Expendables

Table 3.1.: Overview of chemicals

Name	Supplier
Agarose	Sigma Aldrich (Darmstadt, Germany)
Ethidium bromide	Carl Roth (Karlsruhe, Germany)
Ampicilin	Sigma Aldrich (Darmstadt, Germany)
Acetic acid	Carl Roth (Karlsruhe, Germany)
Glycerol	Carl Roth (Karlsruhe, Germany)
β-Mercaptoethanol	Sigma Aldrich (Darmstadt, Germany)
Calcium chloride	Carl Roth (Karlsruhe, Germany)
Chloroform	Carl Roth (Karlsruhe, Germany)
Ethylenediaminetetraacetic acid (EDTA)	Sigma Aldrich (Darmstadt, Germany)
Ethanol	Carl Roth (Karlsruhe, Germany)
Methanol	Carl Roth (Karlsruhe, Germany)
Glycerol	Carl Roth (Karlsruhe, Germany)
Hydrochloric acid	Carl Roth (Karlsruhe, Germany)
Isopropanol	Carl Roth (Karlsruhe, Germany)
Potassium acetate	Carl Roth (Karlsruhe, Germany)
LB Medium/Agar	Carl Roth (Karlsruhe, Germany)
Magnesium chloride	Carl Roth (Karlsruhe, Germany)
3-(N-Morpholino)propansulfonic acid (MOPS)	Sigma Aldrich (Darmstadt, Germany)
NaCl	Carl Roth (Karlsruhe, Germany)
Di-Sodium carbonate	Carl Roth (Karlsruhe, Germany)

o-Nitrophenyl-β-D-galactopyranosid	Sigma Aldrich (Darmstadt, Germany)
Polyethylenimine	Sigma Aldrich (Darmstadt, Germany)
Paraformaldehyd	Sigma Aldrich (Darmstadt, Germany)
Tris(hydroxymethyl)aminometh (TRIS)	Carl Roth (Karlsruhe, Germany)
Triton-X 100	Sigma Aldrich (Darmstadt, Germany)
Tween20	Carl Roth (Karlsruhe, Germany)
Sodium dodecylsulfate	Sigma Aldrich (Darmstadt, Germany)
Dithiothreitol	Sigma Aldrich (Darmstadt, Germany)
Dimethylsulfoxide	Sigma Aldrich (Darmstadt, Germany)
2-methylnicotinic acid	Sigma Aldrich (Darmstadt, Germany)
1,1'-carbonyldiimidazole	Sigma Aldrich (Darmstadt, Germany)
Phenol	Sigma Aldrich (Darmstadt, Germany)
Urea	Sigma Aldrich (Darmstadt, Germany)
Polyacrylamide (19:1, 30%)	Carl Roth (Karlsruhe, Germany)
Coelenterazine	Promega (Mannheim, Germany)
Luciferine	Promega (Mannheim, Germany)

Table 3.2.: Overview of expendable materials

Name	Manufacturer
Eppendorf reaction tubes (1.5 ml, 2.0 ml)	Eppendorf (Hamburg, Germany)
Multiply-μStrip Pro 8 PCR tubes	Sarstedt (Nrmbrecht, Germany)
Polyproylen tubes (15 ml, 50 ml)	Sarstedt (Nrmbrecht, Germany)
Pipet tips (10 μL, 100 μL, 1000 μL)	Greiner (Frickhausen, Germany)
Glass pipet (2 ml, 5 ml, 10 ml)	Costar (Corning NY, USA)
Sterile syringe	BRAUN Melsungen AG (Melsungen, Germany)
Sterile syringe filter (0.22 μm, 0.45 μm)	Millipore (Billerica, USA)
Cell culture flasks	Becton-Dickinson (Heidelberg, Germany)
Cell culture dishes	Falcon BD (Heidelberg, Germany)
Multiwell culture plates	Falcon BD (Heidelberg, Germany)
96-well white flat-bottom	NUNC (Roskilde, Denmark)
Scalpel	Swann-Morton (Sheffield, UK)

Microscopy glass slides	Menzel (Braunschweig, Germany)
Cover slips	Menzel (Braunschweig, Germany)
Latex/ Nitrile gloves	Kimberly-Clark (Dallas, TX, USA)
BioMax MR Film	Kodak (Rochester, NY, USA)
BioMax MS Film	Kodak (Rochester, NY, USA)
BioMax Light Film	Kodak (Rochester, NY, USA)
Glassware	Schott (Jena, Germany)
Phosphorscreen	BioRad (Hercules, CA, USA)

Table 3.3.: Kits and commercial systems

Name	Manufacturer
PhusionFlash High Fidelity Master Mix	Thermo Fischer Scientific (Waltham, MA, USA)
Restriction enzymes	NEB (Ipswich, MA, USA)
DNA Ladder EcoRI λDNA	Invitrogen (St. Leon-Rot, Germany)
T4 DNA Ligase	NEB (Ipswich, MA, USA)
Extract II Gel Extraction Kit	Machery & Nagel (Freiburg, Germany)
NucleoBond PC 100 Plasmid Extraction Kit	Machery & Nagel (Freiburg, Germany)
NucleoBond PC 500 Plasmid Extraction Kit	Machery & Nagel (Freiburg, Germany)
Penicillin-Streptomycin (100x)	Gibco-BRL (Karlsruhe, Germany)
DMEM	Gibco-BRL (Karlsruhe, Germany)
OPTIMEM	Gibco-BRL (Karlsruhe, Germany)
Trypsin-EDTA	PAA Laboratories (Pasching, Austria)
jetPEI	Polyplus Transfection SA (Illkirch-Graffenstaden, France)
Lipofectamine2000	Thermo Fischer Scientific (Waltham, MA, USA)
Effectene	Qiagen (Hilden, Germany)
Grace Insect Cell Medium	Gibco-BRL (Karlsruhe, Germany)
RNAsin	Promega (Mannheim, Germany)
SensiMixPlus SYBR	Invitrogen (Darmstadt, Germany)
siRNA negative control	Sigma Aldrich (Darmstadt, Germany)

dNTPs	Invitrogen (Darmstadt, Germany)
rNTPs	Invitrogen (Darmstadt, Germany)
SuperScript III RT	Invitrogen (Darmstadt, Germany)
Western Lightning ECL	PerkinElmer (Waltham, MA, USA)
QuantiGene ViewRNA ISH Cell Assay Kit	Affymetrix (Santa Clara, CA, USA)
Fluoromount-G	Sigma Aldrich (Darmstadt, Germany)

3.2. Plasmids

Table 3.4.: Basic plasmids

Name	Description
pAPM-L1221	Lentiviral vektor for shRNA expression, puromycin resistance gene
pBSK-3'-JFH-dg	T7 expression plasmid for *in vitro* assay template
pFKT7-JFH-1-3'	7 expression plasmid for *in vitro* assay template
pET16	Plasmid for IPTG inducible protein expression
pET21	Plasmid for IPTG inducible protein expression
pFastBac-DualGFP	Baculovirus plasmid for protein expression in Sf9
pFK-i389-LucubiNS3-3'-dg-JFH	Monocistronic luciferase-Replicon, JFH-1 NS3-3', HDV ribozyme at 3'end.
pFK-i341-PiLucNS3-3'-dg-JFH	Bicistronic luciferase-Replicon, JFH-1 NS3-3', Polio IRES driven luciferase, HDV ribozyme at 3'end.
pFK-JCR2a-dg-WT	Full-length J6/JFH-1 luciferase reporter virus
pTM-NS3-3'	T7 promoter-driven protein expression plasmid

pMD.G2	Lentiviral plasmid, which encodes for the surface protein (env)
pCMVΔ31	Lentiviral plasmid, which encodes for the replication machinery (gag/pol)
pWPI-BLR	Lentiviral protein expression plasmid with EIF1A promoter
pUC19	High copy plasmid, used for generation of *in vitro* transcripts

3.3. Technical Equipment and Software

Table 3.5.: Overview of centrifuges, PCR cycler and other technical appliances

Name	Manufacturer
Biofuge Pico	Heraeus (Hanau, Germany)
Gelelectrophoresis system	Qiagen (Hilden, Germany)
Electrophoresis Power Source	Qiagen (Hilden, Germany)
NanoDrop Light	Thermo Fischer Scientific (Waltham, MA, USA)
Sorvall RC5C Plus Centrifuge	Thermo Fischer Scientific (Waltham, MA, USA)
GlassLine Refrigerator	Liebherr Holding GmbH (Kirchdorf an der Iller, Germany)
Freezer -20°C	Gram (Sarstedt, Germany)
Freezer -80°C	Thermo Fischer Scientific (Waltham, MA, USA)
ThermoMixer	Eppendorf (Hamburg, Germany)
Precision 2864 Water Bath	Thermo Fischer Scientific (Waltham, MA, USA)
Vortexer	Bibby Scientific Limited (Staffordshire, UK)
Analysis balance M4600 Delta Range	Mettler (Giessen, Germnay)
pH-meter 766 Calimatic	Knick (Berlin, Germany)
TPersonal 48 Thermal Cycler	Biometra (Gttingen, Germany)

BioRad CFX96	BioRad (Hercules, CA, USA)
UV GelDoc 2000	Intas (Ahmedabad, India)
PipetBoy acu integra	INTEGRA Biosciences (Fernwald, Germany)
Pipets (10 μL, 100 μL, 1000 μL)	Gilson (Hamburg, Germany)
Dispenser Multipipette	Eppendorf (Hamburg, Germany)
Leica DM-IL HC microscope	Leica Camera AG (Solms, Germany)
Leica DM-IL microscope	Leica Camera AG (Solms, Germany)
Leica DFC 420C CCD camera	Leica Camera AG (Solms, Germany)
Leica DM 6000B microscope	Leica Camera AG (Solms, Germany)
HERAsafe sterile work bench	Thermo Fischer Scientific (Waltham, MA, USA)
HERAcell 240 incubator	Thermo Fischer Scientific (Waltham, MA, USA)
Magnetic stirrer L-71	A. Harfenstein (Wrzburg, Germany)
Shaker HS250	IKA Labortechnik (Staufen im Breisgau, Germany)
Lumat LB 9508 Tube Luminometer	Berthold Technologies (Bad Wildbad, Germany)
Mithras LB 940 Plate Luminometer	Berthold Technologies (Bad Wildbad, Germany)
Gene Pulser II Electroporation System	BioRad (Hercules, CA, USA)

Table 3.6.: Software

Name	Developer
Creative Suite 6	Adobe (Dublin, Ireland)
Kile	Kile Development Team
Prism 5	GraphPad (La Jolla, CA, USA)
CFX Manager	BioRad (Hercules, CA, USA)
CLC Main Workbench v6.5	CLC bio (Mhltal, Germany)
Primer3	Lincoln Stein
VARNA	Ponty and Leclerc[292]
SAFA	Das et al.[293]
LEICA Suite	Leica Camera AG (Solms, Germany)

Office Suite 365	Microsoft (Redmond, WA, USA)

3.4. Oligonucleotides

All primers were designed using either the integrated tool of CLC Main Workbench v5, or VectorNTI v11. The oligonucleotides were purchased from Sigma Aldrich (Darmstadt, Germany). Refer to supplementary **tab. C.2** to **tab. C.1** for a complete list of used primers.

RNA oligonucleotides were ordered at MWG (Ebersberg, Germany). Sequences of hsa-miR-122-5p and -3p were acquired from miRBase. However, an additional 3' U was added based on the review of Jopling[188], which stated this sequence as the most abundant variant in hepatocytes. For the inactive mutant miR-122 A4U, the adenine at position 4 was changed to uracil, and the complementary exchange was performed on the 3p-strand. Duplexes were generated by mixing of 5p- and 3p-strand, 2 min denaturing at 95°C, and cooling to room temperature on the bench top.

3.5. Bacteria and Cell Lines

The bacterial strain used or plasmid amplification was *E. coli* DH5α from Invitrogen (Darmstadt, Germany). BL21 E. coli were used for IPTG inducible protein production. DH10Bac (Thermo Fischer Scientific, Waltham, MA, USA) were used for bacmid generation, to produce baculovirus.

Table 3.7.: Overview of used cell lines

Name	Type
HEK293T	Adherent human epithelial cell line, expresses SV40 large T-antigen
Hep3B	Human hepatoma cell line with HBV integrate, no miR-122 expression
HepG2	Human hepatoma cell line, no miR-122 expression
Huh7 "Lunet"	Human hepatoma cell line, HCV cured
Huh7.5	Human hepatoma cell line, highly permissive Huh7 subclone
Sf9	Insect cell line for baculovirus based protein production
BSRT7	Baby Hamster Kidney cell line, expressing T7 polymerase

4. Methods

4.1. Cloning

4.1.1. Polymerase Chain Reaction (PCR)

The PhusionFlash Master Mix (Thermo Fischer Scientific, Waltham, MA, USA) was used for PCR-based DNA amplification. $0.5\,\mu$M of the respective primers were mixed with up to $500\,$ng of template, and diluted with water to a final volume of $10\,\mu$l. Then, $10\,\mu$l of the master mix was added and the PCR was performed according to the manufacturer's instructions.

Deletions of sequences within a given template were generated via fusion PCR. This two-step method makes use of two primer pairs: one pair of "outer" primers was designed as usual at the very ends of the template with an incorporated restriction site, as desired. Two "inner" primers were placed directly 3' adjacent to the desired mutation site with a 5' complementary overhang of approximately $15\,$nt. With the corresponding inner and outer primers, two PCR fragments were generated with complementary sequences at the respective overlap region. Via these sequences, the amplification products of the first PCR were fused in a second step, using the outer primer pair.

4.1.2. Restriction of DNA Templates

For analytic purposes, $\approx$500$\,$ng of DNA were used in the reaction. 1u per μg of restriction enzyme (NEB, Ipswich, MA, USA) was used, and the mixture was incubated for 1 h at 37°C, or as indicated for specific enzymes. In case of plasmids to be used for ligation, 1 u of calf intestine phosphatase (NEB, Ipswich, MA, USA) was added after 30 min, and the mixture was incubated for another 25 - 30 min at 37°C. This step was performed to remove the 5'-phosphates from the cleavage sites, to counteract spontaneous re-ligation of the vector.

4.1.3. Agarose Gel Electrophoresis

Depending on the expected size of the DNA fragment, 1 to 2% agarose gels were prepared in TAE buffer (40 mM TRIS,1 mM EDTA, 40 mM acetic acid) with 10 μL of a 10 mg/ml ethidium bromide (EtBr) solution per 100 ml. The DNA was complemented with loading dye. The gel was run at 100 V for 25 to 45 min. 10 μL DNA ladder mix were loaded on at least one lane, to estimate the sizes of the analyzed fragments. UV-analysis was performed using the INTAS UV system (Intas Ge iX Imager, Ahmedabad, India), and images were printed for each gel.

4.1.4. Gelextraction

If gel electrophoresis was used to purify DNA fragments, bands of the desired size were excised with a clean scalpel on an UV transilluminator, at low energy UV light (λ=365 nm), to minimize double-strand breaks. The gel pieces were transferred to 1.5 ml reaction tubes, and the enclosed DNA was extracted with the column-based MN ExtractII kit (Macherey-Nagel, Düren, Germany), as instructed by the manufacturer.

4.1.5. Ligation

1 u of T4 DNA ligase (NEB, Ipswich, MA, USA) per 20 μL of rection mix was employed for ligation of DNA fragments with compatible ends. Usually, molar ratios of 1:5 to 1:3 (Vector:Insert) were used, to ensure a high insertion rate, whilst avoiding multiple insertions. For each reaction, approximately 100 ng of vector were used in order to achieve a satisfactory transformation rate, later in the process. The corresponding amount of insert was calculated by the following formula:

$$m_{insert}(ng) = \frac{m_{vector}(ng) \cdot l_{insert}(kbp) \cdot 5}{l_{vector}(kbp)}$$

Finally, the reaction was incubated for 2 h at room temperature, or alternatively over night at 16°C, and further on used for transformation of competent bacteria.

4.1.6. Transformation of Chemically Competent Bacteria

DH5α *E. coli* were thawed on ice, and 100 μL of the bacteria suspension were mixed with 10 μL ligation mix. After 10 min incubation on ice, the bacteria were transformed for 45 s at 42°C in a water bath, and cooled on ice. 900 μL of lysogeny broth (LB) medium

were added, and the culture was grown for 1 h at 37°C in a shaker incubator. For the amplification of a purified plasmid, the suspension was added to 4 ml of LB-Amp, and grown over night at 37°C in a shaker incubator. In case of a freshly ligated construct, the culture was collected for 3 min at 3,000 rpm, the pellet was taken up in 200 μL of LB and streaked on an LB agar plate, supplemented with ampicillin. Clones were picked with a sterile pipet tip after incubation at 37°C, 4 ml of LB-Amp were inoculated and grown at 37°C under agitation.

4.1.7. Transformation of Electrocompetent Bacteria

0.2 cm electroporation cuvettes were pre chilled on ice for 30 min before use. 1 ml LB medium was prepared per reaction in a reaction tube. 40 μl electrocompetent E. coli cells were then thawed on ice. Next, 1-3 μl of salt free DNA-solution was transferred into a pre-cooled eppendorf tube and mixed with 40 μl of bacteria, and transferred into the electroporation cuvette. The mixture was incubated for 1 min on ice. The pulse settings were set to 25 μF, 2.5 kV and 200 Ω. After electroporation, 1 ml of LB-Medium was added and the bacteria were transferred to a fresh eppendorf tube, incubated 20-60 min at 37°C and seeded on appropriate selective LB-Agar. The remaining cells were cryo-conserved by adding 15% glycerol and frozen at -20°C.

4.1.8. Isolation and Analysis of Plasmid DNA from Bacteria

Plasmid extraction was conducted using a column-based approach. Depending on the desired amount of isolated DNA, 4 ml up to 500 ml of transformed *E. coli* culture were used as input. For small-scale extractions the Miniprep kit was applied, larger volumes were processed with the Maxiprep kit (Macherey-Nagel, Dren, Germany). In both cases, the manufacturer's protocols were used. The obtained plasmids were subjected to analytical restriction, to estimate the success of the ligation. If the correct band pattern was produced, the samples were sequenced by the commercial service provider GATC, Freiburg.

4.1.9. Glycerol Stocks

For long term storage, transformed bacteria were grown in sterile LB medium, containing antibiotics, and collected by centrifugation. The pellet was resuspended in 500 μL LB medium and 500 μL sterile 86% glycerol. Then the cultures were stored at -80°C.

4.2. Cell Culture

The human HEK293T, HepG2, Huh7.5, Huh7 "'Lunet"', and Hep3B cell lines were used for the different applications. Under normal culturing conditions, all cell lines were grown in polysterene culture dishes (Falcon BD, Heidelberg, Germany), in Dulbecco's Modified Eagle Medium (DMEM), complemented with 10% FCS, 1% sodium pyruvate and 1% penicillin/streptavidin. The cells were grown to confluency in an incubator (37°C, 5% CO_2), and splitted as required. All cells were counted prior to transfection or electroporation, using a Neubauer chamber.

4.2.1. Transient Transfection of RNA and DNA

Electroporation of cells

Cells were trypsinized, washed and resuspended in cytomix (120 mM KCl, 0.15 mM $CaCl_2$, 10 mM K_2HPO_4/KH_2PO_4 (pH 7.6), 25 mM Hepes, 2 mM EGTA, 5 mM $MgCl_2$) including freshly added 2 mM ATP and 5 mM glutathione. The final concentration was $1.5 \cdot 10^7$ (for Hep3B or Huh7.5) or $1 \cdot 10^7$ (for Huh7) cells per ml. $6 \cdot 10^6$ cells were electroporated with 10 μg of replicon RNA. Depending on the experiment 50 pmol wild type or mutant miR-122 duplex RNA were added per 10 μg of electroporated RNA. As a control for short term translation assays, 5 μg of a capped Renilla transcript were also added. Cells were then seeded onto 6-well plates, incubated at 37°C, and subsequently lysed (1% Triton-X-100, 25 mM Gly-Gly, pH 7.8, 15 mM $MgSO_4$, 4 mM EGTA, 1 mM DTT added directly prior to use) and frozen at the desired time points. Luciferase activity of the lysates was measured in a tube luminometer.

Tranfection with Polyethylenimine

After trypsin treatment, $5 \cdot 10^5$ cells were plated in a 6-Well plate (Falcon BD, Heidelberg, Germany) either 24 h prior to transfection. The aspired confluency ranged between 60 and 80%. For transfection with polyethylimine (PEI, Polyplus Transfection SA, Illkirch-Graffenstaden, France), 1 μg of the expression vectors were taken up in 100 μL OPTIMEM medium and complemented with 10 μL PEI. The used cell numbers, DNA concentrations and reagent volumina for different well sizes were chosen according to the supplied protocol. After brief vortexing, the mixture was incubated 20 min at room temperature. The medium in the wells was changed to 2 ml serum-free OPTIMEM, to minimize cytotoxic effects. The tranfection mix was then added drop-wise, and the plate

was gently tilted for homogeneous distribution. The cells were then incubated (37°C, 5% CO_2) until harvest and analysis for gene expression.

Transfection with Lipofectamine2000

After trypsin treatment, cells were plated either 24 h to reach an aspired confluency ranged between 60 and 80% at the time of transfection. Depending on the scale of transfection the volume of Lipofectamine2000 (Thermo Fischer Scientific, Waltham, MA, USA), specified by the manufacturer's protocol was diluted in OPTIMEM in a reaction tube. In a separate tube, 5 µg of plasmid was added to the same volume of OPTIMEM. After 5 min incubation at room temperature, both solutions were mixed and incubated again for 20 min before addition to the cells. After 6 h the medium was changed, to prevent cytotoxic effects. The cells were then incubated (37°C, 5% CO_2) until harvest and analysis for gene expression.

Transfection with Effectene

After trypsin treatment, cells were plated either 24 h to reach an aspired confluency ranged between 60 and 80% at the time of transfection. The protocol was employed as described by the manufacturer. 5 µg of plasmid DNA was first mixed with Enhancer and transfection buffer for DNA condensation, and kept at room temperature for 25 minutes. Effectene Reagent (Qiagen, Hilden, Germany) was then added and the mixture was incubated for 10 minutes to allow Effectene:DNA complexes to form. The complexes were mixed with DMEM medium, and added directly to the cells. The cells were then incubated (37°C, 5% CO_2) until harvest and analysis for gene expression.

Transfection with MirusLT1

For pTM based protein expression in Huh7 Lunet, producing T7 polymerase, Mirus LT1 was used as transfection reagent. 6-Well plates were used and treated according to manfacturer's instructions. 24h post transfection cells were harvested and processed.

Transfection with CaPO$_4$

After trypsin treatment, HEK293T cells were plated either 24 h, or at least 4 h prior to transfection, to ensure proper settling. The aspired confluency ranged between 60 and 80%. 10-20 µg DNA were diluted in 450 µl sterile H_2O, and supplemented with 50 µl of 2.5 M $CaCl_2$. Then, 500 µl 2x HBS-Buffer (Thermo Fischer Scientific, Waltham,

MA, USA) were added and the mixture was incubated at room temperature for 20 min. The solution was added drop-wise to the cells. After 2 h the medium was screened for precipitates, indicating a successful transfection. The medium was changed 4 h post transfection. The cells were then incubated (37°C, 5% CO_2) until harvest of the supernatant for lentivirus transduction.

4.2.2. Generation of Lentiviruses and Stable Cell Lines

Retroviral plasmids were transfected with $CaPO_4$ into a HEK293T packaging cell line. The vectors for virion production were pMD.G2, which encodes for the surface protein (env), pCMVΔ31 for the replication machinery (gag/pol), and the pWPI construct containing the gene of interest, which carries a packaging signal. The used ratio of pCMVΔ31, pWPI and pMD.G2 was 3:3:1. After 4-6 h the medium was changed. The efficiency of transfection was evaluated by microscopic analysis of the precipitate formation in the medium. The supernatant of the cells containing the assembled lentivirus was collected after 48 and 72 h, filtered through a 0.45 μm syringe filter, and stored at -80°C until use. Target cells were seeded to a final density of 30-50% confluency at the time of transduction in a 12-Well plate. Over a period of two days, the recipient cells were treated three times with 0.5-1 ml of filtered supernatant from the producer cells. 6 h after the last transduction, the medium was changed and the selection compound was added. Untransduced cells were used as a control, to ensure the efficiency of selection.

4.3. Protein Production and Detection

4.3.1. Baculovirus-production for Expression of HCV Non-Structural Proteins in Sf9 Cells

For baculovirus production, the bac-to-bac protocol from Thermo Fischer Scientific (Waltham, MA, USA) was used. In brief, the NS3-5B expression cassette was cloned into the pFastBac-DualGFP vector, and amplified in DH5α E. coli. For recombination into the baculovirus bacmid, 1 ng of plasmid was transformed into DH10Bac E. coli and selected on LB agar plates containing kanamycin, gentamicin, tetracycline, Bluo-gal, and IPTG. White colonies were picked and transferred into a 3 ml liquid culture. The bacmid DNA was extracted, and the correct insert was determined by PCR. Empty bacmids would lead to a 300 bp product, while the correct insert should show a band at

9000 bp. The bacmid was transfected into Sf9 cells, using Cellfectin II (Thermo Fischer Scientific, Waltham, MA, USA) according to the manufacturer's instructions. The cells were incubated at 28°C and checked for GFP expression after 24 up to 72 h. At 72 h post transfection, the supernatant was clarified by filtration through a 0.2 *mu*m syringe filter, and stored at 4°C. Fresh Sf9 cells were inoculated with the virus stock, incubated at 28°C and checked regularly for GFP expression. The amount of produced HCV protein was determined by western blot.

4.3.2. Preparation of HCV Non-Structural Proteins Expressed in E. coli

E. coli BL21 were electroporated, as described above, with a pET-plasmid carrying the gene-of-interest and an ampicilin resistance gene. An agar plate was streaked with a seeding tool from a glycerol stock and single clones were picked to inoculate a 5 ml ampicilin starter culture. After over night growth, the culture was used to inoculate a 500 ml culture, which was grown to an OD_{600} of 0.6-0.7. Then the cultures were cooled to room temperature. For NS5A expression, 3% ethanol were added. After 20 min, the expression culture was induced with 0.1 mM IPTG (**fig. 4.1**) and incubated at 20°C. For NS3, the culture was pelleted after 4 h, for NS5A the incubation was carried out over night. After centrifugation, the pellets were kept on ice and resuspended in lysis
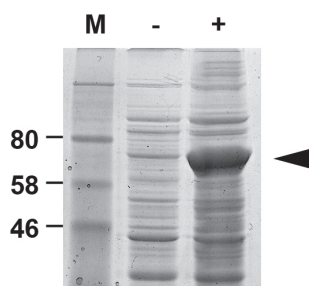
Figure 4.1.: IPTG induction control. SDS polyacrylamide gel stained with coomassie brilliant blue. The arrow head indicates the expected size for his-tagged NS3. Whole cell lysates were lysed in Laemmli buffer and loaded before (-) and after (+) over night induction with IPTG.

buffer containing lysozyme, benzonase and a protease inhibitor. The pH of the buffer was chosen based on the isoelectric point of the desired protein. Since the solubility is strongly decreased at that pH, the conditions were adapted to higher values, up to pH 8.8 with Tris/HCL.

After lysis for 30 min on ice, the suspension was sonicated 6 times for 30 s. Afterwards, the soluble and insoluble fraction were separated by centrifugation. The supernatant was filtered and transferred into a new falcon. It was then adjusted to 500 mM NaCl and 10 mM imidazole. After brief incubation at 4°C, 1 ml NiNTA slurry was added, followed

by another incubation at 4°C for 45 min. The beads were washed twice with buffer containing 50 mM imidazole, and then loaded onto a gravitational flow column. After another wash with 5 ml 50 mM imidazole, the stringency was increased to 75 mM or 100 mM imidazole for NS3 or NS5A, respectively. The protein was eluted in one fraction with 200 mM L-histidine. All samples were analyzed by SDS PAGE, to check for purity and quantity of the obtained protein.

4.3.3. Western Blot

For protein analysis, the cells were lysed by addition of Laemmli loading buffer (2% w/v SDS, 10% glycerol, 50 mM DTT, 0.01 w/v bromophenol blue). This was followed by denaturization at 95°C for 5 min. The proteins in the samples were then separated on a 10% SDS PAGE gel, and blottet onto a methanole activated PVDV membrane over 1.5 h at $2 \, \text{mA cm}^{-2}$, using the semi dry method. For this purpose, two filter papers, the membrane, the gel, and another two filter papers were soaked with semi dry blotting buffer (25 mM TRIS, 250 mM glycin, 0.1% SDS, pH 8.3), stacked, and placed onto the transfer system. Alternatively, wet blotting was performed with a current 350 mA for 1-2 h, or 100 mA over night at 4°C. In succession to the blotting process, the membrane was blocked with 5% low fat milk powder in PBS (MPBS) for 30 min. Then the primary antibody (1:1000 - 1:500 in MPBS+0.5% Tween20) was applied and incubated for at least 1h, at room temperature, or over night at 4°C, followed by 3 washes with PBS-T and addition of the second antibody (1:10000 in MTBS-T), coupled to horse radish peroxidase (HRP). The following 1 h incubation was carried out at room temperature. Finally, the blot was washed (2x PBS-T, 1x PBS) and chemiluminescence was measured in an Intas Ge iX Imager (Intas, Ahmedabad, India), after addition of the HRP substrate.

4.4. In Vitro Assays

4.4.1. Helicase Assay

The helicase activity of purified NS3 and NS3/4A was assessed in a DNA-based unwinding assay. A 54-mer, a 30-mer, and a capture oligonucleotide, complementary to the 30-mer, were purchased from Sigma-Aldrich (Darmstadt, Germany, **tab. 4.1**). The 30-mer was radiolabeled with T4 PNK (NEB) in the supplied buffer, using $10 \, \mu\text{Ci} \, \gamma\text{-}^{32}\text{P-}$ATP per pmol substrate. The excess nucleotides were removed by trap filtration in an

Illustra MicroSpin G25 column (GE Healthcare). An equimolar amount of the 54-mer was added, and the mixture was heated to 95°C and slowly cooled to room temperature to anneal the oligos. 0.8 pmol of each enzyme used in the following reaction were

Table 4.1.: Oligonucleotides used for helicase assay.

Name	Sequence
54-mer	GACTACGTAC TG*TTAACCGC CGCCCAGGTG TGAGGAGTAC CAGGCCA*GAT CTGC
30-mer	TGGTACTCCT CACACCTGGG CGGCGGTTAA
capture	TTAACCGCCG CCCAGGTGTG AGGAGTACCA

preincubated 5 min at room temperature. After addition of H_2O, 10x unwinding buffer and the labeled dsDNA, the proteins were allowed to form active complexes at 37°C for additional 5 min. Then, the capture oligo was added in 30-fold excess, to prevent reannealing. After taking a sample (no ATP, 0 min), 5 mM ATP were added to start the reaction. Samples were prepared for 1, 5, 10, 20, and 30 min reaction time. After the denoted period, the helicase activity was abolished by addition of 1 reaction volume stop solution (20 mM EDTA, 0.5% SDS). 10 μL of glycerol loading dye were added to each 20 μL of sample. As positive control, 0.1 pmol labeled dsDNA in unwinding buffer were denatured at 95°C in the presence of 3 pmol capture oligo. All samples were stored at -20°C. 15 μL of each sample were loaded onto a 12% native PA gel, and run at 3-4 V·cm^{-1}. The bands were visualized on a phosphoimager (BioRad, Hercules, CA, USA), and the quantitation analysis was performed with the provided QuantityOne software (BioRad, Hercules, CA, USA).

4.4.2. RdRP assay

First, 2.5 μL RdRP buffer (20 mM Tris pH7, 25 mM KCl, 1 mM EDTA, 1 mM DTT + 12.5 mM MgCl2), 0.25 μL 100mM DTT, 0.5 μL RNAsin and 9 μL RNAse-free H_2O were mixed on ice ("RdRP Mix"). In a seperate tube, the NTP mix was prepared, containing 2.5 μL 10x cold rNTPs (10mM GTP/ATP/UTP, 100 μM CTP), and 1 μL $\alpha-^{32}$P-CTP (1 μl = 10 μCi). The proteins were preincubated with the RdRP Mix for 15 min at RT. Meanwhile, the RNA was denatured for 2 min at 95°C, then flash-cooled for 2 min on ice. The RNA was then added to the RdRP Mix and incubated at 37°C for 5 min. The polymerization reaction was started by addition of the NTP mix, and incubated at the

desired temperature for 1 h. The reaction was terminated with 1 mM aurintricarboxylic acid in 1x TE buffer.

For the scintillation counter-based assay, the reaction was precipitated in 1 ml 5% TCA, and incubated on ice for 30 min. The mixture was filtered through a 10 mm round Whatman filter on a vacuum device.The precipitated oligonucleotides were retained in the filter, while unincorporated nucleotides were removed by 5 washes with 0.1%TCA solution. The filter was then transferred into a scintillation tube and covered with Ultima Gold scintillation reagent (PerkinElmer, Waltham, MA, USA). The counts per minute were detected in a Beckman LS 6000 Liquid Scintillation Counter (Beckmann Coulter, Brea, California, USA). An empty filter was used as negative control.

For the gel based assay, the RNA was subsequently isolated by phenol:chloroform extraction and isopropanol precipitation. The resulting pellet was dissolved in 10 μL formamide loading dye and denatured for 5 min at 65C. 5 μL were loaded on a preheated 6% polyacrylamide gel, containing 8 M urea. The gel was run at 20 W for 2 h, fixed in 10% methanol/acetic acid and dried. The produced RNA products were detected by autoradiography using phosphor screens. The bands were visualized on a PMI phosphoimager (BioRad, Hercules, CA, USA) and the quantitation analysis was performed with the provided QuantityOne software (BioRad, Hercules, CA, USA).

4.5. RNA Synthesis, In Vitro Transcription and Structure Determination

4.5.1. In Vitro transcription

In vitro transcripts for electroporation were generated from 10 μg pFK-plasmid in IVT buffer with 16 mM $MgCl_2$, 4 mM rNTPs, 1.7 μg BSA (NEB) and 10 μl of homemade T7 polymerase. The reactions were performed 4 h or over night at 37°C. The RNA was purified by phenol:chloroform extraction and isopropanol precipitation. RNA integrity was assessed by agarose gel electrophoresis. For capped transcripts, m7G analog (Sigma Aldrich, Darmstadt, Germany) was added to a final concentration of 20 mM.

4.5.2. In Silico RNA Structure Calculation

For in silico folding of the 5 terminal 120 nt of HCV, the online versions of mfold, RNAFold and RNAalifold were used without constraints. For RNAalifold analysis, 3

full-length sequences of each genotype were obtained from HCVdb.org. Visualization was performed with VARNA.

4.5.3. Gel Purification of RNA

RNA of the 5'UTR fragments was *in vitro* transcribed and purified, as described above. Approximately 20 - 30 μg were loaded on a 5% Urea gel (20x20 cm), and run for 1 h at 20 W. Bands were visualized by UV shadowing and extracted with an RNAse-free spatula. The gel piece was crushed using a scalpel and transferred into a clean eppendorf tube. Then, 500 μl of extraction buffer was added and the RNA was eluted for 48 h at 4°C on a rotator. The supernatant was transferred into a new tube, the remaining gel was rinsed with another 250 μl of buffer, and the supernatant was pooled with the previously collected sample. RNA was extracted by phenol:chloroform, and precipitated with isopropanol at -20°C. After two EtOH washes, the pellet was resuspended in deionized water.

4.5.4. SHAPE

SHAPE assays and synthesis of NAI were performed as reported by Spitale et al.[294], with minor modifications. Briefly, *in vitro* transcripts were denatured at 95°C, and refolded in presence of miR-122-5p or -3p at 37°C for 15 min. Different $MgCl_2$ concentrations (0, 1 and 6.6 mM) were tested. NAI or DMSO were added and incubated for another 10 min, before phenol:chloroform extraction. Purified RNA was subjected to reverse transcription (RT) with a ^{32}P-labeled primer, and the cDNA was analyzed on a urea PAA gel, followed by autoradiography using phosphor screens. The bands were visualized on a phosphoimager (BioRad, Hercules, CA, USA) and subsequently assigned and quantified with SAFA[293].

4.5.5. NMR

RNA fragments were produced by *in vitro* transcription, as described before. For NMR sample preparation, 50 – 100 μg of linearized template was used per ml of reaction, in a total volume of up to 10 ml. The RNA was diluted in 5 volumes 8 M urea. The resuspended RNA was purified by FPLC, and dialyzed against water for 24 h, to remove salts. The water was exchanged five times during the course of dialysis. Salt-free samples were subjected to lyophilization. The lyophilized RNA was resuspended in RNAse free

H_2O at a concentration of $2\,mg/ml$, and denatured at 95°C before flash-cooling on ice. The transcript was concentrated to around $1\,mM$ in $75\,\mu l$ using Amicon centrifugation concentrators (Merck Millipore, Darmstadt, Germany). After concentration, an equal amount of 2x folding buffer ($20\,mM$ HEPES, $200\,mM$ NaCl, $10\,mM$ $MgCl_2$) was added and the samples were transferred to $3\,mm$ Shigemi tubes (Shigemi Inc, Allison Park, PA, USA). The samples were incubated for 15 minutes at 37°C, before measurement in an 850 or 950 MHz Bruker spectrometer (Billerica, MA, USA) at the desired temperature. 1D and 2D NMR spectra were visualized and evaluated with Bruker Topspin software.

4.6. Direct and indirect detection of HCV RNA

4.6.1. HCV RNA detection by qRT-PCR

For first-strand cDNA synthesis, $10\,\mu M$ gene specific primers, and dNTPs were added to $1\,\mu g$ of total RNA, and filled up to $10\,\mu L$ with DEPC treated H_2O (**tab. 4.2**). This mixture was incubated for 5 min at 65°C and then chilled on ice for at least 2 min, before adding $10\,\mu L$ the reverse transcriptase mix (**tab. 4.3**). To start the reaction, the

Table 4.2.: Composition of the RNA mix for first-strand cDNA synthesis

Component	Amount
RNA ($1\,\mu g/\mu L$)	$1\,\mu L$
Primer	$1\,\mu L$
dNTPs ($10\,\mu M$)	$1\,\mu L$
H_2O	to $10\,\mu L$

Table 4.3.: Composition of the RT mix for first-strand cDNA synthesis

Component	Amount
RT buffer	$2\,\mu L$
$MgCl_2$ (25 mM)	$4\,\mu L$
DTT (0.1 M)	$2\,\mu L$
RNAseOUT	60 u
SuperScript III	200 u

sample was placed into a thermo cycler. The following program was applied:
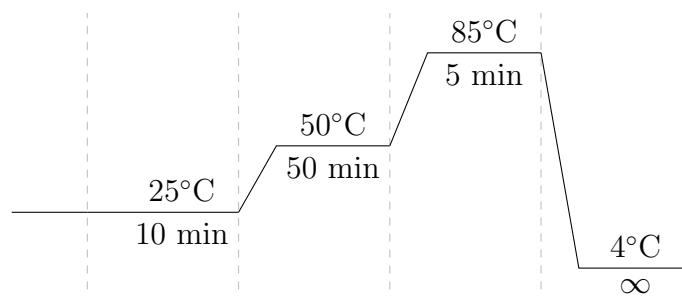
Comparative quantification of DNA was performed with quantitative PCR (qPCR), using SYBRGreen. The obtained data is presented in cycle threshold (CT) values. This unit defines the first cycle the specific fluorescence signal is above background level. Comparison in abundance of two or more templates is only possible, if they are amplified at the same rate, and no side products are made. cDNA of template-negative cells, and H_2O controls were employed to detect unspecific priming, or contaminations, respectively. 40 cycles withe the following PCR program were performed:
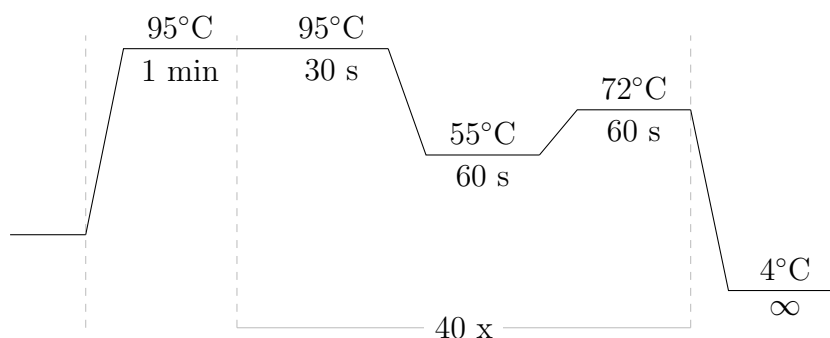
To compare the relative expression of different mRNAs, the $\Delta\Delta C_T$-method was used, with human GAPDH mRNA as calibrator (set to 1). Then, the difference between the C_T values of the control and miRNA of interest was used to calculate the relative amounts in different cell lines.

At the end of each run, a melting curve analysis was performed, to detect possible side products or primer dimers. Upon denaturing of the DNA dimers, the complex with the dye is destroyed, and the fluorescence signal disappears. The decrease of fluorescence is plottet against the temperature. Therefore, for a single product, only one sharp peak should be visible. More peaks would indicate additional products of different length.

4.6.2. HCV RNA detection by Northern blot

$6\cdot10^6$ electroporated cells were immediately put on ice, spun down and resuspended in cold PBS with $5\,\text{mM}$ aurintricarboxylic acid (PBS-ATA) as input control ($0\,\text{h}$). For later time points, $6\cdot10^6$ (1-$24\,\text{h}$) or $3\cdot10^6$ (48-$72\,\text{h}$) were seeded on a $10\,\text{cm}$ dish, and incubated at $37°\text{C}$ for the desired time. a fraction of cells At later time points, cells were scraped into put on ice immediately, spun down and resuspended in cold PBS-ATA.

Cells were lysed with $750\,\mu\text{l}$ of GITC solution. Genomic DNA was sheared by pipetting. Then, 1/10 volume $2\,\text{M}$ NaAc (pH 4.5) and 1 volume acidic phenol were added. After addition of 1/5 volume chloroform, the mixture was vortexed and incubated on ice

for 15 min. The phases of the milky solution were separated again by 10 min centrifugation at 13,000 rpm, 4°C, and the RNA-containing upper phase was transferred into a new tube, avoiding carry-over from the interphase. Now the RNA was precipitated by addition of 1 volume isopropanol. After 30 min incubation at -20°C, the RNA was pelleted by centrifugation for 15 min at 14,000rpm, 4°C. Finally, the pellet was washed once with 70% ethanol, and dissolved in an appropriate volume of water. The RNA was quantified by NanoDrop (Thermo Fischer Scientific, Waltham, MA, USA) measurement, and stored at -70°C. Denaturing glyoxal agarose gel electrophoresis was performed for Northern blot analysis. 1-1.5% agarose (depending on the size of the RNA) was dissolved in H_2O, then $NaPO_4$ pH 7.0 to final concentration of 10 mM was added. During sample preparation, up to $10\,\mu g$ RNA in a volume of $10\,\mu l$ were mixed with $4.1\,\mu l$ 100 mM $NaPO_4$ pH 7.0, $6\,\mu l$ 6M deionized glyoxal, and $20.5\,\mu l$ DMSO, incubated at 50°C for 1 h, cooled on ice, and mixed with $10.9\,\mu l$ glyoxal loading buffer. $25\,\mu l$ of the sample were loaded onto the gel. Electrophoresis was performed in 10 mM $NaPO_4$ pH 7.0 at $4\,V/cm$ gel. To keep the pH constant, the buffer was constantly mixed by magnetic stir bars after the sample had migrated into the gel.

RNA was transferred to positively charged nylon membranes (Hybond-N+; Amersham Biosciences, Freiburg, Germany) with 50 mM NaOH (0.2 bar under pressure for 1h, vacuum transfer machine (Keutz, Giessen, Germany) and cross-linked by UV-irradiation. To block unspecific binding of the probe to the membrane, it was incubated for 15 min at 68°C in 10 ml hybridization solution containing $100\,\mu g$ heat denatured salmon sperm DNA. Positive-strand HCV RNA was detected by hybridization with $\alpha-^{32}$P-labeled negative sense riboprobe complementary to nt 5979 to 6699 of the HCV JFH-1 isolate in hybridization solution at 68°C ON. Hybridization with a β-Actin-specific riboprobe was used to monitor equal sample loading in each lane of the gel. Membranes were washed twice with 2x SSC/0.1% SDS for 15 min at 68°C, and then washed three times with 0.2x SSC/0.1% SDS for 15 min at 68°C, briefly dried and signals were detected by autoradiography. As standards for the positive-strand RNA defined quantities (10^9, 10^8, and 10^7 RNA molecules per $25\,\mu l$) of the corresponding *in vitro* transcripts were used.

4.6.3. Strand-specific HCV RNA detection by in situ hybridization

The QuantiGene ViewRNA ISH Cell Assay Kit (Affymetrix, Santa Clara, CA, USA; Cat. No. QVC 001) was used for *in situ* hybridization. Cells were fixed with 4% PFA, rinsed with PBS and then permeabilized with 70% EtOH at 4°C for 1 h. After washing

with PBS, the supplied QS protease was applied for 5 min at RT in a 1:4000 dilution. Then the cells were rinsed and 1:100 probe set (in Probe Set Diluent QF prewarmed to 40°C) was added for 3 h at 40°C. Excess probes were removed with the supplied Wash Buffer. Next, cells were incubated with PreAmplifier Mix (PreAmplifier Mix 1:25 in pre-warmed Amplifier Diluent QF) for 30 min at 40°C. After thorough washes with Wash Buffer, the Amplifier Mix Solution (Amplifier Mix 1:25 in pre-warmed Amplifier Diluent QF) was applied for 30 min at 40°C. After another wash with Wash Buffer, the final Label Probe Mix Solution (Label Probe Mix 1:25 in pre-warmed Label Probe Diluent QF) was added for 30 min at 40°C. Then the cells were washed with PBS and subjected to immunofluorescence staining as described below.

4.7. Immunofluorescence Assay

Cells were grown on a cover slip, placed into each well of a multi-well plate, and transfected the following day. 24 h post transfection, the cells were washed twice with PBS. Afterwards, they were fixated with 4% para-formaldehyde (PFA) for 15 min, and washed again. To disrupt the plasma membrane, and allow intracellular immunostaining, the cells were treated with Triton X-100 for 5 min. Then, 10 min blocking with 3 mg/ml BSA in PBS, were followed by 1-2 h incubation with primary antibody (1:100 in PBS+3 mg/ml BSA). 50 μL of antibody solution were pipetted on a piece of parafilm, and the cover slip was placed on the droplet. Subsequently, the slides were washed and blocked again, and exposed to the secondary, labeled antibody (1:1000), for another hour in the dark. Finally, glass slides were prepared with a drop of DAPI-solution, and the cover slip was gently placed on top. The cover slips were fixed with fluoromount (Sigma Aldrich, Darmstadt, Germany), and the slides stored at 4°C in the dark until use.

4.7.1. Luciferase Assay

For assaying the *firefly* luciferase activity from reporter replicons, cells were washed once with PBS, lysed directly on the plate in ice cold lysis buffer (350 μl/6-well) and frozen. Upon thawing, lysates were resuspended by pipetting and 100 μl were mixed in a measuring tube with 360 μl of assay buffer (with freshly added 1 mM DTT and 20 mM ATP). After the addition of 200 μl of a 200 μM luciferin solution in 25 mM Gly-Gly, the luciferase activity was measured in a tube luminometer (Lumat LB9507; Berthold, Freiburg, Germany) for 20 s. All luciferase assays were done in duplicate measurements.

For *renilla* measurements, 20 μl of lysate were mixed with 100 μl assay buffer without ATP/DTT, but supplemented with 1,43 μM coelenterazine (Promega, Mannheim, Germany), and measured for 10 s.

Dual-luciferase assays from the same tube were performed with 40 mul of lysate. Firefly activity was recorded after mixing with 100 μl assay buffer with ATP/DTT, and 70 μl/ml of 1 M luciferin stock solution. Luminiscence was measured for 10 s. Then, *renilla* quencing buffer was added and the sample was measured again for 10 s, after a delay of 60 s, to allow sufficient quenching of the *firefly* activity.

4.8. Detection of miRNA by RT-PCR

4.8.1. Stem-loop qRT-PCR

This method for the amplification of small RNAs was first described by Chen et al.[295]. The main advantages of this approach is the generation of qPCR compatible products even from a small pool of RNA. The procedure is based on primers of about 60 nt in length, with a stem-loop structure. Primer design was performed with the online tool "miRNA Primer Designer" (http://www.leonxie.com/miRNAprimerDesigner.php), and a reference miRNA gene (miR-23b) was selected based on the results of Lamba et al.[296]. Six nucleotides at the 3' end confer specificity for a mature miRNA, the rest of the primer is kept constant. First a mix of multiple stem-loop primers, adjusted to 10 μM each, dNTPs and H_2O (primer mix, **tab. 4.4**) were incubated at 65°C for 5 min. After chlling on ice, the RT mix (**tab. 4.5**) was added, to a final volume of 19 μL. At last, 1 μg of RNA was added. In contrast to a conventional RT-PCR, a pulsed RT program

Table 4.4.: Composition of the primer mix for stem-loop cDNA synthesis

Component	Amount
dNTPs (10 μM)	1 μL
Stem-loop Primer Mix	1 μL
H_2O	11.25 μL

Table 4.5.: Composition of the RT mix for stem-loop cDNA synthesis

Component	Amount
Buffer	4 μL
DTT (0.1 M)	1 μL
RNAsin (40U/μL)	0.5 μL
SuperScript III (200U/μL)	0.25 μL
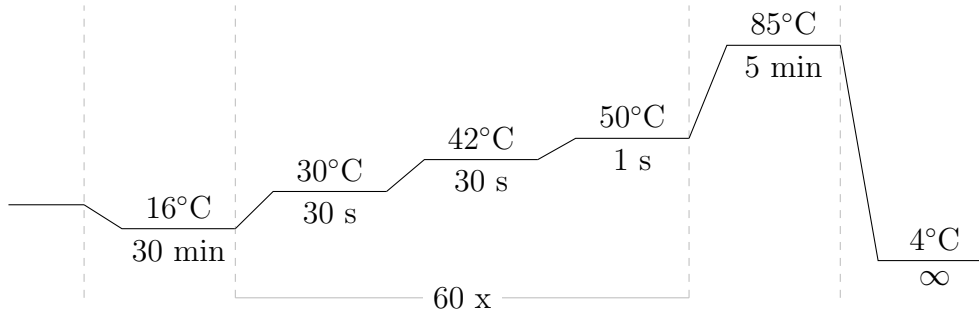
was used.

Comparative quantification of DNA was performed with quantitative PCR as described before. To compare the relative expression of different miRNAs, the $\Delta\Delta C_T$-method was used, with human miR-23b as calibrator (set to 1). As for the conventional qPCR, at the end of each run, a melting curve was produced, to detect possible side products or primer dimers.

4.9. Pull-Down Assays

4.9.1. Immunoprecipitation

Cells were washed twice with PBS and scraped in 1 ml sterile PBS. 10% were spun down, resuspended in $50\,\mu$l Laemmli buffer, and used as input. After centrifugation (10 min at 8000g, 4°C), the supernatant was discarded, and the pellet was resuspended in 1 ml lysis buffer, followed by incubation on ice for 15 min. To aid lysis, the suspension was vortexed briefly and pipetted up and dwn with a $100\,\mu$l pipette. Then, the cell debris and nuclei were removed by a centrifugation at 10000 g for 10 min. The lysate was transferred into a fresh tube and 2-8 mul of antibody was added, then incubated under rotation for 2 h at 4°C. In the meantime, $10\,\mu$l Protein G-coated beads were washed with 1 ml lysis buffer (1 min at 3000g, 4°C). The buffer was removed before lysate was added, and mixed with the beads by pipetting. Then, the mixture was incubated over night at 4°C under rotation. The next day, beads were washed three times with lysis buffer, and the protein was eluted by boiling for 10 min in $50\,\mu$l of Laemmli buffer. Beads were spun down and the supernatant was transferred to a fresh tube carefully to avoid carry-over of beads. The samples were then analyzed by western blotting.

4.9.2. Biotin-miRNA Pull-down

Pull-down of a biotinylated miRNA was performed, based on the protocol of Wani and Cloonan[297]. In brief, 200 pmoles biotin tagged miRNA were electroporated together with 10 μg of an HCV replicon. Two electroporations were pooled on a 15cm dish and incubated at 37°C for 72h. On the day of harvest, streptavidin-coated magnetic dynabeads were washed (Wash buffer: 5 mM Tris-Cl pH 7.5, 0.5 mM EDTA, 1M NaCl), NaOH treated (Solution A: 0.1 M NaOH, 0.05 M NaCl followed by Solution B: 0.1M NaCl) to remove RNAses, and blocked with 1 mg/ml BSA and tRNA in sterile H_2O at room temperature for 2h on a rotating mixer. The cells were scraped and washed twice with cold, sterile PBS. The pellet was resuspended in 300 μl lysis buffer (10 mM KCl, 1.5 mM $MgCl_2$, 10 mM Tris-HCl pH 7.5, 5 mM DTT, 0.5% NP-40) containing 1x complete protease inhibitor and 40 U/mlRNAsin. The suspension was frozen at -20°C and thawed at room temperature to increase lysis efficiency. The lysate was cleared by centrifugation at 4∘C, and the supernatant was transferred to a new tube. NaCl was added to a final concentration of 1 M. The blocked beads were washed three times with bead wash buffer, and the lysate was then added. The mixture was incubated at room temperature for 30 min under rotation. Afterwards the beads were washed three times (10 mM KCl, 1.5 mM MgCl2, 10 mM Tris-Cl pH 7.5, 5 mM DTT, 0.5% NP-40, 40 U/ml RNAsin ,1x Complete Mini protease inhibitor, 1 M NaCl) and then resuspended in 1 ml TRIZOL reagent. Protein and RNA were extracted following the manufacturers instructions.

4.9.3. Electrophoretic Mobility Shift Assay

The RNA of interest was dephosphorylated (CIP) and 5' end labeled with $\gamma-^{32}P$ using T4 PNK. Then the labeled RNA was incubated with purified protein under suitable binding conditions The 25 μl reaction mix contained 1x Binding buffer, RNA (50,000 cpm) and the purified protein (serial dilutions from excess to less than equimolar). The mixture was incubated for 30 min at 37°C. After incubation, 5 μl EMSA loading dye was added. 5 μl of the the sample was loaded onto a 5% native polyacrylamide gel. The rest was frozen at -20°C.

5. Results

5.1. Purification of HCV Replicase Components

The first aim of this study was to determine potential roles of NS3 and NS5A in the initiation of HCV RNA synthesis. Prior to determining the roles of different non-structural proteins in HCV replication, it was necessary to establish a robust and reliable assay to address the contribution of each protein alone. This can only be achieved *in vitro*, since the cell culture system inheres a high degree of complexity, in which a variety of host factors can significantly influence the outcome of an experiment. Hence, a highly reduced and controlled model system is better suited to identify the individual functions of a single viral protein, as well as functions which rely on the action of cellular co-factors. Additionally, requirements of the RNA template can be addressed more easily. The 3' terminal 450 nucleotides, including the 5B-CRE structure of the JFH-1 positive strand RNA was used as a basic template. The RNA templates were generated by in vitro transcription. An authentic 3' end is essential for the replicase assay, because it represents the natural initiation site for NS5B. Therefore, the transcripts were either generated on a PCR-based template, or using a plasmid (pFKT7-JFH-1-3') with a suitable restriction site at the end of the template. It has been determined that the ideal template consists of a short single stranded 3' end, followed by a stem-loop structure. Such an architecture is present at the 3' (-) terminus, which is also readily recognized by NS5B *in vitro* (**fig. 5.1**A). In contrast, the (+)-strand is a poor template for terminal initiation of the polymerase, due to its extensive secondary structure. However, the helicase activity of NS3, or a yet to be determined mechanism involving NS5A, might facilitate efficient replication. Especially for the helicase this hypothesis is conceivable, since it could convert the hairpin into a single stranded region, more suitable for NS5B initiation (**fig. 5.1**B). To study the viral replicase *in vitro*, first, a sufficient amount of protein must be produced and purified. Two strategies were employed to produce proteins for reconstitution of the functional replicase. Either the *in cis* expression of all proteins in an eukaryotic system, which relies on the natural cleavage of the polyprotein.

This strategy would more closely resemble the natural context of HCV infection, in a sense that the proteins will undergo most stages of maturation and post-translational modification. However, due to the large size of the complete ORF and transfection efficiency, the amount of produced protein might be limiting. Alternatively, the individual production of each protein in bacteria was pursued. While especially the natural phosphorylation pattern of NS5A will likely not be obtained in this system, it has the advantage of being relatively easy and suitable for large scale protein production (**fig. 5.1**C).
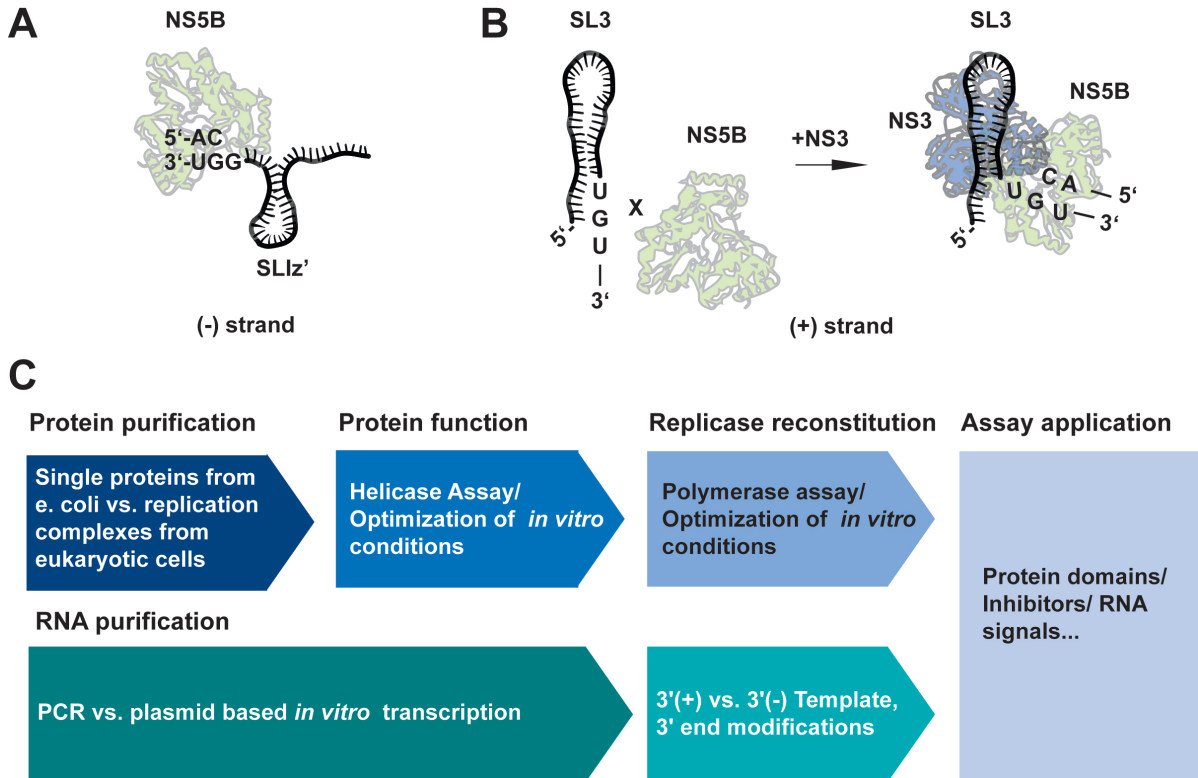
Figure 5.1.: Working hypothesis and establishment of an *in vitro* RdRP assay. A | Initiation of NS5B is highly efficient at the single stranded 3' end of the (-)-strand of the HCV genome. **B |** The hairpin structure at the 3' end of the (+)-strand of HCV prevents the viral polymerase to initiate RNA replication. Thus, the helicase activity of NS3 might be required to unwind the stem, and thereby create a suitable template for NS5B. **C |** To establish an *in vitro* replicase assay, the non-structural proteins NS3, 5A and 5B were purified via different methods. The optimal conditions for the helicase function of NS3 was tested. In parallel, the production of RNA template was optimized. Finally, the template-dependent impact of NS3 and 5A on RdRP function was assessed. In the future, this assay could be used to investigate the roles of individual protein domains or chemical compounds *in vitro*.

5.1.1. Tagging of NS proteins and Determination of their Replication Fitness

To effectively extract complete replicase complexes, common tag has to be introduced into the non-structural proteins 3-5B. Ideally, the tagged proteins should support replication in cell culture, since this would verify that all individual components are functional, and a possible failure to replicate *in vitro* is not due to aberrant folding or impairment of protein function. On the other hand, the functionality in the cell culture system is not necessarily a predictor for the *in vitro* situation. Deletion of the membrane anchor of NS5B for instance, abolishes replication in cell culture, but even enhances *in vitro* RNA polymerization. The positions for the tags were in part based on a publication that investigated how viral replication was affected by 15,nt long insertions at random sites in the open reading frame[298]. For NS3, a tag can be added at the 5' terminus, without significantly impairing the proteins function in replication (**fig. 5.2**A). A site in 4B was already described to tolerate a tag insertion, given an additional compensatory mutation[49], and was not tested here. Domain 3 of the NS5A protein is completely dispensable for replication, and thus easy to modify (**fig. 5.2**B). NS5B proved to be the most difficult protein to tag, without abrogating replication. According to the study of Arumugaswami et al.[298] and considering structural properties and accessibility (ideally an unstructured loop at the surface) several positions were tested. Insertions were introduced after amino acid 42 (1), 246 (2), 248 (3), 264 (4) and 326 (5). In another approach, the tag was inserted directly after the C-terminal linker region (post-linker, PL), however, also this strategy could not produce a viable construct (**fig. 5.2**C). For the latter position, also a FLAG and an HA-tag were introduced, but neither of these supported efficient replication. Only one mutant, 4, exhibited low levels of replication after 72 h, with raw values at around 10-fold over background (**fig. 5.2**C). It remains to be evaluated, whether a different tag could improve the replication behavior. Additionally, selection experiments could be conducted, in which the negative effects of the tag might be compensated by mutations acquired during serial passaging. However, due to the low replication efficiency of the tagged NS5B variants and the necessity to combine all tags into a single replicon, which would further dampen efficiency of the system, different methods of ectopic polyprotein production were explored.
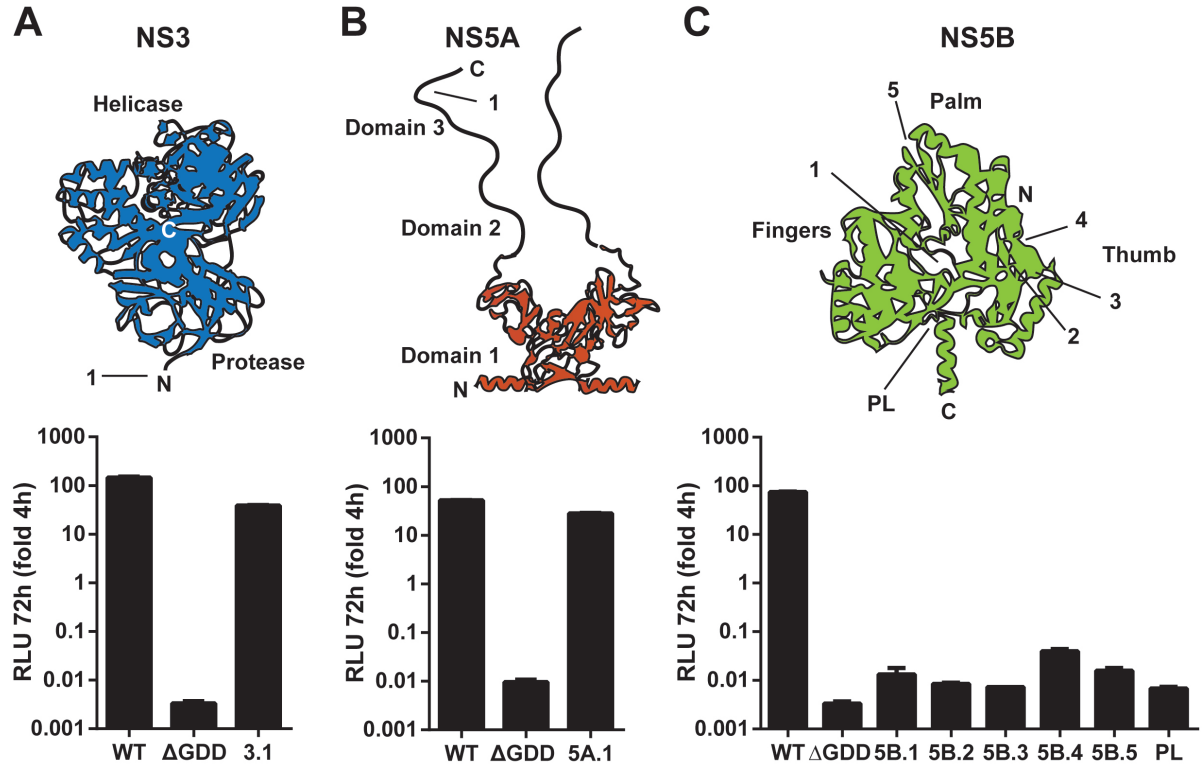
Figure 5.2.: Replication capacity of hexa-histidine tagged JFH-1 replicons. Upper panels: schematic structure of the HCV NS proteins NS3 helicase, **A |** ; NS5A **B |** and NS5B **C |**. Numbers indicate the his-tag insertion site(s). Lower panels: impact of His-tag insertion on replication efficiency of a subgenomic luciferase replicon with His-tag insertion, compared to a wt-replicon (WT) and a replication deficient mutant (ΔGDD). Replication efficiency is expressed in relative light units (RLU) in cell lysates of Huh-7 cells 72 h after transfection, relative to 4 h, to normalize for transfection efficiency.

5.1.2. Expression of the Complete Replicase Open Reading Frame in Eukaryotic Cells

The most natural condition to express the proteins of the replicase machinery is in a context encompassing NS3-5B, which are necessary and sufficient to support RNA replication. This can only be achieved in eukaryotic cells, since the open reading frame is too large for efficient expression in bacteria. Apart from this, the eukaryotic system offers several additional advantages. The two most important are the *in cis* processing, which might significantly affect protein folding kinetics, and secondly, post-translational modification, which relies on host factors not present in prokaryotes. Two different strategies were tested to achieve high protein yields: Firstly, a mammalian cell line (BSRT7) expressing T7 polymerase was used in conjunction with a T7 promoter bearing plasmid. Secondly, the expression with a baculovirus system in insect cells (Sf9). Several trans-
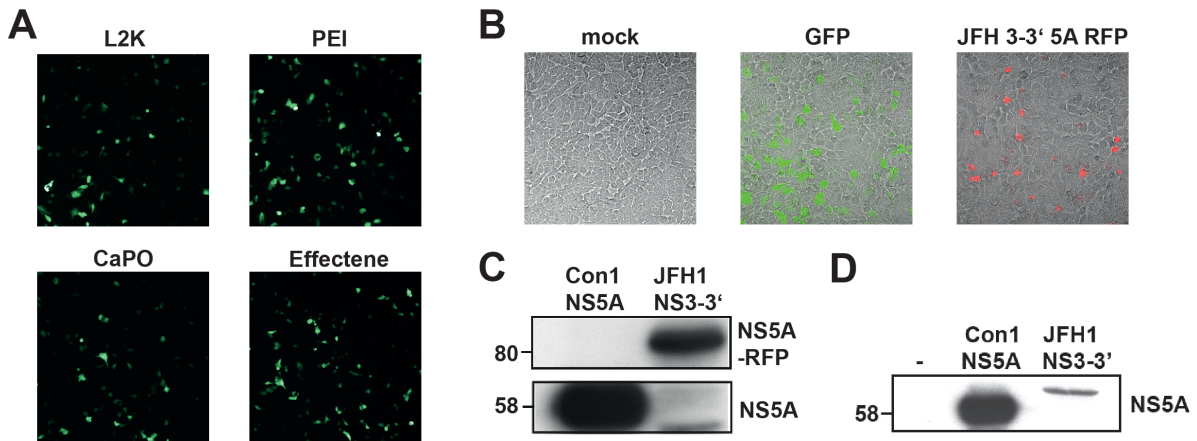
Figure 5.3.: Non-structural protein expression in BSRT7 and Sf9 cells. A | Evaluation of different transfection methods for BSRT7 cells using a GFP reporter plasmid. Shown is the GFP expression 24 h post transfection. PEI transfection was the most efficient in BSRT7 cells. **B |** Expression of HCV NS3-5B, harboring an RFP within domain 3 of NS5A. The expression of the RFP reporter was around 50% of the GFP control. **C |** Western blot analysis of NS5A expression in BSRT7 cells. A plasmid encoding the NS3-5B polyprotein from isolate JFH-1 under transcriptional control of the T7-promoter was transfected into BSR-T7 cells. Con1 NS5A expressed in Sf9 cells was used as a control. Lysates corresponding to equal cell numbers were loaded per lane. **D |** Expression of NS5A in Sf9 cells infected with baculoviruses carrying the coding sequence for JFH NS3-5B. Naïve Sf9 cells served as negative control. The same Con1 NS5A expressing Sf9 cell line as in **C** was used as positive control.

fection methods were compared for their effectiveness in BSRT7 cells. PEI was found to be the most efficient reagent, with approximately 50% of cells expressing GFP from a transfected reporter plasmid (**fig. 5.3**A). However, the much larger plasmid encoding

the viral proteins, including an RFP within NS5A, could not be delivered to the cells with the same efficiency. In addition, the expression levels were much lower compared to control Sf9 cells expressing Con1 NS3-5A (**fig. 5.3**B, C). The transfection of baculoviral vectors, containing the replicase cassette and GFP as separate cistrons, and subsequent inoculation of Sf9 cells only yielded very few GFP expressing cells (not shown). Western blotting confirmed that only minute amounts of viral protein were produced (**fig. 5.3**D). The expression in neither of these systems could produce sufficient amounts of protein for the desired purpose. Therefore, this approach was not further pursued, and no efforts were put into purification of replicase proteins using these expression models. Instead, the strategy was revised, and the proteins of interest were expressed individually in E. coli.

5.1.3. Expression of Single Proteins in E. coli

The proteins NS3, 5A and 5B were produced in bacteria. NS4B is assumed to be mainly responsible for membranous web formation, and not RNA replication itself. Therefore, it should not exert any function in an *in vitro* assay, and was not purified. Since all proteins of the HCV replicase complex are either integral membrane proteins, or at least tightly associated with lipids, the purification strategy was optimized to ensure maximum yield and purity. Efficient protocols exist for bacterial production of a version of NS5B, lacking the C-terminal 21 amino acids (NS5BΔC21), which has been shown to be much more soluble. Also, this truncated variant is more active *in vitro*, than the full length enzyme. NS3, 5A and the full-length 5B, however, are more complex to isolate in a soluble form. NS5A and full-length NS5B aggregate easily upon over-expression in bacteria. To aid correct folding 3% EtOH were added to the culture medium before induction, and expression was found to be best in an over night culture at 18°C. To increase solubilization and prevent aggregates in the lysis buffer, the pH was adjusted according to the theoretical pI of the individual proteins based on their amino acid sequence. The larger the difference between pI and pH, the greater the chance to keep the protein soluble. For NS5A (pI=5.15) and NS5B (pI=9.04) the buffer was kept at 7.5. In contrast, NS3 has an expected pI of 6.99, so the pH was raised to 8.8.

With these adjustments, satisfactory yields of protein could be obtained. The proteins were of sufficient purity, with very little contaminating bands (**fig. 5.4**).
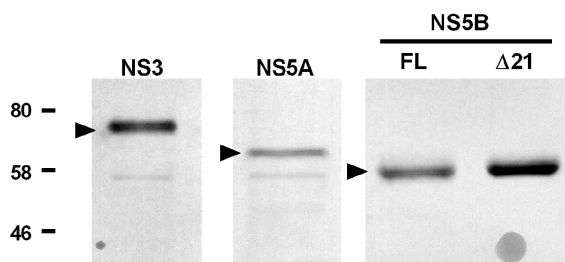
Figure 5.4.: Bacterial expression and purification of HCV non-structural proteins. Around $1 \mu g$ of eluted protein was loaded on a 10% PAA gel and stained with coomassie brilliant blue. Arrow heads indicate the band for the protein of interest. Protein amounts were approximated by NanoDrop measurement.

5.1.4. Reconstitution of the Viral Replicase In Vitro

After purification of the replicase proteins, the next goal was to assess the modulatory effects of NS3 and NS5A on the function of the viral polymerase NS5B. NS3 is a multifunctional enzyme, which contains a protease, and a helicase/NTPase domain. The relevant function in the replicase is likely associated to the helicase, which might prepare the RNA template for efficient NS5B initiation. Therefore, its enzymatic activity was determined and reaction conditions were tested that would allow enzymatic activity of polymerase and helicase in the same reaction. In contrast, the phospho-protein NS5A does not posses any known enzymatic function, but binds to several viral and host proteins, as well as to uridylate-rich RNA. How and if it is involved in initiation of (-)-strand synthesis is not yet understood. Thus, no further testing was possible beforehand for this protein.

NS3 Helicase Assay

Before the interaction of the purified replicase components were tested, the NS3 helicase was subjected to an *in vitro* assay, to confirm its functionality. Besides the wild type enzyme, also an ATPase dead mutant (Q460H[62]) and the helicase domain alone (ΔP) were used. These his-tagged variants of the viral protease/helicase were also expressed in E. coli and purified via NiNTA chromatography (**fig. 5.5**A). The enzyme kinetics and efficacy were determined in a DNA based unwinding assay, adapted from[62] (**fig. 5.5**B). Furthermore, specificity of the observed effect was probed by inhibition of the helicase by the small molecule inhibitor manoalide (MNLD). This compound has been described to inhibit helicase function, ATPase and nucleic acid binding capabilities of HCV NS3 and related cellular helicases[63]. As expected, a dose dependent effect could be observed with an IC_{50} of $1.1 \mu M$ (**fig. 5.5**D, E). Thus, manoalide is approximately 15 times more potent inhibiting NS3 on a DNA duplex compared to the RNA template ($IC_{50}=15 \mu M$), tested by Salam et al.[63]. VX950, a potent protease inhibitor, had no effect on total

helicase activity (**fig. 5.5**F) or the enzyme kinetics (supplementary **fig. C.1**). The small polypeptide NS4A is an essential co-factor of NS3 during natural infection. It folds into the protease domain, and anchors the enzyme to the membrane. To evaluate its role *in vitro*, an NS3/4A fusion-protein was expressed and purified. Previously, it has been shown, that the pH significantly influences the helicase activity of NS3/4A. At acidic pH, helicase activity was detected, while neutral pH inhibited protein function. We could observe the same effect in the established helicase assay (**fig. 5.6**D-E). While the NS3 helicase activity was readily detectable at pH6, no unwinding was found at physiological pH7.5. This phenotype remained unchanged upon addition of either NS5A or 5B in equimolar amounts. Since NS5B activity is greatly reduced in an acidic environment[299,300], NS3 was used without NS4A at pH7.5 in the subsequent assays. In order to further optimize assay conditions, a potential temperature-dependence of the helicase was addressed. At room temperature (25°C), the DNA duplex was unwound only very inefficiently. Furthermore, 37°C, or 41°C (the physiological temperature inside the liver) were tested, which both proved to be more suitable for unwinding activity (**fig. 5.7**A). At early time points 41°C could increase helicase activity compared to 37°C, but the maximum amount of unwound template after 30 min was equal in both conditions. To mimic cell culture conditions as close as possible, the following optimization experiments were conducted at 37°C. Next, the cooperative effect of NS5B was addressed. It has already been shown that NS5B has a stimulatory effect on NS3 helicase activity[62]. The reported stimulation was dose dependent, and readily observable at excess concentrations of NS5B. Thus, NS5BΔC21 was added to the unwinding reaction. In agreement with the published data, no stimulation could be observed at equimolar amounts in the optimized helicase buffer. However, using a buffer optimized for RdRP activity had a marked effect on NS3, and the unwound DNA fraction after 30 min was decreased by approximately 50%. Interestingly, this effect could be reversed by adding NS5B in a 1:1 molar ratio (**fig. 5.7**B and C).

In summary, the NS3 helicase function was greatest using the full length enzyme, but without NS4A as co-factor. As for the optimal *in vitro* conditions, elevated temperatures greater than 25°C were needed for optimal activity. Since the final replicase assay depends on full functionality of NS5B, an RdRP buffer was tested for its effect on helicase function. It was found that this buffer was not ideal for NS3. However, interaction with the polymerase was sufficient to restore full helicase activity. These data also indicate that NS3 and NS5B were capable of functional interaction under the chosen *in vitro* conditions.
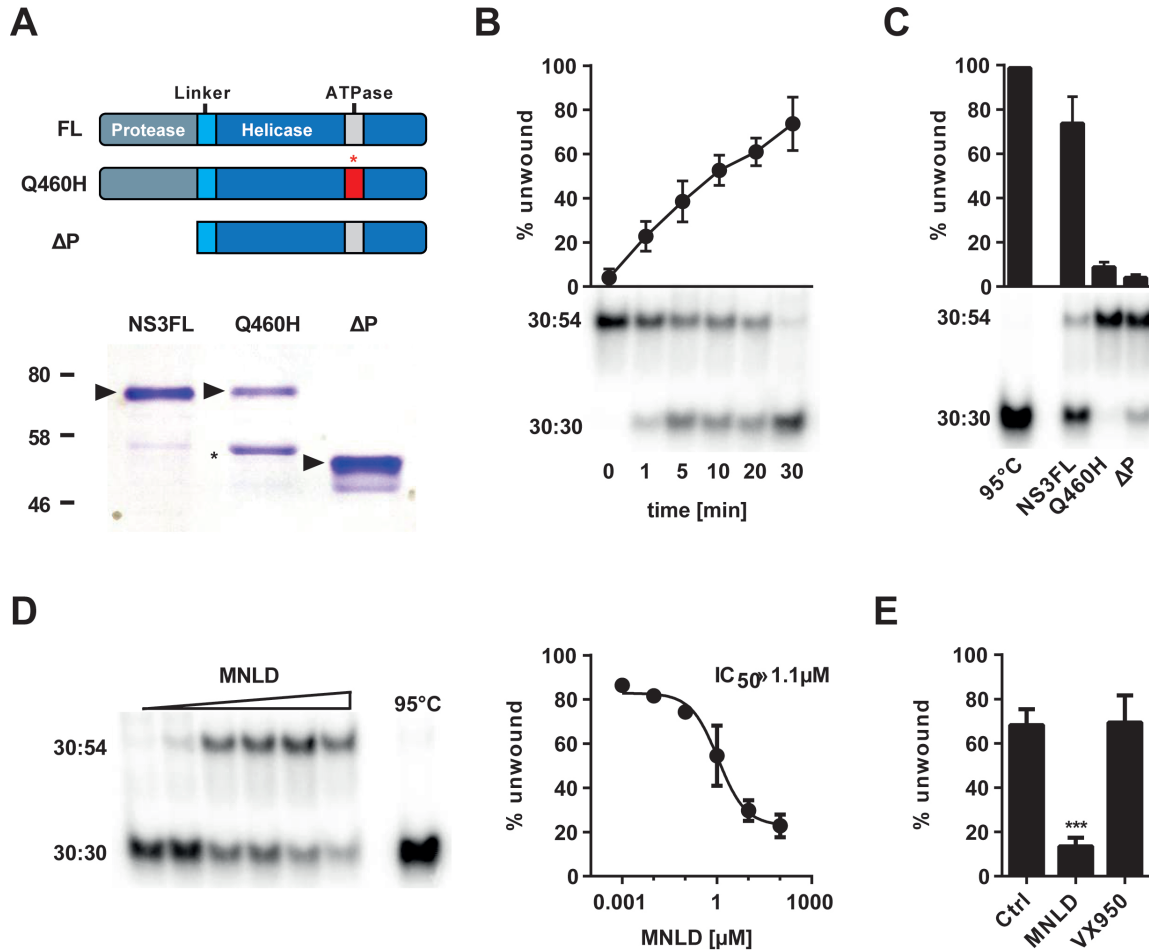
Figure 5.5.: Expression and determination of activity of NS3 variants. A | Schematics of the NS3 variants used, and representative SDS-PAGE gel stained with coomassie blue, demonstrating the successful purification of the proteins. Arrow heads mark the expected size of each construct. The nature of lower band (*) in the Q460H mutant preparation is not known. **B |** Kinetics of NS3 action were determined by a DNA based unwinding assay. Duplexes of a 54 and a radioactively labeled 30 nucleotide long DNA fragment were incubated with full-length NS3 and a 30-fold excess of a 30 nt capture oligo. The reaction was started by addition of ATP and incubated for up to 30 min. The reaction was loaded onto a non-denaturing PAA gel and the ratio of the initial duplex (54:30) and hybrids with the capture oligo (30:30) was determined by auto-radiography. (n=5) **C |** Unwinding performance of the different mutants was tested as described in textbfB. Shown are endpoint values after 30 min at 37°C . Heat-denatured samples were used as positive control (95°C). **D |** Manoalide (MNLD) is an inhibitor of NS3 activity and was used to verify a specific effect of the enzyme. Representative auto-radiography image showing the effect of increasing MNLD concentration on NS3 helicase activity. The effect of increasing concentrations of MNLD on NS3 unwinding activity was quantified (n=2), and the IC_{50} was calculated. **E |** Comparison of MNLD with the protease inhibitor VX950, both at $100\,\mu M$ concentration (n=2). Shown are endpoint values after 30 min at 37°C . Error bars represent S.D.
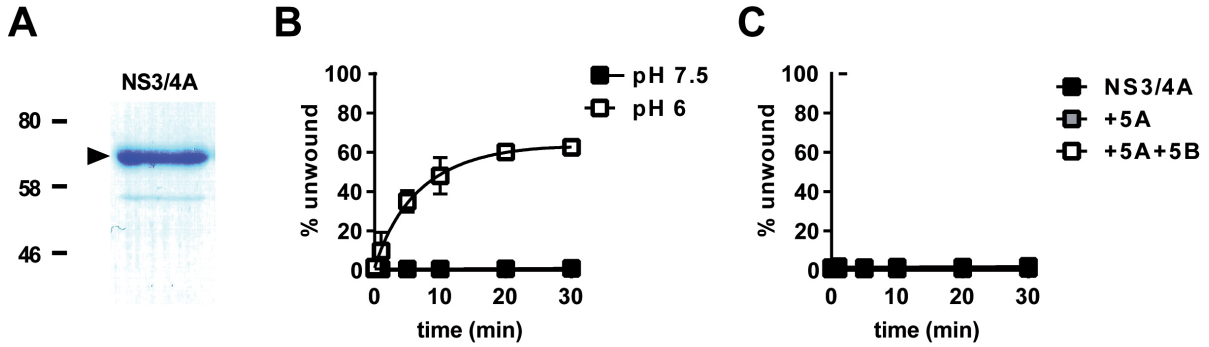
Figure 5.6.: Effect of NS4A on NS3 activity *in vitro*. A | Coomassie stained SDS-PAGE of purified NS3/4A. **B |** pH-dependent performance of an NS3/4A fusion protein. Purified NS3/4A was subjected to the helicase assay described in **fig. 5.5** at different pH values (n=2).In brief, 30 nt DNA oligo was labeled and hybridized with an unlabeled 54 nt fragment. The duplex was incubated with the enzyme, excess levels of a 30 nt capture oligo and ATP. The resulting large (54:30, native) and small (30:30, unwound) duplex were separated by PAA gel electrophoresis, detected by auto-radiography and quantified. Shown is the amount of unwound duplex over 30 min at 37°C. Error bars represent S.D. **C |** The same assay as in **B** was performed at pH7.5, but after addition of equimolar amounts of other non-structural proteins (NS5A and 5B) to assess, whether possible protein:protein interactions might overcome pH dependence of NS3/4A.
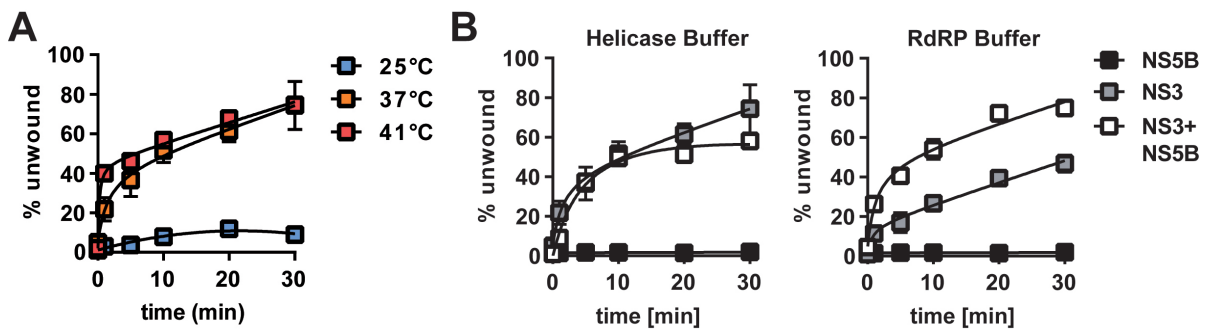
Figure 5.7.: Optimization of conditions for NS3 activity *in vitro*. A | To address the influence of temperature on NS3 unwinding kinetics, the DNA-based helicase assay was performed at 25°C, 37°C and 41°C (n=2), as described above. In brief, 30 nt DNA oligo was labeled and hybridized with an unlabeled 54 nt fragment. The duplex was incubated with the enzyme, excess levels of a 30 nt capture oligo and ATP. The resulting large (54:30, native) and small (30:30, unwound) duplex were separated by PAA gel electrophoresis, detected by auto-radiography and quantified. **B |** The final aim to reconstitute the viral replicase demands optimal activity of all enzymes *in vitro*. Therefore the different buffer systems, either optimized for NS3 ("helicase buffer", n=2) or NS5B ("RdRP buffer", n=1) were used in the helicase assay. NS5B alone was used as a negative control. Shown is the amount of unwound duplex over 30 min. Error bars represent S.D.

Impact of NS3 on NS5B RNA Polymerization

After successful validation of NS3 activity, interaction with NS5B, and optimization of *in vitro* conditions, it was attempted to unravel the role of NS3 in NS5B-driven RNA replication. Previously, it has been described that in CSFV NS3 can increase NS5B RNA polymerization activity through direct interaction at distinct regions[65]. *In vitro*, NS5B has been described to use several modes of initiation: i) primer-dependent/copy-back: the end of newly made RNA product is annealed to another RNA template and used as primer to initiate a subsequent round of polymerization. This mechanism produces RNAs larger than the original template. ii) terminal *de novo*: First synthesis of a 2-3 nt primer at the very 3' end of the template, then the polymerase switches from initiation to elongation mode. This mechanism is used to initiate at the 3' terminus, producing exactly template-sized RNAs. This is suspected to be the preferred mechanism in the natural infection. iii) Internal *de novo*: as in ii), but using an internal single-stranded region, as it has been shown for picornaviruses[301,302].

To test whether HCV NS3 is capable of stimulating NS5B processivity or initiation capacity, both proteins were incubated to different ratios, and complemented with either a cytidin homo-polymer, or a natural hetero-polymer, comprising the 3' end of the HCV (-) strand, including the known cis-acting replication elements. As readout for polymerase activity, the incorporation of radio-labeled nucleotides into the nascent RNA was quantified by liquid scintillation counting[104] (**fig. 5.8**A). The homo-polymer is unstructured and therefore elongation can progress at maximum velocity. Additionally, it allows for efficient initiation virtually anywhere on the template. The 3'(-)-strand sequence also contains an ideal platform for initiation at the 3' end, but features several secondary structures. These might be favorable for more specific recognition of the viral RNA, but also restrict internal initiation on this template. Moreover, since the intrinsic processivity of NS5B is rather low[?], the stems might also slow down or abort polymerization.

NS3 acts as a 3'-5' helicase, and could theoretically initiate at a short single stranded region 3' of the first stem and unwind the structured template, thereby aiding efficient initiation or polymerization of NS5B. Indeed, the active wild type NS3 was able to stimulate incorporation of radioactive nucleotides by approximately 3-fold, whereas the inactive mutants did not (**fig. 5.8**B). This dependence on helicase activity suggests a specific effect, which goes beyond pure stabilization of NS5B, and argues for a function of active NS3, facilitating NS5B initiation and/or processivity.
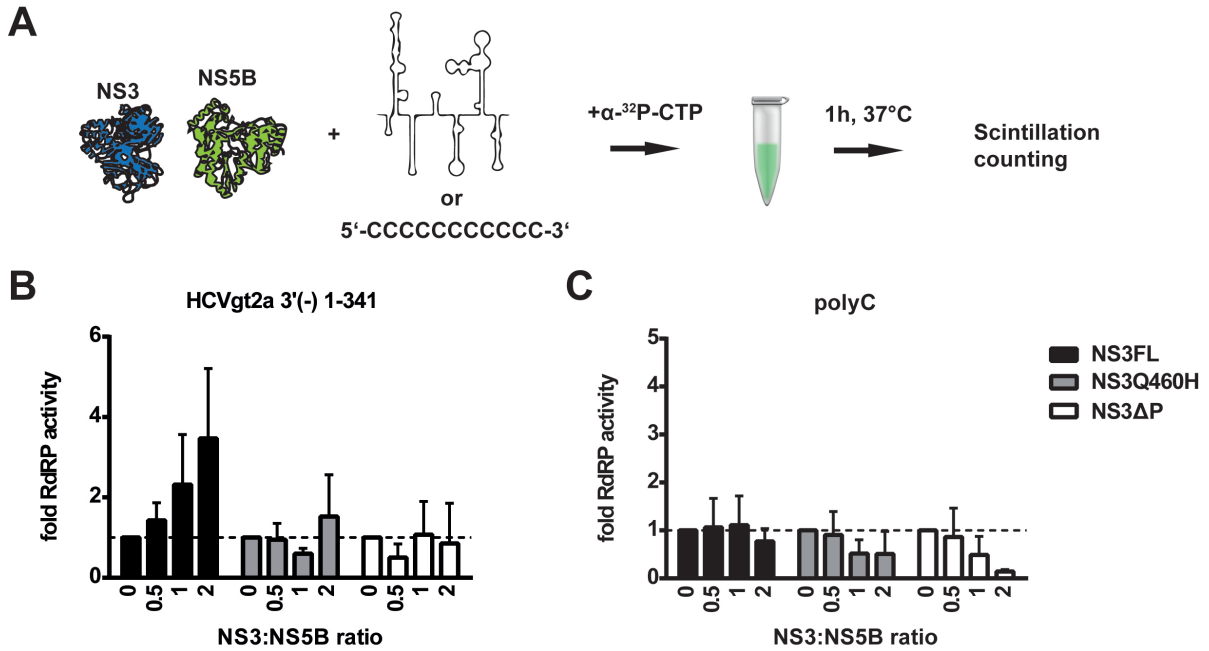
Figure 5.8.: Effect of NS3 variants on NS5B activity *in vitro*. A | Schematic representation of the used assay to study RdRP activity by incorporation of radioactively rNTPs. NS3 and NS5BΔC21 were pre-incubated on ice in different ratios. Then, either a natural and highly structured template (*in vitro* transcribed 3'(-) nucleotides 1-341 of the JFH-1 strain), or a cytidylate homopolymer was added. The reaction was started by addition of rNTPs containing radioactively labeled CTP and incubated for 60 min at 37°C. The reaction was TCA precipitated, and the polymerase products captured on a Whatman filter. Excess nucleotides were removed by stringent washing, and the radioactivity incorporated into newly formed RNA products was measured in a scintillation counter. **B |** Effect of NS3 variants on NS5B performance, using the 3' terminal 341 nucleotides. NS5B was incubated with full-length NS3 or inactive variants Q460H and ΔP. **C |** Effect of NS3 variants on NS5B performance, using a polyC template. NS5B was incubated with full-length NS3 or inactive variants Q460H and ΔP (n=3). The values of each experiment were normalized to the activity of NS5B alone. Error bars represent S.D.

In contrast, on the polyC template the incorporation of nucleotides was not improved by NS3 addition, which might mean that NS5B is maximally active on this template, and no further stimulation is possible. In fact, increasing amounts of the helicase dead mutants even decreased RdRP activity on this template (**fig. 5.8**C). Since the active enzyme did not show this phenotype, one could speculate that NS5B processivity might be enhanced actually be pulled along the template by NS3. This mechanism would require interaction with NS5B, the RNA template and an active ATPase, which mediates the structural shift necessary for moving along the template. The Q460H mutant is ATPase defective, while ΔP is supposedly impaired in RNA binding. Therefore, interaction of these mutants with the polymerase could lead to a functional block, by retention at the initiation site (Q460H), or sequestration away from the template (ΔP).

These data show that NS3 activates NS5B-dependent RNA synthesis through its helicase/NTPase function. Likely this involves physical interaction of both proteins. However, it cannot be deduced from these results, if the generated product was initiated *de novo* from the extreme 3' end, which would be necessary in the natural context, or by internal initiation, which has also been described to occur *in vitro*. Therefore, a qualitative analysis of reaction products was performed using a gel-based system as readout. Here, the natural 3' terminal 450 nt of the (+)-strand were used (**fig. 5.9**A). The polymerase alone was not able to initiate efficiently on this template (**fig. 5.9**B). In concurrence with the liquid scintillation counting assays, the overall RdRP activity was increased by functional NS3, but not by inactive mutants (**fig. 5.9**C). Additionally, a specific increase of the presumed full-length product was observed in presence of NS3 (**fig. 5.9**A,C,D)), as judged by higher amounts of a radiolabeled product of template size (450 nt). At different temperatures, the observed phenotype was modulated. Lowering the temperature, led to a decreased the amount of NS3 needed for maximal stimulation (0.5-fold molar ratio, **fig. 5.9**C). Moreover, the specific enhancement of *de novo* product seemed to be favored over the general RdRP activation. At higher temperature the opposite effect became evident (**fig. 5.9**D). Interestingly, in all cases a 2-fold excess of NS3 led to reduced specific product, compared to equimolar amounts. However, the effect RdRP stimulation was retained at excess concentrations of NS3, at least at higher temperatures.

As shown previously, the natural compound MNLD readily inhibits NS3 nucleic acid unwinding, and to a lesser extent its ATPase activity[63]. The impact of MNLD on NS5B is not known. To test the influence of NS3 inhibition on RdRP activity, these compounds were added to the assay with a NS3:NS5B ratio of 1:1. The compounds
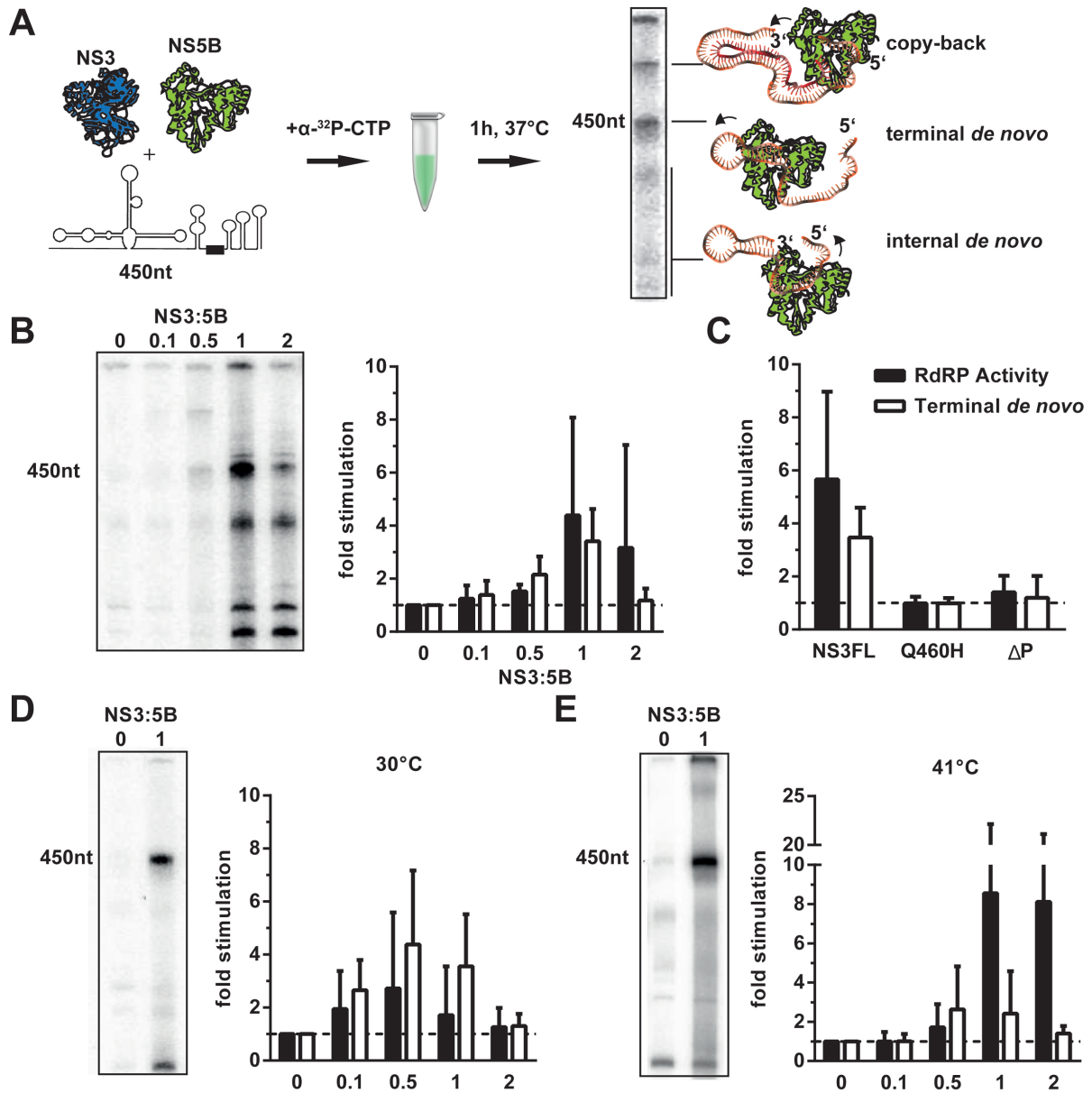
Figure 5.9.: Effect of NS3 variants on NS5B *de novo* initiation *in vitro*. **A** | Schematic representation of the gel-based assay, and assignment of obtained bands. The initial experiments were performed at 37°C, using different NS3:NS5B ratios. 3'(+) RNA, and rNTPs with $\alpha-^{32}$P-CTP were added, and radioactively labeled products were separated by denaturing PAGE, and visualized by auto-radiography. Bands above 450 nt were considered copy-back products, template-sized RNAs were assumed to be terminal *de novo* products. Lower bands could be a result of internal initiation. The density of a whole lane was used as value for RdRP activity. The band at 450 nt was normalized to the corresponding lane. **B** | Representative auto-radiography image, and quantification of terminal *de novo* product, and RdRP activity. **C** | Effect of NS3 variants on NS5B performance. NS5B was incubated with equimolar amounts full-length NS3 or inactive variants Q460H and ΔP. General and specific RdRP stimulation were quantified and normalized to the values obtained with NS5B alone. **D-E** | Temperature dependence of NS3-mediated RdRP stimulation. The assay was performed at 30°C, to facilitate protein:protein interaction, or 41°C to mimic conditions in the human liver. Error bars represent S.D. of three independent experiments.

were preincubated with the proteins in different concentrations. While a stimulation of NS5B by NS3 was still visible in all conditions, the nature of the template was different at inhibitory concentrations, giving ride to large amounts of copy-back product. Strikingly, the template-sized and all smaller products were effectively eliminated in a dose-dependent manner (**fig. 5.10**A). To test for any effect on NS5B alone, a template with a tri-cytidylate attached to the 3' terminus was used. NS5B can initiate on its own at this short single-stranded region. Interestingly, MNLD alone did also affect NS5B terminal *de novo* initiation, while a faint band appeared at the size of the suspected copy-back product (**fig. 5.10**B). However, this was not as pronounced as in the case of NS3 addition. Possibly because NS3-mediated stimulation of the general RdRP activity is required for this effect.

Additionally, biogenic polyamines (i.e. spermidine (SPDN)), inhibited NS3 with IC_{50} values around 0.5 mM, but stimulated NS5B by up to 6-fold at similar concentrations, leading to achievement of the maximal enzyme velocity[303]. For SPDN, the inhibitory concentration for NS3 has not been tested in our system, so a larger concentration range form 10 μM to 10 mM was covered. As for MNLD, the compound was able to increase the copy-back fraction. However, addition of NS3 was not essential in this case, as the compound itself actively stimulates NS5B[303] (**fig. 5.10**C). This means, a general stimulatory effect on the V_{max} of NS5B can be mediated by NS3, even after inhibition of the helicase. However, the mechanism of initiation seems to be affected, since terminal *de novo* product is not efficiently made under these conditions.

In conclusion, we found no increase of the copy-back fraction of newly synthesized RNA after addition of active NS3, whereas internally initiated or abortive fragments appeared in concurrence to the template-sized product. The data are in line with a reported 1:1 stoichiometry of functional NS3:5B complexes[67]. The most specific effects on *de novo* initiation were seen at 30°C, which might be due to more stable protein:protein and Protein:RNA interactions. Suppression of the helicase activity by chemical inhibitors led to a loss of *de novo* product, instead copy-back products were generated in larger proportions. Additionally, MNLD and SPDN seem to act on NS5B, favoring a primer dependent mode of initiation. This speaks for two separate functions of NS3: first, at the initiation step, for which the helicase is needed, and second, a stimulation of processivity which likely depends mostly on the NTPase activity of NS3.
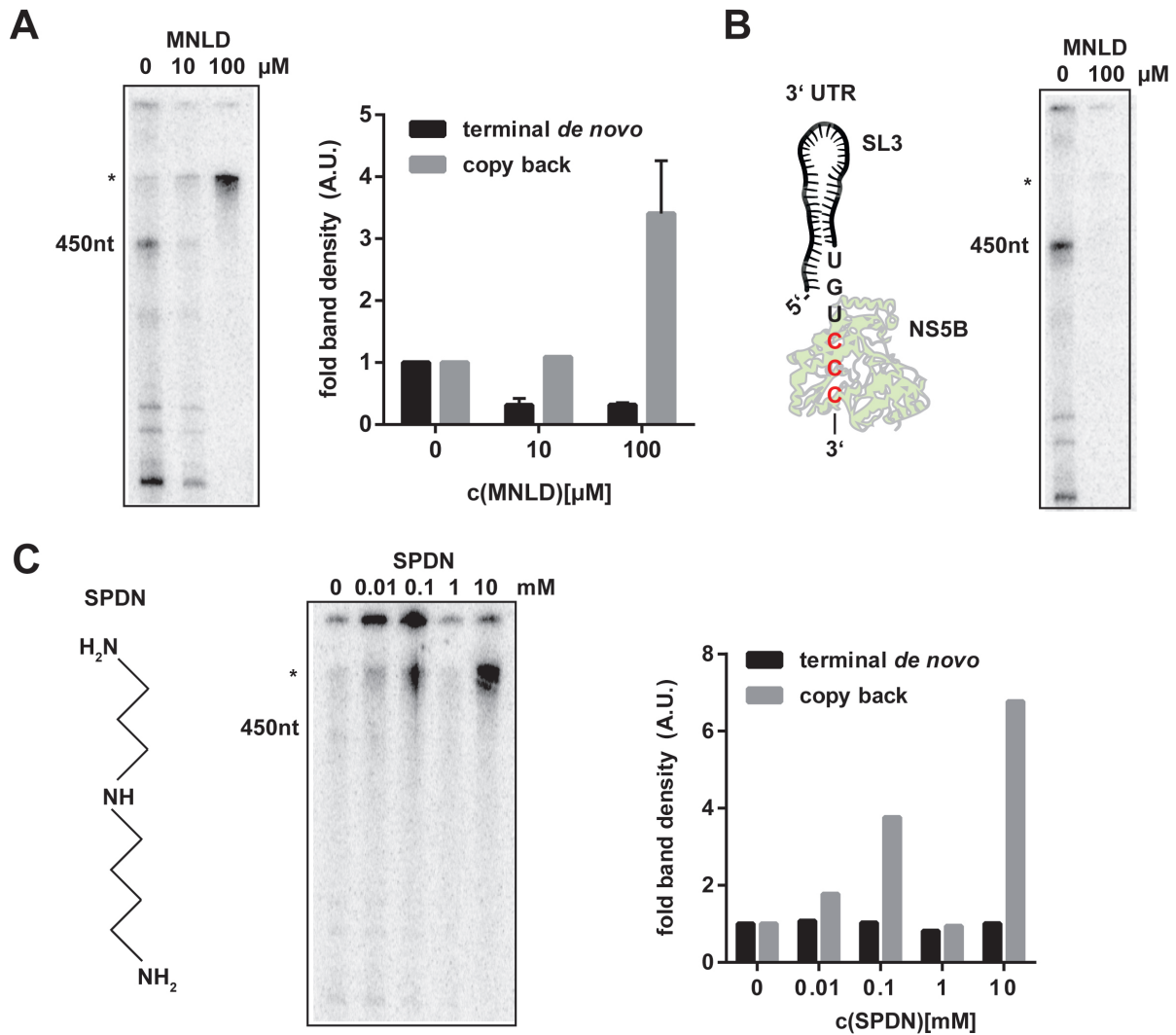
Figure 5.10.: Small molecule inhibition of NS3 and its impact on NS5B stimulation.A NS3 and NS5BΔC21 were pre-incubated on ice in different ratios. Then, the natural *in vitro* transcribed 3' 450 nt of the (+)-strand (JFH-1) and different concentrations of Manoalide (MNLD) were added. As stated above, the reaction was started by addition of rNTPs containing radioactively labeled CTP and incubated for 60 min at 37°C. The resulting labeled fragments were separated by denaturing PAA gel electrophoresis and visualized by auto-radiography. Densities of the terminal *de novo* and copy-back product (*) were quantified relative to the whole lane (n=2). **B** | The standard heteropolymeric 3'(+) template was modified with 3 cytidylates at the 3' end to enable NS5B initiation without NS3. **C** | Chemical structure of Spermidine (SPDN). A similar effect as with MNLD is seen for spermidine under equivalent assay conditions. The copy-back product is marked by an asterisk. The 1 mM value was not considered due to apparent loss of sample. Error bars represent S.D.

The Role of NS5A

Next, the role of the viral phospho-protein NS5A was interrogated. NS5A is a key factor for efficient RNA replication of numerous host factors engaged in RNA synthesis and biogenesis of the viral replication compartment. However, few facts are known about the contribution of the interplay of NS3, 5A and 5B. Thus, different ratios of all three NS proteins were mixed, and the impact on *de novo* initiation was investigated. A slightly
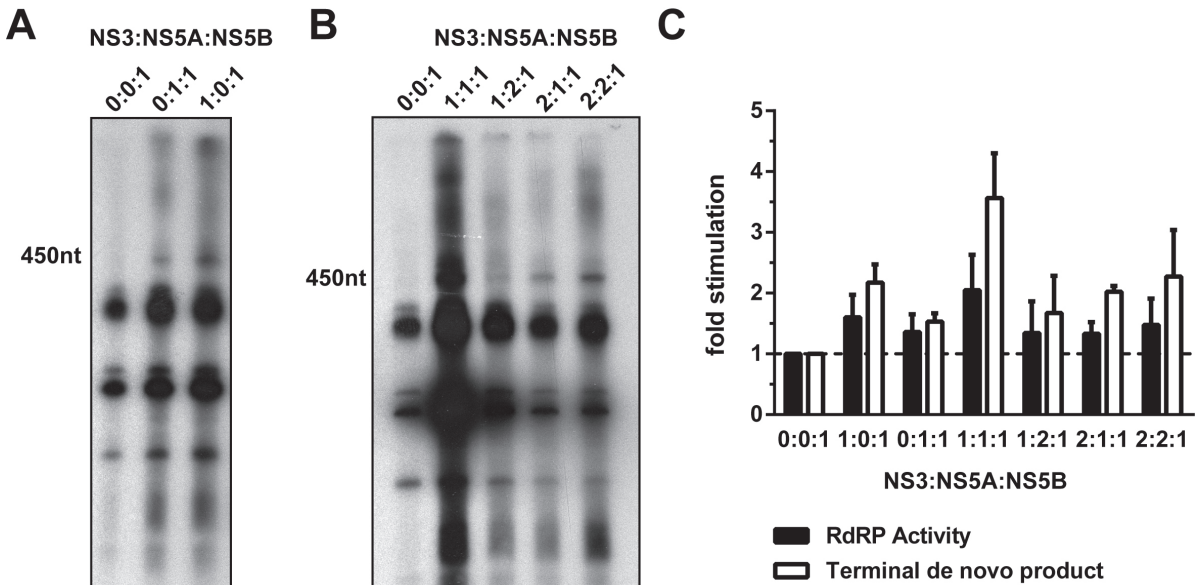
Figure 5.11.: Modulation of NS5B by NS5A. NS3, NS5A and NS5BΔC21 were pre-incubated on ice in different ratios. Then, the natural *in vitro* transcribed 3' 450 nt of the (+)-strand (JFH-1) were added as template. As before, the reaction was started by addition of rNTPs containing radioactively labeled CTP and incubated for 60 min at 37°C. The resulting labeled fragments were separated by denaturing PAA gel electrophoresis and visualized by auto-radiography. **A** | Auto-radiography images showing the effect of each auxiliary protein alone (NS3 or NS5A), or **B** | the combination of NS3 and 5A in different amounts. Numbers above the lanes indicate the used molar ratios relative to NS5B (NS3:NS5A:NS5B). **C** | Quantification of auto-radiography images (n=2). RdRP activity indicates the density of the whole lane. Densities of the terminal *de novo* product (450 nt) were quantified relative to the whole lane. Error bars represent S.D.

increased production of the suspected *de novo* product could be observed in presence of NS5A, without the need for NS3. However, this effect was less pronounced than the helicase-mediated stimulation (**fig. 5.11**A, C). The NS5A-mediated mechanism seemed to be distinct from the one exerted by NS3, since an additive effect was noted, when both proteins were added in equimolar amounts. In this case, a substantial increase of overall RdRP activity and terminal *de novo* product formation was noted (**fig. 5.11**B,

C, [1:1:1]). This phenotype was only observed in this particular condition. As described before, 2-fold excess of NS3 reduced the *de novo* product (**fig. 5.11**B, C [2:1:1]). A similar trend was also seen in presence of increased amounts of NS5A, while the decrease of RdRP activity was somewhat less pronounced (**fig. 5.11**B, C [2:2:1]). Indeed, excess NS5A even seemed to attenuate the stimulatory function of NS3 slightly (**fig. 5.11**B, C [1:2:1]). This is in line with the previously proposed separate effects on NS5B function. Also, the strongly increased polymerase activity only in the case of equimolar amounts of all proteins underscores the need for a well-balanced complex formation.

These data suggest a supporting/modulatory role of NS5A, by enhancing the NS3-mediated effects, and increasing terminal *de novo* initiation at optimal molar ratios of all three proteins. Recruitment and correct positioning of the NS3:NS5B complex would therefore be a likely mode of action by NS5A in this context.

Remaining Technical Challenges

While the assay worked in principle, many experiments showed a high degree of variability. The most common issues are summaized in **fig. 5.12**. A constant source of uncertainty resulted from a significant quantity of abortive products produced in the in vitro transcription reaction, as shown in **fig. 5.12**A. Moreover, a few times, another unidentified band appeared close to the presumed full length product (**fig. 5.12**B). Some protein batches were contaminated with minute amounts of RNAse, which led to the degradation of most of the sample (**fig. 5.12**C). The desired reproducibility was not always achieved when only one component was changed in the reaction, i.e. a different batch of protein (**fig. 5.12**D). While all batches of protein and RNA template were checked for contamination or degradation, respectively (**fig. 5.12**E, F), this was not sufficient to predict, whether an individual purification would yield comparable results. Conclusively, the overall quality of the used components needs to be improved and has to remain consistent between batches. Gel-purification of the used RNA, and an additional size exclusion chromatography step for the proteins could be employed to generate high quality components. Therefore, additional studies will be required beyond the scope of this thesis to setup a more robust *in vitro* system.

Overall, these observations support a model of a minimal replicase containing NS3, NS5B and viral RNA. NS5A could further augment the NS3-mediated effect on *de novo* initiation of RNA synthesis. However, the experimental model could not be established towards sufficient robustness to allow more in depth studies (**fig. 5.12**). Open questions remain, in particular concerning the involvement of NS5A in RNA replication, as the
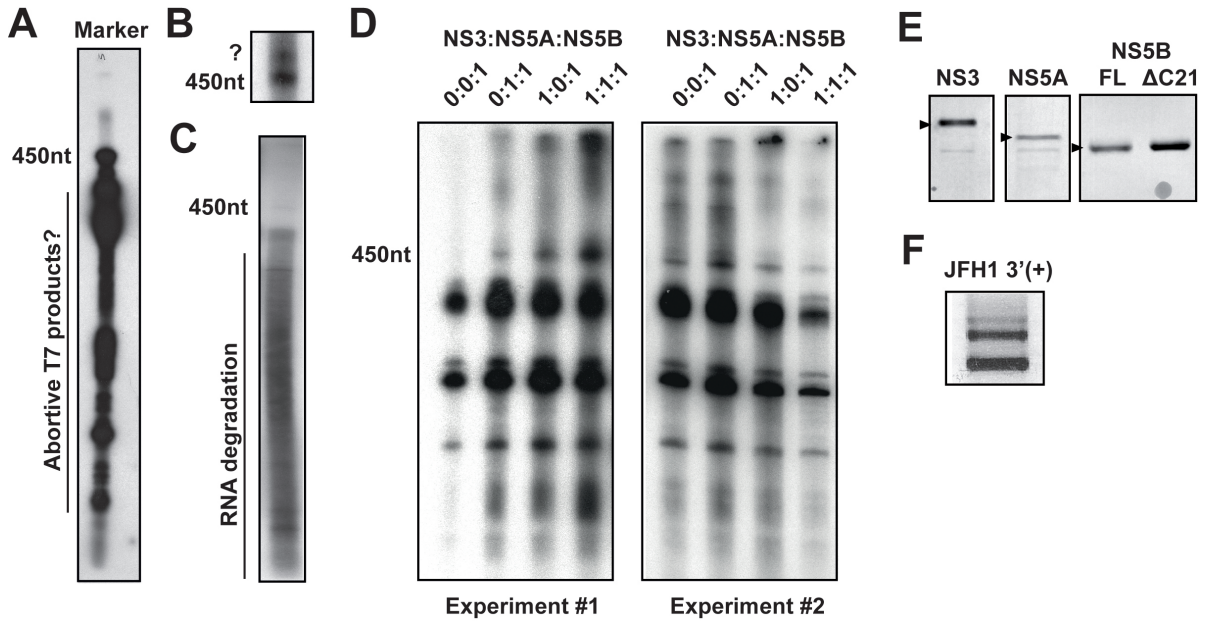
Figure 5.12.: Persisting technical problems. **A** | A large number of lower molecular weight bands appeared in the marker, which was generated by hot in vitro transcription. A possible reason for this is premature termination of the T7 polymerase. **B** | A second band close to the terminal de novo product was detected in several experiments. The nature of this RNA remains unclear. **C** | Some protein preparations were contaminated with RNAses. **D** | Different protein and/or RNA batches lead to very different results. Shown are two experiments performed in the same way, but with a different NS3 preparation. **E** | Protein purity was checked by SDS PAGE, stained with Coomassie Brilliant Blue. **F** | RNA integrity was determined by agarose gel electrophoresis. Multiple bands represent different conformations of the RNA.

protein was produced in bacteria and several studies have pointed out that the post-translational modification of NS5A is crucial for correct protein function.

5.2. Dissecting the Roles of miR-122 in the HCV Life Cycle

The mode of action of miR-122 as a viral dependency factor has been attributed to a variety of functions. The most recent paradigm on the molecular mechanism is a physical stabilization of the viral RNA (**fig. 5.13**A). Other reports have also claimed, that replication initiation is enhanced (**fig. 5.13**B), as well as translation of the viral polyprotein (**fig. 5.13**C). While these studies have already worked on different leads to find the true mode of action, most pursued a single hypothesis, and relied on different cell culture systems. Initially, it was attempted to specify the quantitative contribution of this small non-coding RNA at different phases of the viral RNA metabolism, and to subsequently elucidate the corresponding mechanism of each function.
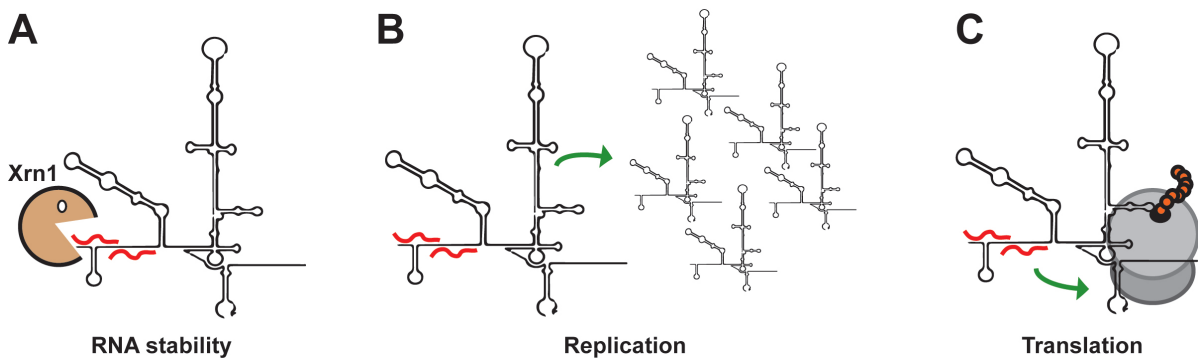
Figure 5.13.: Comparison of HCV replication in different cell lines upon miR-122 supplementation. A | miR-122 protects the HCV 5' end against cleavage by the host exonuclease Xrn1[304]. **B** | RNA amplification is enhanced after miR-122 binding[207]. **C** | Translation activity of the viral IRES is increased, and the association of the 40S ribosomal subunit is bound more efficiently[209].

5.2.1. Establishment of a miR-122 Activated Cell Culture System

To investigate the mechanisms responsible for the effects of miR-122 on the HCV life cycle, a cell line without miR-122 expression was required. HEK293T as a non-hepatic cell line, as well as HepG2 and Hep3B cells are described to have undetectable miR-122 levels, and are therefore unable to sustain HCV replication natively. However, by supplementation of the miRNA, transfected HCV RNA can be efficiently amplified. Initially, we used a co-electroporation approach of JFH-1 monocistronic reporter replicons together with synthetic miRNA duplexes (**fig. 5.14**). None of the tested cell lines could

reach the reporter activity achieved in the control Huh7.5 cell line. Nevertheless, 293T and Hep3B replicated >100- or >1000-fold over background levels (ΔGDD), respectively (**fig. 5.14**B). Since Hep3B cells performed best in the comparison of the different tested cell lines, as they showed the highest permissivity for HCV after introduction of miR-122. These cells were therefore selected for subsequent experiments. All attempts to induce HCV replication in HepG2 were unsuccessful even in presence of miR-122. In contrast, 293T and Hep3B cells could readily support HCV replication (**fig. 5.14**B). In addition, the amounts of miRNA present in the naïve and electroporated cells were detected by qPCR. Only background levels of miR-122 were detected without duplex addition, whereas the electroporated cells showed levels even higher than Huh7.5 cells after 48 h (**fig. 5.14**C). However, it is likely that not all of the miRNA is active, which might be partly be the reason for the lower replication activity, compared to Huh7.5. By means of *in situ* hybridization and western blot, detecting the expression of non-structural proteins, a robust translation and replication could be visualized. No detectable levels of reporter activity, viral protein or RNA were present during the 72 h time course when no miR-122 was added (**fig. 5.14**B, D, E).

In addition, Hep3B cells were transduced with lentiviruses encoding either the wild type pre-miR-122 stem-loop, or a mutated version with a single nucleotide exchange within the seed region (A4U), rendering it unable to bind canonical targets. Complementary mutations in the HCV 5' UTR (m1,2) will in turn only allow for binding of miR-122 A4U, and not the wild type replicon (**fig. 5.15**A). The lentiviral integrate also contained a puromycin N-acetyl-transferase gene for selection. To confirm the activity of the introduced miR-122 variants, a known miR-122 target gene (PACT[304]) and several controls were tested for regulation by western blot. While the wild type miR was able to repress PACT expression to around 60%, the A4U version did not alter the expression levels. The control genes (ACTB, GAPDH) were not affected by over-expression of either miR-122 variant (**fig. 5.15**B). The miR-122 expression levels of the cells were determined by stem-loop RT qPCR. The miR-122 level in the generated cell lines is approximately half of the amount found in Huh7.5 cells, a hepatic cell line highly permissive for HCV. In addition, let7a levels were also tested and found to be unaffected by overexpression of functional miR-122, arguing for a largely unaffected RNAi system (**fig. 5.15**C,D). After validation of the functional miRNA expression, different HCV reporters were tested, either a wild type construct or the m1,2 mutant, bearing the compensatory mutations U26A and U41A for the A4U miR-122. As expected, neither replicon was viable in native Hep3B cells. The miR-122 wild type cells only supported the wild type
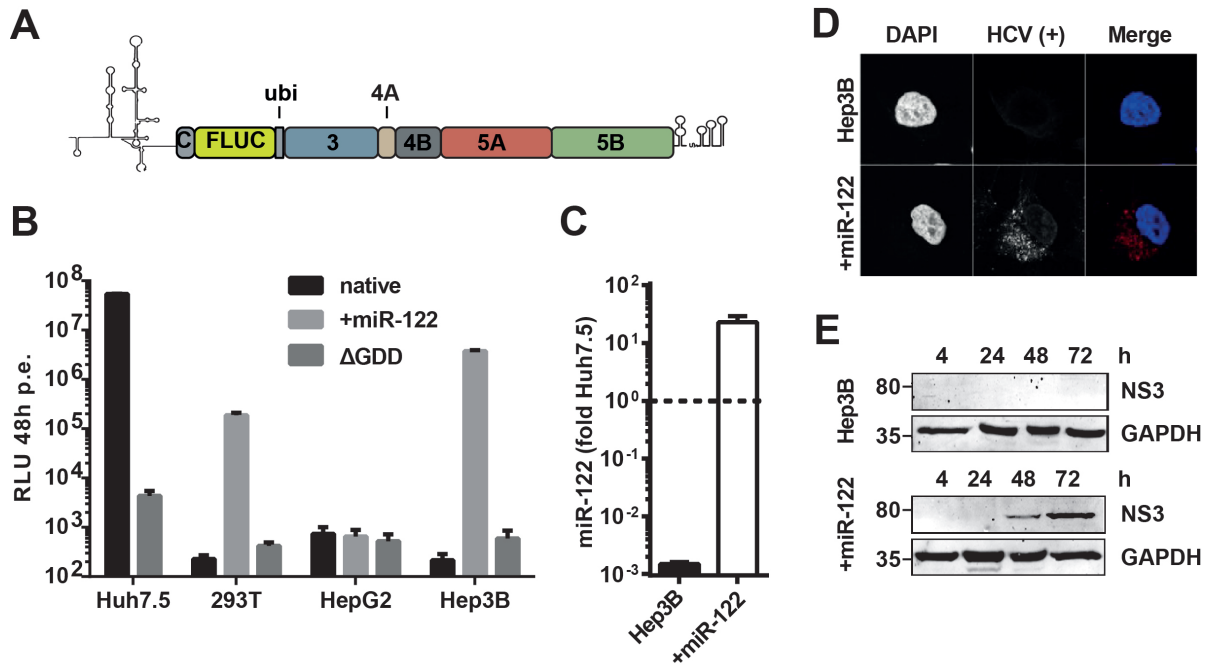
Figure 5.14.: Comparison of HCV replication in different cell lines upon miR-122 supplementation. A | Schematic of the monocistronic luc-ubi reporter replicon of the JFH-1 strain. **B |** Three different cell lines were electroporated with JFH-1 monocistronic replicons in presence or absence a synthetic miR-122-duplex. Cells were lysed and luciferase activity (RLU) was measured after 4 h (input control, not shown), and 48 h at the peak of replication activity. The replication deficient ΔGDD (deletion in the catalytic center of NS5B) mutant served as negative control. Highly permissive Huh7.5 cells were used as positive control. **C |** qPCR quantification of miR-122 in naïve Hep3B cells, compared with cells electroporated with miR-122 duplex. miR-expressing Huh7.5 cells served as control. **D |** Replicon RNA was transfected with or without wild type miR-122, and cells were stained with HCV- specific probes (red). Nuclei were visualized with DAPI (blue). **E |** Western blot analysis of viral protein expression over 72 h. GAPDH was used as loading control.

replicon, whereas the mutant miR-122 exclusively stimulated the corresponding mutant replicon. The maximal reporter activity and the replication kinetics were comparable in both cases. Moreover, the initial translation stimulation was achieved also for the A4U miR-122 binding to m1,2 (**fig. 5.15**E,F). Therefore, the general mechanism of action seemed not to be impaired for the mutant miR-122. This means that all relevant functions of miR-122 could be reconstituted by exogenous supplementation of a synthetic duplex and can be replaced by a mutant miR. Thus, Hep3B cells are a suitable model system for the study of miR-122 dependent effects on the HCV life cycle.

To characterize the influence of miR-122 on the viral replication capacity, we used a number of mono- and bicistronic replicons. The major difference between these reporters
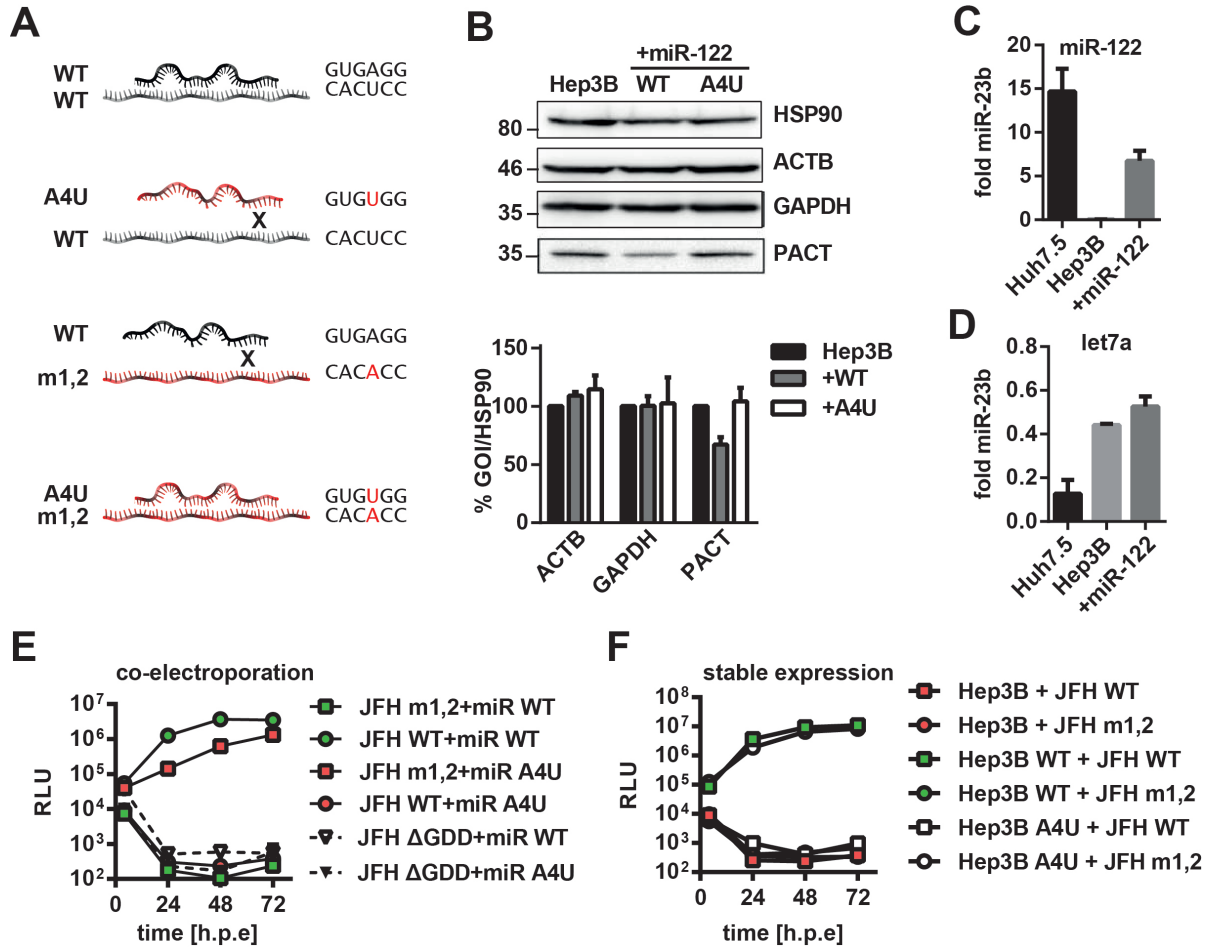
Figure 5.15.: Establishment of Hep3B cells stably expressing miR-122. A | Binding of miR-122 to a target RNA. Mutation of a single nucleotide within the seed region (A4U) restricts binding to the natural target site. Conversely, the complementary exchange in the target leads to abolishment of interaction with wild type, but restores binding of the A4U mutant. **B |** Western blot of control genes in cells stably expressing miR-122 WT or A4U. HSP90, ACTB and GAPDH have no known or predicted target sites for miR-122, and are not differentially regulated in all cell lines. PACT is a known target of the miRNA and is downregulated only in cells expressing WT miR-122. All gene expression levels were normalized to those of HSP90.**C |** qPCR quantification of miR-122 or **D |** let7a in native and miR-122 expressing Hep3B cell lines. Huh7.5 were used as a control. Luciferase reporter activity of wild type or mutant replicons in Hep3B cells clistE with co-electroporated or **F |** stably expressing wild type or mutant miR-122.

was the IRES responsible for translation of the viral proteins (**fig. 5.16**A). First, the influence of miR-122 on the translation of the incoming RNA was interrogated using the luciferase activity at 4 h post electroporation. The most notable effect was observed in the monocistronic context, where translation of the whole ORF depends on the HCV IRES, and therefore on miR-122. The luciferase activity was increased over 6-fold, while all other constructs were much less affected (**fig. 5.16**B). Next, the replication kinetics was addressed. Unexpectedly, we found that miR-122 was not essential for replication, since a monocistronic construct could replicate in miR-122 deficient Hep3B cells, if translation was uncoupled from the HCV IRES, in this case by insertion of a Polio IRES (PI-luc-ubi, **fig. 5.16**C). Importantly, the HCV IRES used in this setting lacked the cis-acting element of the core coding region and was thus not able to initiate translation, but contained only the sequences needed for RNA replication. This phenotype could also be found for both tested bicistronic replicons, which harbored an EMCV IRES proximal to the viral ORF (PI-luc and luc, respectively). Hence, miR-122 independent replication was independent of the nature of the IRES element driving translation of the viral proteins, as long as this was not the HCV IRES. These data also assigned a crucial function of miR-122 to the translation of non-structural proteins, since only the monocistronic replicon requiring the HCV- IRES for translation of the polyprotein was replication incompetent in absence of miR-122 (luc-ubi, **fig. 5.16**C). Of note, enhanced stability of the viral genomes mediated by miR-122 binding could likely be excluded as a factor in this approach, since all replicons contain the same 5' UTR sequence. However, addition of miR-122 could still enhance translation and replication in the bicistroic, as well as in the Polio-IRES dependent monocistronic replicon, albeit to a lower extent compared to the monocistronic replicon (luc-ubi), which did not replicate at all in absence of miR-122. This stimulating effect on miR-independent replicons could be attributed to the published RNA stabilizing effect.

To gain a more quantitative view on the role of miR-122 in different parts of the viral RNA metabolism, bicistronic replicons were constructed, in which elements necessary for replication and translation were separated by duplication of the HCV 5' UTR and could thus be directly compared (**fig. 5.17**A). The first copy of the 5'UTR (i1) was required for regulation of viral RNA replication and to maintain stability of the viral genome, but had no function in translation. To monitor replication independently of miR-122 activity, a Polio-IRES driven *renilla* luciferase gene was inserted. Translation of the second cistron was dependent on the HCV IRES, bearing a *firefly* luciferase reporter to visualize translation of the viral proteins (**fig. 5.17**A). The architecture of
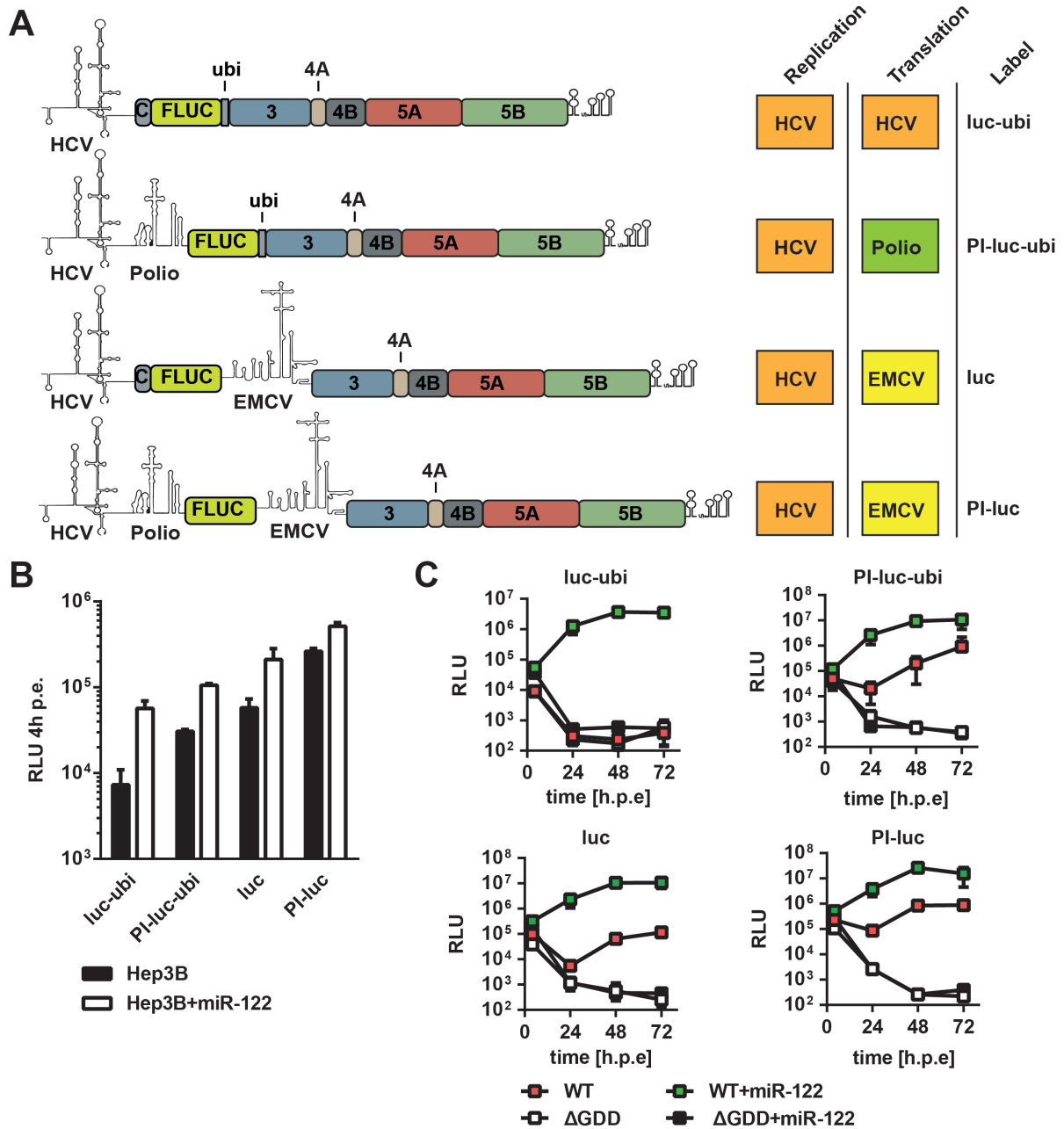
Figure 5.16.: Importance of translation of HCV NS proteins for replication. A | Schematic representation of the different replicons used. The functional RNA elements responsible for RNA replication or translation of the viral proteins are indicated in the boxes on the right. **B |** Initial translation, as measured by firefly luciferase activity (RLU), 4 h post electroporation. Shown are the comparisons between miR-122 WT and A4U supplementation in the different classes of replicons. Polymerase-dead variants (ΔGDD) of the replicons were used in these experiments to exclude potential influences of early replication. **C |** Kinetics of replication, measured by luciferase expression over a time course of 72 h post electroporation. Shown are the comparisons between miR-122 WT and A4U supplementation in the different classes of replicons. A polymerase-dead mutant (ΔGDD) was used as negative control. Values represent means of three independent experiments with S.D..

this construct therefore allowed to independently mutate the miR-122 binding sites in both copies of the HCV 5'UTR to assess the functional role of miR-122 in viral replication/stability and IRES-function/translation, respectively. The functionality of the construct was tested in different cell lines, and in presence or absence of miR-122. In Hep3B cells, functional miR-122 had to be co-electroporated or stably expressed to facilitate translation/replication of the construct. Without miR addition, no replication was detectable.Surprisingly, *renilla* luciferase activity was significantly lower, and only distinctly detectable in the highly permissive Huh7.5 cells (**fig. 5.17**B). However, a robust increase in *firefly* luciferase activity of approximately 100-fold was achieved by addition of miR-122 in Hep3B cells (**fig. 5.17**B). In Huh7.5 cells, the peak luciferase activity was around 10 to 20-fold higher than in Hep3B cells expressing miR-122 WT. Thus, the *firefly* values were initially used for quantification. Furthermore, single point mutants disrupting the miR-122 binding to its recognition sequences were introduced to each of the IRES elements separately or in combination. In addition, miRNAs with complementary mutations were used for rescue experiments. By this approach, individual functions of the miRNA could be probed separately. While the wild type replicon did only replicate in presence of wild type miRNA, but not with A4U, the control replicon with mutations in both UTRs exhibited the inverse phenotype. Surprisingly, abrogation of the interaction of miR-122 at the 5' end (i1 m1,2) only had a slight negative effect on replication, which could be restored by addition of the rescue miR. In contrast, the mutations in i2 affected replication more dramatically. In presence of wild type miRNA only basal levels of replication could be achieved. However, the replication of this mutant could be rescued by co-transfection of the mutant miR-122. The replication kinetics of the dual luciferase replicons, as measured by *firefly* luciferase expression, differed from those observed with other bicistronic replicons in earlier experiments . Therefore, direct detection of the viral RNA was performed by northern blotting, in order to see whether RNA integrity or replication were affected. Also at the RNA level, the dual luciferase reporters exhibited slightly delayed kinetics, and a lower replication efficiency compared to a monocistronic replicon (**fig. 5.17**D). In addition, it was noted that a lower molecular weight band appeared after 48 h, which was approximately the size of a monocistronic construct (**fig. 5.17**D, asterisks). Over the course of 72 h this truncated RNA gained intensity in the wild type replicon, and became the dominant fraction. Both point mutants showed lower maximal luciferase activities in the previous assays, which was also reflected in decreased RNA levels. However, the lower band was also detectable at 48-72 h in the i1 m1,2 and at 48 h in the i2 m1,2 mutant (**fig. 5.17**D). This could
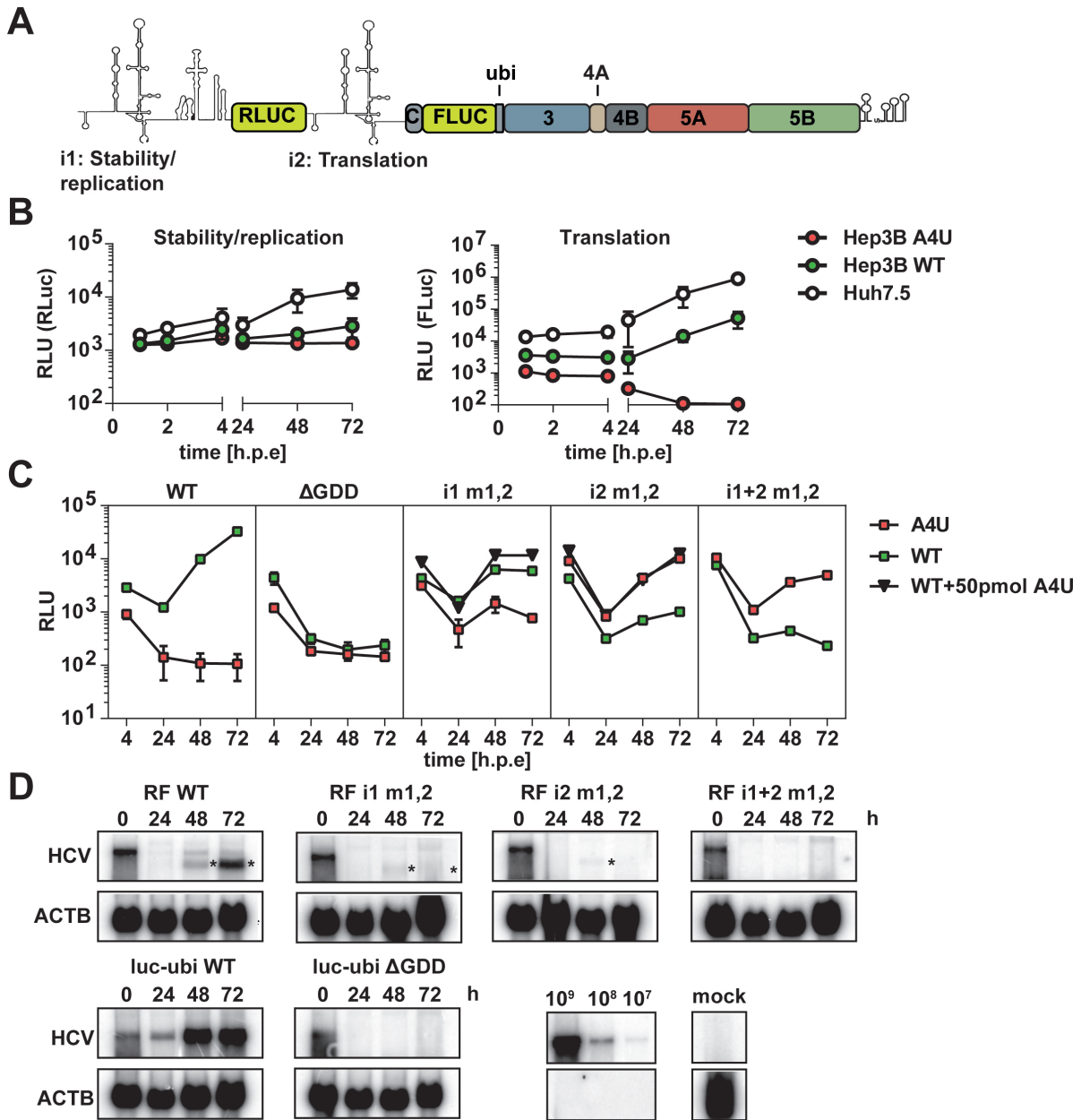
Figure 5.17.: Quantification of miR-dependent translation and replication. A | Schematic representation of the dual luciferase replicon. **B |** *Renilla* and *firefly* expression after electroporation in Huh7.5 or Hep3B cells. **C |** Replication capacity of dual IRES replicons upon miR-binding site mutation of IRES 1 (i1 m1,2) and 2 (i2 m1,2)in Hep3B cells stably expressing miR-122 WT (green squares) or A4U (red squares). To define the maximal replication capacity for the single IRES mutants, miR-122 A4U duplex was co-electroporated into miR-122 WT producing cells (black triangles). **D |** Northern blot detection of viral RNA over 72 h in Hep3B cells, supplemented with miR-122 WT. Body-labeled radioactive RNA probes directed against the coding region of the NS-proteins was used to detect HCV RNA. β-Actin served as a loading control. Upper panels: RNA amounts of wild type and point mutants of the dual- luciferase construct. Truncated RNAs, which appeared for the RF replicons after 48 h, are marked with an asterisk. Lower panels: monocistronic replicon (luc-ubi) wild type and ΔGDD were used as controls. Fixed amounts of *in vitro* transcribed replicon RNA were loaded as standard. Mock electroporated Hep3B cells were used as negative control.

hint towards a recombination event, which occurred at early time points (4-24 h), and gave rise to a monocistronic fragment, likely consisting of the second cistron. Possible mechanisms would be a homologous recombination at SLI, or internal initiation of the viral RdRP at the start of the second cistron during (+)-strand synthesis. In both cases, the *renilla* luciferase gene would have been removed in the majority of replicating RNAs, which consequently accounted for the strong differences of *firefly* and renilla *activities*.

Overall, the results of the comparison between the different mono- and bicistronic replicons showed that HCV can only replicate in absence of miR-122, if translation is not mediated by the HCV IRES. This finding emphasized the importance of initial translation during the HCV replication cycle. However, a detailed quantification was not yet possible, due to recombination events within the used dual luciferase replicon.

5.2.2. Sequences and Structures in Domain I of the 5' UTR Necessary for Translation

As the results of the previous experiments pointed towards a strongly translation-associated effect, we asked, how miR-122 can enhance translation efficiency by binding to domain I of the IRES. However, removal of domain I has no negative effect on IRES function[240]. Furthermore, it is known that optimal activity of the HCV IRES depends on its secondary and tertiary structure[247] (**fig. 5.18**A, B). The complementary 3'(-) region adopts a well-described and functionally relevant fold[244] (**fig. 5.18**D). Particularly the region containing the terminal 150 nt is essential for replication, and disruption of the secondary structure leads to severe loss of viral fitness. Therefore, the highly structured shape of the complementary region (SL-IIz') opposes the paradigm of a completely relaxed state on the (+)-strand. Consequently, domain I might adopt a fold, which interferes with the formation of essential structures in the IRES. Especially the adjacent SLII could be affected, resulting in a dysfunctional IRES. Based on this hypothesis *in silico* folding of the first 120 nucleotides was performed, which include domain I and II. Interestingly, all tested algorithms predicted a stem-loop, encompassing nucleotides 21-105, which are exactly the borders of the 3'(-) SL-IIz' as energetically most favorable option (**fig. 5.18**C). Obvious similarities were observed between the base (nts 21 - 35, 85 - 105) and tip regions (nts 48 - 65) of the hypothesized domain I/II stem-loop and the corresponding structure on the 3'(-) end (**fig. 5.18**C, E). This is not particularly surprising, since it can be assumed that complementary sequences will likely adopt similar shapes, except for parts where U:G base paring occurs. Strikingly, all five U:G base

pairs within the 3' terminal 120 nucleotides are clustered within a 9-base pair stretch (**fig. 5.18**E). Accordingly, this central part of the (+)-strand counterfeit of SLIIz' is strongly destabilized and expected to assume a single stranded conformation. It is also worth noting that this segment overlaps exactly with the second seed binding region for miR-122. The reported fold of domain II (**fig. 5.18**A, B) could not be obtained, unless additional constraints were applied. Strikingly, disallowing the nucleotides involved in miR-122 binding to form base pairs, prevented the domain I structure and yielded the functional fold of the IRES. These predictions indeed suggested that miR-122 binding to the 5' UTR of the HCV positive strand might contribute to the correct folding of the IRES. As mentioned above, the *in silico* model predicts a fold closely related to the 3'(-)
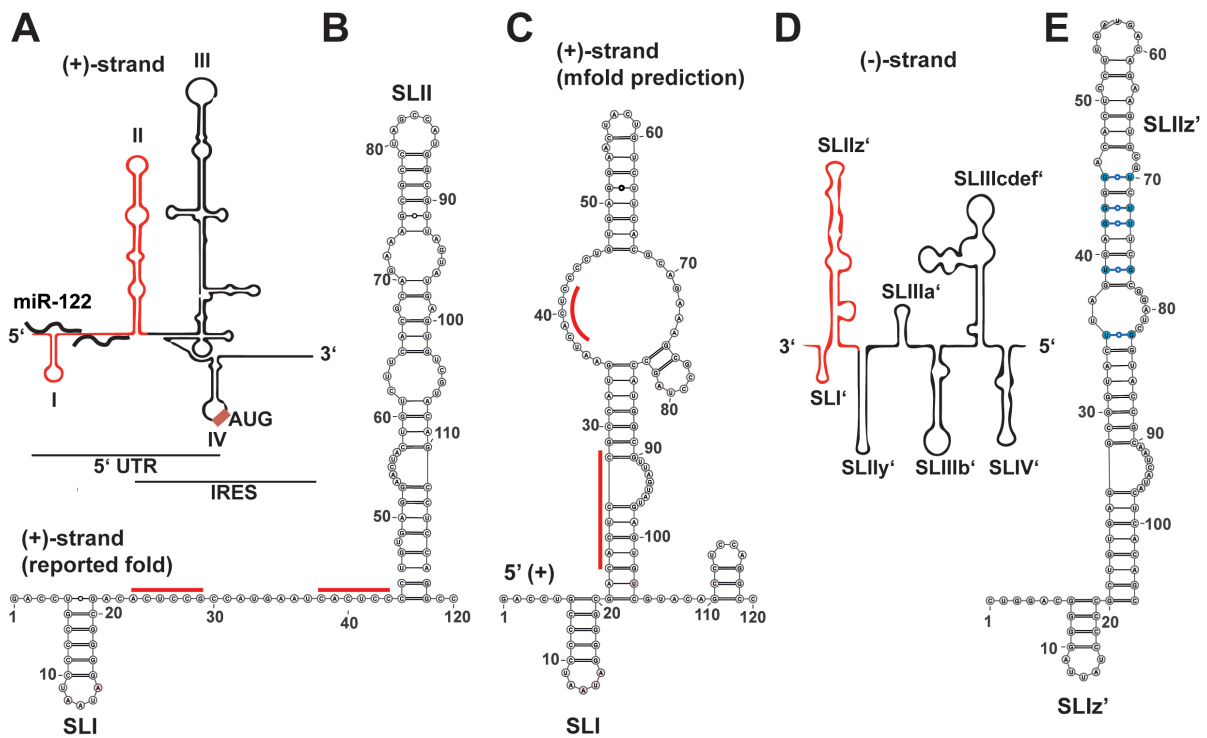
Figure 5.18.: *In silico* **analysis of domain I/II of the HCV 5' UTR. A |** Schematic representation of the complete 5' UTR and IRES of HCV. The two miR-122 binding sites within domain I are indicated. The region of domain I and II, which was used for *in silico* prediction is colored in red. **B |** mfold prediction of the first 120 nt of the HCV (+)-strand, when both seed binding sequences (indicated by red lines) were prohibited from forming base pairs. **C |** The same sequence as in **B**, but without constraints. Seed binding sequences are again marked with red lines. **D |** Schematic representation of the complementary sequence to the 5' UTR at the 3'(-) end. The region, which was used for *in silico* prediction is colored in red. **E |** mfold predicted structure of the 3' 105 nt of the (-)s-strand. U:G base pairs are depicted in blue.

end structures. Therefore, the results obtained in the *in silico* analysis conflicted with the commonly proposed structural model of domain I/II. Hence, the structure of this region was examined in greater detail. In order to experimentally address the structure of the 5' 120 or 389 nt, these RNA fragments were *in vitro* transcribed and gel purified. The purity and integrity of the resulting RNA was checked by urea PAGE, and staining with methylene blue. The obtained RNA was free of appreciable contamination and could be isolated in satisfactory yields (**fig. 5.19**A). Prominent secondary structures, and hybridization of miR-122-5p to its target under the chosen *in vitro* conditions, were investigated by native PAGE, stained with methylene blue. As a non-binding control, the complementary strand of the miR-122 duplex (3p) was used. It was observed that miR-122-5p does bind to both fragments, as the target RNA shifted to a higher molecular weight, and concurrently the miR-122-5p band showed decreased intensity, compared to the 3p-control (**fig. 5.19**B, C). Seven distinct bands were observed for the 389 nt fragment, pointing towards a number of secondary structures (**fig. 5.19**B). Importantly, no lower molecular weight bands were detected in the denaturing gel, arguing against truncated/abortive fragments in the preparation. In this setting, no change of the band pattern was observed between the miR-122-5p or -3p condition. Expectedly, the 120 nt RNA presented a much cleaner picture in the native gel, since there are fewer options for intramolecular interactions. However, at high contrast three more bands could be detected (**fig. 5.19**B). The quantification of bound miR molecules to their target showed that both miR-binding sites were occupied on the 389 nt, while only one site was bound efficiently on the 120 nt fragment. This might be a result of the lower miR:template ratio ($\approx$2:1) , compared to the 389 nt fragment ($\approx$8:1). These data provide evidence that indeed the 5' UTR can fold into several different structures. In addition, miR-association was possible under the chosen *in vitro* conditions, and likely both binding sites were recognized, given a sufficient molar excess of the miR over its respective target. However, post-folding binding of miR-122 seemed not capable of resolving the non-canonical folds of the 5' UTR.

A more sophisticated approach was applied with the help of our collaboration partners in Grenoble, where the smaller fragments should be analyzed by NMR. This technique is able to discern dynamic states of a macromolecule in solution. The general principle is the measurement of energy transfer from an external magnetic field to atomic nuclei. Nuclei of ^{1}H, ^{13}C or ^{15}N can be excited, due to their specific spin and energy properties. When these atoms relapse into their basal energy state after application of the force field, the emitted energy can be recorded. The exact energy that acts upon a specific nucleus is
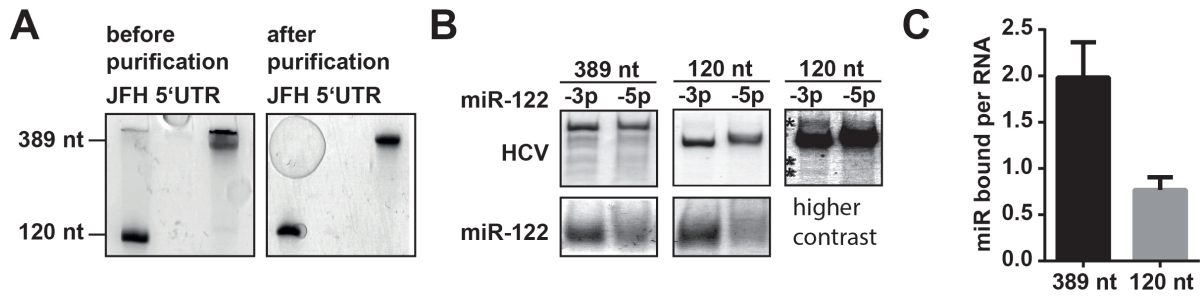
Figure 5.19.: Characterization of HCV 5'UTR fragments. A | Denaturing urea PAGE with ~1 µg of *in vitro* transcribed RNA, before and after gel purification. **B** | Native PAGE using 1.5 µg of the 389 nt (≈12 pmol) and 120 nt (≈40 pmol) fragment after denaturation and refolding for 15 min at 37°C in presence of 100 pmol miR-122-5p or -3p (non-binding control). **C** | Quantification of miR molecules bound to the respective target RNA. Calculation was done by comparing the density of miR-122 signals between the binding and the non-binding control.

dependent on the surroundings, i.e. other nuclei and electrons, which influence the local magnetic field. Therefore, the excitation state and consequently the emitted frequencies vary between different atoms in a higher order structure, and give an individual spectrum for each molecule.

First, we optimized the RNA production to generate large amounts of highly pure RNA. Apart from the full-length IRES (389 nt), three truncations were generated: the first 120 nucleotides, comprising domain I and II, only the SLII sequence (40-120) and one harboring the predicted alternative structure (1-105). These samples were used to record 1D ^{1}H spectra. In this case, only the hydrogen atoms engaged in the imino bonds between the bases were specifically activated by the magnetic field. Therefore, each peak in the obtained spectrum should theoretically represent one imino bond. However, only the hydrogens of U:G and C:G base pairs (and some non-Watson-Crick pairings), are easily detectable. U:G pairs will result in a double peak, while C:G only gives a single peak. The experiments were performed at 6.6 mM $MgCl_2$, and several temperatures from 5 to 30°C. Strikingly, while the linewidth usually is reduced at low temperatures, in the case of the 120 nt and 105 nt fragments, the spectrum became very noisy. This can be due to different conformers, which are trapped in their current state at low temperatures, when the available energy is increased the most stable structure is favored, and thus becomes the dominant spectrum. This hypothesis was further supported by the fact that this temperature dependence was not seen for the SLII fragment (40-120), which is predicted to strongly favor a particular secondary structure (**fig. 5.20**A). After the determination of optimal recording conditions, the 1D spectra of each fragment was
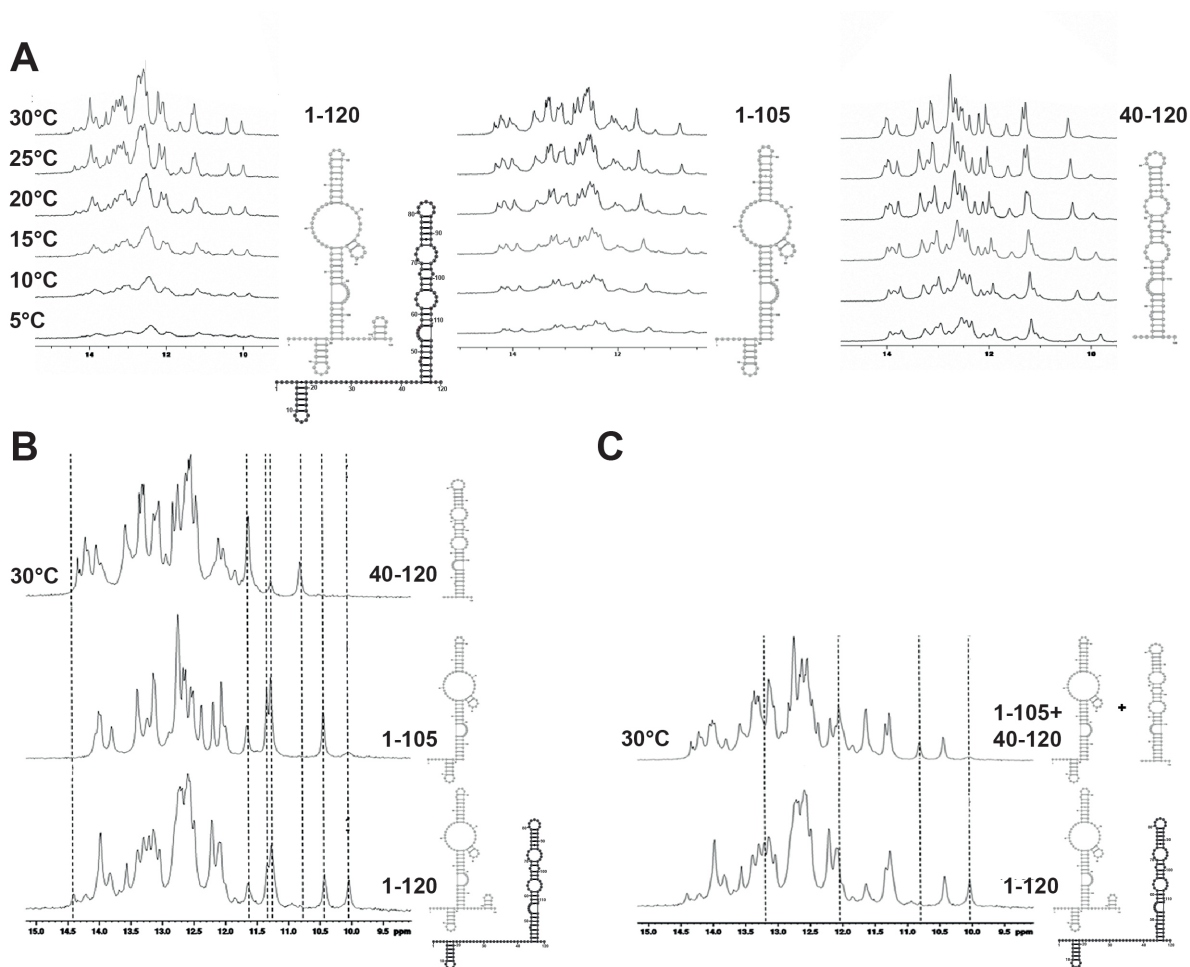
Figure 5.20.: 1D NMR spectra of HCV 5'UTR domain I and II. A | To assess the optimal temperature for the following experiments, 1D ^{1}H spectra of the first 120 nt of the HCV 5' UTR were recorded at 5 to 30°C. The RNA concentrations used in this initial experiment were 0.8 to 1.2 mM. **B |**. Comparison of 1D ^{1}H spectra recorded of three truncations of the HCV 5' UTR, 1-105 (1.2 mM), 40-120 (0.8 mM) and 1-120 (0.3 mM) at 30°C. **C |** While some mismatches remain, the combination of peaks generated in **B** fit the 1-120 spectrum considerably better than the ones obtained for the individual sub-fragments. Mismatched peaks are marked with a line. The corresponding predicted folds for each construct are depicted at the respective spectra. Since the 120 nt fragment is likely present as ensemble of conformers, the predicted and the canonical structure are shown.

compared. There was no strong overlap between each individual peak map. However, several peaks missing in the 120 nt spectrum, as compared to the others could be restored by addition of both fragments, even though not all signals could be matched (**fig. 5.20**B, C). While the 1D spectra are a good indicator whether two structures are identical, it is not possible to assign a peak to a specific base pair. This means, even closely related structures can have very different spectra. In order to determine specific secondary structural elements, 2D NMR was performed (**fig. 5.21** and **fig. 5.22**). The optimal temperature for the 120 nt construct was determined to be at 30°C, while in contrast to the 1D spectrum, the 105 nt fragment gave varying signals, the strongest one at 15°C, which was used for analysis in this experiment.

Here, the signals come from the imino bonds (ω_1), and the magnetization transfer between hydrogen atoms in close proximity (ω_2). As expected, several characteristic peaks for the SLII stem-loop were detected, in the 120 nt fragment as well as in 40-120 nt truncation. There were only few peaks that were missing in the 40-120 template, which are likely representative of the SLI stem. This is corroborated by the fact that the 105 nt RNA did not present the SLII peaks, however, the signals absent in the 40-120 nt fragment could be seen. The rest of the cross-peaks did not show any overlap, which is in line with the predicted abolishment of SLII in this mutant (**fig. 5.22**).

Overall, these experiments in conjunction with the native gel analysis could provide further evidence for the existence of an ensemble of structures in solution, which could be influenced by association of miR-122 to the RNA. Moreover, it seems that the alternative states are not defined as one or two stable conformations, but rather the dynamic transition of a number of structures, with the canonical fold as a dominant fraction. Only such a model would explain the fact that most of the signal is lost in the background.

In parallel, SHAPE was used as an approach (**fig. 5.23**) to verify the architecture of domain I and II biochemically[305]. This type of structure probing relies on stochastic chemical labeling (acylation) of flexible nucleotides. In a subsequent reverse transcription reaction, the polymerase stalls at these modified residues, giving rise to several fragments, which can be separated on a denaturing gel. Each band will thus represent a nucleotide not engaged in a higher order structure. Since most complex RNAs in solution can adopt numerous folds, depending on the thermal energy of the surroundings, this will also be reflected in the band pattern. Therefore, the *SFold* algorithm was used, which can produce a histogram plot with the probabilities of a nucleotide being free, based on the 1000 thermodynamically most favorable structures of a given RNA[306]. Interestingly, while the overall SHAPE pattern was similar to previously published data, the mapping
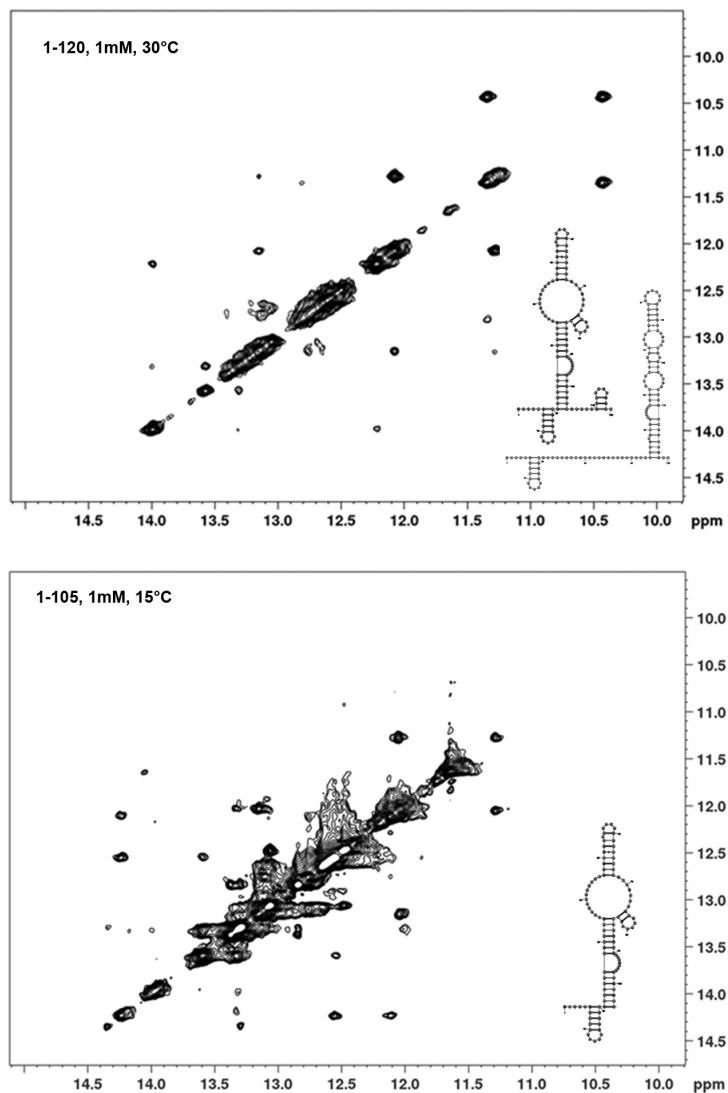
Figure 5.21.: 2D 1H-1H-NOESY spectrum of HCV 5'UTR fragments. 2D 1H-1H-NOESY spectra were recorded for the 120 (top) and 105 nt (bottom) fragments. The temperatures at which the measurement was performed is indicated. The mfold predicted structures are shown as inset. Since the 120 nt fragment is likely present as ensemble of conformers, the predicted and the canonical structure are shown.
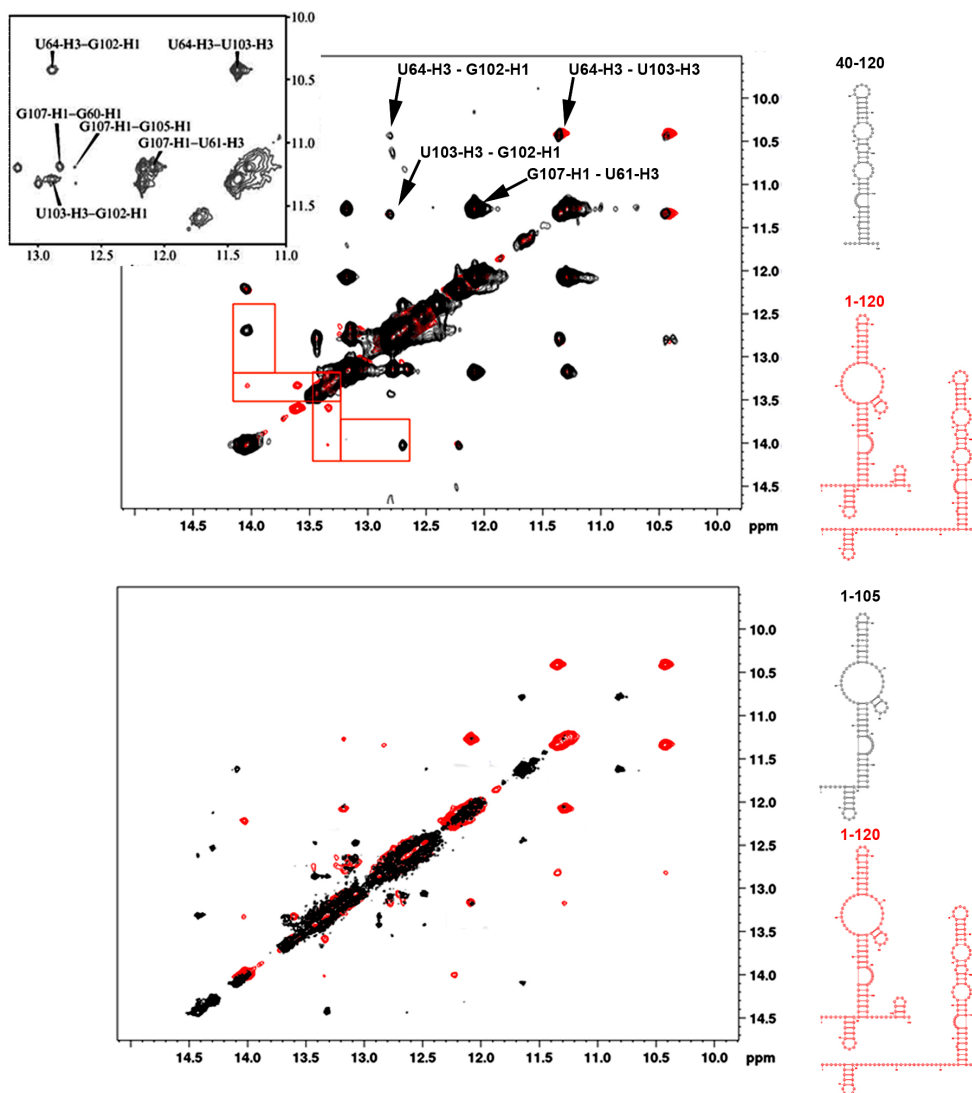
Figure 5.22.: Comparison of 2D NMR spectra of the different fragments. Overlay of the 40-120 nt part, resembling SLII, with the full 120 nt fragment (top). Mismatched singular peaks are marked with a red box. Characteristic cross-peaks, which indicate the presence of SLII (arrows) are indicated. The inset shows the corresponding region of the original publication, in which they were first described (Lukavsky et al.[250]). The lower panel shows the overlay of the 120 nt and 105 nt fragments. The mfold predicted structures are shown on the right. Since the 120 nt fragment is likely present as ensemble of conformers, the predicted and the canonical structure are shown.

of reactive nucleotides against the current folding model revealed significant mismatches (**fig. 5.23**A,B). Some of these could be resolved by fitting to our predicted alternative structural element, especially the lack of reactivity of residues 20-35 and 61-65, whereas some inconsistencies remained. The most striking unresolved peak in reactivity (nts 49-51) was included as a constraint in the following prediction refinement(**fig. 5.23**C-E). This small change was sufficient to favor a structure even more closely resembling the SLIIz' stem loop, with a much smaller central bulge, however, still containing the complete seed binding region. Moreover, this led to a better overall fit of experimental data and predicted structure. The final structure only contains minor regions ($<=4\,$nt) which are not reactive. Only the region between nt 90-98 shows no labeling, while it should be accessible in the predicted, as well as in the published fold. This could also be a result of tertiary structure or intra-/intermolecular interactions.

To further test the involvement of domain I in the IRES formation, we created a panel of mutants to stabilize or destroy SLII of the IRES. Hence, all mutants had at least one defective miR-binding site. The structures of all designed constructs were tested by *in silico* predictions. In addition, some were tested for the predicted fold using native PAGE analysis and SHAPE chemistry. An obvious approach to disrupt the putative interactions of the miR-binding region (MBR) with other downstream sequences is to delete it completely (**fig. 5.25**). It is also an approximation of the canonical IRES element, which additionally lacks SLI. Further increments of shorter deletions were also created ($\Delta15$, $\Delta10$), all starting at nt 21, to functionally map relevant sequences in this region in more detail. Besides the deletion variants, several mutations were designed: One class was modified by changing short sequences within domain I to adenine, thereby preventing their original bonding with other sequences. Either five (pA5) or ten (pA10) adenines were inserted starting from position 21. Another method was the introduction of stable stems in the supposedly relaxed region of domain I. This was either achieved by changing nts 31-40 to the reverse complement sequence (C(omplementary) mutant, **fig. 5.26**), or by replacing the sequence between nt 21 to 35 with a C:G-hairpin. All of these sequences stabilized the canonical SLII fold, according to mfold prediction. Also, two negative controls were created. The M25 mutant was predicted to destroy the alternative fold, but not stabilize SLII. The ISL construct (inhibitory stem-loop) was modified in the region of the U:G cluster, to eliminate the central bulge in the proposed alternative structure, and therefore stabilize this form (**fig. 5.27**). In the following, a set of three mutants ($\Delta20$, C, and ISL), which will be in the focus of this study, is described in more detail.
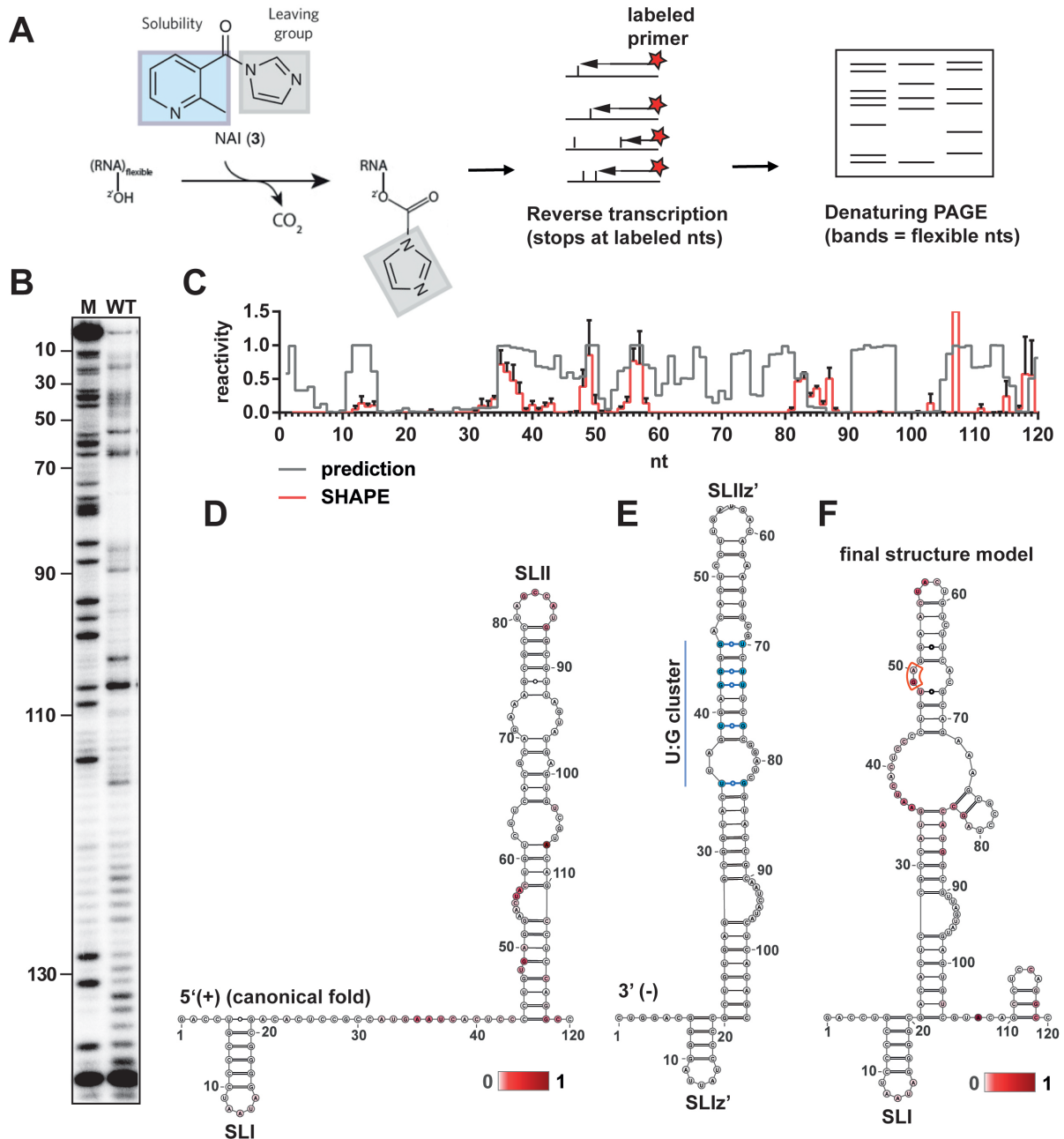
Figure 5.23.: SHAPE analysis of domain I/II of the HCV 5' UTR. A | Schematic of the SHAPE method. NAI can transfer its leaving group to flexible nucleotides. Modified residues will terminate the following RT reaction with a radioactively labeled primer. The resulting fragments were visualized by auto-radiography after urea PAGE. **B |** Representative auto-radiography image for the WT sequence at 1 mM $MgCl_2$. Marker (M) shows all A residues. **C |** Plot of SHAPE reactivities (red line) against the predicted probability of the respective residue being single stranded (gray line, generated by SFold). Shown are means with S.E.M. of 3 independent experiments. **D |** Overlay of SHAPE reactivity with the canonical model of the first 120 nt of the HCV positive strand. Nucleotides are colored white to red, according to their average normalized SHAPE reactivity. *In silico* folding was performed with the mfold online tool. **E |** Structure prediction of the 3'(-) SLIIz'. U:G base pairs are depicted in blue (U:G cluster). **F |** Predicted 2D structure with incorporation of SHAPE-based constraints in the folding prediction.

First, it was tested, whether the mutants also showed the extensive range of secondary structures, which was observed in the wild type RNA. The mutations were designed to stabilize a specific form of the structure, which should result in a suppression of the additional bands in the gel. Indeed, the mutant RNAs presented themselves as a single band, without appreciable alternative forms on a native gel (**fig. 5.24**B). Quantification of the major "top" band and the lower bands could however not detect a difference in the band pattern between incubation with the non-binding (3p) or binding (5p) strand of miR-122 (**fig. 5.24**B).
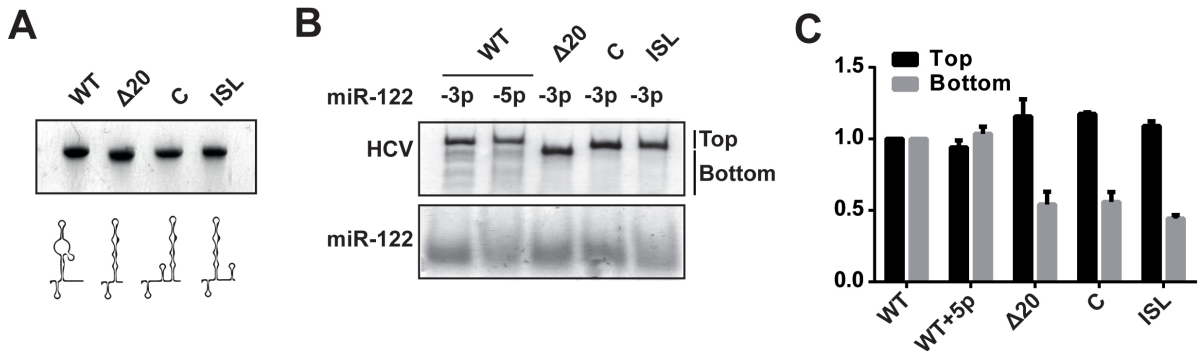
Figure 5.24.: Characterization of HCV 5'UTR fragments. A | Denaturing urea PAGE with ∼1 μg of different variants of the *in vitro* transcribed 389 nt HCV 5' UTR/IRES fragments, stained with methylene blue. Shown are wild type, Δ20, C and ISL RNA after gel purification. Below are the mfold predictions for the first 120 nt of the respective construct. **B** | Native PAGE of the 389 nt fragment after denaturation and refolding for 15 min at 37°C in presence of miR-122-5p or -3p (non-binding control). RNA was stained with methylene blue. **C** | Quantification of "top" and "bottom" bands as indicated in *B*. Densities were normalized to wild type and miR-122-3p. Error bars represent SD from quantification of two gels from the same sample.

Δ20

Δ20 mutant was designed as approximation of the canonical IRES sequence, omitting possible interactions of domain I with downstream sequences. Only the small stem-loop SLI was retained, and nucleotides 21-41 were deleted. Via SHAPE structure probing, the construct was tested for its correct fold. This construct was predicted to strongly favor SLII formation, while completely lacking any miR-122 recognition sites. **fig. 5.25** shows the rationale of mutant design and structural probing by SHAPE. Most predicted free nucleotides were detected, with the exception of two small bulge regions around nt 65 and 73 (**fig. 5.25**A, B). In the secondary structure view, the nucleotides are colored

according to their SHAPE reactivity (**fig. 5.25**C). The predicted fold of SLII is identical between the mutant and wild type (**fig. 5.25**D).
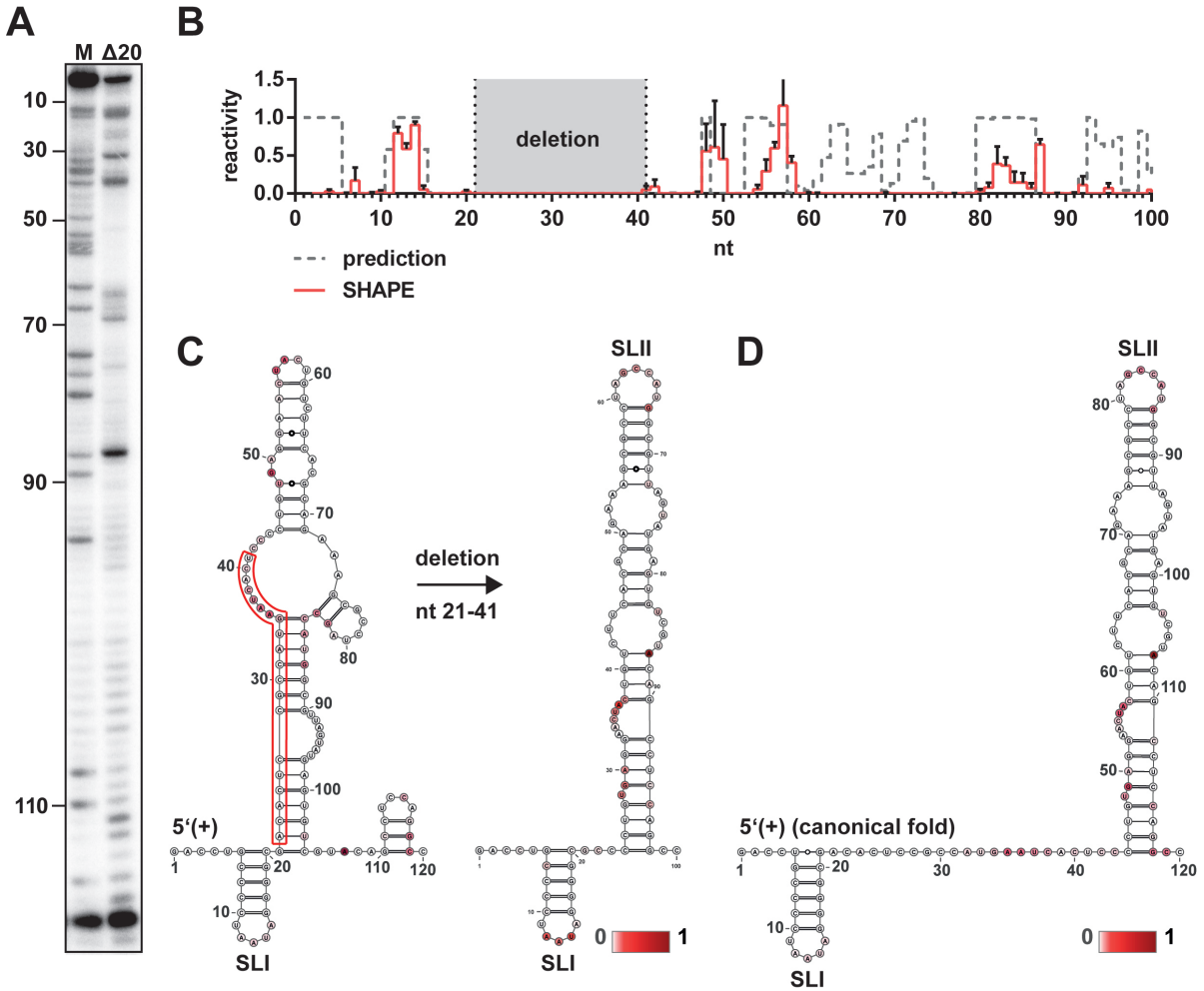
Figure 5.25.: Characterization of the Δ20 mutant. A | Representative autoradiography image of the SHAPE pattern at $1\,\text{mM}$ $MgCl_2$. Marker (M) shows all A residues. **B |** The corresponding histogram plot with the average normalized reactivities of 2 independent experiments. Error bars represent S.E.M. **C |** Secondary structure prediction of the first $120\,\text{nt}$ of HCV in the native state and impact of the deletion. Region of the mutation is marked with a red box. **D |** Canonical fold of the HCV 5'UTR domains I and II. SHAPE reactivities as determined in **fig. 5.23** are indicated.

C

The C mutant was designed following a different scheme, in order to keep length and complexity of the sequence constant. A small stem-loop was introduced into the MBR

by exchanging the region predicted to be involved in the alternative structures, including parts of miR-binding site #2, by its complementary sequence (**fig. 5.26**C). This should force a strong interaction, which would compete with the translation attenuating conformations, thereby also favoring the SLII fold. Importantly, site #1 remains intact, but is also engaged in a stem-loop, as it is predicted for the wild type (**fig. 5.26**C). The SHAPE data mostly confirmed the predicted fold, while again the region around nt 70 was not efficiently labeled, as seen for the wild type and $\Delta 20$ alike (**fig. 5.26**B). The loop of SLI was hardly visible in this mutant, but detectable (**fig. 5.26**A). Also for this mutant, the predicted structure of domain II was in agreement with the functional SLII fold (**fig. 5.26**D).

ISL

The inhibitory stem-loop mutant was generated to serve as a negative control. Since a stem-loop resembling the 3'(-) fold was predicted to be the energetically most stable conformation, however, bearing a large bulge in the central region of the stem, nucleotide exchanges were introduced in this segment to stabilize this structure (**fig. 5.27**C). This intervention destroys site #2, site #1 remains unaffected. Since this mutant should not be able to form SLII efficiently, it is expected that translation will be greatly diminished. The SHAPE pattern showed a high reactivity between nt 90 and 120, which correlated very well with the predicted fold. However, the RT reaction was much less efficient for the subsequent nucleotides. Most predicted regions showed some reactivity on the gel, but due to the following normalization process these could not be appreciated in the histogram plot (**fig. 5.27**A, B). Still, the qualitative pattern supported the desired fold of this mutant.

In summary, the native gel analysis as well as SHAPE data argued for the desired fold of the tested mutants, even though some regions were not as efficiently labeled as expected. In particular, the mutants seemed to suppress the various secondary structures, which could be detected in the wild type. Therefore, domain I seemed to participate in folding of the HCV IRES.

Functional Characterization of Domain I Mutants

Overall, the experimentally determined structures of the mutants seemed to be in good agreement with the calculated ones. In a subsequent effort to functionally characterize the mutants, their replication capacity was tested in a monocistronic context(**fig. 5.28**).
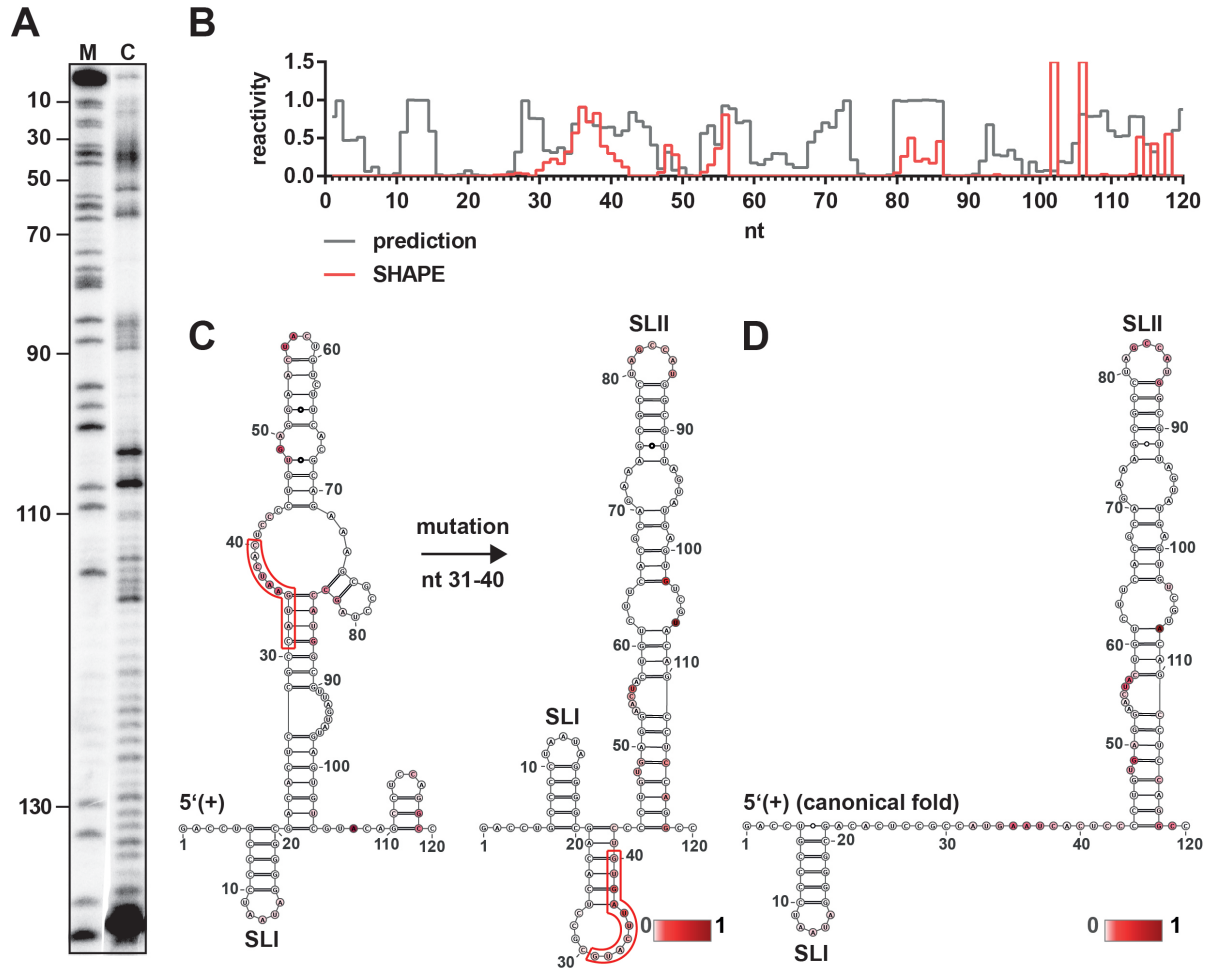
Figure 5.26.: Characterization of the C mutant. A | Representative autoradiography image of the SHAPE pattern at 1 mM MgCl$_2$. Marker (M) shows all A residues. **B |** The corresponding histogram plot with normalized reactivities. **C |** Secondary structure prediction of the first 120 nt of HCV in the native state and impact of the mutation. Region of the mutation is marked with a red box. **D |** Canonical fold of the HCV 5'UTR domains I and II. SHAPE reactivities as determined in **fig. 5.23** are indicated.
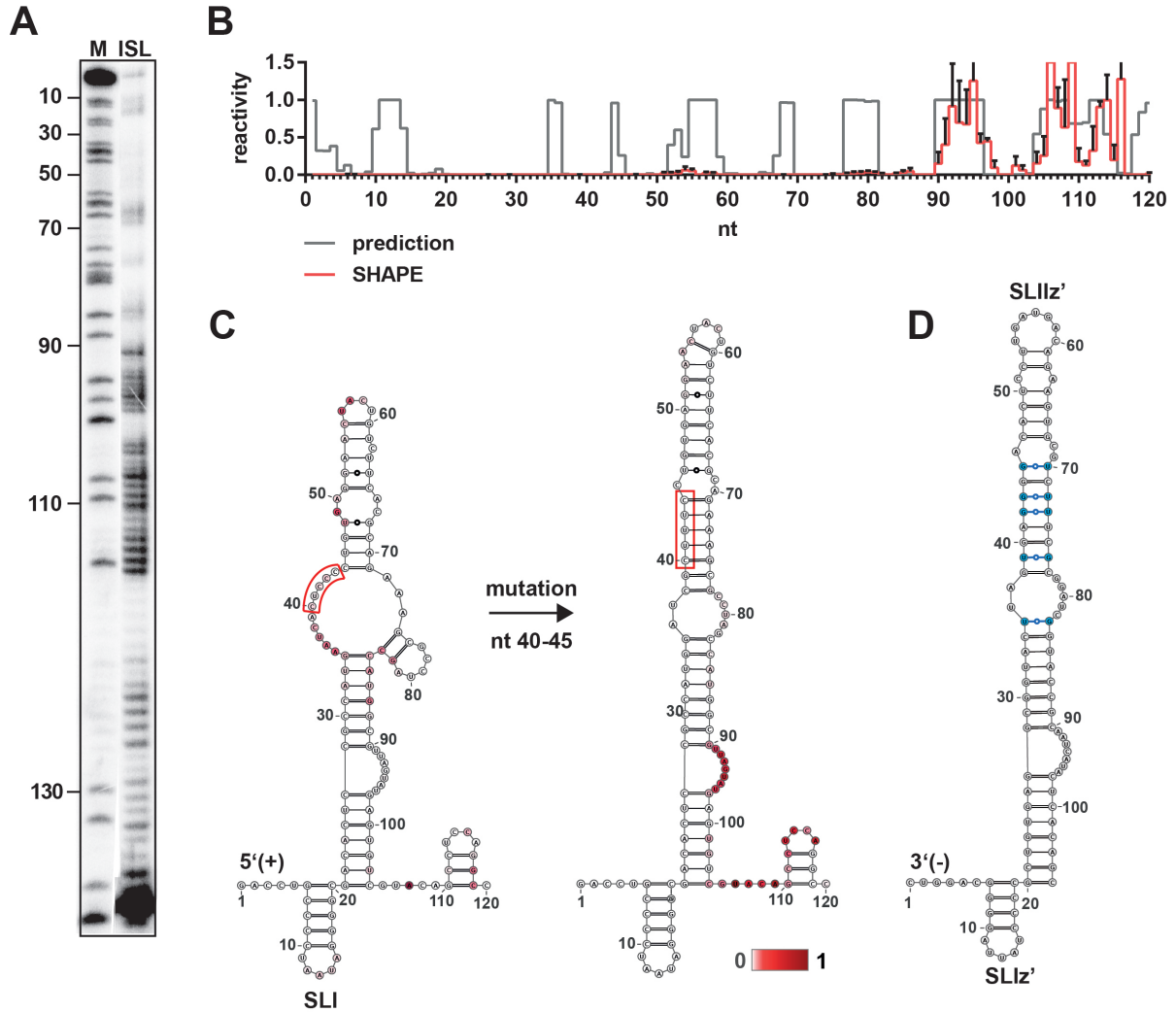
Figure 5.27.: Characterization of the ISL mutant. A | Representative autoradiography image of the SHAPE pattern at $1\,mM$ MgCl$_2$. Marker (M) shows all A residues. **B |** The corresponding histogram plot with the average normalized reactivities of 2 independent experiments. Error bars represent S.E.M. **C |** Secondary structure prediction of the first 120 nt of HCV in the native state and impact of the mutation. Region of the mutation is marked with a red box. **D |** Fold of the complementary 3'UTR stem-loops I and II.

Mutations in domain I likely disrupt structure elements in the 3'(-) end, which are critical for replication. All but one of the mutants were replication deficient. Only the pA5 mutant could replicate to low levels even in absence of miR-122 (**fig. 5.28**pA5), and will be investigated further in future experiments. Preliminary *in silico* analysis suggested that this mutant leaves a significant part of the structural elements of the 3'(-) end intact, which might be sufficient to explain this phenotype.
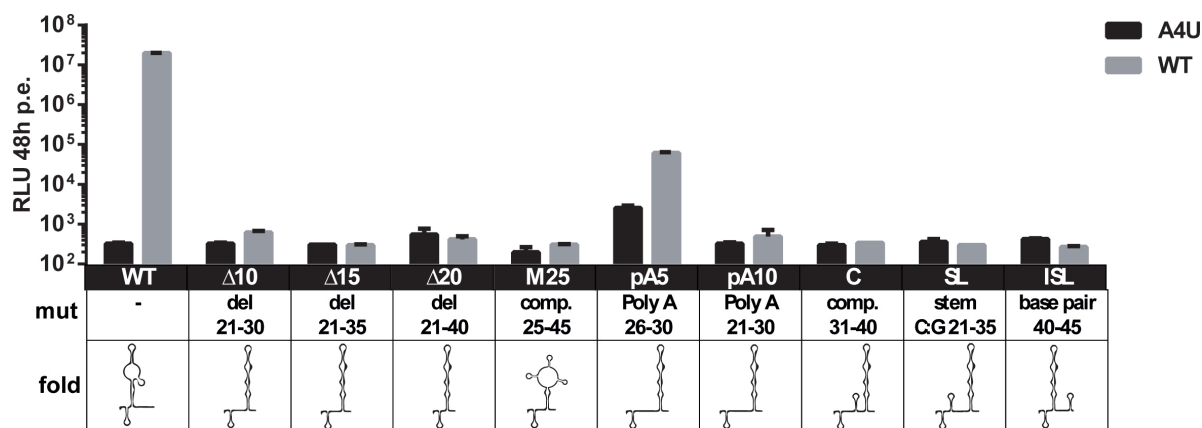
Figure 5.28.: Replication capacity of domain I mutants. Hep3B cells were electroporated with JFH-1 monocistronic replicons in presence of synthetic miR-122 WT or A4U. Cells were lysed and luciferase activity (RLU) was measured after 4 h (input control, not shown), and 48 h at the peak of replication activity. The replication deficient ΔGDD (deletion in the catalytic center of NS5B) mutant served as negative control. The upper panels of the table show the location and type of mutation for each construct, as well as the thermodynamically most stable structure calculated with mfold.

The mutants, which were predicted to abolish alternative structures interfering with IRES function, and instead form the SLII stem-loop, were chosen for translation experiments (**fig. 5.29**A). To this end, all mutant IRES elements were introduced into a replication deficient monocistronic replicon, transfected into Hep3B cells, in presence of wild type or A4U miR-122. In parallel, a capped RNA coding for renilla luciferase was transfected, to assess transfection efficiency. Translation was quantified at early time points after transfection via the ratio of firefly to renilla activity. This allowed to measure the combined impact of translation and stability. Importantly, all SLII-forming mutants showed increased translation at early time points, without any measurable effect of miR-122 addition. The most striking phenotype was observed for the Δ20 mutant, devoid of the complete miR-binding region. Here, the translation activity 1 h post electroporation was enhanced to several fold above the wild type replicon in presence of miR-122. This effect proportionally declined with the size of the deletion (Δ15, Δ10). While the Δ20

mutant showed up to 5-fold increased translation activity, excision of 15 nt could only raise the luciferase levels by approximately 3-fold. Finally, the 10 nt deletion mutant showed 1 h values close to the wild type in presence of miR-122 (**fig. 5.29**B, Δ10 - 20).

Similarly, introduction of short adenylate stretches in the base of the predicted alternative structure enhanced translation at 1 h post electroporation. These mutants should be structurally identical to the wild type with bound miRNA. Indeed, also the initial translation efficiency was comparable to wild-type. Interestingly, the pA5 mutant was even more efficient at 1 h post electroporation, than pA10 and the wild type control (**fig. 5.29**B, pA5, pA10).

In another approach, the MBR was mutated to form stable secondary structures (**fig. 5.29**B, C, SL), which would also abolish the interactions with downstream sequences. As for the other mutations, early phase translation was enhanced to positive control levels. There was no difference in the behavior between these mutants.

Both controls showed the expected behavior, the random mutation control (**fig. 5.29**B, M25) could not increase translation significantly over the level of wild type without miR-122. This phenotype could not be rescued by addition of miR-122 WT. Moreover, the SLII disrupting ISL mutant decreased translation efficiency even further (**fig. 5.29**B, ISL). The observed reduction of luciferase activity was possibly due to changes in translation efficiency, or reduced stability upon degradation by exonucleases. To assess the quantitative effect of the reported miR-122 mediated protection from the exonucleases Xrn1 and Xrn2, short term northern blot kinetics of selected mutants were performed. Importantly, the reported stabilization of the wild type RNA could also be detected in Hep3B cells. However, correlation could be observed between stability of each construct and its translation efficiency (**fig. 5.30**). Indeed, the Δ20 mutant with the strongest translation phenotype was the least stable. In contrast, the ISL mutant was very stable, but could not be translated efficiently. This anti-proportional phenotypes could argue for a translation-dependent decay mechanism in absence of RISC binding.

In summary, in these experiments the predicted and partially validated stabilization of SLII correlated strongly with increased translation. In contrast, mutants which did not form SLII or even actively disturbed this structure, could not enhance translation, or even reduced it, respectively. Therefore, it was concluded that the structure played a significant role in the process. Moreover, the influence of stability on wild type HCV RNA could be reproduced in Hep3B cells. However, the increased translation of the mutants seemed to be independent from this effect, because mutants, which lacked miR-122 binding, and at the same time showed enhanced translation activity, were degraded
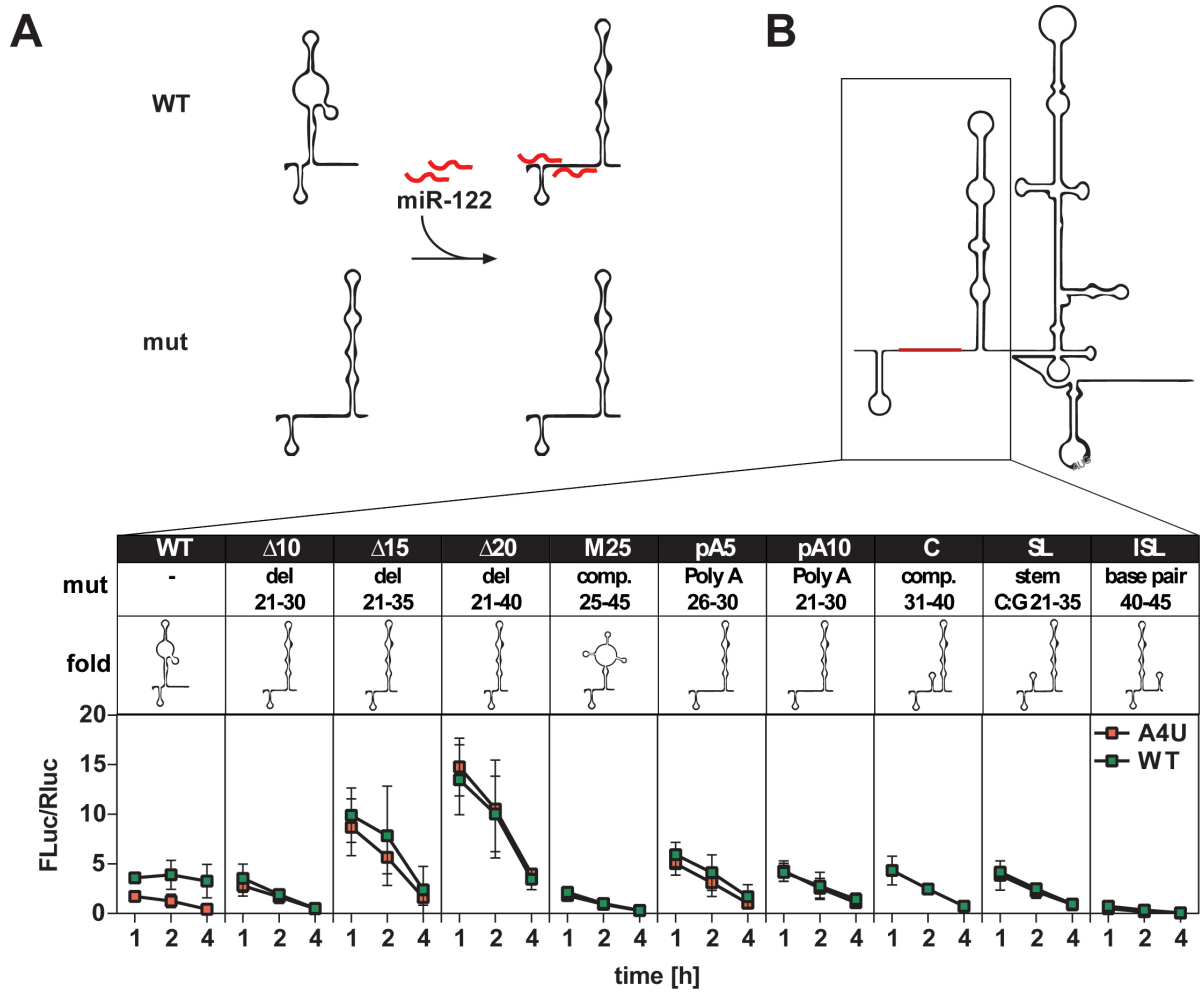
Figure 5.29.: Role of domain I in translation. A | Proposed structural switch by miR-122 in the context of WT, and design of mutants, which should stabilize the translation stimulating fold without the need for miR-122. *In silico* folding was used to predict the most stable conformation of all mutants. The mutations were then introduced into replication deficient replicons (luc-ubi ΔGDD). **B |** Overview of the HCV 5' UTR and IRES. The box indicates the first 120 nt, containing domain I and II in the reported fold. The red line indicates the region harboring the mutations. The upper panels of the table show the location and type of mutation for each construct, as well as the thermodynamically most stable structure calculated with mfold. The mutants were subsequently tested for their translation capability in luciferase assays. The reporter replicons were electroporated into Hep3B cells wit A4U or WT miR-122. A capped *renilla* luciferase mRNA was co-electroporated as internal control. After 1, 2 and 4 h, cells were lysed and *firefly* and *renilla* luciferase activity were measured. The ratio of FLuc and RLuc was calculated in order to normalize the results. Values represent means with S.D. of at least 3 independent experiments.
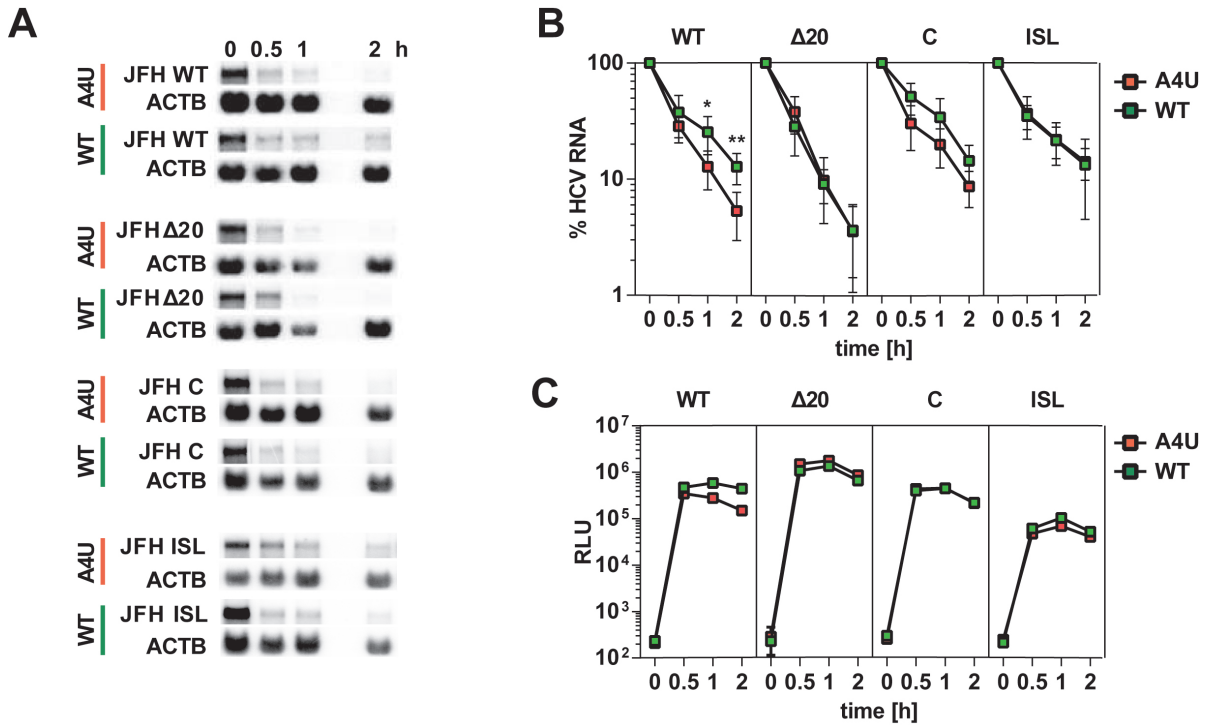
Figure 5.30.: RNA stability of selected domain I mutants. A | The stability of several domain I mutants was compared with the WT replicon via northern blot, in presence of either wild type or mutant miR-122. **B |** Quantification of northern blot data. The values represent means with S.D. from 3 independent experiments. **C |** Respective luciferase data for all time points. Values represent means with S.D. of at least 3 independent experiments.

as fast or even faster than the wild type RNA.

These observations led to the conclusion that translation of the IRES was influenced by domain I, likely due to formation of alternative secondary structures. Prevention of such interactions, by mutation or deletion of sequences within this region significantly augmented the first round(s) of translation, which could not be explained by enhanced RNA stability.

Xrn1 and Xrn2 Involvement in HCV RNA Decay

Xrn1 and 2 have been implicated as key regulators of HCV RNA decay. Therefore, preliminary knock-down experiments were performed using transient siRNA transfection. 48 h later, monocistronic replicons were electroporated with miR-122 WT or A4U. After 4 h, translation of the input RNA was measured by luciferase assay. Overall, the stimulation after miR-122 addition was slightly lower than in previous assays, which might be a result of the preceding transfection procedure. The knock-down efficiencies in both

transfections were determined by western blotting and quantified. The protein levels of Xrn1 were reduced by 80%, and 70% in case of Xrn2, suggesting that Xrn2 was not involved in HCV RNA degradation in this experimental setting. Xrn1 k.d. resulted in an overall increase in luciferase activity, arguing for increased RNA stability. Moreover, the difference between wild type and A4U miR-122 was decreased to around 1.5-fold 4 h after electroporation, compared to 4-fold in case of the control transfection. Increased stability of the input RNA will likely lead to prolonged production of protein, albeit to lower levels. Therefore, the overall difference after 4 h was smaller. In contrast, no difference could be seen in the enhancement of translation after Xrn2 knock-down, compared to a non-targeting control miRNA.
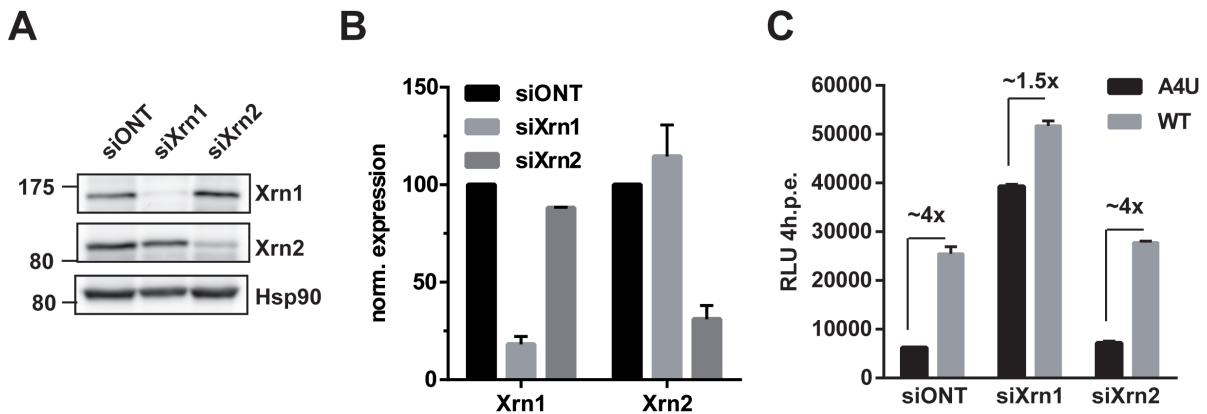
Figure 5.31.: Influence of Xrn1 and 2 knock-down on HCV translation. A Xrn1 and 2 were knocked down by siRNA and their expression levels after 48 h were detected by western blot. **B** The detected bands were quantified relative to HSP90 levels, in order to determine the relative knock-down efficiencies. **C** The siRNA transfected Hep3B cells were electroporated with replication deficient reporter replicons (luc-ubi ΔGDD). Luciferase activity (RLU) was measured 4 h after electroporation.

Another interesting observation was that, in spite of the initial boost of translation, the protein production did not seem to be sustained over multiple rounds. Calculating the slope of the *firefly/renilla* ratio, relative to the 1 h value, all mutants, and also the wild type in absence of miR-122, showed a significant decrease over time. However, addition of miRNA duplex was sufficient to stabilize the levels of luciferase activity significantly (**fig. 5.32**A). In case of the Xrn1 k.d. a similar effect on the kinetics of luciferase activity were noted. While overall luciferase activity was increased, the stimulation by miR-122 was as pronounced as in the siONT control.

In essence, Xrn1, but not Xrn2, controlled HCV RNA degradation at early time points after electroporation. However, neither the mutants, nor Xrn1 depletion could compen-
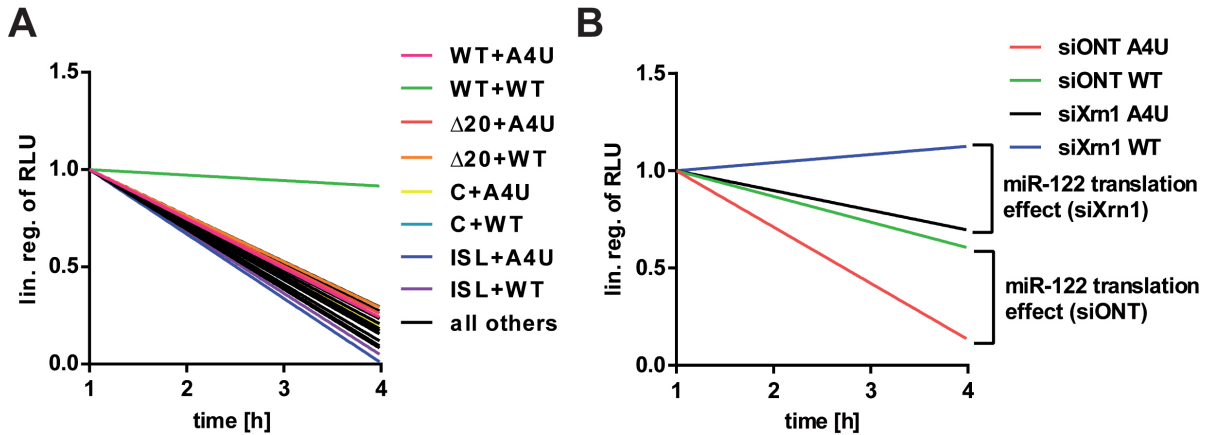
Figure 5.32.: Faster decay of translational activity in absence of miR-122. A |
Hep3B cells were electroporated with replication deficient reporter replicons (luc-ubi ΔGDD),
containing the previously described domain I mutations. Luciferase activity (RLU) was mea-
sured 1, 2 and 4 h after electroporation. After normalization of all samples to the 1 h value,
the linear regression of the luciferase activity in all mutants and the wild type was calculated.
Selected mutants are depicted in color. **B |** siONT or siXrn1 transfected Hep3B cells were
electroporated with replication deficient reporter replicons (luc-ubi ΔGDD). Luciferase activ-
ity (RLU) was measured 1, 2 and 4 h after electroporation. After normalization of all samples
to the 1 h value, the linear regression of the luciferase activity in all mutants and the wild type
was calculated.

sate for all functions of the bound RISC, as the production of new protein seized after
a short initial burst. This was deduced from the fact that the luciferase activity after
1 h decayed approximately with the half life of the firefly luciferase protein ($t_{1/2} \approx 2$ h).
Therefore, stability and translational enhancement were dependent on separate mecha-
nisms.

Impact of Mg^{2+} and miR-122 Binding on the Secondary Structure of Domain I and II

Since we hypothesized that miR-122 alters the secondary structure of the IRES, the in-
fluence miR-122 annealing was investigated. It is known, that the concentration of Mg^{2+}
is an important variable for the folding of the HCV IRES[307], and also for RNA:RNA
hybridization. Several studies have examined the influence of metal ions on the ultra-
structural properties by means of gel-shift and atomic force microscopy, however, there
has not been any in-depth biochemical analysis of the secondary structure. It has been
described that significant rearrangements occur in the concentration range of 2-3 mM
$MgCl_2$. This is close to the predicted intracellular free magnesium levels, which are

believed to be around 0.5-3.5 mM. Most SHAPE experiments done so far, used much higher concentrations for folding, which might bias the result. Especially the folding of SLII can be influenced, since the hinge of SLII coordinates three Mg^{2+} ions, which gives this stem-loop its characteristic, and functionally relevant L-shaped appearance. Therefore, experiments were performed using 0, 1 or 6.6 mM $MgCl_2$ in the folding buffer. The 5' proximal 389 nt of JFH-1 were used either in their wild type sequence pre-incubated with the 3p- or 5p-arm of miR-122, or the mutants Δ20, C and ISL. DMSO controls were loaded for each condition for normalization. As expected, the MBR is significantly reduced in reactivity only if miR-122-5p was supplemented (**fig. 5.33**A). This confirms that AGO-less binding of miR-122 occurs under these conditions. However, since some regions, especially at the first binding site, are not reactive in either condition, no claims can be made, as to whether both sites are bound. The peak at nt 21 is likely an artifact, since it appeared only irregularly. It is directly in front of SLI, which is a very stable structure and might terminate the RT reaction. As expected the band patterns differed in several positions between the three conditions (**fig. 5.33**A, B). Interestingly, the reactivity of the predicted tip of the SLII stem-loop, was strongly affected by magnesium concentration. At low levels all of the nucleotides gave a clear signal, which waned with increasing concentrations. This might hint towards a tertiary structure component, or another Mg^{2+} organizing loop, where the flexibility of the participating nucleotides is affected. The band representing U103 was only detectable at higher Mg^{2+} concentrations. The mutants however presented the nt 103 band even in absence of miR-122, arguing for a shift towards functional fold even under physiological levels of magnesium, and in absence of miR-122. While free nucleotides are only predicted at this position in the canonical fold, the nucleotides 114-116 should in contrast only be reactive when SLII is not efficiently formed, as they are part of the small predicted stem at the 3' terminal portion of domain II(**fig. 5.33**C). Indeed, the latter ones were only labeled in the lower range of $MgCl_2$ concentration. Instead, reactivity was shifted towards nts 119-120, which are located just 3' of the SLII base. Also miR-122 annealing efficiency was impaired at lower concentrations, which is an indication that the hybridization energy alone might not suffice to fully reconstitute the processes in the cell in this system. An interesting observation was the fact that at 0 mM as well as at the highest concentrations no significant impact of miR-122 binding was apparent, resulting likely from reduced hybridization of target and miRNA, and maximal shift towards the "active" conformation, respectively (**fig. 5.33**A,B). At intermediate magnesium levels, however, several bands were quantitatively affected. Intriguingly, U103 became stronger at 1 mM
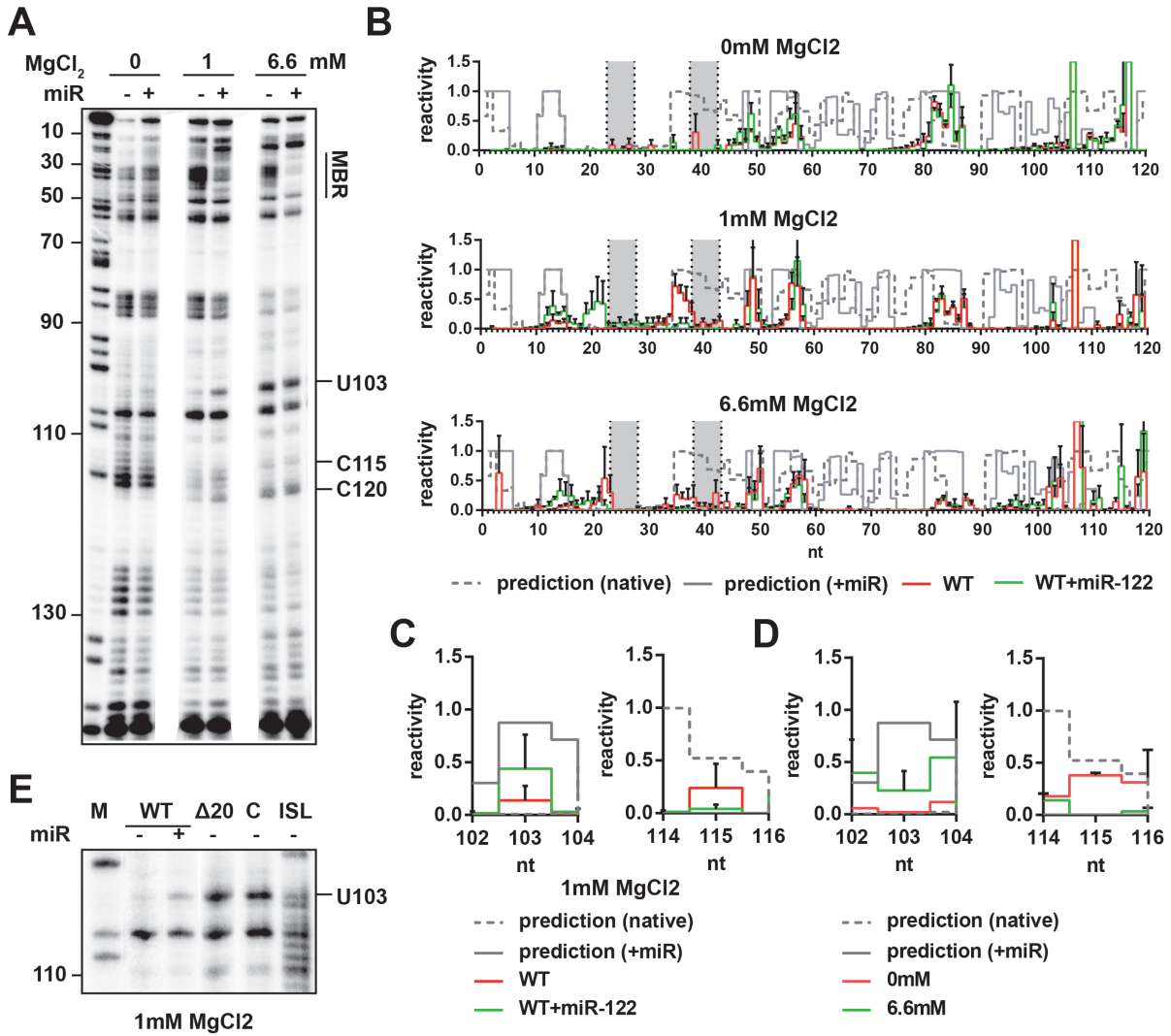
Figure 5.33.: **A** | Auto-radiography image of the results obtained for the WT sequence at 0 - 6.6 mM $MgCl_2$. Marker (M) shows all A residues. **B** | Histogram plots of nucleotide reactivities at different magnesium levels and in presence of miR-122-5p (green) or a control (miR-122-3p, red). Shown are means with S.E.M. of 3 independent experiments. **C** | Magnification of miR-122 responsive regions downstream of the MBR. At 1 mM $MgCl_2$ the band corresponding to nucleotide position 103 is intensified, while position 115 is decreased. **D** | Characteristic bands from **C**, affected by Mg^{2+} levels. The shift of intensities at higher concentrations resembles the situation after addition of miR-122-5p. **E** | Comparison of U103 SHAPE reactivities in wild type RNA and selected domain I mutants.

MgCl$_2$, and the reactivity of the 114-116 bands were shifted to a greater proportion at this concentration (**fig. 5.33**C). Of note, also the translation enhancing mutants $\Delta 20$ and C showed increased reactivity at this residue (**fig. 5.33**E). This argues for a dynamic equilibrium of structures, which can be biased by miR-122 binding, favoring the canonical IRES structure. It can be assumed that miR-122 incorporated into the RISC is much more efficient in binding to the HCV RNA under low divalent cation conditions. Moreover, the quite large protein complex might also facilitate state conversion. So the changes that are occurring in the natural infection might be more drastic.

All in all, the effects of Mg^{2+} concentration were quite drastic, and superseded those of miR-122 addition. Only at concentrations of $1\,\mathrm{mM}$, which is close to intracellular free magnesium levels, differences at specific nucleotides were observed in the SHAPE pattern upon miR-122 annealing. Assuming an array of different structures in solution, these data suggest a magnesium-dependent shift of this equilibrium, which could be supported by miR-122 association at low Mg^{2+} levels.

Conclusively, these experiments could show that translation is a key feature of the miR-dependent activity, which stimulates HCV propagation. Phenotypical data, generated with domain I mutants, supported the notion that the MBR could take part in translation-abrogating structures within domain I and II. Moreover, it was confirmed that the structure of the IRES in solution was strongly affected by magnesium concentration. Under specific conditions, this effect was also moderately enhanced by annealing of miR-122.

5.2.3. In Search for a Host Factor

While our results so far pointed to a significant contribution of miR-122 to stabilizing the IRES and preventing alternative secondary structures. However, based on the prolonged translation activity during the first $4\,\mathrm{h}$ after electroporation of HCV RNA, we wanted to evaluate the impact of recruiting host proteins by miR-122. The RISC complex is a highly dynamic RNP, which can be reconfigured for a variety of purposes, where the central Argonaute protein acts as a hub to recruit different auxiliary factors. Hence, it is conceivable that binding of the RISC to the HCV RNA is necessary to assemble a translation enhancing and -sustaining protein complex at the IRES. This could for instance join the 5' and 3' ends of the genome to circularize the RNA, which is a prerequisite for efficient polysome assembly and steady state translation. In order to find candidate proteins, a literature search was performed, which brought to light two studies: one

examined AGO-associated protein complexes[308], the other determined factors binding to the HCV RNA[309]. In a first approach, these lists host factors were compared, and a

HCV RNA binding proteins   **RISC associated proteins**
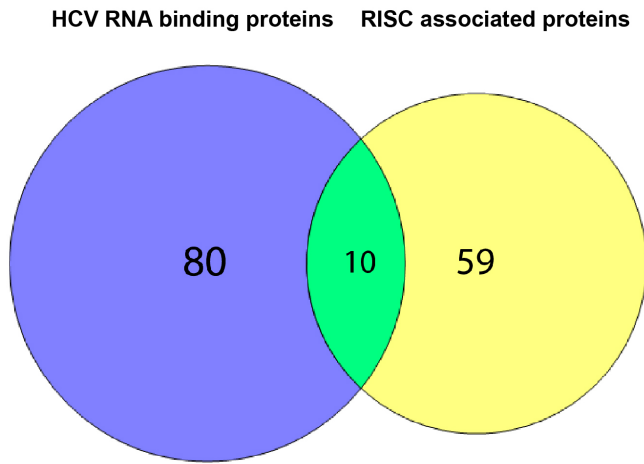
Figure 5.34.: Comparison of factors associated to HCV and AGO complexes. Venn diagram of the proteins found in pull-down experiments to interact with HCV RNA (Upadhyay et al.[309], blue) or present in different AGO complexes (Höck et al.[308], yellow). Ten proteins were detected in both approaches, and are therefore viable candidates in HCV translation regulation (see **tab. 5.1**).

roster of matching proteins was generated (**fig. 5.34** and **tab. 5.1**,**tab. 5.2**). Known cellular elongation factors and ribosomal proteins were excluded, since these are motile on the RNA and therefore unlikely to act as linkers between genome ends. A curious result, which was found in this analysis was the strong enrichment of known relevant proteins for HCV IRES-mediated translation in AGO1 complex III (IGF2BP1, NF45, MOV10 in **tab. 5.1**; HuR, HSP90, hnRNPC/L, NSAP-1 in **tab. 5.2**). Some of these were not found in association with AGO2, which is thought to be the key regulator of miR-122-mediated HCV stimulation. In contrast, AGO2 was found to bind several regulators of replication/assembly, such as YB-1, DDX3/5/6, and NF45. Intruigingly, DDX5 could only be found in complex II of AGO2, which also includes YB-1 and NF45. This might point towards a possible influence of the bound AGO protein on the functional impact. According to this data, 5'-bound AGO1 could stimulate translation, while AGO2 rather enhances replication. Some factors were only present in of the two lists, but well known to be involved in HCV translation and replication, as determined by other studies. These are summarized in **tab. 5.2**.

To attain the composition of the specific RNP for the 5' binding sites of HCV, biotinylated miR-122 was used to capture HCV RNA, and the associated proteins. Since any duplex miRNA is expected to be incorporated into a RISC, and thus will pull down many associated proteins, we used the mutated miR-122 and the corresponding replicon. This increases specificity, since canonical miR-122 targets will not be efficiently targeted, and 3' binding sites in the HCV genome are also excluded. Thus, using either wild type or a

Table 5.1.: Proteins identified in association with HCV and Argonaute complexes. Given are functions in the viral life cycle and location of their respective binding sites, if known. The containing AGO complexes are named according to Höck et al.[308].

Protein	Accession	HCV function	HCV RNA binding	AGO complex
YB-1	181486/55451	Replication/ Assembly	?	AGO1: II AGO2: II, III
HSP60	306890	?	?	AGO1: I AGO2: I
Upf1	1575536	?	?	AGO1: III AGO2: -
DDX5	226021	Replication	?	AGO1: - AGO2: II
hnRNP U	32358	?	?	AGO1: II, III AGO2: II, III
hnRNP H	5031512	?	?	AGO1: II AGO2: -
PABPN1	693937	?	?	AGO1: III AGO2: II, III
IGF2BP-1	7141072/ 56237027	Translation	3'UTR	AGO1: II, III AGO2: III
NF45	532313	Translation/ Replication	5'+3'UTR	AGO1: II, III AGO2: II, III
MOV10	14424568	Translation	5'UTR	AGO1: III AGO2: III

mutant replicon, any additional proteins detected in the mutant pull-down are potential candidates for further evaluation.

Table 5.2.: Additional proteins identified in complex with either HCV genome or Argonaute only found in one list, but linked to the respective other in separate reports.

Protein	Accession	HCV function	HCV RNA binding	AGO complex
DDX3	698980011	Replication[310]	?	AGO1, AGO2[311]
DDX6	574957069	Replication[312]	?	AGO1, AGO2[313]
HuR	1022961	Translation	3' UTR	AGO1: III AGO2: -
NF90	1082856/5006602	Translation/ Replication	5'+3'UTR	?
HSP90	153792589	Translation[284]	?	AGO1: II, III AGO2: -
hnRNP C	117189974	Translation	3' UTR[276]	AGO1: II, III AGO2: II, III
hnRNP L	52632382	Translation[271]	5' UTR	AGO1: III AGO2: -
hnRNP D	52632382	Translation[314]	5' UTR[314]	AGO1-3[315,316]
NSAP1	5031511	Translation[265]	5' CDS	AGO1: II, III AGO2: -

In a first approach electroprations of Hep3B cells were performed with wild type or m1,2 replicon and 3'-biotinylated miR-122 A4U. Unbiotinylated miR-122 was used as background control (**fig. 5.35**A). After 72 h the cells were harvested and RNA and protein were extracted from the pulled down material. To validate the assay, the presence of RISC components as well as known interactors with the viral genome were verified by western blotting. In subsequent experiments, co-precipitated HCV RNA was quantified by Taqman qPCR. As for the protein fraction, the pull-down yielded small, but detectable amounts of AGO2, HSP90 and DDX6, while the control IP with unbiotinylated miRNA was devoid of protein. The common RISC proteins DDX6 and AGO2 were enriched around 10-fold compared to the control. HSP90 was also present

in the pull-down, albeit to a lesser amount (**fig. 5.35**B, C).

To determine the influence of miR-122 binding on the pulled down protein fraction, biotinylated miR was co-electroplated with the corresponding mutant (binding) or wild type (non-binding) replicon. No significant difference could be detected between the HCV-binding or non-binding miRNA, for the tested RISC proteins. This was within the expectation, since RISC incorporation of the biotinylated miRNA should be largely independent of HCV (**fig. 5.35**D-F). In contrast to AGO2 and DDX6, proteins that associate to HCV, but not to the RISC should be enriched. Quantification of the western blot gave the expected result (**fig. 5.35**G). Because the overall quantity of pulled-down protein was rather low (around 0.5% of input), in the following approach the number of electroporations used for pull-down was doubled, and the amount of input was reduced to 0.1%, resulting in more equal loading of input and pull-down fractions. The first tested candidate was a subunit of the eIF3 complex (eIF3η) . This protein is a part of the preinitiation complex, interacting with the 40S ribosomal subunit, and therefore a marker for active translation. Since the RISC mainly inhibits translation, and triggers disassembly of the initiation complex, eIF3 should not co-purify significantly with microRNPs. In parallel to Hep3B cells, these pull-downs were also performed in Huh7.5 cells. Indeed, the pull-down from both cell lines showed a significant enrichment of eIF3η, when miR-122 was able to bind the co-electroporated replicon RNA, compared to the non-binding control (**fig. 5.35**H, I). Subsequently, the the pull-down material was subjected to mass spectrometry, to gain high-throughput data on all differentially enriched proteins. However, the results were not yet available at the time of submission of this thesis.

Overall, our results so far pointed towards a substantial role of miR-122 in stimulating translation of the HCV polyprotein, probably by stabilizing the secondary structure of the IRES: Firstly, the results with mono- and bicistronic replicons showed the importance of translation. Secondly, mutants lacking miR-122 binding sites, but stabilized the IRES structure, showed enhanced translation. However, since these mutants were not replication competent, it was difficult to assign the quantitative impact of translation stimulation on overall replication efficiency. In particular, since previous studies suggested that each HCV genome is translated ca 10.000 times prior to replication[45]. Thus, even a moderate change in translation efficiency might have a massive impact on overall replication efficiency. Moreover, the enhancement of the domain I mutants only lasted over a short time period, leading to the assumption that additional mechanisms, such as recruitment of host factors by the RISC might support ongoing translation. To
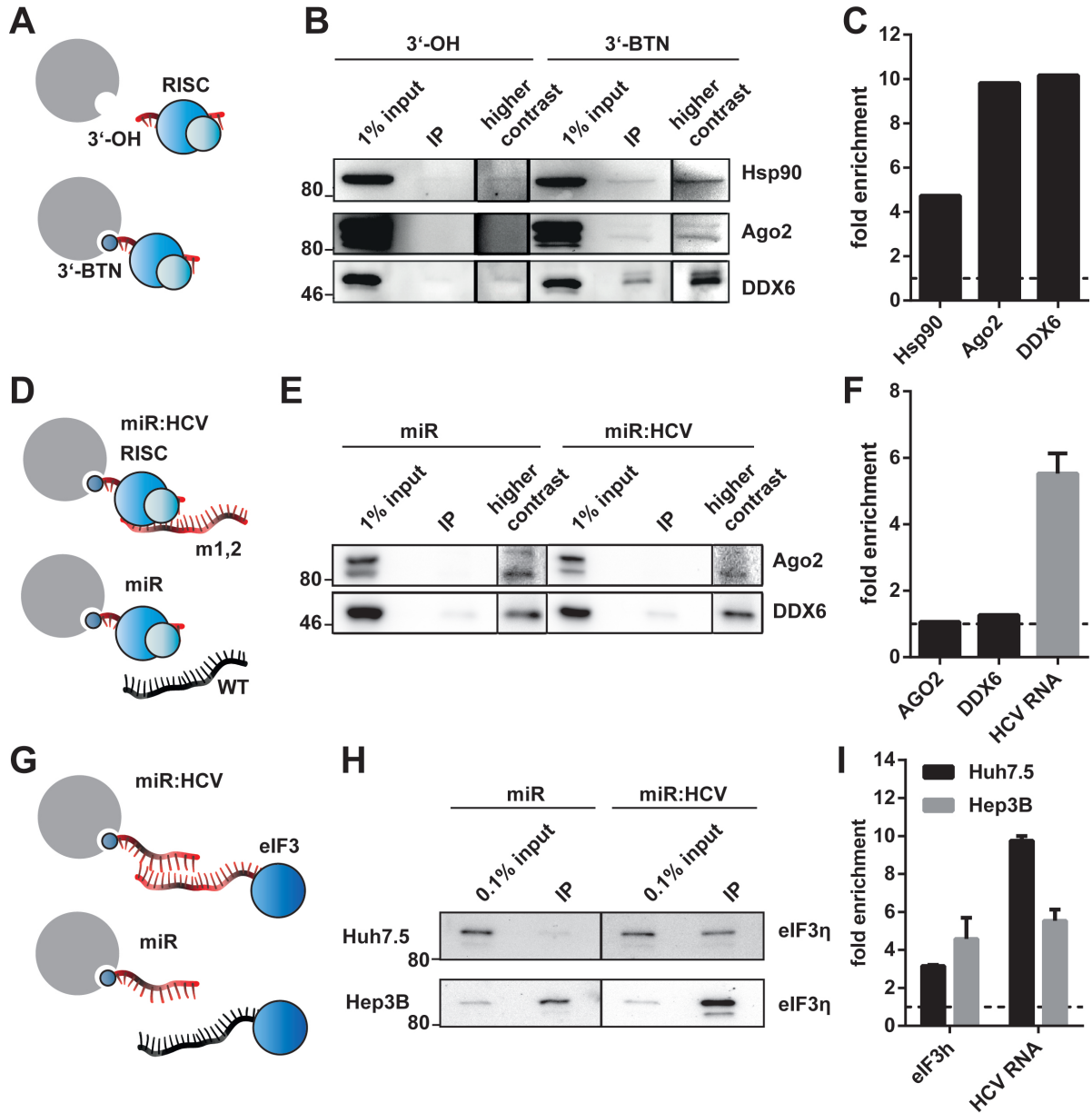
Figure 5.35.: Pull-down of specific HCV:miRNPs with biotinylated miRNA. A4U miR-122 (red) was used for these experiments to reduce background due to canonical miR-122 target binding. **A** | The background of the assay was assessed by comparison of proteins pulled down with biotinylated versus unbiotinylated miR-122. **B** | While the absolute amount of protein detected by western blot is low, **C** | a significant enrichment of miR-associated proteins was achieved. **D** | Since RISC assembly should be equally efficient, independent of target binding. **E** | Western blot analysis of the processed samples showed detectable amounts of protein. **F** | Quantification confirmed that RISC members AGO2 and DDX6 are pulled down with similar efficiency in both conditions. **G** | Non-RISC binding, but HCV associated proteins should only be co-purified via HCV-bound RISC. **H** | Western blot against eIF3η showed a marked increase in pull-down efficacy with a matching miR:HCV pair. **I** | Normalized to input, a more than 3-fold enrichment was detected in both, Hep3B and Huh7.5 cells

investigate this further, have established a system, which allowed us to pull down miR-122 bound HCV molecules. This technique can be used in future studies to identify host factors, which facilitate RISC-dependent translation stimulation.

5.2.4. Evaluating The Role of miR-122 in Replication

Since it was already established that the role of miR-122 in replication is important, in addition to its effect on translation, the mechanism of action on this regulatory level was also being investigated. During the search for possible mechanisms of miR-122 induced activation of replication, a peculiar fact was noted. The 3' terminal nucleotides of the major fraction of miR-122 molecules are identical with the ones at the 3' end of the HCV genome (UGU). Since the rate limiting step of *de novo* RNA synthesis by the viral RdRP is the initiation, which requires the generation of a 2-nt primer. The single stranded nature of the miR-122 overhang, as opposed to the stable stem at the 3'(+) end, and the concomitant close association with the viral genome, could support a model of a trans-priming mechanism (**fig. 5.36**A). The 3' nucleotide of the initiation dimer is essential in the progression from initiation to elongation. Thus, we designed a miR-122 mutant with a 3' terminal CU, instead of GU, as well as a corresponding HCV replicon. In the mutant replicon, the structural integrity of the 3' terminal stem was maintained by introduction of a compensatory mutation on the other arm of the hairpin. If the hypothesis were true, the primer generated from the mutated miR would be AG, and could therefore not initiate on a 3'-UG template, and would consequently abolish replication. The generated replicons were electroporated into Hep3B cells, with either wild type or mutant miR-122. The replication of the GC mutant was completely abolished in Hep3B cells, and could not be rescued by the addition of the GC miR-122. Concurrently, the wild type replicon was not impaired by addition of GC miR-122, compared to the wild type molecule (**fig. 5.36**B). While there seems to be no priming at the end of miR-122, it also became apparent that binding of miR-122 and probably the associated RISC is the most important feature of any miR-related mechanism. The 3' unpaired sequence might indeed be fully exchangeable. To further investigate any potential role of unpaired regions of miR-122, more mutants were designed, with more severe sequence alterations (**fig. 5.36**C). All mutants were tested for their replication stimulating activity with wild type JFH-1 replicons. Only two of the mutants showed any attenuating effect. A moderate 3-fold repression of replication, but not on the level of translation, was noted in case the overhang was exchanged for the complementary
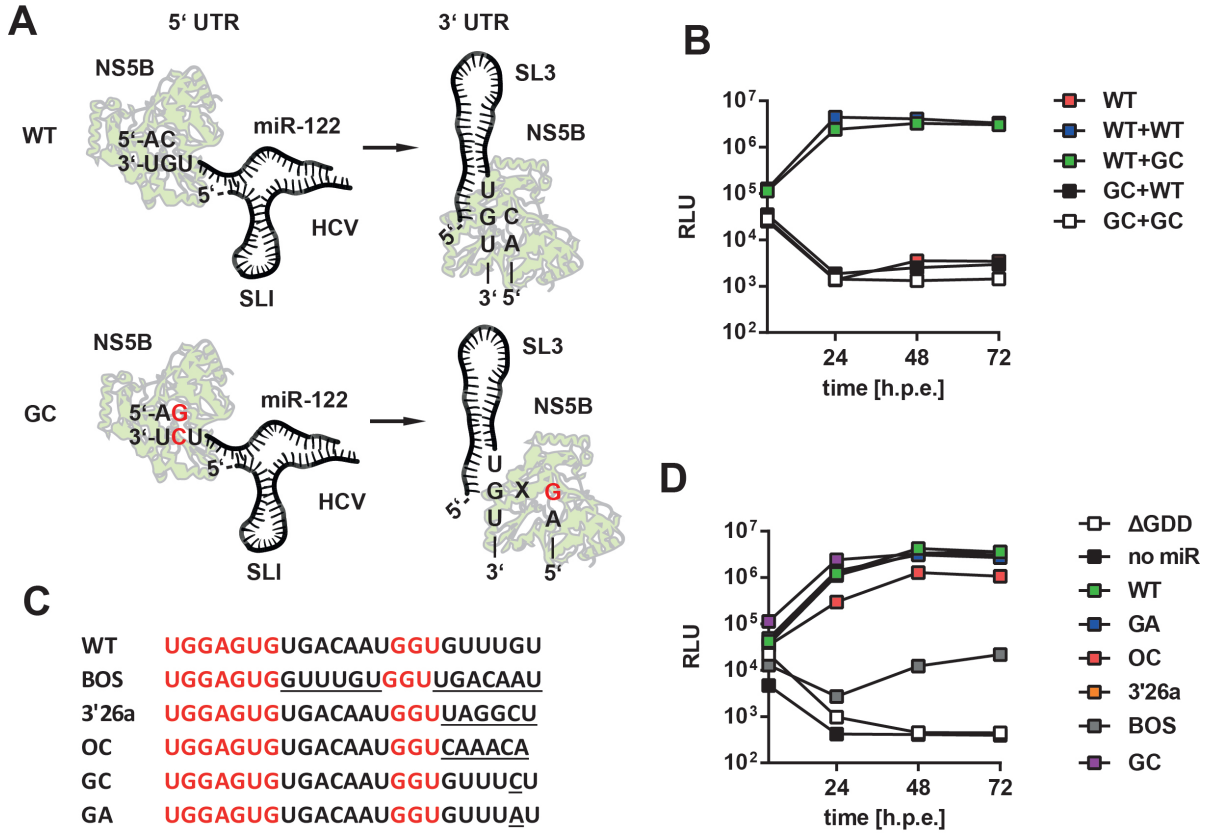
Figure 5.36.: Effects of altered miR-122 sequences on HCV replication. A | Model
of a trans-priming mechanism at the 3' end of miR-122 to initiate replication. The overhang
of miR-122 at the 5' end might be recognized by NS5B, and used as a template for generation
of an AC-primer. After translocation to the 3' end, RNA synthesis is initiated. When the
penultimate nucleotide of the miR is modified, the resulting di-nucleotide should not be able
to serve as primer for replication. **B |** Luciferase assay with miR and HCV 3'-GC mutants.
Alteration of the penultimate nucleotide of miR-122 has no effect on HCV replication and
cannot rescue a replication-dead replicon with the same mutation in the 3' SL3. **A |** Sequences
of the miR-122 mutants. Base-paired regions are colored in red, mutated bases are underlined.
D | Test of additional mutants. Most variants do not exhibit any change in HCV stimulation,
only significant changes in nucleotide composition or switch of entire regions are deleterious.

sequence (OC). Interestingly, the replacement with the 3' sequence of miR-26a (3'26a) had no effect. This might be an indication that certain sequence features are indeed needed, the terminal U, or a UG rich region in general, albeit they are not supposed to directly bind to the HCV genome. A more striking impairment was observed for the variant, in which the central bulge was switched with the 3' overhang (BOS). Here, translation, as well as replication, was significantly lower than for the wild type (**fig. 5.36**D). These changes, however, are drastic, and might affect additional processes, including RISC-dependent strand selection, or simply binding efficiency. Therefore, the primary sequence of miR-122 3' of the seed region seems not to be the most important feature for HCV replication, although drastic sequence modifications can significantly impair miR-122 functions.

Another possible way of increasing replication, would be the active translocation of genomic RNA by the RISC to the replication sites. At some point, translation needs to be terminated in order to assemble the replicase complex on the HCV RNA. The determinants for this process are widely unknown. A recent publication stated that PCBP2, a trans-activating factor of the HCV IRES, might be displaced by the RISC[207]. Assuming such a model, the RNA would be associated to the RISC after termination of translation. The miRNA-mediated RNA processing also involves intracellular transport mechanisms, leading to accumulation of the miRNPs in P-Bodies. Together with the fact that several P-Body proteins are also recruited to these viral factories[317,318], it seemed a plausible hypothesis that the RISC could in that way play a role in recruiting the viral RNA to the replication sites after translation. Assuming a highly dynamic RISC composition, bound AGO complexes could, possibly in collaboration with NS proteins, shift the viral RNA from translation to replication. To test this hypothesis, imaging experiments were performed in Hep3B cells electroporated with JFH-1 replicons. After 48 h, the cells were fixed and HCV RNA was visualized by *in situ* hybridization, followed by immuno-staining of AGO2 and Hsp90. Both proteins have been shown to influence several parts of the viral life cycle. Surprisingly, very little co-localization was observed between the proteins and the HCV genome (**fig. 5.37**). Instead, several signals of AGO2 and HCV RNA were directly apposed to each other.

In summary, these data could confirm that the binding of a miRNP to the HCV 5' UTR is of utmost importance, whereas the sequence of the miR plays a minor role. Only drastic changes of the primary sequence, which potentially disrupted the proper annealing to the target RNA impaired HCV replication. At the peak of replication, 48 h post electroporation of an HCV replicon, no co-localization of AGO2 and the HCV
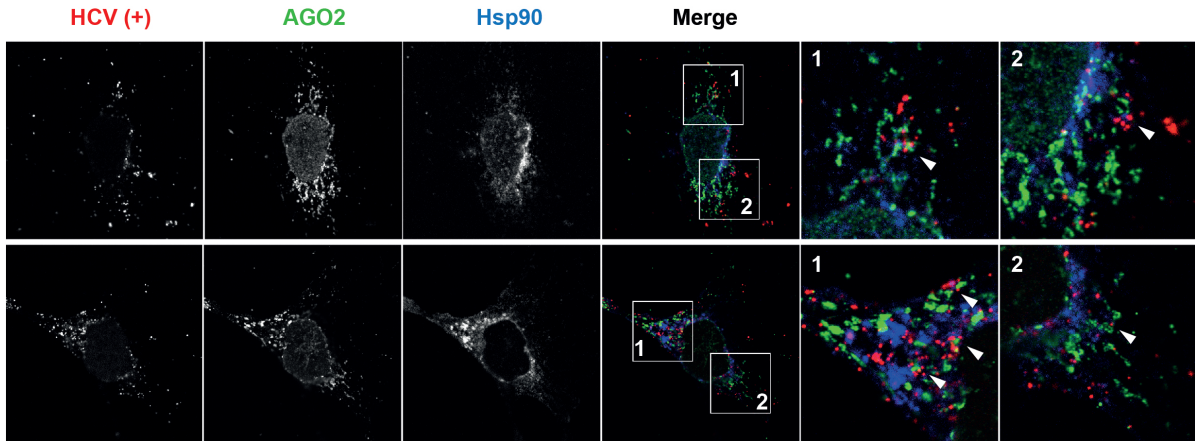
Figure 5.37.: Localization of HCV RNA and host proteins. Hep3B cells were electroporated with HCV replicon and wild type miR-122. 48 h later they were fixed and stained for HCV (+)-RNA (red), AGO2 (green) and Hsp90 (blue), both proteins involved in viral translation. Little co-localization was observed for these host factors with HCV RNA. However, clustering of AGO2 around HCV RNA or vice versa was observed. White arrowheads indicate regions where HCV RNA and host proteins accumulate.

(+)-strand could be detected in the microscopic analysis. Also, studies have found that the dependence on miR-122 decreases, after replication has been established. This observation could point towards the exclusion of AGO complexes from replication sites.

5.2.5. Identification and Characterization of Additional miR-binding Sites in the HCV Genome

So far, the analysis focused on the two well-characterized mir-122 binding sites at the 5' end of the genome. However, it has been published that the HCV genome contains more than the two best described seed binding sites, which are conserved over several genotypes. However, these sites remain poorly characterized. Therefore, we aimed to determine, whether these exhibit any functionality. Additionally, it was attempted to identify possible new miR-122 sites. In this approach, we screened the genomes of several genotypes for the central seed binding hexamer CACUCC. Three novel binding sites in the coding region of NS5B were successfully identified (**fig. 5.38**A). One of these (4) was found to be conserved throughout all tested sequences, the two others (3 and 4*) were only partly conserved. Genotype 2a harbored a miR-binding site only at position (3), while sequences of genotype 1a and 3a contained site 4*. Genotypes 1b, 4, 5 and 6 were positive for both. It was also noted that the novel miR-binding sites 3 and 4 of gt2a and 4 are very close to each other (~60 nt), and might act in a synergistic way. Since

Table 5.3.: Identification of miR-122 binding sites in the HCV genome. The reported MBRs are indicated by the citation. Nucleotides in bold were targeted by mutations.

no.	start	end	MBR Sequence	gt	published
1	23	28	CCCCUAAUAGGGGCGACACUCCG	all	Jopling et al.[153]
2	38	43	ACACUCCGCCAUGAAUCACUCCC	all	Jopling[319]
3	8778	8784	UGACCAGAGACCCAACCAC**U**CCA	2, 4, 5, 6	
4	8815	8821	CUGGGAAACAGUUAGACAC**U**CCC	all	
5	9219	9225	AGACCAAGCUCAAACUCAC**U**CCA	all	Nasheri et al.[320]
6	9406	9412	CGGCACACACUAGGUACAC**U**CCA	all	Jopling et al.[153]

the main aim of this part was to investigate the functional involvement of these sites in the complete viral life cycle, it was necessary to use a system capable of replication and virion production. However, most genotypes do not efficiently produce infectious particles in cell culture. The chimeric genotype 2a virus (JcR2A) is the exception, therefore only the sequences of gt2a were examined in this approach. The location, primary sequences and references for the MBRs are summarized in **tab. 5.3**. To assess the quality of the binding site, several features, such as conservation, location and sequence similarity were examined by *in silico* analysis(**fig. 5.38**A). Moreover, it is well established that structure elements within the binding region can strongly influence RISC association and activity. Hence, the structural conformation of the putative binding sites and the resulting hybridization energies were predicted with SFold/StarmiR (**fig. 5.38**A). It was observed, that certain features of the primary sequence were prominently appearing. Site 3 was overall very C/G rich, a C(U)GUU motif was found in most sequences. For site 4 the most apparent feature was a GGGAAA cluster. Site 5 contained the most highly conserved 5' flanking sequence. Notably, this site is located directly upstream of the secondary structure element 5BSL, which is critical for HCV replication. Therefore, the primary sequence might be more important in this region. Site 6 lies in the variable region of the HCV 3' UTR, therefore only little sequence homology was detected. Notably, most sequences contained a 3'-terminal adenine or guanine, and an upstream nucleotide triplet which could mediate secondary interactions of miR-122 nucleotides 14-16 (5'-GGU-3'). Such sequence attributes have been shown to improve miRNA annealing and activity. This, and the fact that most of the surrounding sequence was not conserved at all, could indicate that all these sites have functional relevance (**fig. 5.38**A). Hence,

we first tested the canonical functionality of the individual and combinations of the sites (**fig. 5.38**B, C). In line with the following genetic experiments, the sequences present in genotype 2a were used. A simple way of testing the physical and functional interaction of a miRNA with a putative target sequence, is to introduce the binding site downstream of a reporter gene, and assess whether the expression of the protein is regulated by transfection of the miRNA. Three copies of the MBR, spanning approximately 40 nt upstream of the seed binding sequence, were cloned behind a renilla luciferase gene, a firefly reporter plasmid was used as transfection control. The canonical function of miRNAs is the translational inhibition of their respective target RNA. Therefore, a functional interaction would lead to reduced *renilla* luciferase expression in this assay. In these reporter based experiments, it was found that site 3 and 6 were able to efficiently repress the *renilla* luciferase activity. Possible synergistic effects were addressed by combining a single copy of each of the four sites, however, no additional repression could be achieved. Next, we asked how these sites might act on the viral life cycle. Thus, single point mutants and combinations thereof were introduced into JFH-1 reporter replicons (**fig. 5.39**A). For the sites in the coding region, special attention was paid not to disrupt the amino acid sequence, while still being able to target all sites with the same rescue miRNA. Only for site 4 a mutation on the protein level had to be introduced, which led to a Ser to Thr exchange. These mutants were electroporated into Huh7 Lunet, which are highly permissive for HCV replication, or Hep3B cells, in order to check for cell type specific phenotypes. The latter were supplemented with synthetic miR-122 WT to facilitate HCV replication. The 4 h values, representing translation of input RNA, were increased to a certain extent for some mutants. All effects on translation were more pronounced in the Huh7 cells, but similar in Hep3B cells. (**fig. 5.39**B). However, these mutations had only little effect on replication in this setting. In Huh7 Lunet cells, the mutations manifested in a slightly decreased replication of 60-90% of wild-type. The combination of mutations in sites 3-5 led to a 3-fold drop of viral RNA amplification. In Hep3B cells, the mutations had practically no influence on replication, with the exception of the 3-5 mutant, which was reduced to around 60% of wild type replication capacity (**fig. 5.39**C). Since no negative influence of binding site mutations could be observed at the stage of viral replication, these studies were then extended to full-length JcR2A (**fig. 5.40**A), to test a possible involvement in subsequent steps of the viral life cycle. These experiments were performed in Huh7.5 cells, with or without co-electroporation of the A4U miR-122, which is able to bind the mutated sequences. Replication of the JcR2A constructs was tested as for the replicons. The relative replication values were similar to
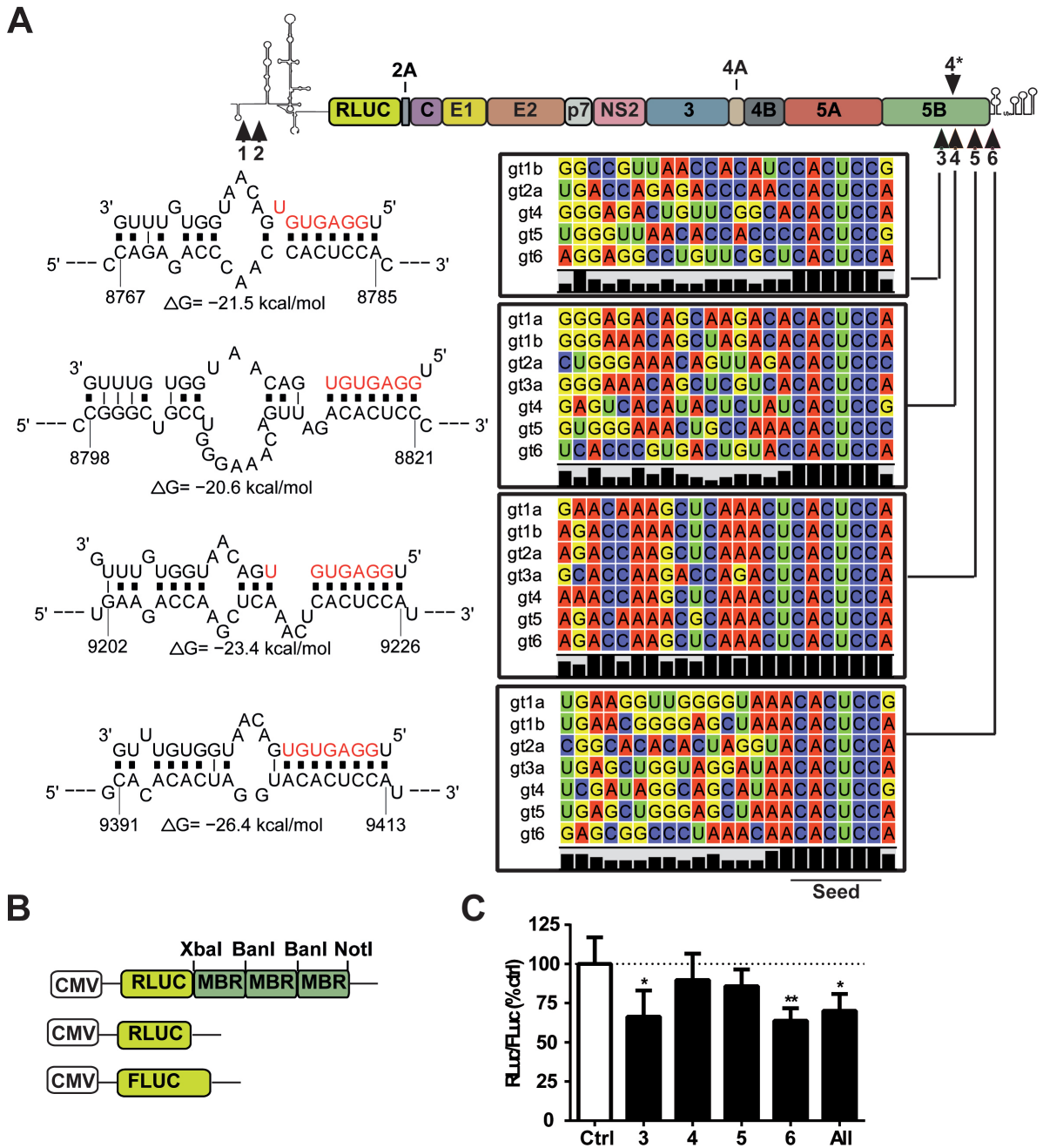
Figure 5.38.: Identification and characterization of additional miR-122 binding sites. A | Seed binding hexamers were searched within the HCV genome of different genotypes. The 5' flanking regions of the identified seed-binding sequences were tested for conservation between genotypes (black bars). StarmiR was used to calculate binding structures and hybridization energies. gt2a sequences were used as a template for the prediction. **B |** Reporter constructs for the assessment of canonical activity of the putative MBRs. Three copies of an approximately 40 nt region harboring the MBR were cloned 3' of a *renilla* luciferase gene. A control vector with *firefly* luciferase was co-transfected. **C |** *Renilla* activity values were normalized to the corresponding *firefly* expression. Ratios of all constructs were then normalized to the control vector, without miR-122 binding sites. Values represent means with S.D. of 5 independent experiments. *: p≤0.05, **: p≤0.01.
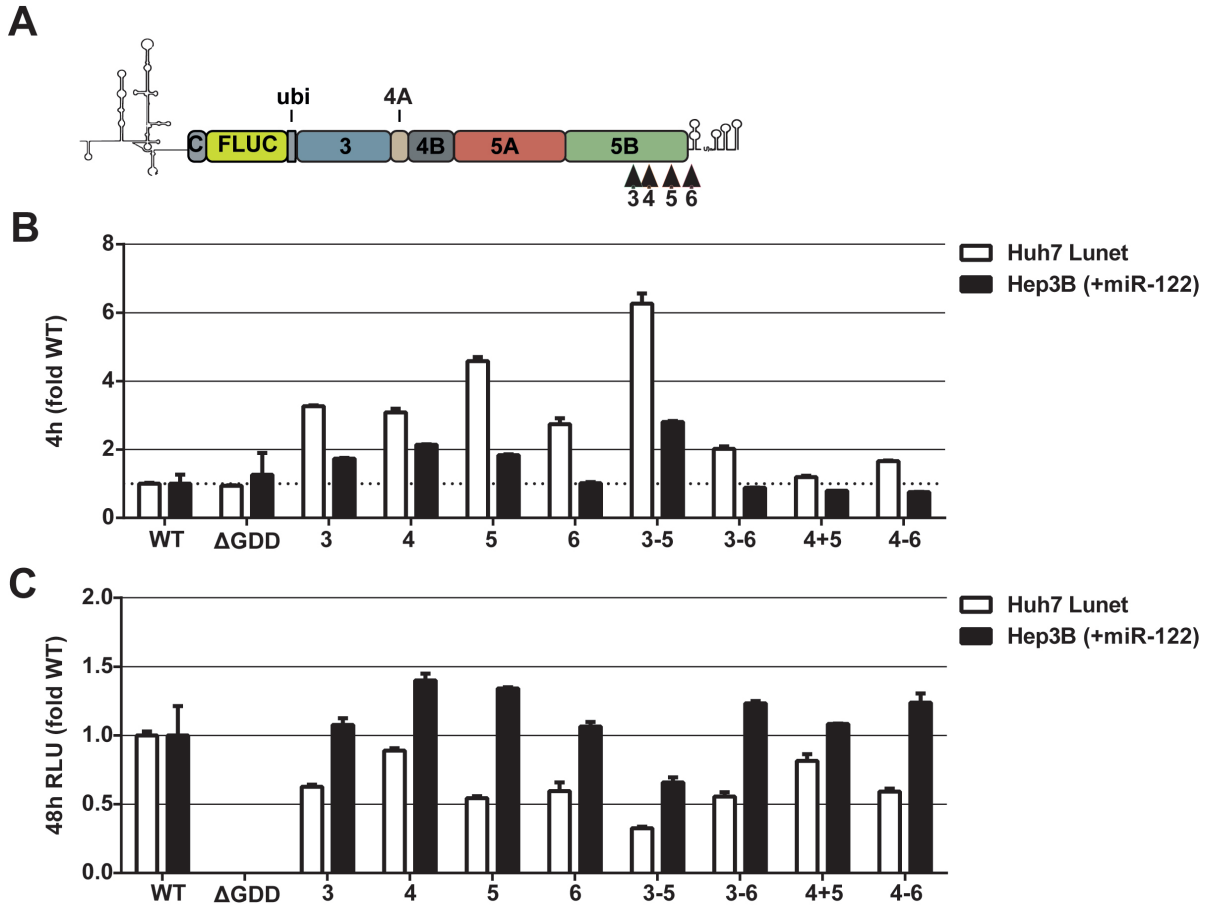
Figure 5.39.: Effect of additional miR-122 binding sites on replication. A | Schematic of a monocistronic JFH-1 reporter replicon. Black arrow heads indicate the position of the mutated miR-binding sites. **B |** Mutant JFH-1 replicons were electroporated into Huh7 Lunet or Hep3B cells, to test for cell type specific effects. The latter were co-transfected with miR-122 duplex. To determine translation efficiencies, the cells were lysed, and *firefly* luciferase activity was measured 4 h post electroporation. The luciferase activities of the mutants was normalized to wild type. **C |** To probe the replication capacity, electroporated cells were lysed after 48 h, and *firefly* luciferase activity was measured. The luciferase activities of the mutants was normalized to wild type. Values represent means with S.D. of 2 independent experiments.

those obtained in the replicon experiments, and did, with the exception of the 3-5 mutant, not vary significantly from the wild type construct. Interestingly, addition of miR-122 A4U reduced the replication capacity of several mutants by approximately 2-fold. The most profound effect was seen for the 3-6 mutant, in which all sites are A4U responsive (**fig. 5.40**C). After 72 h, supernatants were transferred to a new batch of Huh7.5 cells, and incubated for another 72 h. Then, the ratio of luciferase activity obtained from the electroporated and infected cells was calculated to determine the relative release of specific infectivity. The mutant with nucleotide exchanges in all 3' binding sites (3-6) replicated as efficiently as wild type, but was strongly impaired in particle production (5 to 10-fold reduction). This was also the case for the single site mutants targeting position 3 and 6. Addition of the miRNA with a compensatory mutation, however, could not reproducibly restore the relative amounts of released infectivity. Interestingly, for the mutants targeting site 4 and 5 alone, no strong effect could be observed (**fig. 5.40**D). This was in coherence with the functional assays (**fig. 5.38**C), in which site 4 and 5 also did not appear to be functional in isolation. The 4+5 mutant, in contrast, had a strong impact on assembly/release, which might suggest a cooperative function of these sites.

The results obtained in these experiments argue for a functional involvement of the miR-122 binding sites within the coding region and 3' UTR during the production of viral progeny. While the stage of replication was largely unaffected, initial translation seemed to be increased by abrogation of miR-binding to these sites. Overall, this could be indicative of a regulatory switch, in which RNA leaving the replication is either targeted for translation (5' sites) or packaging into virions (CDS/3' sites). Moreover, the strong replication and assembly phenotype of mutations in sites 3-5, and the intermediate suppression of both processes mediated by the 4-6 mutant, suggest a highly complex regulation, which requires all binding sites in conjunction.
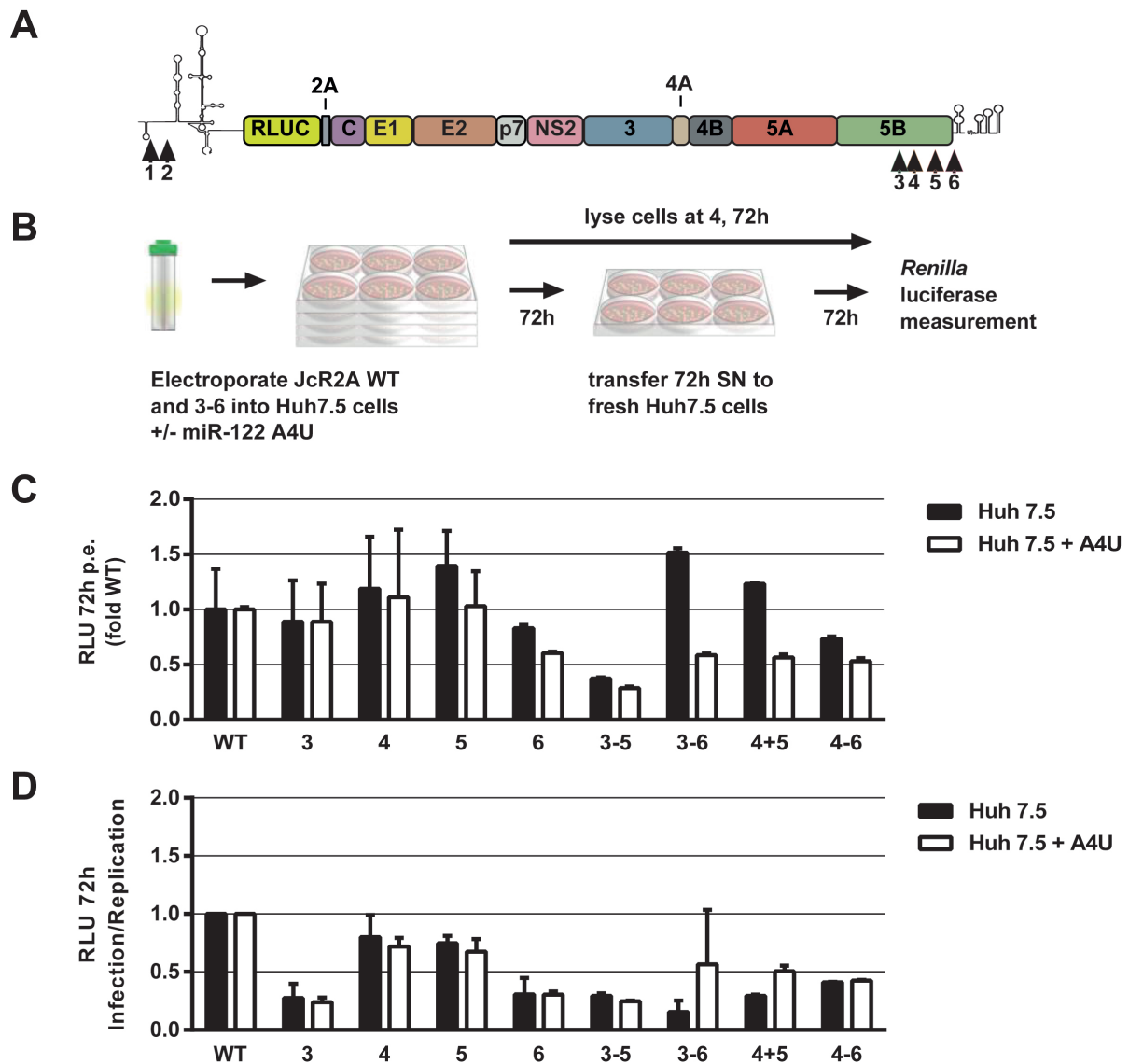
Figure 5.40.: Effect of additional miR-122 binding sites on replication, assembly and release. A | Representation of a JcR2A full-length reporter virus. Black arrow heads indicate the position of the mutated miR-binding sites. **B |** To address a potential role in assembly and release, the same mutations were introduced into a JcR2A reporter virus, and the constructs electroporated into Huh7.5 cells. The cells were lysed 4 and 72 h post electroporation and luciferase activity was measured, as described before. The supernatant of the 72 h time point was collected, and used to inoculate naïve Huh7.5 cells. These infected cells were incubated at 37°C for another 72 h, lysed, and luciferase activity determined. The luciferase activities of the infected cells after 72 h was normalized to the corresponding values of the electroporated cells. This ratio was assumed as the efficiency of infectious particle release.

6. Discussion

The hepatitis C virus is a widespread pathogen, and one of the main etiological agents for liver disease. The replication within the cell is entirely cytoplasmic, and driven by the viral proteins NS3-5B. Three of these proteins were investigated in this study: NS3 acts as a protease/helicase, that recruits the small peptide NS4A as co-factor. The phosphoprotein NS5A interacts with several host and viral factors but has no enzymatic function. NS5B is the viral polymerase. Most of the highly efficient antiviral drugs developed during the last decade target components of this complex[14–17], called the viral replicase. However, only limited information is available about the determinants for the interplay between these proteins, and the involvement of specific RNA signals, so called cis acting replication elements (CRE), that modulate RNA amplification. In particular, the mechanism of (-)-strand synthesis remains enigmatic, since the 3' end of the plus strand is not a suitable platform for initiation of NS5B[107]. In particular, the helicase function of NS3 was of interest, since it might be required to remove unfavorable RNA structures, ultimately leading to enhanced initiation. Hence, this study aimed to establish *in vitro* tools to investigate these questions in a controlled way.

Another goal was to clarify the mechanism of action of the liver specific miR-122 on the life cycle of HCV. While miRNAs usually repress bound target RNAs, in case of HCV two binding sites in the 5' UTR strongly increase translation[209], replication[207] and RNA stability[203]. However, the mechanistic details and quantitative contribution of these functions have remained unclear. Thus, we established tools to investigate each of the proposed functions. Moreover, we searched for additional miR-binding sites in the HCV genome and characterized their influence in the complete infectious cycle of HCV.

6.1. Functional characterization of purified HCV proteins

The first part of the thesis aimed to generate an *in vitro* model assessing the contribution of the NS3 helicase and NS5A to initiation of RNA synthesis. To this end, proteins were individually expressed, purified and relevant enzymatic activities were tested to ensure their functionality. In the established DNA unwinding assay, based on the study of Zhang et al.[62], it was confirmed that the protease domain is a vital component for helicase activity. This concurs with previously published data, which state that the RNA binding, as well as contact to NS5B were facilitated by the protease[62,321]. Proteolytic activity was, however, not a prerequisite for its influence on RNA unwinding capability. This was clearly demonstrated by addition of the protease inhibitor VX950 at a concentration of $100\,\mu$M, which entirely inhibited protein cleavage by NS3[14]. Even under these conditions, there was no discernible effect on helicase activity, while manoalide (MNLD)[63] strongly impaired duplex dissociation at the same molarity (**fig. 5.5**).

In agreement with these results, also the absence of the protease co-factor NS4A did not impair helicase activity. However, the data showed that the properties of the holo-enzyme differed from those of NS3 alone, especially in terms of their individual pH optima (**fig. 5.6**). This could also be observed in an earlier study of Kyono et al.[322]. In the *in vitro* setting, the lack of lipid membranes might have led to aberrant folding of NS4A, which interfered with protein activity. The lower pH could have compensated for this by altering the charge of the protein, and thereby inducing a functional conformation. Lam et al.[323] found that nucleic acid binding properties of the holo-enzyme and the helicase domain were in fact improved at low pH. Moreover, a recent publication also reported a pH dependent structural shift of the protein, which modulated its NTPase and helicase function[324]. Therefore, it is also possible that this effect was not an artifact of *in vitro* conditions, but rather a property that enables alternative functions of the enzyme in different environments. In this context it might be interesting to address the *in cellulo* pH of replicase compartments, to probe for a physiological relevance of an acidic environment. A lowered pH could argue for a protonation-dependent functional switch, possibly between protease and helicase activity. The fact that addition of NS5B rescued helicase activity of NS3 in suboptimal buffer conditions (**fig. 5.7**) could also be interpreted as a result of conformational changes. The main interaction site is located in the protease domain, which was able to modulate helicase function and RNA binding[62]. A stabilizing effect of a favorable conformation might explain the observed effect.

Another possibility arises from the fact that nucleic acid binding also activates NS3[325]. Therefore, merely enhanced recruitment of NS3:5B complexes to the template could be the underlying mechanism for this activating phenotype.

6.2. Role of NS3 helicase in replication

The main hypothesis of this part of the study, was a possible unwinding activity of NS3, exerted on the extensive 3'-X-tail structures of the HCV positive strand. These stable stem-loops impair RdRP initiation. Transformation of the helical regions to single stranded RNA would create optimal initiation sites for the viral polymerase NS5B. Conversion of stable stem-loop formations by NS3 has been demonstrated *in vitro*[326]. The *in vitro* replication data gained in this study by comparing NS5B performance on a hetero- and a homo-polymeric template showed that the polymerase was functionally enhanced on a structured RNA (**fig. 5.8**). In addition, the level of activation was strongly dependent on the nature of the 3' end of the template. If the RNA terminus was engaged in a stem, the stimulatory effect of NS3 is even more pronounced than in the context of a single stranded region at the initiation site. Also, inactive mutants, either ATPase deficient (Q460H)[327], or impaired in RNA binding (ΔP) were not capable of increasing polymerase activity (**fig. 5.8** and **fig. 5.9**). Overall, these data argue for a major role of the NS3 helicase function in initiation, which is the rate limiting step during viral replication[108]. An auxiliary role in elongation might be exerted by increasing overall processivity of the viral polymerase. A similar approach to study the effect of NS3 on viral RNA replication has been taken by Piccininni et al.[64], who were not able to observe template-sized product in their assay. In their experiments, addition of NS3 stimulated NS5B activity, but resulted in the generation of a significantly larger RNA. However, no functional analysis of helicase activity was performed in this study. Along those lines, it is interesting to note that a similar phenotype could be observed in our hands, when the NS3 inhibitor MNLD at effective concentrations, or high doses of spermidine were added (**fig. 5.10**). Polyamines are potent inhibitors of NS3 helicase activity, but strongly activate NS5B[303]. MNLD also seemed to inhibit NS5B terminal *de novo* initiation, however, using a combination of both proteins, the higher molecular weight band was strongly increased. At the same time, the template-sized product was markedly reduced. This is indicative of an "unspecific" RdRP-stimulatory function of NS3, which was not associated with RNA helicase activity. While this apparently conflicted with the data obtained in this study and by Piccininni et al.[64], using a helicase dead mutant,

which was unable to exert any stimulatory effect, there was one hint towards a possible explanation. While the inhibitory concentration of MNLD was at around $1\,\mu$M, the IC_{50} for the NTPase was significantly higher ($70\,\mu$M according to Salam et al.[63]). Therefore, a profound residual NTPase activity was retained at $100\,\mu$M[63]. Both mutants were however ATPase defective, as determined by Piccininni et al.[64] for their variant, and for the Q460H mutant in the study of Kim et al.[327]. While the exact mode of action remains elusive, the potential involvement of the NTPase activity provides grounds for further experiments, using other NS3 mutants, which leave the ATPase intact.

Moreover, a tight physical and functional association of the replicase proteins has been described earlier[62], and could also be confirmed in this study. It is conceivable that this is a prerequisite for optimal protein function. For CSFV this was already shown by mutational analysis of NS3:NS5B interaction sites[65]. This might simply be achieved by bringing the replicase components into close proximity, or potentially through induction of a certain conformational state. Intriguingly, our data showed that there were reciprocal effects of temperature on the interplay between viral helicase and polymerase (**fig. 5.9**). At lower temperatures it is likely that protein:protein, as well as protein:RNA interactions were stabilized. In this case, a very specific effect on terminal *de novo* initiation was apparent, which even surpassed the general boost of the RdRP. In line with a potentially stronger interaction, these effects were present even at low NS3:NS5B ratios. With increasing temperature, the strongest effect could be observed at equimolar protein amounts. Of note, while the average stimulation of terminal *de novo* product was around 3-4-fold for all temperatures, unspecific RdRP initiation was increased proportionally. This might be attributed to several reasons. The most obvious would be the observed higher catalytic velocity of NS3 at higher temperatures, which in turn led to more dissociation of secondary structures on the template, accounting for more internal initiation, as more single stranded regions became available. Alternatively, these could represent abortive elongation products, resulting from decreased processivity of NS5B at higher temperatures[299].

These data showed that NS3 and NS5B are sufficient for the assembly of a functional replicase *in vitro*. The helicase activity of NS3 enabled NS5B *de novo* initiation on a difficult template and moderately increases its processivity. On an ideal template, like the 3'(-) end[107], the effects are less pronounced, which corroborates the notion that NS3 mostly acts at the stage from initiation to elongation of NS5B. On the other hand, NS5B also significantly stimulated NS3 activity *in vitro*[67]. This means that both enzymes depend to some extent on their interaction to function efficiently.

6.2.1. Involvement of NS5A

The role of NS5A in replication is not fully understood. It participates in a wide network of protein:protein interactions, involving host and viral factors. One host factor used for viral replication is replication protein A[328]. It is recruited by NS5A, and supports the attachment of NS5B to the HCV genome. It is known that the protein binds RNA, importantly it shows a strong affinity for the poly U tract in the HCV 3' UTR[77,78]. It also interacts with NS3[329] and NS5B[330,331], which could hint towards a role as a hub for recruitment of the replication machinery. Its different phosphorylation states might also define the subset of interaction partners needed for the various functions in the viral life cycle. It has been shown that NS5A can increase the RdRP activity of NS5B in a template-dependent manner[332]. In this study, the role of NS5A in initiation of (-)-strand synthesis was addressed. As shown in **fig. 5.11**, the contribution of NS5A seemed to be a general stimulatory effect on NS5B. This could be deduced from the fact that terminal *de novo* initiation was not favored, but the overall activity of the RdRP was increased. The effect was weaker than the one exerted by NS3. The combination of NS3 and NS5A augmented the effect of NS3, and facilitated terminal *de novo* product formation. This is in line with a recent study that used a rolling circle RNA polymerization model. Mani et al.[328] found that NS5A exploited the host protein replication factor A to tie a preexisting NS3:NS5B complex to the template. While the used template was poorly amplified by the replicase, addition of NS5A and RPA could markedly increase initiation and polymerization. However, the importance of RPA in cellulo has not been determined so far. Generally, the impact of RPA might point to a requirement for a single stranded binding protein, a role which might be served by other viral proteins like core or NS4B, both being shown to bind RNA, or differentially phosphorylated NS5A isoforms, which cannot be generated *in vitro*.

In addition, numerous cellular RNA binding proteins have been identified in previous studies to contribute to HCV replication, which might serve this function *in vivo*[88,333–338]. In contrast to our study, the helicase domain of NS3 was sufficient to stimulate NS5B, which might be a result of the specific assay conditions (i.e. salts, pH). One remaining substantial concern is the post-translational modification of NS5A. Since the protein was produced in bacteria, the way of interaction with either of the other non-structural proteins might be affected. Therefore, future experiments will need to address the influence of NS5A in different phosphorylation states on the RdRP, either alone, or in concert with NS3. Such approaches will need to make use of NS5A produced in mammalian

cells, or phosphorylated *in vitro.*

6.2.2. Remaining Technical Challenges And Perspectives

While the overall trend in most experiments was reproducible, the results showed a high variation, depending on the batch of protein and RNA used. Therefore, different issues arose in the course of this study (supplementary **fig. 5.12**). Foremost, the strength of the NS3-mediated activation of NS5B was very inconsistent, ranging from almost none to 20-fold. Then, a template-sized band could sometimes be seen with NS5B alone, which might be due to contaminating proteins, or aberrant RNA folding. In some experiments, the appearance of a second band very close to template size made it difficult to judge which one was the true *de novo* product. Also, the used marker (either generated by hot *in vitro* transcription, or end-labeled) did show several truncated fragments, arguing for abortive T7 products, or RNAse contamination. Since these fragments likely represent templates for NS5B, the presence of unspecified smaller RNAs in the reaction was a major concern for the interpretation of any phenotype produced in this assay. It was therefore clear that the major flaw was the variable quality of RNA and protein preparations, which need to be addressed in the future. Subsequent studies will have to make use of higher quality template, to generate more consistent phenotypes. A robust assay could then be used for different applications, such as the functional specification of template and protein regions in the context of replication. Moreover, this method could be applied to clarify the mechanism of action for different antiviral drugs which target replicase components.

6.3. miR-122 Promotes Viral Translation

The liver specific miR-122 is an important host factor for HCV, contributing to the viral tropism in a non-canonical mode of action, by enhancing viral propagation. Several paradigms exist, which aim to explain the stimulatory effects exerted by miR-122 on the life cycle of HCV. The currently favored model is the direct shielding of the viral genome against host exonucleases (specifically Xrn1)[339,203]. Only the elongation phase of RNA replication seems not to be affected[206]. Moreover, mechanistically conflicting roles in translation and replication have been proposed. While Henke et al.[198] claimed that miR-122 association facilitates 40S ribosomal subunit binding, another recent report suggested a translation abrogating effect, through the displacement of ITAFs

(PCBP2)[207]. Moreover, a recent study suggested that miR-122 function is specifically altered during HCV replication[340]. This shaping of the cellular environment could be of relevance for the balance between viral replication and translation, since several factors associated with HCV are themselves predicted or validated targets of miR-122, e.g. PACT[304], OCLN[341], IGF2BP1 (predicted by TargetScan).

Others have used non-hepatic HeLa cells[342] or rabbit reticulocyte lysates[209] to study HCV translation. Obviously, such systems pose a high risk of *in vitro* artifacts. In particular, there is no functional RISC loading of introduced duplex miRNA in the RRL system, so pre-annealing of the miR-122 guide strand to the genome becomes necessary, which represents a very artificial system[209,198]. In fact, *in vitro* and *in cellulo* translation activation has already been shown to rely on functionally distinct mechanisms[342]. All of these factors have made it difficult to evaluate the biological relevance or quantitative role in the natural infection. Therefore, in our studies we interrogated the effect of transient miR-122 supplementation on different reporter replicon constructs in Hep3B cells, a hepatic cell line, which does not express miR-122 natively[343]. We found that, in line with published data[155], the miRNA was able to support replication of a monocistronic replicon in these cells (**fig. 5.15**). In addition, bicistronic replicons could partially overcome the dependence on this host-factor (**fig. 5.16**), which has also been described by others for one of the tested constructs[155]. In addition, we could show that this effect was also achieved, when protein expression of a monocistronic replicon was put under the control of a PV IRES. While substantial replication was observed without miR-122 in these translationally uncoupled HCV reporters, addition of miR-122 could still increase the maximal replication and initial translation levels. This might be due to either the published shielding of the genome, faster progression towards replication, or possibly recruitment of translation-activating factors in the course of RISC association to the HCV IRES, which could then be passed along to the upstream IRES elements. A similar capturing mechanism has also been described for picornaviral IRES structures, which have been shown to enhance translation of upstream cistrons[344]. In any case, these data very clearly favored a role of miR-122 in promoting translation above a certain threshold level, which in turn led to efficient replication. If this was achieved by other means, this was sufficient for active replication in absence of miR, arguing that other possible activities, i.e. enhanced genome stability[203], or initiation of replication[207], were advantageous, but not essential. Moreover, the use of a mutant miR-122 (A4U) could stimulate translation and replication of a corresponding mutant replicon (**fig. 5.15**). Since this miRNA could not efficiently bind to canonical miR-122 target sequences, the

regulatory properties of miR-122 seemed to be of little importance to HCV replication, at least in the transient cell culture setting.

To quantify all possible contributions in the context of replication, a bicistronic replicon was created, which should allow for a distinction between phenotypes arising from replication/stability, or translation. However, recombination of the replicon RNA after electroporation precluded the generation of quantitative data (**fig. 5.17**).

Conclusively, it was shown that increased translation, rather than RNA stability/replication was the initial step for the action of miR-122. Nonetheless, subsequent events were also enhanced by miR-122 supplementation, arguing for additive effects during the course of HCV replication.

6.4. The impact of domain I on IRES function

In an approach to find the mechanism of miR-122 in HCV translation, we were addressing the question, whether binding of the RISC complex could act as an RNA chaperone, to invoke a structural switch in the 5' UTR of HCV, which regulates translation activity. In previous studies focusing on IRES structure domain I was omitted in most cases, since it was deemed functionally irrelevant[240]. In our model, however, we propose that while it likely does not enhance translation, it rather negatively regulates IRES function[241,242], by interacting with other sequences. A functionally related mechanism has been proposed before, in which a sequence within the core coding region beyond domain IV, was suggested to interact with domain I. This interaction was supposed to involve the miR-122 binding region and would be disrupted by RISC association[345]. This hypothesis was later falsified by introduction of specific mutations introduced in the interacting sequence[346]. Also, the fact that the 389 nt IRES element used in monocistronic replicons is fully translation competent, and responsive to miR-122 stimulation, precludes a relevant involvement of this stem-loop in miR-122 dependent activation of IRES function. Hence, we focused on the local structure adjacent to the miR-binding region. Several structural features of the IRES have been proposed to play important roles in binding and positioning host translation machinery to initiate cap-independent translation[259,347,256,257,348,291]. We envision that, by preventing translation attenuating conformations in domain I, miR-122 binding creates a bias towards the local structure, which has been described as SLII of the HCV IRES (**fig. 5.18**). The aforementioned attenuating elements have been predicted by different RNA structure algorithms, and the complementary strand is known to form a stem-loop at this position. Moreover, we

could observe that the translation efficacy of an HCV IRES dependent construct was increased by >5-fold at early time points after HCV RNA transfection by the addition of miR-122. Accordingly, we designed mutants, which should fold into the SLII confirmation natively, circumventing the need for miR-122. Indeed, all mutants designed that way could stimulate translation at least to the level of wild type in presence of miR-122. Some even exceeded the translation activity of the positive control by up to 3-fold, whilst specific controls were not able to enhance translation. The observed effect was limited to the time points up to 2 h post electroporation, since there seemed to be a block at the stage of re-initiation for all mutants. The luciferase activity decayed roughly with the half life of the protein, which is around 2 h. Only in the case of the wild type positive control, the levels remained nearly unaltered even at 4 h post transfection. This effect cannot be attributed to RNA stability, in spite of the fact that the decay of wild type RNA was indeed slowed by miR-122. This point can be exemplified by focusing on the C mutant (**fig. 5.29**, **fig. 5.30**). Here, the initial 1 h values of luciferase activity closely resembled the wild type levels (3.5-fold RLuc for WT and 4.3-fold for C). Also, the RNA decay kinetics were very similar (with and without miR-122) with a half life of approximately 30 minutes (**fig. 5.30**). The reason for this increased stability of the mutant without miR-122 has not been investigated, but might be due to the introduced stem-loop structure. In any case, initial translation and RNA breakdown were nearly identical, still the rate of protein decay was accelerated. This is, precluding any effect on protein stability itself, indicative of a large protein amount generated in one or two rounds of translation, followed by ribosome drop-off.

In addition, the influence of Xrn1 and 2 on HCV translation was investigated by knock-down experiments. It has been established that Xrn1 knock-down protects HCV RNA from degradation[203]. Indeed, silencing of Xrn1 could also significantly enhance luciferase activity in the translation assay (**fig. 5.31**). However, luciferase expression over time was still enhanced by miR-122 WT compared to A4U (**fig. 5.32**). Therefore, the effects of miR-122 on stability of the RNA and translation activity rely on separate mechanisms. In addition, knock-down of Xrn2 had no effect on luciferase expression, which argues against a role in HCV RNA degradation, as proposed by[204].

The obtained data, based on the domain I mutants, support the initial hypothesis that the IRES structure is influenced by miR-122 association, which in turn leads to more efficient translation initiation. However, the fast decay of translation activity of all mutants, compared to the wild type with bound RNA, suggested an additional mechanism, which depends on the miRISC itself. Moreover, stability and translation

activity were shown to be mechanistically independent.

6.4.1. Influence of miR-122 and Mg^{2+} on IRES Structure

The marked effect on first-round translation activity, even though it was not sustained, correlated with structural constraints introduced by specific mutations (**fig. 5.29**). The biochemical approach to validate the secondary structure via SHAPE chemistry could not detect a significant fraction of a single alternative structure **fig. 5.23**. Accordingly, the native gel analysis showed several secondary structures of the wild type RNA, but none for the domain I mutants **fig. 5.24**. Also the obtained NMR data indicated the presence of a number of conformers (**fig. 5.20**), which may be intermediate folding states. The RNA also seemed to progress from one state to the other dynamically, since at low temperatures, the obtained NMR peaks were broadened and the noise increased, arguing for a number of structurally diverse forms. As shown in **fig. 5.23**, the region around the second miR-122 binding site (nt 38-43) was unpaired in almost all predicted structures (calculated probability 0.65 - 1), and was highly reactive. In contrast, the signal for the directly adjacent nucleotides 21-35 was severely decreased. Precluding a technical error only occurring in this particular region, this phenotype contradicted the notion, that this part is entirely relaxed. The fact that this was seen for the 120 nt long fragment as well (supplementary **fig. C.4**), can be interpreted to conclude that these nucleotides are engaged in some way with other sequences in this region. Secondly, the experimental validation of all tested domain I mutant structures showed high degrees of conformity with the prediction (**fig. 5.25**-**fig. 5.27**). This increased the overall confidence in the *in silico* data.

The native gel, NMR and SHAPE experiments did confirm that a fraction of the RNA natively adopts the canonical fold. This was in line with the predictions derived from the phenotypical data shown in **fig. 5.29**: translationally active RNA is formed even in absence of miR-122, so a significant fraction probably contains SLII.

The structure of the complete 5' 389 nt of HCV was then investigated by means of SHAPE analysis under different ion conditions and in presence or absence of miR-122. MgCl$_2$ is known to have a significant impact on the folding of the HCV IRES and miR-122 hybridization, as has been reported by several groups[349,307,350]. Moreover, the exact ion-dependent secondary structure has not been established for the 5' terminal part. Thus, we performed folding experiments using different Mg^{2+} concentrations, and some mutants enhancing or reducing translational activity. For the wild type IRES,

there were marked changes that appeared with increasing ion availability. A phenotype also observed by Mortimer and Doudna[349] (supplementary data). In the intermediate condition (1 mM), which should be close to cellular free magnesium levels, miR dependent changes could be observed, which seemed to alter the structure in a way similar to the highest magnesium levels. This might also be a limitation of studies performed on RNA structure before, since mostly unphysiologically high magnesium concentrations were used, which improves folding, but also introduces a source of *in vitro* artifacts. Translation initiation, measured by sucrose density fractionation, is also increased at concentrations of 5 mM $MgCl_2$, as compared to 2.5 mM[347]. While this study claimed to use intracellular concentrations of magnesium, no distinction was made between free, ionized Mg^{2+}, which only constitutes around 1-5% of the total amount[351], while the vast majority is complexed with nucleotides/nucleic acids and proteins[351,352], and is thus not available for the HCV IRES. This leaves a "usable" intracellular concentration of only 0.1-3.5 mM in a normal cell. This is a range at which the HCV IRES was seemingly impaired in initiating translation, according to the data of Lancaster et al.[347].

Finally, the appearance of certain reactivity peaks in presence of high $MgCl_2$ or excess miR-122-5p, was indicative of fixation of certain structures under these conditions (**fig. 5.33**, U103). In agreement with the hypothesis that at these high concentrations of divalent cations the HCV IRES folds spontaneously, no changes could be achieved by miR-122 at 6.6 mM magnesium, albeit very efficient binding to its target, as indicated by a marked loss in reactivity within the MBR (**fig. 5.33**A). That would mean, a maximally folded equilibrium was already established, which was also corroborated by the NMR data, gathered under high magnesium concentrations.

These data support a model, in which the RNA structure was stabilized by mir-122, reducing the dependence on Mg^{2+} ions, or poising the structure to coordinate the available ions more efficiently. Moreover, the presence of a functional RISC in the cell might be needed to exert the strongest possible effect on its target, which cannot be attained by mere hybridization.

6.4.2. A pioneer round of translation at the IRES?

Cap-dependent translation in eukaryotic cells is usually split in two distinct phases, characterized by discernible RNPs associated to the mRNA[215,218,213,217]. The first round of translation is usually dependent on the cap binding complex CBP20/80, which interacts with polyA binding proteins and initiation factors. CBP20/80 and PABPN1 are only

found on mRNAs in this pioneer round of translation[218]. Likewise, if the transcript is spliced, the exon-junction complex remains associated during this stage[217]. When the first ribosome has assembled and encounters an EJC before it has reached a stop codon, this is recognized as a signal for an aberrant transcript. This triggers a quality control mechanism called non-sense mediated decay[216]. For a correctly spliced message, after the first ribosome has run through the coding region, a major change in RNP composition is induced in order to form the polysome and start steady-state translation[218].

The phenotype in the case of the HCV domain I mutants was quite reminiscent of the proceedings taking place during non-sense mediated decay. In particular, only active translation triggers this type of RNA decay, which could also be interpreted from the results at hand: the most strongly translated $\Delta 20$ mutant RNA was degraded at a rate even faster than wild type in absence of miR-122, while the ISL mutant abolishing translation near completely was as stable as wild-type with miR (**fig. 5.30** $\Delta 20$, ISL). Generally, one would not easily assume a role of NMD in HCV RNA turnover, since the HCV genome is not spliced, and mammalian intronless genes are usually NMD resistant[353]. To date, there have been no reports so far implicating the EJC/NMD machinery with HCV translation, but some peculiar facts hint towards a possible connection. Firstly, several NMD components, including the central factor Upf1, which is essential for recruitment and activation of the effector endonucleases, have been found in proteomic approaches to be present on HCV RNA, and to interact with viral proteins[309,354]. Also, Xrn1 the nuclease claimed to be responsible for HCV degradation, is the enzyme that eliminates the 5'-uncapped RNA fragments resulting from NMD cleavage[355]. Furthermore, it is known that IRES-mediated translation can trigger NMD, without the need for CBP-components[356], while AGO2 binding to a given mRNA can actively inhibit NMD[357,358]. Recently, two studies also showed a direct antiviral effect of NMD by limiting translation of (+)-sense RNA viruses in plants and mammals. The effects were seen to be dependent on central effector components Upf1, SMG5 and SMG7[359,360].

In conclusion, a putative inhibitory effect of NMD on the viral RNA, and hijacking of AGO2 by HCV, in order to prevent degradation of its genome, is a plausible hypothesis, which might be promising a starting point for further studies. Especially the determination of the translation-associated RNP could hold novel insights into the regulation of the HCV IRES.

6.4.3. Potential candidates for a translation-activating host factor

The observation that alterations in domain I, which natively stabilize SLII were still not able to induce translation over a longer time period (**fig. 5.32**A), argues for a specific function of miR-binding. This will in the cell always be accompanied by the RISC complex, and an array of auxiliary factors. It is very likely, that one of these proteins stimulates steady state translation. Considering the notion that the first round of translation could obviously be initiated without the need for a RISC complex in the domain I mutants (**fig. 5.29**), it follows that re-initiation is the step where the miR-guided RNP might act. For efficient multi-round translation, mRNAs need to adopt a circular form. It has been shown in fact that regions of the 3'UTR are essential for full translation activity. Thus, the function of the factor in question, could be responsible to bridge both ends of the viral genome. This could either be AGO itself, or an interacting protein, binding to the 3' UTR of HCV.

One of the few occasions, where miRNA-mediated up-regulation of translation has been described in human cells, is TNFα. Here, a complex containing AGO2 and FXR1 is required for activation of protein synthesis[361,362]. FXR1 is known to bind to AU-rich elements in the 3' UTR of the *tnfa*-mRNA, and during starvation it can interact with AGO2 to stimulate TNFα expression. The detailed mechanism that promotes the switch of the AGO2-dependent machinery from RNA decay to translation activation is however still elusive. FXR1 itself would rather be unlikely as the interaction-partner in suspicion, since the translation stimulating complexes were shown to form during cell cycle arrest, while the HCV IRES is most active in the mitotic G2/M stages[363]. Moreover, in the mouse, Tsai et al.[364] found that the polysome assembled more efficiently on RIP140 mRNA, after binding of miR-346 to a binding site in the 5' UTR. While the exact mechanism has not been elucidated in this case, AGO2 knockdown did not significantly impair this effect, which could hint towards a role of the other AGO-members[364]. Thus, the proof-of-principle has been established that the RISC can participate in translation activation under specific conditions.

In the following, some factors will be discussed, which could be promising candidates for a translation enhancing/sustaining function for the HCV IRES. To reiterate, assuming a bridging function between the 3' and 5' end, the factor in question needs to interact with the 3' UTR, and a component of the RISC, likely an AGO protein. An indirect interaction might also be possible, however, only direct interactions will be assumed here to minimize the complexity of the initial model.

Nuclear Factors Associated with dsRNA

NF90 and NF45 are dsRNA binding proteins which cooperate functionally with each other and further proteins and regulatory RNAs to regulate gene expression and stabilize mRNAs. Furthermore, both factors are commonly found in Argonaute-containing complexes, which make them appealing candidates for being the bridging component needed for efficient HCV translation. The interaction of both has been shown to stimulate gene expression of cellular proteins, and activate cell proliferation[365,366]. In respect to cellular mRNA, it has been described that NF90 is also involved in RNA transport processes[367], which could also play a role in delivering viral RNA to the sites of particular processes, be it replication or translation. NF90 has already been implicated in the replication cycle of the HCV related pestivirus BVDV[368], and binding sites for NF90 and NF45 were detected in both UTRs of HCV[369,268].

Insulin-like growth factor-2 mRNA-binding proteins

IGF2BP-1 is a member of the ZIP-code like protein family, with two more homologs, accordingly termed IGF2BP-2 and -3. The family name is derived from the drosophila homologue which targets specific mRNAs to certain sites. These proteins are exclusively localized in the cytoplasm and form RNPs with a variety of mRNAs[370,371]. Many of those are important oncogenes, i.e. KRAS, c-MYC[372], therefore dysregulation of IGF2BPs is associated with tumor metastasis[373,374]. A hallmark feature of target association is the recognition of naked RNAs, which are likely protected from premature decay IGF2BPs. IGF2BP1 binds the poly-U region of the HCV genome[121] and is a known interactor of RISC complexes[375]. IGF2BP-2 and -3 are found either associated to HCV or the RISC, respectively[308]. It cannot be excluded that these might also be involved in translation modulation in the context of HCV. Interestingly, an interaction with the protease (Npro) of the related pestivirus family has been shown[376].

Y-Box protein 1

YB1 is a DNA and RNA binding protein, which resides in the nucleus and the cytoplasm[377]. Its major functions include transcription, splicing and translation regulation. The name is deduced from its Y-Box-promoter affinity, which regulates HLA class II genes, among others[378–380]. It stabilizes exported mRNA (e.g. GMCSF, c-MYC) by sequence specific interaction[381,382]. A secreted version of the protein acts as strong mitogen and can influence proliferation and migration of neighboring cells[383]. An involvement in

the non-coding RNA machinery has been claimed as well[384]. YB1 has been described as a dependency factor of HCV replication, while it restricts virion assembly. Mechanistically, it is known that YB1 exerts its effects on the viral life cycle in part by binding to NS3[285,385].

PolyA-binding protein N1

The class of poly-A binding proteins regulate translation initiation, by associating to the 3' poly A element of mRNAs in the nucleus. PABPN1 can recruit and stimulate the poly A polymerase activity, thereby stabilizing target transcripts through the elongation of their poly A tail[386]. The protein is shuttled to the cytoplasm in complex with the mRNA[387]. During the pioneer round of translation, it modulates NMD, and is removed from the RNP in a translation-dependent manner[218]. Steady-state translation requires only PABPC1[218,355]. It has been found to be associated with the HCV genome[309], but there has been no report of functional interaction with HCV so far. However, the fact that several other factors included in the pioneer round of translation and the associated NMD pathway have also been found to bind HCV RNA might suggest a possible functional link[309,354].

Human antigen R

HuR is a predominantly nuclear RNA-binding protein, which preferentially targets the 3' UTR of mRNAs. Especially poly U and AU-rich elements are avidly bound[388]. It can regulate the nuclear export of its target messages, and thereby influence gene expression. Prominent targets are the proto-oncogenes survivin and p53[389,390]. Deregulation of HuR has been implicated in tumor growth and metastasis[391–393]. Moreover it interferes with miR-122-binding to the CAT-1 mRNA and relieves its repression[182]. Sindbis virus recruits HuR to a U-rich region in its 3' UTR, stabilizing the viral genome. This is accompanied by a translocation of HuR into the cytoplasm, which also leads to impairment of its cellular functions[394,395]. An AU-rich element present in the CSFV genome is also targeted[396]. HuR has been linked to HCV translation stimulation, which is achieved by binding to the viral polyU element in the 3' UTR[120]. The exact mechanism has not been clarified so far.

The role of AGO1

The comparison of HCV and RISC associated factors led to the striking observation that most proteins, which play a role in IRES mediated translation, are actually in a complex assembled around AGO1 ("complex III" from Höck et al.[308]). The few studies that looked at the different Argonaute proteins apart from AGO2 in HCV modulation yielded controversial results. While some reports found that AGO2 is the key player boosting HCV RNA accumulation[397,339], another group saw all Argonaute proteins (and many other components of the RNAi machinery) as important host factors in their siRNA approach[152]. Curiously, in this case the knockdown of AGO4 was the most effective in inhibiting HCV replication. A more recent study also showed direct, miR-dependent association of AGO1 to HCV RNA, albeit AGO2 was still more efficiently bound[208]. It is important to consider a likely interaction between the Argonaute proteins and their respective complexes. Moreover, little is known about the determinants of miRNP-assembly. This might again be dependent on the cell-type and environmental factors, so that the study of Höck et al.[308], which was performed in HeLa lysates, might be a good starting point, but could fail to describe the situation in the liver. Thus, the proteins found only in AGO1 complexes by Höck et al.[308], could also be associated to AGO2 in liver cells. Alternatively, different functions in the viral life cycle might be performed by different AGO-species.

The review of the literature brought to light several candidate proteins, which interact with the HCV 3' UTR, as well as the RISC. Hence, these factors could join the 5' and 3' end of the viral genome during translation, to facilitate polysome formation. Notably, AGO1 was found to bind many of the factors known to modulate HCV IRES-mediated translation, which could imply that AGO2 is not the only Argonaute protein involved in HCV regulation.

6.5. The effect of miR-122 in HCV replication

The annealing of miR-122 to the 5' end of the HCV genome is characterized by a 6-nucleotide U-rich overhang. This is thought to prevent recognition of the uncapped viral 5' terminus by exonucleases, like Xrn1[203]. Moreover, it has been shown that deletion of the 3' nucleotides can severely affect miR-122-dependent HCV stimulation[202]. This might have been be a result of inefficient incorporation into the RISC, which is strongly selective for correctly sized RNA duplexes. Another study has also found that either

shortened or elongated synthetic miR molecules were impaired in their influence on HCV[208]. While some work has been done in the context of translation, using short luciferase reporter constructs[346], we wanted to study the miR-122 sequence determinants for replication in more detail. A central hypothesis was the possible primer generation of NS5B at the single-stranded portion of the bound microRNA, since the 3' UG dimer at the end of the miR would be a perfect primer template (**fig. 5.36**). Moreover, the structural appearance, a short pyrimidine-rich region, close to a helical element, resembles an ideal initiation template for NS5B[107]. Also, the genome is circularized to facilitate replication, which brings the 5' and 3' termini in close proximity[398]. Thus, primer generation at the microRNA would be an elegant solution to effectively initiate (-)-strand synthesis. However, we could show that at least the supplementation of a synthetic duplex could not rescue a corresponding mutant in Hep3B cells, arguing against an initiation at the bound miR-122. Importantly, this phenotype strongly favors a primer generation site apart from the 3' terminus, since the priming would otherwise be unaffected by the mutation of the penultimate nucleotide. Furthermore, we tested a panel of other mutants to assess their influence on HCV replication. The general phenotype of different mutations introduced in the overhang and bulged regions of the miRNA was also investigated. Most perturbations of the non-binding miR-regions were tolerated without impairing HCV replication. The exchange of all overhang nucleotides to their complementary counterparts resulted in a 70% reduction of replication, while translation remained seemingly unaffected. A terminal UG-rich sequence might therefore have some impact on miR-122 activity. This might also explain why addition of the miR-26a 3' region has no effect, as it also harbors 3 pyrimidines and two gunaines. Importantly, a recent report suggests binding of hnRNP K to flexible, pyrimidine-rich sequences in mature miR-122[399]. While hnRNPK does not influence replication[400], a similar mechanism involving another miR-binding protein might be responsible for the observed effect. A switch of the bulged and overhang region massively affected replication (100-fold reduction), and initial translation (4-fold reduction). This could also be due to the 1 nt difference in length between the two regions, making the bulge slightly smaller, which might affect the target binding affinity in general.

Furthermore, RNA localization may be influenced by RISC binding. Since several components of the miR-silencing pathway are involved in HCV replication[318,401,317], we asked whether these could recruit the AGO-bound genome to the sites of viral replication. In an imaging based approach, electroporated HCV (+)-strand RNA was stained *in situ*, and in parallel to AGO2 and Hsp90, a chaperone involved in many steps of the HCV

life cycle[402,403,284]. Unexpectedly, while the signals for protein and RNA were in close proximity in some regions, no direct co-localization was observed (**fig. 5.37**). It was not clear, if this was due to a very transient interaction, a suboptimal time point (48 h post electroporation), or technical limitations. Therefore, no definitive conclusions could be drawn from this experiment.

Recent studies performed by Masaki et al.[207] suggest that part of the mechanism could be the displacement of PCBP2, a host factor that stimulates translation. The authors claimed that this leads to a shift of the fraction of HCV RNA engaged in translation towards replication.

Unfortunately, the mechanisms of miR-122 supporting viral RNA replication could not be elucidated further in this study.

6.6. Effects of miR-122 binding to sites in the CDS and 3' UTR

In the same report that found the first binding site in the 5' UTR, an additional one has been described within the variable region of the 3' UTR[153]. While this region is not essential for RNA replication *in vivo*[404], deletions impaired viral propagation in the replicon system by an unknown mechanism[118], which might be linked to miR-122. Later on, another site was identified in the coding region of NS5B[320]. However, these additional sites have only been poorly characterized, likely because of their negligible effect on viral replication. In our study, possible additional binding sites were investigated by searching the full-length genomes of six genotypes for the core hexamer CACUCC. Indeed, several putative miR binding sites were detected in the sequences, two of them were also conserved among genotypes. Insertion of point mutations had only limited effects on RNA amplification kinetics of HCV replicons in Huh7 Lunet, as well as in Hep3B cells with exogenously supplemented miR-122 (0.3-fold to 1.5-fold of wild type). Interestingly, some mutants showed enhanced translation (up to 6-fold), which could imply directly opposing effects of miR-binding to either end of the genome, which has been described for the known sites 5 and 6[320]. For site 6, this could also be deduced from a reporter assays, in which this MBR could significantly lower the expression of a preceding *renilla* luciferase gene. All other sites, except site 3, could hardly act as translational repressors. Also, no synergistic effects were detected using all sites in conjunction. However, the results obtained with the artificial reporters did not correlate completely with the phenotype seen

in the replicons. For instance, point mutations within sites 4 and 5 could enhance initial translation to a certain degree, which could argue for additional influence of the flanking sequences, or effects dependent on certain combinations of binding sites not tested so far. In any case, these sites seem to be functional, and their conservation speaks for a relevant role in the HCV life cycle. The restricting effects on translation/replication would suggest distinct and position-dependent complexes, which are recruited to exert a specific function.

To date, an impact of miR-122 on assembly and release has been proposed only once, and focusing on the 5' UTR sites[405]. Since replication kinetics were only moderately affected by the identified 3' sites, these were also tested for a function in later stages of viral propagation. The mutant sites were cloned into JcR2A reporter viruses and Huh7.5 cells were electroporated with or without the matching miR-122 mutant. For the single mutants, as in the replicon context, no notable effect could be seen. However, supplementation of miR-122 A4U lowered the replication capacity of mutant 6. Notably, this phenotype was dominant in all mutants harboring a defective site 6. This corroborates the reporter assays and the previous report of Nasheri et al.[320], which showed that this site could function to repress the upstream ORF to some extent. The supernatants containing the released virions were used to inoculate fresh Huh7.5 cells, and luciferase activity was measured 72 h later. The replication of the electroporated cells after 72 h was used as baseline to normalize the amount of reinfection (**fig. 5.40**). All viruses, except for the single mutations site 4 and 5, were severely impaired in their relative release of infectivity, compared to wild type. However, the addition of synthetic miR-122 A4U duplex during electroporation could not rescue the assembly/release phenotype. This could be in part due to the experimental setup. One has to take into account that exogenously delivered duplex RNA in high doses will be incorporated in a different fashion than intracellularly expressed miRNA. In an earlier publication NS3 was observed to form a complex with YB1, which modulates virus production and replication[285,385]. YB1 is also an interaction partner of AGO1 and 2. Therefore, the assembled RISC-complexes might be different and dependent on viral proteins. In that case, the bound complexes formed by synthetic miR might not be able to act synergistically. Follow-up experiments will be performed using Huh7.5 cells, stably expressing miR-122 A4U, to circumvent these potential pitfalls. Furthermore, nothing is known about the regulatory events that dictate where miR-122 binds on the HCV genome. Finally, it cannot be excluded that miR-122 wild type is needed for activation of assembly/release. A possible explanation might be the significant effect of HCV replication on miR-122 function,

which has been described by Luna et al.[340]. The authors saw a marked upregulation of miR-122 target genes. One of these might play a role in assembly, packaging or release of the virion. Assuming that sequestration of miR-122 might be dependent on the concerted action of all binding sites in the genome, the introduced mutations would disturb this function. Therefore, no rescue can be achieved by miR-122 A4U addition. In this case, specific inhibition of miR-122 might be a way to rescue assembly in these mutants. Also it will have to be clarified whether the defect lies in the actual assembly step, or whether infectious virions are only retained within the cell.

In summary, the characterization of additional miR-122 binding sites in the HCV genome showed that at least two of these sites have an impact on assembly/release. These findings led to the discovery of a complex regulatory mechanism, which should be explored in more depth in the future.

6.7. Towards a comprehensive model of miR-122:HCV interaction

In the course of this study, we have shown that miR-122 is indispensable for HCV replication, and have quantified the influence at individual steps of the viral life cycle. Mutants lacking miR-122 binding sites, but stabilizing the IRES structure were equally or more efficient at what appears to be a pioneer round of translation, as the wild type with bound miR-122. Thus, the stabilization of essential structures by miR-122 association might be the first step of poising the RNA for translation. Suppression of adverse conformations and favoring of SLII formation would provide a surface for 40S docking[254,247,259], which is the basis of preinitiation complex formation. The recruitment of the first ribosome is therefore accelerated in these mutants even in absence of RISC binding. However, further rounds of translation were not efficiently initiated. This led to the conclusion that the AGO-associated complex itself is essential at the stage of polysome assembly. This might be facilitated through an interaction of the RISC with a factor binding to the 3' UTR, leading to genome circularization. This end-joining has been proposed to be an essential step for induction of steady-state translation[406]. The aspects of genome stability and initiation of replication were found to play subordinate roles, and support the life cycle through an additive mechanism. The RNA stabilizing effect of the miR could be reproduced in this study, could however not account for the effects seen on viral propagation. While point mutations in the 5' miR-122 binding
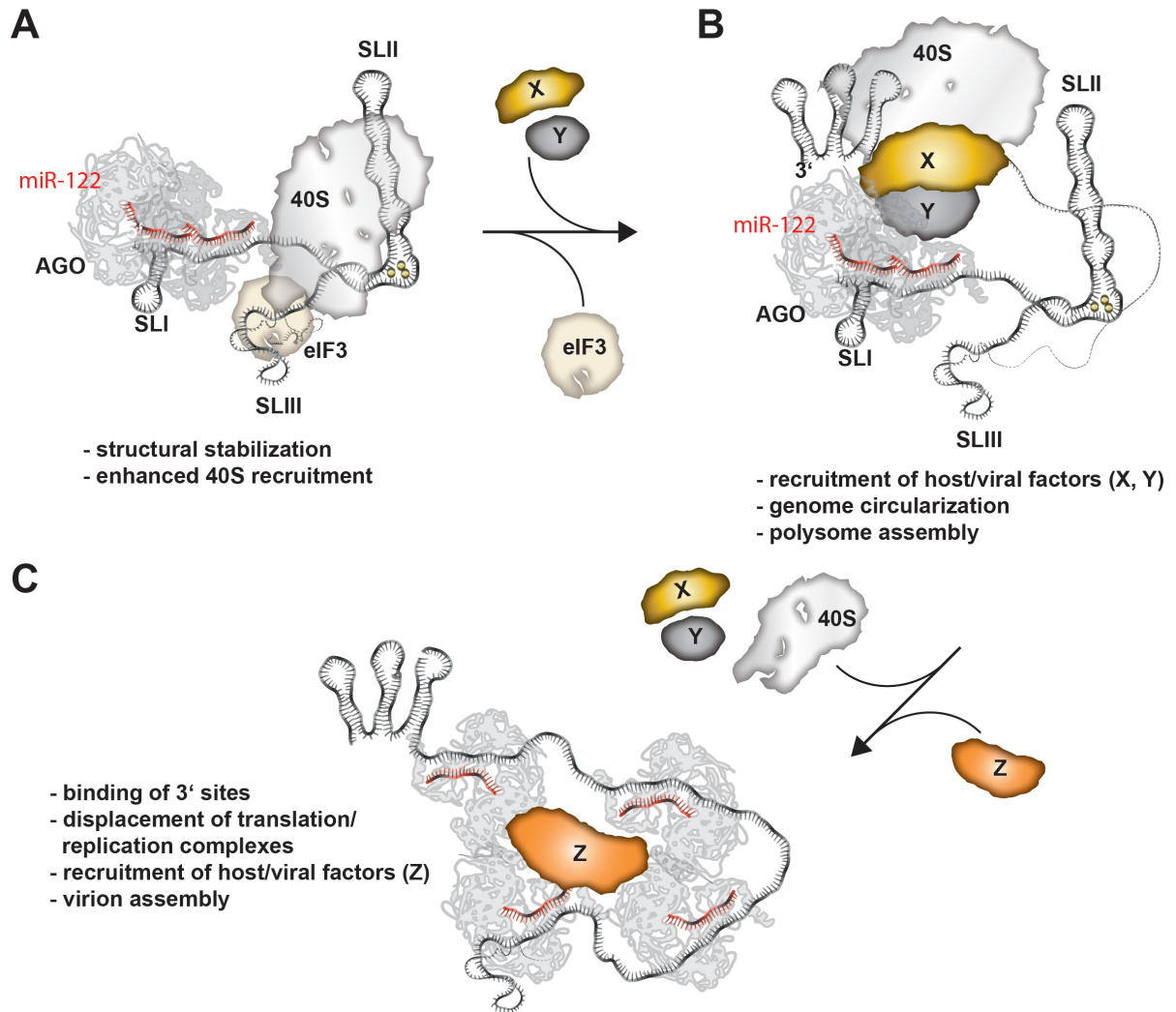
Figure 6.1.: Model of miR-122:HCV interaction A | Initially, miR-122 association to the 5' terminus of HCV might stabilize a translation-competent conformation of the IRES. Thereby, the miRISC enables enhanced binding of the 40S ribosomal subunit and initiation factors (i.e. eIF3). **B |** After the initial round of translation, genome circularization is required for efficient reinitiation of the ribosome. This seemed to be impaired, when miR-122 and the associated RNP is not present. Therfore, recruitment of host/viral factors might interact with the RISC to create a bridge between the genome termini. **C |** In later stages of viral replication, HCV needs to shunt some of the genomic RNA towards packaging to generate progeny virions. Binding of miRISC to 3' recognition sites seemed to suppress translation/replication, while increasing the fraction of RNA available for virion assembly.

sites are detrimental for viral translation, targeting of newly discovered 3' located sites could increase translation. This was accompanied by a marked decrease in viral progeny generation. Therefore, we propose a dynamic shift of HCV associated RISCs which might differ in protein composition. The modulatory effect of NS3 in complex with YB1[285] imply that HCV might actively modify RISCs in the course of infection.

The miRNP-based determinants for the translation/replication/assembly-switches will be of particular interest for subsequent studies. More efforts will have to be invested into localization studies and biochemical approaches to unravel the mechanism by which miR-122 augments replication. Overall, this study provides several new perspectives, and the basis for a deeper understanding of this unique virus-host interaction.

A. Abbreviations

A. Abbreviations

A. Abbreviations

B. Bibliography

[1] Stephen M Feinstone, et al. Transfusion-associated hepatitis not due to viral hepatitis type a or b. *N. Engl. J. Med.*, 292(15): 767–770, 1975.

[2] V. M. Villarejos, et al. Evidence for viral hepatitis other than type a or type b among persons in Costa Rica. *N. Engl. J. Med.*, 293 (26):1350–1352, 1975.

[3] Q. L. Choo, et al. Isolation of a cdna clone derived from a blood-borne non-a, non-b viral hepatitis genome. *Science*, 244(4902): 359–362, 1989.

[4] Jane P. Messina, et al. Global distribution and prevalence of hepatitis c virus genotypes. *Hepatology*, 61(1):77–87, 2015.

[5] C. J. Tibbs. Methods of transmission of hepatitis c. *J. Viral Hepat.*, 2(3):113–119, 1995.

[6] Miriam J. Alter. Epidemiology of viral hepatitis and hiv co-infection. *J. Hepatol.*, 44(1 Suppl):S6–S9, 2006.

[7] Raymond T. Chung. Acute hepatitis c virus infection. *Clin. Infect. Dis.*, 41 Suppl 1:S14–S17, 2005.

[8] J. Bukh, et al. Biology and genetic heterogeneity of hepatitis c virus. *Clin. Exp. Rheumatol.*, 13 Suppl 13:S3–S7, 1995.

[9] Laurent Castera, et al. Hepatitis c virus-induced hepatocellular steatosis. *Am. J. Gastroenterol.*, 100(3):711–715, 2005.

[10] T. J. Liang, et al. Pathogenesis, natural history, treatment, and prevention of hepatitis c. *Ann. Intern. Med.*, 132(4):296–305, 2000.

[11] Joseph F Perz, et al. The contributions of hepatitis b virus and hepatitis c virus infections to cirrhosis and primary liver cancer worldwide. *J. Hepatol.*, 45(4):529–538, 2006.

[12] Shih-Sung Chuang, et al. Hepatitis c virus infection is significantly associated with malignant lymphoma in Taiwan, particularly with nodal and splenic marginal zone lymphomas. *J. Clin. Pathol.*, 63(7):595–598, 2010.

[13] N. M. Dixit and A. S. Perelson. The metabolism, pharmacokinetics and mechanisms of antiviral activity of ribavirin against hepatitis c virus. *Cell. Mol. Life Sci.*, 63(7-8):832–842, 2006.

[14] Kai Lin, et al. Vx-950, a novel hepatitis c virus (hcv) ns3-4A protease inhibitor, exhibits potent antiviral activities in hcv replicon cells. *Antimicrob. Agents Chemother.*, 50(5):1813–1822, 2006.

[15] Kenneth Berman and Paul Y. Kwo. Boceprevir, an ns3 protease inhibitor of hcv. *Clin Liver Dis*, 13(3):429–439, 2009.

[16] Robert A. Fridell, et al. Resistance analysis of the hepatitis c virus ns5A inhibitor bms-790052 in an in vitro replicon system. *Antimicrob Agents Chemother*, 54(9):3641–3650, 2010.

[17] Tarik Asselah. Sofosbuvir for the treatment of hepatitis c virus. *Expert Opin. Pharmacother.*, 15(1):121–130, 2014.

[18] J. Vermehren and C. Sarrazin. New hcv therapies on the horizon. *Clin Microbiol Infect*, 17(2):122–134, 2011.

[19] Lotte Coelmont, et al. Debio 025, a cyclophilin binding molecule, is highly efficient in clearing hepatitis c virus (hcv) replicon-containing cells when used alone or in combination with specifically targeted antiviral therapy for hcv (stat-c) inhibitors. *Antimicrob. Agents Chemother.*, 53(3):967–976, 2009.

[20] Sam Hopkins, et al. The cyclophilin inhibitor SCy-635 suppresses viral replication and induces endogenous interferons in patients with chronic hcv genotype 1 infection. *J. Hepatol.*, 57(1):47–54, 2012.

[21] Eric Lawitz, et al. Safety, pharmacokinetics, and antiviral activity of the cyclophilin inhibitor nim811 alone or in combination with pegylated interferon in hcv-infected patients receiving 14 days of therapy. *Antiviral Res.*, 89(3):238–245, 2011.

[22] Elisabeth S. Hildebrandt-Eriksen, et al. A locked nucleic acid oligonucleotide targeting microrna 122 is well-tolerated in cynomolgus monkeys. *Nucleic Acid Ther*, 22(3):152–161, 2012.

[23] Søren Ottosen, et al. In vitro antiviral activity and preclinical and clinical resistance profile of miravirsen, a novel anti-hepatitis c virus therapeutic targeting the human factor mir-122. *Antimicrob. Agents Chemother.*, 59(1):599–608, 2015.

[24] Meike H. van der Ree, et al. Long-term safety and efficacy of microrna-targeted therapy in chronic hepatitis c patients. *Antiviral Res.*, 111:53–59, 2014.

[25] Troels K H. Scheel, et al. Characterization of nonprimate hepacivirus and construction of a functional molecular clone. *Proc. Natl. Acad. Sci. U. S. A.*, 112(7):2192–2197, 2015.

[26] Maria Teresa Catanese, et al. Ultrastructural analysis of hepatitis c virus particles. *Proc. Natl. Acad. Sci. U. S. A.*, 110(23): 9505–9510, 2013.

[27] Q. L. Choo, et al. Genetic organization and diversity of the hepatitis c virus. *Proc. Natl. Acad. Sci. U. S. A.*, 88(6):2451–2455, 1991.

[28] Y. Tanji, et al. Hepatitis c virus polyprotein processing: kinetics and mutagenic analysis of serine proteinase-dependent cleavage. *J. Virol.*, 68(12):8418–8422, 1994.

[29] R. Suzuki, et al. Processing and functions of hepatitis c virus proteins. *Intervirology*, 42(2-3):145–152, 1999.

[30] C. Wang, et al. A conserved helical element is essential for internal initiation of translation of hepatitis c virus rna. *J. Virol.*, 68(11):7301–7307, 1994.

[31] A. V. Gamarnik and R. Andino. Switch from translation to rna replication in a positive-stranded rna virus. *Genes Dev.*, 12(15): 2293–2304, 1998.

[32] P. Pileri, et al. Binding of hepatitis c virus to CD81. *Science*, 282(5390):938–941, 1998.

[33] Mirjam B. Zeisel, et al. Scavenger receptor class b type i is a key host factor for hepatitis c virus infection required for an entry step closely linked to CD81. *Hepatology*, 46(6): 1722–1731, 2007.

[34] Matthew J. Evans, et al. Claudin-1 is a hepatitis c virus co-receptor required for a late step in entry. *Nature*, 446(7137):801–805, 2007.

[35] Marion Sourisseau, et al. Temporal analysis of hepatitis c virus cell entry with occludin directed blocking antibodies. *PLoS Pathog.*, 9(3):e1003244, 2013.

[36] Joachim Lupberger, et al. Egfr and epha2 are host factors for hepatitis c virus entry and possible targets for antiviral therapy. *Nat. Med.*, 17(5):589–595, 2011.

[37] Emmanuelle Blanchard, et al. Hepatitis c virus entry depends on clathrin-mediated endocytosis. *J. Virol.*, 80(14):6964–6972, 2006.

[38] Laurent Meertens, et al. Hepatitis c virus entry requires a critical postinternalization step and delivery to early endosomes via clathrin-coated vesicles. *J. Virol.*, 80(23): 11571–11578, 2006.

[39] Sibylle Haid, et al. Low ph-dependent hepatitis c virus membrane fusion depends on e2 integrity, target lipid composition, and density of virus particles. *J. Biol. Chem.*, 284 (26):17657–17667, 2009.

[40] A. Grakoui, et al. Expression and identification of hepatitis c virus polyprotein cleavage products. *J. Virol.*, 67(3):1385–1395, 1993.

[41] K. Shimotohno, et al. Processing of the hepatitis c virus precursor protein. *J. Hepatol.*, 22(1 Suppl):87–92, 1995.

[42] Andreas Weihofen, et al. Identification of signal peptide peptidase, a presenilin-type aspartic protease. *Science*, 296(5576):2215–2218, 2002.

[43] Takanobu Kato, et al. Processing of hepatitis c virus core protein is regulated by its

c-terminal sequence. *J. Med. Virol.*, 69(3): 357–366, 2003.

[44] K. Yasui, et al. The native form and maturation process of hepatitis c virus core protein. *J. Virol.*, 72(7):6048–6055, 1998.

[45] Doris Quinkert, et al. Quantitative analysis of the hepatitis c virus replication complex. *J. Virol.*, 79(21):13594–13605, 2005.

[46] Rainer Gosert, et al. Identification of the hepatitis c virus rna replication complex in huh-7 cells harboring subgenomic replicons. *J. Virol.*, 77(9):5487–5492, 2003.

[47] Darius Moradpour, et al. Membrane association of hepatitis c virus nonstructural proteins and identification of the membrane alteration that harbors the viral replication complex. *Antiviral Res.*, 60(2):103–109, 2003.

[48] Darius Moradpour, et al. Membrane association of the rna-dependent rna polymerase is essential for hepatitis c virus rna replication. *J. Virol.*, 78(23):13278–13284, 2004.

[49] David Paul, et al. Morphological and biochemical characterization of the membranous hepatitis c virus replication compartment. *J. Virol.*, 87(19):10612–10627, 2013.

[50] Ralf Bartenschlager, et al. Hepatitis c virus replication cycle. *J. Hepatol.*, 53(3):583–585, 2010.

[51] Mair Hughes, et al. Domain iii of ns5A contributes to both rna replication and assembly of hepatitis c virus particles. *J. Gen. Virol.*, 90(Pt 6):1329–1334, 2009.

[52] Hamed Gouklani, et al. Hepatitis c virus nonstructural protein 5B is involved in virus morphogenesis. *J. Virol.*, 86(9):5080–5088, 2012.

[53] R. De Francesco, et al. The hepatitis c virus ns3 proteinase: structure and function of a zinc-containing serine proteinase. *Antivir. Ther.*, 3(Suppl 3):99–109, 1998.

[54] R. Bartenschlager. The ns3/4A proteinase of the hepatitis c virus: unravelling structure and function of an unusual enzyme and a prime target for antiviral therapy. *J. Viral Hepat.*, 6(3):165–181, 1999.

[55] Martin Baril, et al. Mavs dimer is a crucial signaling component of innate immunity and the target of hepatitis c virus ns3/4A protease. *J. Virol.*, 83(3):1299–1311, 2009.

[56] Stacy M. Horner, et al. Mitochondrial-associated endoplasmic reticulum membranes (mam) form innate immune synapses and are targeted by hepatitis c virus. *Proc. Natl. Acad. Sci. U. S. A.*, 108(35):14590–14595, 2011.

[57] Kui Li, et al. Immune evasion by hepatitis c virus ns3/4A protease-mediated cleavage of the toll-like receptor 3 adaptor protein trif. *Proc. Natl. Acad. Sci. U. S. A.*, 102(8):2992–2997, 2005.

[58] Erwin Daniel Brenndörfer, et al. Nonstructural 3/4A protease of hepatitis c virus activates epithelial growth factor-induced signal transduction by cleavage of the t-cell protein tyrosine phosphatase. *Hepatology*, 49(6):1810–1820, 2009.

[59] Craig A. Belon and David N. Frick. Fuel specificity of the hepatitis c virus ns3 helicase. *J. Mol. Biol.*, 388(4):851–864, 2009.

[60] Meigang Gu and Charles M. Rice. Three conformational snapshots of the hepatitis c virus ns3 helicase reveal a ratchet translocation mechanism. *Proc. Natl. Acad. Sci. U. S. A.*, 107(2):521–528, 2010.

[61] Todd C. Appleby, et al. Visualizing ATP-dependent rna translocation by the ns3 helicase from hcv. *J. Mol. Biol.*, 405(5):1139–1153, 2011.

[62] Chen Zhang, et al. Stimulation of hepatitis c virus (hcv) nonstructural protein 3 (ns3) helicase activity by the ns3 protease domain and by hcv rna-dependent rna polymerase. *J. Virol.*, 79(14):8687–8697, 2005.

[63] Kazi Abdus Salam, et al. Inhibition of hepatitis c virus ns3 helicase by manoalide. *J. Nat. Prod.*, 75(4):650–654, 2012.

[64] Sabina Piccininni, et al. Modulation of the hepatitis c virus rna-dependent rna polymerase activity by the non-structural (ns) 3 helicase and the ns4B membrane protein. *J. Biol. Chem.*, 277(47):45670–45679, 2002.

[65] Ping Wang, et al. Classical swine fever virus ns3 enhances rna-dependent rna polymerase activity by binding to ns5B. *Virus Res.*, 148 (1-2):17–23, 2010.

[66] Rudolf K F. Beran and Anna Marie Pyle. Hepatitis c viral ns3-4A protease activity is enhanced by the ns3 helicase. *J. Biol. Chem.*, 283(44):29929–29937, 2008.

[67] Thomas A. Jennings, et al. Rna unwinding activity of the hepatitis c virus ns3 helicase is modulated by the ns5B polymerase. *Biochemistry (Mosc.)*, 47(4):1126–1135, 2008.

[68] Upasana Ray and Saumitra Das. Interplay between ns3 protease and human la protein regulates translation-replication switch of hepatitis c virus. *Sci Rep*, 1:1, 2011.

[69] Keril J. Blight. Charged residues in hepatitis c virus ns4B are critical for multiple ns4B functions in rna replication. *J. Virol.*, 85(16): 8158–8171, 2011.

[70] Jason Aligo, et al. Formation and function of hepatitis c virus replication complexes require residues in the carboxy-terminal domain of ns4B protein. *Virology*, 393(1):68–83, 2009.

[71] Esther L. Ashworth Briggs, et al. Interaction between the ns4B amphipathic helix, ah2, and charged lipid headgroups alters membrane morphology and ah2 oligomeric state - implications for the hepatitis c virus life cycle. *Biochim. Biophys. Acta*, 1850(8):1671–1677, 2015.

[72] Marika Lundin, et al. Topology of the membrane-associated hepatitis c virus protein ns4B. *J. Virol.*, 77(9):5428–5438, 2003.

[73] Anne M. Paredes and Keril J. Blight. A genetic interaction between hepatitis c virus ns4B and ns3 is important for rna replication. *J. Virol.*, 82(21):10671–10683, 2008.

[74] Naama David, et al. The interaction between the hepatitis c proteins ns4B and ns5A is involved in viral replication. *Virology*, 475: 139–149, 2015.

[75] Shirit Einav, et al. A nucleotide binding motif in hepatitis c virus (hcv) ns4B mediates hcv rna replication. *J. Virol.*, 78(20):11288–11295, 2004.

[76] Qingxia Han, et al. Modulation of hepatitis c virus genome encapsidation by nonstructural protein 4B. *J. Virol.*, 87(13):7409–7422, 2013.

[77] Luyun Huang, et al. Hepatitis c virus nonstructural protein 5A (ns5A) is an rna-binding protein. *J. Biol. Chem.*, 280(43): 36417–36428, 2005.

[78] Toshana L. Foster, et al. All three domains of the hepatitis c virus nonstructural ns5A protein contribute to rna binding. *J. Virol.*, 84(18):9267–9277, 2010.

[79] Xavier Hanoulle, et al. The domain 2 of the hcv ns5A protein is intrinsically unstructured. *Protein Pept. Lett.*, 17(8):1012–1018, 2010.

[80] Xavier Hanoulle, et al. Domain 3 of nonstructural protein 5A from hepatitis c virus is natively unfolded. *Biochem. Biophys. Res. Commun.*, 381(4):634–638, 2009.

[81] Jungwook Hwang, et al. Hepatitis c virus nonstructural protein 5A: biochemical characterization of a novel structural class of rna-binding proteins. *J. Virol.*, 84(24):12480–12491, 2010.

[82] Joseph Marcotrigiano and Timothy Tellinghuisen. Purification and crystallization of ns5A domain i of hepatitis c virus. *Methods Mol. Biol.*, 510:85–94, 2009.

[83] Sebastian M. Lambert, et al. The crystal structure of ns5A domain 1 from genotype 1a reveals new clues to the mechanism of action for dimeric hcv inhibitors. *Protein Sci.*, 23 (6):723–734, 2014.

[84] Rebecca Toroney, et al. Regulation of pkr by hcv IRes rna: importance of domain ii and ns5A. *J. Mol. Biol.*, 400(3):393–412, 2010.

[85] Swarupa Panda, et al. A unique phosphorylation-dependent eif4e assembly on 40S ribosomes co-ordinated by hepatitis c virus protein ns5A that activates internal ribosome entry site translation. *Biochem. J.*, 462(2):291–302, 2014.

[86] Teymur Kazakov, et al. Hepatitis c virus rna replication depends on specific cis- and trans-acting activities of viral nonstructural proteins. *PLoS Pathog.*, 11(4):e1004817, 2015.

[87] Takahiro Masaki, et al. Involvement of hepatitis c virus ns5A hyperphosphorylation mediated by casein kinase i-alpha in infectious virus production. *J. Virol.*, 88(13):7541–7555, 2014.

[88] Ronik Khachatoorian, et al. The ns5A-binding heat shock proteins hsc70 and hsp70 play distinct roles in the hepatitis c viral life cycle. *Virology*, 454-455:118–127, 2014.

[89] Anju George, et al. Hepatitis c virus ns5A binds to the mrna cap-binding eukaryotic translation initiation 4F (eif4F) complex and up-regulates host translation initiation machinery through eif4e-binding protein 1 inactivation. *J. Biol. Chem.*, 287(7):5042–5058, 2012.

[90] Bhaswati Sarcar, et al. Hepatitis c virus ns5A mediated stat3 activation requires cooperation of jak1 kinase. *Virology*, 322(1): 51–60, 2004.

[91] Andrew Street, et al. The hepatitis c virus ns5A protein activates a phosphoinositide 3-kinase-dependent survival signaling cascade. *J. Biol. Chem.*, 279(13):12232–12241, 2004.

[92] Kattareeya Kumthip, et al. Hepatitis c virus ns5A disrupts stat1 phosphorylation and suppresses type i interferon signaling. *J. Virol.*, 86(16):8581–8591, 2012.

[93] S. J. Polyak, et al. Hepatitis c virus nonstructural 5A protein induces interleukin-8, leading to partial inhibition of the interferon-induced antiviral response. *J. Virol.*, 75(13): 6095–6106, 2001.

[94] Y. Tanji, et al. Phosphorylation of hepatitis c virus-encoded nonstructural protein ns5A. *J. Virol.*, 69(7):3980–3986, 1995.

[95] J. Kim, et al. Hepatitis c virus ns5A protein is phosphorylated by casein kinase ii. *Biochem. Biophys. Res. Commun.*, 257(3): 777–781, 1999.

[96] Manuela Quintavalle, et al. The alpha isoform of protein kinase cki is responsible for hepatitis c virus ns5A hyperphosphorylation. *J. Virol.*, 80(22):11305–11312, 2006.

[97] Nicole Appel, et al. Mutational analysis of hepatitis c virus nonstructural protein 5A: potential role of differential phosphorylation in rna replication and identification of a genetically flexible domain. *J. Virol.*, 79(5): 3187–3194, 2005.

[98] Luyun Huang, et al. Purification and characterization of hepatitis c virus non-structural protein 5A expressed in escherichia coli. *Protein Expr. Purif.*, 37(1):144–153, 2004.

[99] Simon Reiss, et al. The lipid kinase phosphatidylinositol-4 kinase iii alpha regulates the phosphorylation status of hepatitis c virus ns5A. *PLoS Pathog.*, 9(5):e1003359, 2013.

[100] Y. Ide, et al. Hepatitis c virus ns5A protein is phosphorylated in vitro by a stably bound protein kinase from hela cells and by camp-dependent protein kinase a-alpha catalytic subunit. *Gene*, 201(1-2):151–158, 1997.

[101] Yung-Chia Chen, et al. Polo-like kinase 1 is involved in hepatitis c virus replication by hyperphosphorylating ns5A. *J. Virol.*, 84 (16):7983–7993, 2010.

[102] S. Bressanelli, et al. Crystal structure of the rna-dependent rna polymerase of hepatitis c virus. *Proc. Natl. Acad. Sci. U. S. A.*, 96 (23):13034–13039, 1999.

[103] Alberdina A. van Dijk, et al. Initiation of viral rna-dependent rna polymerization. *J. Gen. Virol.*, 85(Pt 5):1077–1093, 2004.

[104] Philip Simister, et al. Structural and functional analysis of hepatitis c virus strain jfh1 polymerase. *J. Virol.*, 83(22):11926–11939, 2009.

[105] W. Zhong, et al. Template/primer requirements and single nucleotide incorporation by hepatitis c virus nonstructural protein 5B polymerase. *J. Virol.*, 74(19):9134–9143, 2000.

[106] S. S. Carroll, et al. Only a small fraction of purified hepatitis c rna-dependent rna polymerase is catalytically competent: implications for viral replication and in vitro assays. *Biochemistry*, 39(28):8243–8249, 2000.

[107] C. C. Kao, et al. Template requirements for rna synthesis by a recombinant hepatitis c virus rna-dependent rna polymerase. *J. Virol.*, 74(23):11121–11128, 2000.

[108] Todd C. Appleby, et al. Structural basis for rna replication by the hepatitis c virus polymerase. *Science*, 347(6223):771–775, 2015.

[109] V. Lohmann, et al. Biochemical properties of hepatitis c virus ns5B rna-dependent rna polymerase and identification of amino acid sequence motifs essential for enzymatic activity. *J. Virol.*, 71(11):8416–8428, 1997.

[110] Melanie Schmitt, et al. A comprehensive structure-function comparison of hepatitis c virus strain jfh1 and j6 polymerases reveals a key residue stimulating replication in cell culture across genotypes. *J. Virol.*, 85(6): 2565–2581, 2011.

[111] Shihyun You, et al. A cis-acting replication element in the sequence encoding the ns5B rna-dependent rna polymerase is required for hepatitis c virus rna replication. *J. Virol.*, 78 (3):1352–1366, 2004.

[112] Peter Friebe, et al. Kissing-loop interaction in the 3' end of the hepatitis c virus genome essential for rna replication. *J. Virol.*, 79(1): 380–392, 2005.

[113] Sinéad Diviney, et al. A hepatitis c virus cis-acting replication element forms a long-range rna-rna interaction with upstream rna sequences in ns5B. *J. Virol.*, 82(18):9008–9022, 2008.

[114] Cristina Romero-Lopez and Alfredo Berzal-Herranz. The functional rna domain 5Bsl3.2 within the ns5B coding sequence influences hepatitis c virus IRes-mediated translation. *Cell. Mol. Life Sci.*, 5:1–11, 2011.

[115] Asako Murayama, et al. Rna polymerase activity and specific rna structure are required for efficient hcv replication in cultured cells. *PLoS Pathog.*, 6(4):e1000885, 2010.

[116] N. Yamada, et al. Genetic organization and diversity of the 3' noncoding region of the hepatitis c virus genome. *Virology*, 223(1): 255–261, 1996.

[117] Peter Friebe and Ralf Bartenschlager. Genetic analysis of sequences in the 3' nontranslated region of hepatitis c virus that are important for rna replication. *J. Virol.*, 76(11): 5326–5338, 2002.

[118] MinKyung Yi and Stanley M Lemon. 3 nontranslated rna signals required for replication of hepatitis c virus rna. *J. Virol.*, 77(6):3557–3568, 2003.

[119] A. Kanai, et al. Poly(u) binding activity of hepatitis c virus ns3 protein, a putative rna helicase. *FEBS Lett.*, 376(3):221–224, 1995.

[120] K. Spångberg, et al. Hur, a protein implicated in oncogene and growth factor mrna decay, binds to the 3' ends of hepatitis c virus rna of both polarities. *Virology*, 274(2):378–390, 2000.

[121] Susan Weinlich, et al. Igf2Bp1 enhances hcv IRes-mediated translation initiation via the 3'utr. *RNA*, 15(8):1528–1542, 2009.

[122] Dina Uzri and Lee Gehrke. Nucleotide sequences and modifications that determine rig-i/rna binding and signaling activities. *J. Virol.*, 83(9):4174–4184, 2009.

[123] Gretja Schnell, et al. Uridine composition of the poly-u/uc tract of hcv rna defines non-self recognition by rig-i. *PLoS Pathog.*, 8(8): e1002839, 2012.

[124] G. Barba, et al. Hepatitis c virus core protein shows a cytoplasmic localization and associates to cellular lipid storage droplets. *Proc. Natl. Acad. Sci. U. S. A.*, 94(4):1200–1205, 1997.

[125] E. Santolini, et al. Biosynthesis and biochemical properties of the hepatitis c virus core protein. *J. Virol.*, 68(6):3631–3641, 1994.

[126] T. Shimoike, et al. Interaction of hepatitis c virus core protein with viral sense rna and suppression of its translation. *J. Virol.*, 73 (12):9718–9725, 1999.

[127] Kousuke Nakai, et al. Oligomerization of hepatitis c virus core protein is crucial for interaction with the cytoplasmic domain of e1 envelope protein. *J. Virol.*, 80(22):11265–11273, 2006.

[128] Anne Op De Beeck, et al. Characterization of functional hepatitis c virus envelope glycoproteins. *J. Virol.*, 78(6):2994–3002, 2004.

[129] Anne Goffard, et al. Role of n-linked glycans in the functions of hepatitis c virus envelope glycoproteins. *J. Virol.*, 79(13):8400–8409, 2005.

[130] Roxana E. Iacob, et al. Mass spectrometric characterization of glycosylation of hepatitis c virus e2 envelope glycoprotein reveals extended microheterogeneity of n-glycans. *J. Am. Soc. Mass Spectrom.*, 19(3):428–444, 2008.

[131] Nathalie Saint, et al. Structural and functional analysis of the hcv p7 protein. *Methods Mol. Biol.*, 510:125–143, 2009.

[132] Eike Steinmann, et al. Hepatitis c virus p7 protein is crucial for assembly and release of infectious virions. *PLoS Pathog.*, 3(7):e103, 2007.

[133] Ali M. Atoom, et al. Evidence suggesting that hcv p7 protects e2 glycoprotein from premature degradation during virus production. *Virus Res.*, 176(1-2):199–210, 2013.

[134] Kenneth A. Stapleford and Brett D. Lindenbach. Hepatitis c virus ns2 coordinates virus particle assembly through physical interactions with the e1-e2 glycoprotein and ns3-Ns4A enzyme complexes. *J. Virol.*, 85 (4):1706–1717, 2011.

[135] Min Guo, et al. Phosphatidylserine-specific phospholipase a1 involved in hepatitis c virus assembly through ns2 complex formation. *J. Virol.*, 89(4):2367–2377, 2015.

[136] Chao-Kuen Lai, et al. Hepatitis c virus egress and release depend on endosomal trafficking of core protein. *J. Virol.*, 84(21): 11590–11598, 2010.

[137] Ignacio Benedicto, et al. Clathrin mediates infectious hepatitis c virus particle egress. *J. Virol.*, 89(8):4180–4190, 2015.

[138] Kelly E. Coller, et al. Molecular determinants and dynamics of hepatitis c virus secretion. *PLoS Pathog.*, 8(1):e1002466, 2012.

[139] G. Carloni, et al. Susceptibility of human liver cell cultures to hepatitis c virus infection. *Arch. Virol. Suppl.*, 8:31–39, 1993.

[140] S. Iacovacci, et al. Replication and multiplication of hepatitis c virus genome in human foetal liver cells. *Res. Virol.*, 144(4):275–279, 1993.

[141] M. Ikeda, et al. Human hepatocyte clonal cell lines that support persistent replication of hepatitis c virus. *Virus Res.*, 56(2):157–167, 1998.

[142] V. Lohmann, et al. Replication of subgenomic hepatitis c virus rnas in a hepatoma cell line. *Science*, 285(5424):110–113, 1999.

[143] K. J. Blight, et al. Efficient initiation of hcv rna replication in cell culture. *Science*, 290 (5498):1972–1974, 2000.

[144] J. T. Guo, et al. Effect of alpha interferon on the hepatitis c virus replicon. *J. Virol.*, 75(18):8516–8523, 2001.

[145] Yingjia Zhang, et al. Novel chimeric genotype 1b/2a hepatitis c virus suitable for high-throughput screening. *Antimicrob. Agents Chemother.*, 52(2):666–674, 2008.

[146] N. Krieger, et al. Enhancement of hepatitis c virus rna replication by cell culture-adaptive mutations. *J. Virol.*, 75(10):4614–4624, 2001.

[147] Thomas Pietschmann, et al. Production of infectious genotype 1b virus particles in cell culture and impairment by replication enhancing mutations. *PLoS Pathog*, 5(6): e1000475, 2009.

[148] Takanobu Kato, et al. Efficient replication of the genotype 2a hepatitis c virus subgenomic replicon. *Gastroenterology*, 125(6): 1808–1817, 2003.

[149] Mohsan Saeed, et al. Efficient replication of genotype 3a and 4a hepatitis c virus replicons in human hepatoma cells. *Antimicrob. Agents Chemother.*, 56(10):5365–5373, 2012.

[150] Brett D. Lindenbach, et al. Complete replication of hepatitis c virus in cell culture. *Science*, 309(5734):623–626, 2005.

[151] Keril J. Blight, et al. Highly permissive cell lines for subgenomic and genomic hepatitis c virus rna replication. *J. Virol.*, 76(24): 13001–13014, 2002.

[152] Glenn Randall, et al. Cellular cofactors affecting hepatitis c virus infection and replication. *Proc. Natl. Acad. Sci. U. S. A.*, 104 (31):12884–12889, 2007.

[153] C. L. Jopling, et al. Positive and negative modulation of viral and cellular mrnas by liver-specific microrna mir-122. *Cold Spring Harb. Symp. Quant. Biol.*, 71:369–376, 2006.

[154] Shoumei Bai, et al. Microrna-122 inhibits tumorigenic properties of hepatocellular carcinoma cells and sensitizes these cells to sorafenib. *J. Biol. Chem.*, 284(46):32015–32027, 2009.

[155] Patricia A. Thibault, et al. Microrna-122-dependent and -independent replication of hepatitis c virus in hep3B human hepatoma cells. *Virology*, 436(1):179–190, 2013.

[156] Christopher M. Narbus, et al. Hepg2 cells expressing microrna mir-122 support the entire hepatitis c virus life cycle. *J. Virol.*, 85 (22):12087–12092, 2011.

[157] Takasuke Fukuhara, et al. Expression of microrna mir-122 facilitates an efficient replication in nonhepatic cells upon infection with hepatitis c virus. *J. Virol.*, 86(15):7918–7933, 2012.

[158] Rebecca L. Skalsky and Bryan R. Cullen. Viruses, micrornas, and host interactions. *Annu. Rev. Microbiol.*, 64:123–141, 2010.

[159] Jennifer L. Umbach and Bryan R. Cullen. The role of rnai and micrornas in animal virus replication and antiviral immunity. *Genes Dev*, 23(10):1151–1164, 2009.

[160] Mazhar Hussain, et al. West nile virus encodes a microrna-like small rna in the 3' untranslated region which up-regulates gata4 mrna and facilitates virus replication in mosquito cells. *Nucleic Acids Res.*, 40(5):2210–2223, 2012.

[161] A. R. van der Krol, et al. Flavonoid genes in petunia: addition of a limited number of gene copies may lead to a suppression of gene expression. *Plant Cell*, 2(4):291–299, 1990.

[162] R. C. Lee, et al. The c. elegans heterochronic gene lin-4 encodes small rnas with antisense complementarity to lin-14. *Cell*, 75(5):843–854, 1993.

[163] Al-Kaff, et al. Transcriptional and posttranscriptional plant gene silencing in response to a pathogen. *Science*, 279(5359):2113–2115, 1998.

[164] Yang Li, et al. Rna interference functions as an antiviral immunity mechanism in mammals. *Science*, 342(6155):231–234, 2013.

[165] Yoontae Lee, et al. The nuclear rnase iii drosha initiates microrna processing. *Nature*, 425(6956):415–419, 2003.

[166] Jinju Han, et al. The drosha-dgcr8 complex in primary microrna processing. *Genes Dev.*, 18(24):3016–3027, 2004.

[167] Kyu-Hyeon Yeom, et al. Characterization of dgcr8/pasha, the essential cofactor for drosha in primary mirna processing. *Nucleic Acids Res.*, 34(16):4622–4629, 2006.

[168] J. Graham Ruby, et al. Intronic microrna precursors that bypass drosha processing. *Nature*, 448(7149):83–86, 2007.

[169] Haidi Zhang, et al. Human dicer preferentially cleaves dsrnas at their termini without a requirement for ATP. *EMBO J.*, 21(21):5875–5885, 2002.

[170] E. Lund and J. E. Dahlberg. Substrate selectivity of exportin 5 and dicer in the biogenesis of micrornas. *Cold Spring Harb. Symp. Quant. Biol.*, 71:59–66, 2006.

[171] Daniel Cifuentes, et al. A novel mirna processing pathway independent of dicer requires argonaute2 catalytic activity. *Science*, 328(5986):1694–1698, 2010.

[172] Elisavet Maniataki and Zissimos Mourelatos. A human, ATP-independent, RISC assembly machine fueled by pre-mirna. *Genes Dev.*, 19(24):2979–2990, 2005.

[173] Thimmaiah P Chendrimada, et al. Trbp recruits the dicer complex to ago2 for microrna processing and gene silencing. *Nature*, 436(7051):740–744, 2005.

[174] Géraldine Mathonnet, et al. Microrna inhibition of translation initiation in vitro by targeting the cap-binding complex eif4F. *Science*, 317(5845):1764–1767, 2007.

[175] Motoaki Wakiyama, et al. Let-7 microrna-mediated mrna deadenylation and trans-

lational repression in a mammalian cell-free system. *Genes Dev.*, 21(15):1857–1862, 2007.

[176] S. M. Elbashir, et al. Duplexes of 21-nucleotide rnas mediate rna interference in cultured mammalian cells. *Nature*, 411 (6836):494–498, 2001.

[177] Muller Fabbri, et al. Micrornas bind to toll-like receptors to induce prometastatic inflammatory response. *Proc. Natl. Acad. Sci. U. S. A.*, 109(31):E2110–E2116, 2012.

[178] Shveta Bagga, et al. Regulation by let-7 and lin-4 mirnas results in target mrna degradation. *Cell*, 122(4):553–563, 2005.

[179] Kevin V. Morris, et al. Small interfering rna-induced transcriptional gene silencing in human cells. *Science*, 305(5688):1289–1292, 2004.

[180] Kaleb M Pauley, et al. Formation of gw bodies is a consequence of microrna genesis. *EMBO Rep.*, 7(9):904–910, 2006.

[181] Huili Guo, et al. Mammalian micrornas predominantly act to decrease target mrna levels. *Nature*, 466(7308):835–840, 2010.

[182] Suvendra N. Bhattacharyya, et al. Relief of microrna-mediated translational repression in human cells subjected to stress. *Cell*, 125 (6):1111–1124, 2006.

[183] Daphna Nachmani, et al. The human cytomegalovirus microrna mir-ul112 acts synergistically with a cellular microrna to escape immune elimination. *Nat. Immunol.*, 11(9): 806–813, 2010.

[184] Wenliang Zhu, et al. Dissection of protein interactomics highlights microrna synergy. 2013.

[185] Nikolaus Rajewsky and Nicholas D. Socci. Computational identification of microrna targets. *Dev. Biol.*, 267(2):529–535, 2004.

[186] Dominic Grün, et al. microrna target predictions across seven drosophila species and comparison to mammalian targets. *PLoS Comput. Biol.*, 1(1):e13, 2005.

[187] Robin C. Friedman, et al. Most mammalian mrnas are conserved targets of micrornas. *Genome Res.*, 19(1):92–105, 2009.

[188] Catherine Jopling. Liver-specific microrna-122: Biogenesis and function. *RNA Biol.*, 9 (2):137–142, 2012.

[189] Carolyn Spaniel, et al. microrna-122 abundance in hepatocellular carcinoma and non-tumor liver tissue from Japanese patients with persistent hcv versus hbv infection. *PLoS One*, 8(10):e76867, 2013.

[190] Yu-Qiang Nie, et al. The effect of mirna-122 in regulating fat deposition in a cell line model. *J. Cell. Biochem.*, 115(5):839–846, 2014.

[191] Noemi Rotllan and Carlos Fernández-Hernando. Microrna regulation of cholesterol metabolism. *Cholesterol*, 2012:847849, 2012.

[192] Jessica Wen and Joshua R. Friedman. mir-122 regulates hepatic lipid metabolism and tumor suppression. *J. Clin. Invest.*, 122(8): 2773–2776, 2012.

[193] Shu-Hao Hsu, et al. Essential metabolic, anti-inflammatory, and anti-tumorigenic functions of mir-122 in liver. *J. Clin. Invest.*, 122(8):2871–2883, 2012.

[194] Wei-Chih Tsai, et al. Microrna-122 plays a critical role in liver homeostasis and hepatocarcinogenesis. *J. Clin. Invest.*, 122(8):2884–2897, 2012.

[195] Jun Qian, et al. Modulation of mir-122 on persistently borna disease virus infected human oligodendroglial cells. *Antiviral Res.*, 87 (2):249–256, 2010.

[196] Takeshi Yoshikawa, et al. Silencing of microrna-122 enhances interferon-a signaling in the liver through regulating socs3 promoter methylation. *Sci Rep*, 2:637, 2012.

[197] David P. Bartel. Micrornas: target recognition and regulatory functions. *Cell*, 136(2): 215–233, 2009.

[198] Jura Inga Henke, et al. microrna-122 stimulates translation of hepatitis c virus rna. *EMBO J.*, 27(24):3300–3310, 2008.

[199] Jinhong Chang, et al. Liver-specific microrna mir-122 enhances the replication of hepatitis c virus in nonhepatic cells. *J. Virol.*, 82(16): 8215–8223, 2008.

[200] Isabelle Dichamp, et al. Cellular activation and intracellular hcv load in peripheral blood monocytes isolated from hcv monoinfected and hiv-hcv coinfected patients. *PLoS One*, 9(5):e96907, 2014.

[201] Zhaojing Cheng, et al. Extrahepatic manifestations of chronic hepatitis c virus infection: 297 cases from a tertiary medical center in beijing, China. *Chin Med J (Engl)*, 127(7):1206–1210, 2014.

[202] Erica S. Machlin, et al. Masking the 5' terminal nucleotides of the hepatitis c virus genome by an unconventional microrna-target rna complex. *Proc. Natl. Acad. Sci. U. S. A.*, 108(8):3193–3198, 2011.

[203] You Li, et al. Competing and noncompeting activities of mir-122 and the 5' exonuclease xrn1 in regulation of hepatitis c virus replication. *Proc. Natl. Acad. Sci. U. S. A.*, 110 (5):1881–1886, 2013.

[204] Cecilia D. Sedano and Peter Sarnow. Hepatitis c virus subverts liver-specific mir-122 to protect the viral genome from exoribonuclease xrn2. *Cell Host Microbe*, 16(2):257–264, 2014.

[205] You Li, et al. mir-122 and the hepatitis c rna genome: more than just stability. *RNA Biol.*, 10(6):919–923, 2013.

[206] Rodrigo A. Villanueva, et al. mir-122 does not modulate the elongation phase of hepatitis c virus rna synthesis in isolated replicase complexes. *Antiviral Res.*, 88(1):119–123, 2010.

[207] Takahiro Masaki, et al. mir-122 stimulates hepatitis c virus rna synthesis by altering the balance of viral rnas engaged in replication versus translation. *Cell Host Microbe*, 17(2): 217–228, 2015.

[208] K Dominik Conrad, et al. Microrna-122 dependent binding of ago2 protein to hepatitis c virus rna is associated with enhanced rna stability and translation stimulation. *PLoS One*, 8(2):e56272, 2013.

[209] Michael Niepmann. Activation of hepatitis c virus translation by a liver-specific microrna. *Cell Cycle*, 8(10):1473–1477, 2009.

[210] Oleg Raitskin, et al. Large nuclear rnp particles–the nuclear pre-mrna processing machine. *J Struct Biol*, 140(1-3):123–130, 2002.

[211] Junho Choe, et al. Translation initiation on mrnas bound by nuclear cap-binding protein complex cbp80/20 requires interaction between cbp80/20-dependent translation initiation factor and eukaryotic translation initiation factor 3g. *J Biol Chem*, 287(22):18500–18509, 2012.

[212] Kyoung Mi Kim, et al. A new mif4g domain-containing protein, CTIF, directs nuclear cap-binding protein cbp80/20-dependent translation. *Genes Dev*, 23(17):2033–2045, 2009.

[213] Shang-Yi Chiu, et al. The pioneer translation initiation complex is functionally distinct from but structurally overlaps with the steady-state translation initiation complex. *Genes Dev*, 18(7):745–754, 2004.

[214] Junho Choe, et al. eif4Aiii enhances translation of nuclear cap-binding complex-bound mrnas by promoting disruption of secondary structures in 5'utr. *Proc Natl Acad Sci U S A*, 111(43):E4577–E4586, 2014.

[215] Y. Ishigaki, et al. Evidence for a pioneer round of mrna translation: mrnas subject to nonsense-mediated decay in mammalian cells are bound by cbp80 and cbp20. *Cell*, 106(5):607–617, 2001.

[216] Jungwook Hwang, et al. Upf1 association with the cap-binding protein, cbp80, promotes nonsense-mediated mrna decay at two distinct steps. *Mol Cell*, 39(3):396–409, 2010.

[217] Fabrice Lejeune, et al. The exon junction complex is detected on cbp80-bound but not eif4e-bound mrna in mammalian cells: dynamics of mrnp remodeling. *EMBO J*, 21 (13):3536–3545, 2002.

[218] Hanae Sato and Lynne E. Maquat. Remodeling of the pioneer translation initiation complex involves translation and the karyopherin importin beta. *Genes Dev*, 23(21): 2537–2550, 2009.

[219] J. Pelletier and N. Sonenberg. Internal initiation of translation of eukaryotic mrna directed by a sequence derived from poliovirus rna. *Nature*, 334(6180):320–325, 1988.

[220] Sunnie R. Thompson and Peter Sarnow. Enterovirus 71 contains a type i IRes element that functions when eukaryotic initiation factor eif4g is cleaved. *Virology*, 315(1):259–266, 2003.

[221] S. K. Jang, et al. A segment of the 5' nontranslated region of encephalomyocarditis virus rna directs internal entry of ribosomes during in vitro translation. *J. Virol.*, 62(8):2636–2643, 1988.

[222] Lucy P. Beales, et al. Viral internal ribosome entry site structures segregate into two distinct morphologies. *J. Virol.*, 77(11):6574–6579, 2003.

[223] Christopher U T. Hellen. IRes-induced conformational changes in the ribosome and the mechanism of translation initiation by internal ribosomal entry. *Biochim. Biophys. Acta*, 1789(9-10):558–570, 2009.

[224] J. E. Wilson, et al. Naturally occurring dicistronic cricket paralysis virus rna is regulated by two internal ribosome entry sites. *Mol. Cell. Biol.*, 20(14):4990–4999, 2000.

[225] Martin Holcík, et al. The internal ribosome entry site-mediated translation of antiapoptotic protein xiap is modulated by the heterogeneous nuclear ribonucleoproteins c1 and c2. *Mol Cell Biol*, 23(1):280–288, 2003.

[226] J. K. Pinkstaff, et al. Internal initiation of translation of five dendritically localized neuronal mrnas. *Proc Natl Acad Sci U S A*, 98 (5):2770–2775, 2001.

[227] Noa Liberman, et al. The translation initiation factor dap5 is a regulator of cell survival during mitosis. *Cell Cycle*, 8(2):204–209, 2009.

[228] Shaun Willimott and Simon D. Wagner. Post-transcriptional and post-translational regulation of bcl2. *Biochem Soc Trans*, 38 (6):1571–1575, 2010.

[229] Raquel Amorim, et al. Hiv-1 transcripts use IRes-initiation under conditions where cap-dependent translation is restricted by poliovirus 2A protease. *PLoS One*, 9(2):e88619, 2014.

[230] Nehal Thakor and Martin Holcik. IRes-mediated translation of cellular messenger rna operates in eif2a- independent manner during stress. *Nucleic Acids Res*, 40(2):541–552, 2012.

[231] Ilya M. Terenin, et al. Eukaryotic translation initiation machinery can operate in a bacterial-like mode without eif2. *Nat. Struct. Mol. Biol.*, 15(8):836–841, 2008.

[232] R. Grover, et al. p53 and little brother p53/47: linking IRes activities with protein functions. *Oncogene*, 28(30):2766–2772, 2009.

[233] Arandkar Sharathchandra, et al. IRes mediated translational regulation of p53 isoforms. *Wiley Interdiscip Rev RNA*, 5(1):131–139, 2014.

[234] Kerry D. Fitzgerald and Bert L. Semler. Bridging IRes elements in mrnas to the eukaryotic translation apparatus. *Biochim Biophys Acta*, 1789(9-10):518–528, 2009.

[235] Anton A. Komar and Maria Hatzoglou. Cellular IRes-mediated translation: the war of itafs in pathophysiological states. *Cell Cycle*, 10(2):229–240, 2011.

[236] J. E. Reynolds, et al. Internal initiation of translation of hepatitis c virus rna: the ribosome entry site is at the authentic initiation codon. *RNA*, 2(9):867–878, 1996.

[237] E. Buratti, et al. In vivo translational efficiency of different hepatitis c virus 5'-utrs. *FEBS Lett.*, 411(2-3):275–280, 1997.

[238] W. D. Zhao, et al. Genetic analysis of a poliovirus/hepatitis c virus (hcv) chimera: interaction between the poliovirus cloverleaf and a sequence in the hcv 5' nontranslated region results in a replication phenotype. *J. Virol.*, 74(13):6223–6226, 2000.

[239] Shuetsu Fukushi, et al. Complete 5 noncoding region is necessary for the efficient internal initiation of hepatitis c virus rna. *Biochem. Biophys. Res. Commun.*, 199(2):425–432, 1994.

[240] HuI-HUA Lu and Eckard Wimmer. Poliovirus chimeras replicating under the translational control of genetic elements of hepatitis c virus reveal unusual properties of the internal ribosomal entry site of hepatitis c virus. *Proceedings of the National Academy of Sciences*, 93(4):1412–1417, 1996.

[241] JE Reynolds, et al. Unique features of internal initiation of hepatitis c virus rna translation. *The EMBO journal*, 14(23):6010, 1995.

[242] Byoung J Yoo, et al. 5 end-dependent translation initiation of hepatitis c viral rna and the presence of putative positive and negative translational control elements within the 5 untranslated region. *Virology*, 191(2):889–899, 1992.

[243] Michael Gale, et al. Translational control of viral gene expression in eukaryotes. *Microbiol. Mol. Biol. Rev.*, 64(2):239–280, 2000.

[244] Peter Friebe, et al. Sequences in the 5 nontranslated region of hepatitis c virus required for rna replication. *J. Virol.*, 75(24):12047–12057, 2001.

[245] Peter Friebe and Ralf Bartenschlager. Role of rna structures in genome terminal sequences of the hepatitis c virus for replication and assembly. *J. Virol.*, 83(22):11989–11995, 2009.

[246] Joyce A. Wilson and Adam Huys. mir-122 promotion of the hepatitis c virus life cycle: sound in the silence. *Wiley Interdiscip Rev RNA*, 4(6):665–676, 2013.

[247] P. J. Lukavsky, et al. Structures of two rna domains essential for hepatitis c virus internal ribosome entry site function. *Nat. Struct. Biol.*, 7(12):1105–1110, 2000.

[248] René Rijnbrand, et al. Almost the entire 5 non-translated region of hepatitis c virus is required for cap-independent translation. *FEBS Lett.*, 365(2):115–119, 1995.

[249] C. Wang, et al. Translation of human hepatitis c virus rna in cultured cells is mediated by an internal ribosome-binding mechanism. *J. Virol.*, 67(6):3338–3344, 1993.

[250] Peter J. Lukavsky, et al. Structure of hcv IRes domain ii determined by nmr. *Nat. Struct. Biol.*, 10(12):1033–1038, 2003.

[251] Ryan B. Paulsen, et al. Inhibitor-induced structural change in the hcv IRes domain iia rna. *Proc. Natl. Acad. Sci. U. S. A.*, 107(16):7263–7268, 2010.

[252] Nicolas Locker, et al. Hcv and csfv IRes domain ii mediate eif2 release during 80S ribosome assembly. *The EMBO journal*, 26(3):795–805, 2007.

[253] Megan E. Filbin, et al. Hcv IRes manipulates the ribosome to promote the switch from translation initiation to elongation. *Nat. Struct. Mol. Biol.*, 20(2):150–158, 2013.

[254] Gabriele Fuchs, et al. Kinetic pathway of 40S ribosomal subunit recruitment to hepatitis c virus internal ribosome entry site. *Proc. Natl. Acad. Sci. U. S. A.*, 112(2):319–325, 2015.

[255] Victoria G Kolupaeva, et al. An enzymatic footprinting analysis of the interaction of 40S ribosomal subunits with the internal ribosomal entry site of hepatitis c virus. *J. Virol.*, 74(14):6242–6250, 2000.

[256] Adam J. Collier, et al. A conserved rna structure within the hcv IRes eif3-binding site. *Nat. Struct. Biol.*, 9(5):375–380, 2002.

[257] J. S. Kieft, et al. Mechanism of ribosome recruitment by hepatitis c IRes rna. *RNA*, 7(2):194–206, 2001.

[258] Julien Pérard, et al. Human initiation factor eif3 subunit b interacts with hcv IRes rna through its n-terminal rna recognition motif. *FEBS Lett.*, 583(1):70–74, 2009.

[259] Yaser Hashem, et al. Hepatitis-c-virus-like internal ribosome entry sites displace eif3 to gain access to the 40S subunit. *Nature*, 503(7477):539–543, 2013.

[260] M. Honda, et al. Stability of a stem-loop involving the initiator aug controls the efficiency of internal initiation of translation on hepatitis c virus rna. *RNA*, 2(10):955–968, 1996.

[261] Ting-Hsien Wang, et al. Core protein-coding sequence, but not core protein, modulates the efficiency of cap-independent translation directed by the internal ribosome entry site of hepatitis c virus. *J. Virol.*, 74(23):11347–11358, 2000.

[262] Changyu Wang, et al. An rna pseudoknot is an essential structural element of the internal ribosome entry site located within the

hepatitis c virus 5'noncoding region. *RNA*, 1(5):526–537, 1995.

[263] D. B. Smith, et al. Variation of the hepatitis c virus 5' non-coding region: implications for secondary structure, virus detection and typing. the international hcv collaborative study group. *J. Gen. Virol.*, 76 (Pt 7):1749–1761, 1995.

[264] T. V. Pestova, et al. A prokaryotic-like mode of cytoplasmic eukaryotic ribosome binding to the initiation codon during internal translation initiation of hepatitis c and classical swine fever virus rnas. *Genes Dev.*, 12(1): 67–83, 1998.

[265] Sung Mi Park, et al. Translation-competent 48S complex formation on hcv IRes requires the rna-binding protein nsap1. *Nucleic Acids Res.*, 39(17):7791–7802, 2011.

[266] Naushad Ali and Aleem Siddiqui. The la antigen binds 5 noncoding region of the hepatitis c virus rna in the context of the initiator aug codon and stimulates internal ribosome entry site-mediated translation. *Proceedings of the National Academy of Sciences*, 94(6):2249–2254, 1997.

[267] You Li, et al. hnrnp l and NF90 interact with hepatitis c virus 5'-terminal untranslated rna and promote efficient replication. *J. Virol.*, 88(13):7199–7209, 2014.

[268] Olaf Isken, et al. Nuclear factors are involved in hepatitis c virus rna replication. *RNA*, 13 (10):1675–1692, 2007.

[269] K. Spångberg and S. Schwartz. Poly(c)-binding protein interacts with the hepatitis c virus 5' untranslated region. *J. Gen. Virol.*, 80 (Pt 6):1371–1376, 1999.

[270] Almudena Pacheco, et al. Riboproteomic analysis of polypeptides interacting with the internal ribosome-entry site element of foot-and-mouth disease viral rna. *Proteomics*, 8 (22):4782–4790, 2008.

[271] B. Hahm, et al. Heterogeneous nuclear ribonucleoprotein l interacts with the 3' border of the internal ribosomal entry site of hepatitis c virus. *J. Virol.*, 72(11):8782–8788, 1998.

[272] Byounghoon Hwang, et al. hnrnp l is required for the translation mediated by hcv IRes. *Biochem. Biophys. Res. Commun.*, 378 (3):584–588, 2009.

[273] Henry Lu, et al. Riboproteomics of the hepatitis c virus internal ribosomal entry site. *J. Proteome Res.*, 3(5):949–957, 2004.

[274] Maria Licursi, et al. Promotion of viral IRes-mediated translation initiation under mild hypothermia. *PLoS One*, 10(5):e0126174, 2015.

[275] R. T. Chung and L. M. Kaplan. Heterogeneous nuclear ribonucleoprotein i (hnrnp-i/ptb) selectively binds the conserved 3' terminus of hepatitis c viral rna. *Biochem. Biophys. Res. Commun.*, 254(2):351–362, 1999.

[276] R. R. Gontarek, et al. hnrnp c and polypyrimidine tract-binding protein specifically interact with the pyrimidine-rich region within the 3'ntr of the hcv rna genome. *Nucleic Acids Res.*, 27(6):1457–1463, 1999.

[277] T. Ito and M. M. Lai. An internal polypyrimidine-tract-binding protein-binding site in the hepatitis c virus rna attenuates translation, which is relieved by the 3'-untranslated sequence. *Virology*, 254(2): 288–296, 1999.

[278] A. Anwar, et al. Demonstration of functional requirement of polypyrimidine tract-binding protein by selex rna during hepatitis c virus internal ribosome entry site-mediated translation initiation. *J. Biol. Chem.*, 275(44): 34231–34235, 2000.

[279] Michèle Brocard, et al. Evidence that ptb does not stimulate hcv IRes-driven translation. *Virus Genes*, 35(1):5–15, 2007.

[280] N. Ali and A. Siddiqui. Interaction of polypyrimidine tract-binding protein with the 5' noncoding region of the hepatitis c virus rna genome and its functional requirement in internal initiation of translation. *J. Virol.*, 69(10):6367–6375, 1995.

[281] Hideki Aizaki, et al. Polypyrimidine-tract-binding protein is a component of the hcv rna replication complex and necessary for rna synthesis. *J. Biomed. Sci.*, 13(4):469–480, 2006.

[282] Sally A. Mitchell, et al. The apaf-1 internal ribosome entry segment attains the correct structural conformation for function via interactions with ptb and unr. *Mol. Cell*, 11 (3):757–771, 2003.

[283] Sigrid Cornelis, et al. Unr translation can be driven by an IRes element that is negatively regulated by polypyrimidine tract binding protein. *Nucleic Acids Res.*, 33(10):3095–3108, 2005.

[284] Saneyuki Ujino, et al. The interaction between human initiation factor eif3 subunit c and heat-shock protein 90: a necessary factor for translation mediated by the hepatitis c virus internal ribosome entry site. *Virus Res.*, 163(1):390–395, 2012.

[285] Laurent Chatel-Chaix, et al. A host yb-1 ribonucleoprotein complex is hijacked by hep-

atitis c virus for the control of ns3-dependent particle production. *J. Virol.*, 87(21):11704–11720, 2013.

[286] Yupeng He, et al. The regulation of hepatitis c virus (hcv) internal ribosome-entry site-mediated translation by hcv replicons and nonstructural proteins. *J. Gen. Virol.*, 84 (Pt 3):535–543, 2003.

[287] Eirini Karamichali, et al. Hcv ns5A cooperates with pkr in modulating hcv IRes-dependent translation. *Infect. Genet. Evol.*, 26:113–122, 2014.

[288] Takashi Shimoike, et al. Translational insensitivity to potent activation of pkr by hcv IRes rna. *Antiviral Res.*, 83(3):228–237, 2009.

[289] Jashmin Vyas, et al. Inhibition of the protein kinase pkr by the internal ribosome entry site of hepatitis c virus genomic rna. *RNA*, 9(7): 858–870, 2003.

[290] Stéphanie Dabo and Eliane F. Meurs. dsrna-dependent protein kinase pkr and its role in stress, signaling and hcv infection. *Viruses*, 4(11):2598–2635, 2012.

[291] M. Honda, et al. Structural requirements for initiation of translation by internal ribosome entry within genome-length hepatitis c virus rna. *Virology*, 222(1):31–42, 1996.

[292] Yann Ponty and Fabrice Leclerc. Drawing and editing the secondary structure(s) of rna. *Methods Mol Biol*, 1269:63–100, 2015.

[293] Rhiju Das, et al. Safa: semi-automated footprinting analysis software for high-throughput quantification of nucleic acid footprinting experiments. *RNA*, 11(3):344–354, 2005.

[294] Robert C Spitale, et al. Rna shape analysis in living cells. *Nat. Chem. Biol.*, 9(1):18–20, 2013.

[295] Caifu Chen, et al. Real-time quantification of micrornas by stem-loop RT-PCr. *Nucleic Acids Res.*, 33(20):e179, 2005.

[296] Vishal Lamba, et al. Identification of suitable reference genes for hepatic microrna quantitation. *BMC Res Notes*, 7:129, 2014.

[297] S. Wani and N. Cloonan. Profiling direct mrna-microrna interactions using synthetic biotinylated microrna-duplexes. 2014.

[298] Vaithilingaraja Arumugaswami, et al. High-resolution functional profiling of hepatitis c virus genome. *PLoS Pathog.*, 4(10): e1000182–e1000182, 2008.

[299] V. Lohmann, et al. Biochemical and kinetic analyses of ns5B rna-dependent rna polymerase of the hepatitis c virus. *Virology*, 249 (1):108–118, 1998.

[300] K. Ishii, et al. Expression of hepatitis c virus ns5B protein: characterization of its rna polymerase activity and rna binding. *Hepatology*, 29(4):1227–1235, 1999.

[301] P. E. Lobert, et al. A coding rna sequence acts as a replication signal in cardioviruses. *Proc Natl Acad Sci U S A*, 96(20):11560–11565, 1999.

[302] I. Goodfellow, et al. Identification of a cis-acting replication element within the poliovirus coding region. *J Virol*, 74(10):4590–4600, 2000.

[303] A. N. Korovina, et al. Biogenic polyamines spermine and spermidine activate rna polymerase and inhibit rna helicase of hepatitis c virus. *Biochemistry (Mosc)*, 77(10):1172–1180, 2012.

[304] Shuai Li, et al. Hepato-specific microrna-122 facilitates accumulation of newly synthesized mirna through regulating prkra. *Nucleic Acids Res.*, 40(2):884–891, 2012.

[305] Kevin A Wilkinson, et al. Selective 2 -hydroxyl acylation analyzed by primer extension (shape): quantitative rna structure analysis at single nucleotide resolution. *Nature protocols*, 1(3):1610–1616, 2006.

[306] Ye Ding and Charles E. Lawrence. A statistical sampling algorithm for rna secondary structure prediction. *Nucleic Acids Res*, 31 (24):7280–7301, 2003.

[307] Ana García-Sacristán, et al. A magnesium-induced rna conformational switch at the internal ribosome entry site of hepatitis c virus genome visualized by atomic force microscopy. *Nucleic Acids Res.*, 43(1):565–580, 2015.

[308] Julia Höck, et al. Proteomic and functional analysis of argonaute-containing mrna-protein complexes in human cells. *EMBO Rep.*, 8(11):1052–1060, 2007.

[309] Alok Upadhyay, et al. Affinity capture and identification of host cell factors associated with hepatitis c virus (+) strand subgenomic rna. *Mol. Cell. Proteomics*, 12(6):1539–1552, 2013.

[310] Yasuo Ariumi, et al. Ddx3 dead-box rna helicase is required for hepatitis c virus rna replication. *J. Virol.*, 81(24):13922–13926, 2007.

[311] Vivi Kasim, et al. Determination of the role of ddx3 a factor involved in mammalian rnai pathway using an shrna-expression library. *PLoS One*, 8(3):e59445, 2013.

[312] Rohit K. Jangra, et al. Ddx6 (rck/p54) is required for efficient hepatitis c virus replication but not for internal ribosome entry

site-directed translation. *J. Virol.*, 84(13): 6810–6824, 2010.

[313] Chia-ying Chu and Tariq M. Rana. Translation repression in human cells by microrna-induced gene silencing requires RCk/p54. *PLoS Biol.*, 4(7):e210, 2006.

[314] Ki Young Paek, et al. Rna-binding protein hnrnp d modulates internal ribosome entry site-dependent translation of hepatitis c virus rna. *J Virol*, 82(24):12082–12093, 2008.

[315] Manish Kumar, et al. Nuclear heterogeneous nuclear ribonucleoprotein d is associated with poor prognosis and interactome analysis reveals its novel binding partners in oral cancer. *J Transl Med*, 13:285, 2015.

[316] Xiangyue Wu, et al. Combinatorial mrna binding by auf1 and argonaute 2 controls decay of selected target mrnas. *Nucleic Acids Res*, 41(4):2644–2658, 2013.

[317] Cara T. Pager, et al. Modulation of hepatitis c virus rna abundance and virus release by dispersion of processing bodies and enrichment of stress granules. *Virology*, 435(2): 472–484, 2013.

[318] Yasuo Ariumi, et al. Hepatitis c virus hijacks p-body and stress granule components around lipid droplets. *J. Virol.*, 85(14):6882–6892, 2011.

[319] Catherine L. Jopling. Regulation of hepatitis c virus by microrna-122. *Biochem. Soc. Trans.*, 36(Pt 6):1220–1223, 2008.

[320] Neda Nasheri, et al. Competing roles of microrna-122 recognition elements in hepatitis c virus rna. *Virology*, 410(2):336–344, 2011.

[321] Rudolf K F. Beran, et al. The serine protease domain of hepatitis c viral ns3 activates rna helicase activity by promoting the binding of rna substrate. *J. Biol. Chem.*, 282(48): 34913–34920, 2007.

[322] Kiyoshi Kyono, et al. Expression and purification of a hepatitis c virus ns3/4A complex, and characterization of its helicase activity with the scintillation proximity assay system. *J Biochem*, 135(2):245–252, 2004.

[323] Angela M I. Lam, et al. Enhanced nucleic acid binding to ATP-bound hepatitis c virus ns3 helicase at low ph activates rna unwinding. *Nucleic Acids Res.*, 32(13):4060–4070, 2004.

[324] Gustavo Tavares Ventura, et al. ph-dependent conformational changes in the hcv ns3 protein modulate its ATPase and helicase activities. *PLoS One*, 9(12):e115941, 2014.

[325] J. A. Suzich, et al. Hepatitis c virus ns3 protein polynucleotide-stimulated nucleoside triphosphatase and comparison with the related pestivirus and flavivirus enzymes. *J. Virol.*, 67(10):6152–6158, 1993.

[326] Zhi-Shun Huang, et al. Hcv ns3 protein helicase domain assists rna structure conversion. *FEBS Lett.*, 584(11):2356–2362, 2010.

[327] Dong Wook Kim, et al. Mutational analysis of the hepatitis c virus rna helicase. *J. Virol.*, 71(12):9400–9409, 1997.

[328] Nagraj Mani, et al. Nonstructural protein 5a (ns5a) and human replication protein a increase the processivity of hepatitis c virus ns5b polymerase activity in vitro. *J Virol*, 89(1):165–180, 2015.

[329] Chao-Kuen Lai, et al. Association of hepatitis c virus replication complexes with microtubules and actin filaments is dependent on the interaction of ns3 and ns5A. *J. Virol.*, 82(17):8838–8848, 2008.

[330] Tetsuro Shimakami, et al. Effect of interaction between hepatitis c virus ns5A and ns5B on hepatitis c virus rna replication with the hepatitis c virus replicon. *J. Virol.*, 78(6): 2738–2748, 2004.

[331] Yukihiro Shirota, et al. Hepatitis c virus (hcv) ns5A binds rna-dependent rna polymerase (rdrp) ns5B and modulates rna-dependent rna polymerase activity. *J. Biol. Chem.*, 277(13):11149–11155, 2002.

[332] Elizabeth M Quezada and Caroline M Kane. The hepatitis c virus ns5A stimulates ns5B during in vitro rna synthesis in a template specific manner. *The open biochemistry journal*, 3:39, 2009.

[333] Lu Gao, et al. Interactions between viral nonstructural proteins and host protein hvap-33 mediate the formation of hepatitis c virus rna replication complex on lipid raft. *J Virol*, 78(7):3480–3488, 2004.

[334] Itsuki Hamamoto, et al. Human vap-b is involved in hepatitis c virus replication through interaction with ns5a and ns5b. *J Virol*, 79(21):13473–13482, 2005.

[335] Yun-Sook Lim, et al. Peptidyl-prolyl isomerase pin1 is a cellular factor required for hepatitis c virus propagation. *J Virol*, 85 (17):8777–8788, 2011.

[336] Yun-Sook Lim and Soon B. Hwang. Hepatitis c virus ns5a protein interacts with phosphatidylinositol 4-kinase type iiialpha and regulates viral propagation. *J Biol Chem*, 286(13):11290–11298, 2011.

[337] Y. S. Lim, et al. Nonstructural 5a protein of hepatitis c virus regulates heat shock protein 72 for its own propagation. *J Viral Hepat*, 19 (5):353–363, 2012.

[338] Hirotake Kasai, et al. Involvement of fkbp6 in hepatitis c virus replication. *Sci Rep*, 5: 16699, 2015.

[339] Tetsuro Shimakami, et al. Stabilization of hepatitis c virus rna by an ago2-mir-122 complex. *Proc. Natl. Acad. Sci. U. S. A.*, 109(3):941–946, 2012.

[340] Joseph M. Luna, et al. Hepatitis c virus rna functionally sequesters mir-122. *Cell*, 160(6): 1099–1110, 2015.

[341] Dongmei Ye, et al. Microrna regulation of intestinal epithelial tight junction permeability. *Gastroenterology*, 141(4):1323–1333, 2011.

[342] Dagmar Goergen and Michael Niepmann. Stimulation of hepatitis c virus rna translation by microrna-122 occurs under different conditions in vivo and in vitro. *Virus Res.*, 167(2):343–352, 2012.

[343] Takasuke Fukuhara and Yoshiharu Matsuura. Role of mir-122 and lipid metabolism in hcv infection. *J. Gastroenterol.*, 48(2): 169–176, 2013.

[344] Christiane Jünemann, et al. Picornavirus internal ribosome entry site elements can stimulate translation of upstream genes. *J. Biol. Chem.*, 282(1):132–141, 2007.

[345] Rosa Díaz-Toledano, et al. In vitro characterization of a mir-122-sensitive double-helical switch element in the 5' region of hepatitis c virus rna. *Nucleic Acids Res.*, 37(16): 5498–5510, 2009.

[346] Ashley P E. Roberts, et al. mir-122 activates hepatitis c virus translation by a specialized mechanism requiring particular rna components. *Nucleic Acids Res.*, 39(17):7716–7729, 2011.

[347] Alissa M. Lancaster, et al. Initiation factor-independent translation mediated by the hepatitis c virus internal ribosome entry site. *RNA*, 12(5):894–902, 2006.

[348] E. Buratti, et al. Functional analysis of the interaction between hcv 5'utr and putative subunits of eukaryotic translation initiation factor eif3. *Nucleic Acids Res.*, 26(13):3179–3187, 1998.

[349] Stefanie A. Mortimer and Jennifer A. Doudna. Unconventional mir-122 binding stabilizes the hcv genome by forming a tri-molecular rna structure. *Nucleic Acids Res.*, 41(7):4230–4240, 2013.

[350] J. S. Kieft, et al. The hepatitis c virus internal ribosome entry site adopts an ion-dependent tertiary fold. *J. Mol. Biol.*, 292 (3):513–529, 1999.

[351] B. E. Corkey, et al. Regulation of free and bound magnesium in rat hepatocytes and isolated mitochondria. *J. Biol. Chem.*, 261 (6):2567–2574, 1986.

[352] RK Rude. Magnesium disorders. *Fluids and electrolytes*, 3:421–45, 1996.

[353] L. E. Maquat and X. Li. Mammalian heat shock p70 and histone h4 transcripts, which derive from naturally intronless genes, are immune to nonsense-mediated decay. *RNA*, 7(3):445–456, 2001.

[354] Holly R. Ramage, et al. A combined proteomics/genomics approach links hepatitis c virus infection with nonsense-mediated mrna decay. *Mol. Cell*, 57(2):329–340, 2015.

[355] Fabrice Lejeune, et al. Nonsense-mediated mrna decay in mammalian cells involves de-capping, deadenylating, and exonucleolytic activities. *Mol. Cell*, 12(3):675–687, 2003.

[356] Jill A. Holbrook, et al. Internal ribosome entry sequence-mediated translation initiation triggers nonsense-mediated decay. *EMBO Rep*, 7(7):722–726, 2006.

[357] Junho Choe, et al. microrna/argonaute 2 regulates nonsense-mediated messenger rna decay. *EMBO Rep*, 11(5):380–386, 2010.

[358] Junho Choe, et al. Ago2/mirisc-mediated inhibition of cbp80/20-dependent translation and thereby abrogation of nonsense-mediated mrna decay require the cap-associating activity of ago2. *FEBS Lett.*, 585 (17):2682–2687, 2011.

[359] Giuseppe Balistreri, et al. The host nonsense-mediated mrna decay pathway restricts mammalian rna virus replication. *Cell Host Microbe*, 16(3):403–411, 2014.

[360] Damien Garcia, et al. Nonsense-mediated decay serves as a general viral restriction mechanism in plants. *Cell Host Microbe*, 16 (3):391–402, 2014.

[361] S. S. Truesdell, et al. Microrna-mediated mrna translation activation in quiescent cells and oocytes involves recruitment of a nuclear micrornp. *Sci Rep*, 2:842, 2012.

[362] Shobha Vasudevan, et al. Switching from repression to activation: micrornas can up-regulate translation. *Science*, 318(5858): 1931–1934, 2007.

[363] Arun Venkatesan, et al. Cell cycle regulation of hepatitis c and encephalomyocarditis virus internal ribosome entry site-mediated translation in human embryonic kidney 293 cells. *Virus Res*, 94(2):85–95, 2003.

[364] Nien-Pei Tsai, et al. Microrna mir-346 targets the 5'-untranslated region of receptor-interacting protein 140 (rip140) mrna and up-regulates its protein expression. *Biochem J*, 424(3):411–418, 2009.

[365] L. R. Saunders, et al. Characterization of two evolutionarily conserved, alternatively spliced nuclear phosphoproteins, NFar-1 and -2, that function in mrna processing and interact with the double-stranded rna-dependent protein kinase, pkr. *J Biol Chem*, 276(34):32300–32312, 2001.

[366] Lingfang Shi, et al. NF90 regulates cell cycle exit and terminal myogenic differentiation by direct binding to the 3'-untranslated region of myod and p21Waf1/cip1 mrnas. *J Biol Chem*, 280(19):18981–18989, 2005.

[367] Ingrid Pfeifer, et al. NFar-1 and -2 modulate translation and are required for efficient host defense. *Proc Natl Acad Sci U S A*, 105(11):4173–4178, 2008.

[368] Olaf Isken, et al. Complex signals in the genomic 3' nontranslated region of bovine viral diarrhea virus coordinate translation and replication of the viral rna. *RNA*, 10(10):1637–1652, 2004.

[369] Olaf Isken, et al. Members of the NF90/NFar protein group are involved in the life cycle of a positive-strand rna virus. *EMBO J*, 22(21):5655–5665, 2003.

[370] Vivek L. Patel, et al. Spatial arrangement of an rna zipcode identifies mrnas under post-transcriptional control. *Genes Dev*, 26(1):43–53, 2012.

[371] Tingting Song, et al. Specific interaction of kif11 with zbp1 regulates the transport of b-actin mrna and cell motility. *J Cell Sci*, 128(5):1001–1010, 2015.

[372] Jessica L. Bell, et al. Insulin-like growth factor 2 mrna-binding proteins (igf2Bps): post-transcriptional drivers of cancer progression? *Cell Mol Life Sci*, 70(15):2657–2675, 2013.

[373] Tony Gutschner, et al. Insulin-like growth factor 2 mrna-binding protein 1 (igf2Bp1) is an important protumorigenic factor in hepatocellular carcinoma. *Hepatology*, 59(5):1900–1911, 2014.

[374] Nadine Stöhr and Stefan Hüttelmaier. Igf2Bp1: a post-transcriptional "driver" of tumor cell migration. *Cell Adh Migr*, 6(4):312–318, 2012.

[375] Markus Hafner, et al. Transcriptome-wide identification of rna-binding protein and microrna target sites by par-clip. *Cell*, 141(1):129–141, 2010.

[376] Matthew Jefferson, et al. Host factors that interact with the pestivirus n-terminal protease, npro, are components of the ribonucleoprotein complex. *J Virol*, 88(18):10340–10353, 2014.

[377] You Fang Zhang, et al. Nuclear localization of y-box factor yb1 requires wild-type p53. *Oncogene*, 22(18):2782–2794, 2003.

[378] V. Montani, et al. Major histocompatibility class ii hla-dr alpha gene expression in thyrocytes: counter regulation by the class ii transactivator and the thyroid y box protein. *Endocrinology*, 139(1):280–289, 1998.

[379] S. L. Pratt and N. D. Horseman. Identification of two y-box binding proteins that interact with the promoters of columbid annexin i genes. *Gene*, 214(1-2):147–156, 1998.

[380] Shinong Wang and Raimund Hirschberg. Y-box protein-1 is a transcriptional regulator of bmp7. *J Cell Biochem*, 112(4):1130–1137, 2011.

[381] Doreen Weidensdorfer, et al. Control of c-myc mrna stability by igf2Bp1-associated cytoplasmic rnps. *RNA*, 15(1):104–115, 2009.

[382] E. E. Capowski, et al. Y box-binding factor promotes eosinophil survival by stabilizing granulocyte-macrophage colony-stimulating factor mrna. *J Immunol*, 167(10):5970–5976, 2001.

[383] Björn C. Frye, et al. Y-box protein-1 is actively secreted through a non-classical pathway and acts as an extracellular mitogen. *EMBO Rep*, 10(7):783–789, 2009.

[384] Teresa T. Liu, et al. Noncoding rnas that associate with yb-1 alter proliferation in prostate cancer cells. *RNA*, 21(6):1159–1172, 2015.

[385] Laurent Chatel-Chaix, et al. Y-box-binding protein 1 interacts with hepatitis c virus ns3/4A and influences the equilibrium between viral rna replication and infectious particle production. *J. Virol.*, 85(21):11022–11037, 2011.

[386] Yvonne Kerwitz, et al. Stimulation of poly(a) polymerase through a direct interaction with the nuclear poly(a) binding protein allosterically regulated by rna. *EMBO J*, 22(14):3705–3714, 2003.

[387] David G. Bear, et al. Nuclear poly(a)-binding protein pabpn1 is associated with rna polymerase ii during transcription and accompanies the released transcript to the nuclear pore. *Exp Cell Res*, 286(2):332–344, 2003.

[388] Andrew Barker, et al. Sequence requirements for rna binding by hur and auf1. *J Biochem*, 151(4):423–437, 2012.

[389] Kotb Abdelmohsen, et al. 7Sl rna represses p53 translation by competing with hur. *Nucleic Acids Res*, 42(15):10099–10111, 2014.

[390] James M. Donahue, et al. The rna-binding protein hur stabilizes survivin mrna in human oesophageal epithelial cells. *Biochem J*, 437(1):89–96, 2011.

[391] Libero Lauriola, et al. Expression of the rna-binding protein hur and its clinical significance in human stage i and ii lung adenocarcinoma. *Histol Histopathol*, 27(5):617–626, 2012.

[392] Yasuyoshi Miyata, et al. High expression of hur in cytoplasm, but not nuclei, is associated with malignant aggressiveness and prognosis in bladder cancer. *PLoS One*, 8(3):e59095, 2013.

[393] Zhongpeng Zhu, et al. Cytoplasmic hur expression correlates with p-gp, her-2 positivity, and poor outcome in breast cancer. *Tumour Biol*, 34(4):2299–2308, 2013.

[394] Michael D. Barnhart, et al. Changes in cellular mrna stability, splicing, and polyadenylation through hur protein sequestration by a cytoplasmic rna virus. *Cell Rep*, 5(4):909–917, 2013.

[395] Kevin J. Sokoloski, et al. Sindbis virus usurps the cellular hur protein to stabilize its transcripts and promote productive infections in mammalian and mosquito cells. *Cell Host Microbe*, 8(2):196–207, 2010.

[396] Muthukumar Nadar, et al. Hur binding to au-rich elements present in the 3' untranslated region of classical swine fever virus. *Virol J*, 8:340, 2011.

[397] Joyce A. Wilson, et al. Human ago2 is required for efficient microrna 122 regulation of

171

hepatitis c virus rna accumulation and translation. *J. Virol.*, 85(5):2342–2350, 2011.

[398] Linya Wang, et al. Poly(c)-binding protein 2 interacts with sequences required for viral replication in the hepatitis c virus (hcv) 5' untranslated region and directs hcv rna replication through circularizing the viral genome. *J. Virol.*, 85(16):7954–7964, 2011.

[399] Baochang Fan, et al. Heterogeneous ribonucleoprotein k (hnrnp k) binds mir-122, a mature liver-specific microrna required for hepatitis c virus replication. *Mol Cell Proteomics*, 2015.

[400] Marion Poenisch, et al. Identification of hnrnpk as regulator of hepatitis c virus particle production. *PLoS Pathog*, 11(1):e1004573, 2015.

[401] Adam Huys, et al. Modulation of hepatitis c virus rna accumulation and translation by ddx6 and mir-122 are mediated by separate mechanisms. *PLoS One*, 8(6):e67437, 2013.

[402] Terence N. Bukong, et al. Ethanol facilitates hepatitis c virus replication via up-regulation of gw182 and heat shock protein 90 in human hepatoma cells. *Hepatology*, 57(1):70–80, 2013.

[403] Terence N. Bukong, et al. Exosomes from hepatitis c infected patients transmit hcv infection and contain replication competent viral rna in complex with ago2-mir122-Hsp90. *PLoS Pathog.*, 10(10):e1004424, 2014.

[404] M. Yanagi, et al. In vivo analysis of the 3' untranslated region of the hepatitis c virus after in vitro mutagenesis of an infectious cdna clone. *Proc Natl Acad Sci U S A*, 96 (5):2291–2295, 1999.

[405] Tetsuro Shimakami, et al. Base pairing between hepatitis c virus rna and microrna 122 3' of its seed sequence is essential for genome stabilization and production of infectious virus. *J. Virol.*, 86(13):7372–7383, 2012.

[406] Yun Bai, et al. Hepatitis c virus 3'utr regulates viral translation through direct interactions with the host translation machinery. *Nucleic Acids Res.*, 41(16):7861–7874, 2013.

C. Supplementary Data

C.1. Influence of VX950 on NS3 Unwinding Kinetics

Besides the end point values shown in **fig. 5.5**, also kinetic data of the NS3 helicase activity with or without effective concentrations of the protease inhibitor VX950. Inhibition of the NS3 protease has no effect on kinetics or maximal template unwinding in this assay. These data suggest that inhibition of the protease activity did not impair
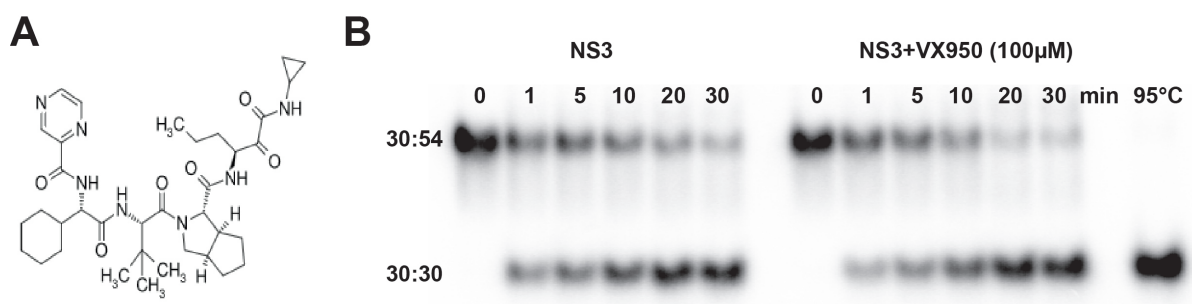
Figure C.1.: Impact of protease inhibition on NS3 helicase function. A | Structure of VX950. **B |** Native gels showing the NS3 activity over a time frame of 30 minutes, either with or without the compound.

helicase activity or RNA binding capability of NS3.

C.2. Growth Inhibition of miR-122 Expressing Hep3B Cells

miR-122 has been shown to have anti-proliferative effects on tumor cell lines. To validate the physiologic activity of miR-122 in the stably transduced Hep3B cell lines, these cells were tested for their growth kinetics by WST-1 assay (Promega, Madison, WI, USA). The experiments show that miR-122 was active and exerted all described effects in Hep3B cells. The cell growth of Hep3B cells was slightly impaired after introduction of wild type miR-122, compared to miR-122 A4U. Addition of the miR-122 inhibitor miRVANA® (Thermo Fischer Scientific, Waltham, MA, USA) alleviates the effect. Importantly, the A4U mutant did not affect cell proliferation.
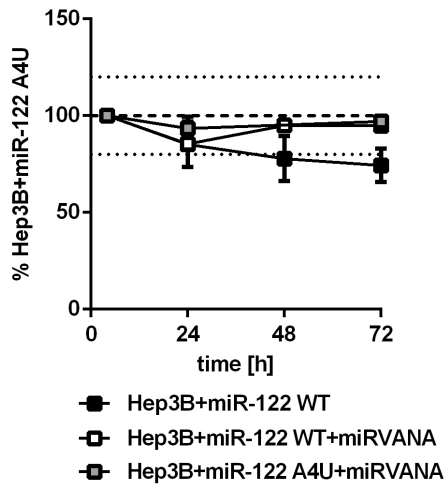
Figure C.2.: Growth kinetics of Hep3B cells stably expressing miR-122. Cell growth estimation was performed by WST assay. Approximately 10,000 cells were seeded in hexaplicate per timepoint on 96-Well plates. The initial cell number was determined 4-6 h after seeding, to allow settling of the cells. This value was used for normalization. Subsequent measurements were performed after 24-72 h. The individual points are means of 2 experiments, error bars represent S.D.

The apparent growth inhibition after miR-122 overexpression in Hep3B cells was in line with previously published data for other hepatoma cell lines[154]. These data provide further evidence for a physiological function of exogenously expressed miR-122 in Hep3B cells.

C.3. Generation of a Hep3B GFP-AGO2 Cell Line

To enable a live tracking of AGO2 containing complexes in future experiments, a Hep3B cell line with AGO2 knock-down and simultaneous overexpression of a GFP-tagged substitute (pWPI-GFP-AGO2) was generated. The shRNA sequence was designed to target the 3' UTR of the endogenous mRNA, to avoid interference with the exogenous version. shRNA mediated knock-down and expression of GFP-AGO2 were successful and the
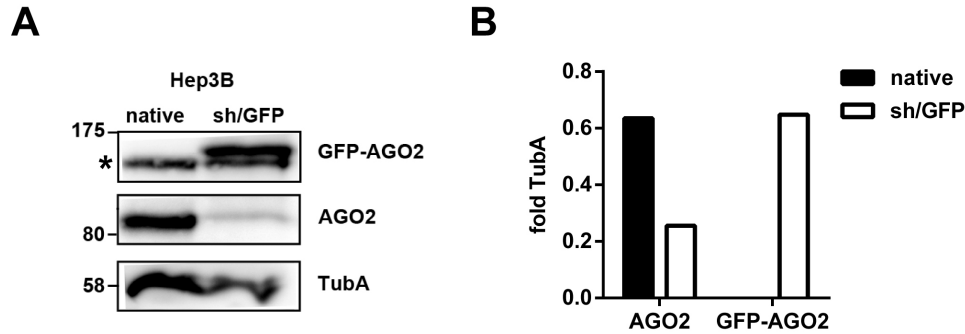
Figure C.3.: Establishment of a Hep3B cell line with GFP-AGO2. A | Western blot against AGO2 and α-Tubulin in the parental and transduced Hep3B cells. **B** | Quantification of western blot data. AGO-Protein amounts were normalized to α-Tubulin.

relative levels of the tagged protein were comparable to the endogenous levels of the parental cell line. The used primer sequences can be found in **tab. C.1**. The successful

Table C.1.: shRNA stem-loop oligos.

Label	Sequence
S-shAGO2-3001	TCGAGAAGGT ATATTGCTGT TGCTCAAACT AGCTGTGAAT CTCGAAAGAT TCACAGCTAG
A-shAGO2-3001	AATTCCGAGG GACAGCCAGC ATCGAACATG ATTCGTCATG TTCGATGCTG GCTGTCAACA

generation of this cell line provides a tool for live imaging based approaches, e.g. to follow AGO2 relocalization after HCV infection.

C.4. mfold Prediction of Domain I Mutants

In the following, the mfold predictions with the lowest ΔG for the designed domain I mutants are listed. The structure is given in VIENNA format.

WT

```
gaccugcccc uaauaggggc gacacuccgc caugaaucac uccccuguga ggaacuacug
.....((((( .....))))) (((((((((( ((((...... ......(((( (((.(....)
ucuucacgca gaaagcgccu agccauggcg uuaguaugag ugucguacag ccuccaggcc
))))))))... ....((.... .)))))))))) .......))) ))))....( ((....))).
```

WT (w/ miR-122)

```
gaccugcccc uaauaggggc gacacuccgc caugaaucac uccccuguga ggaacuacug
....(((((( .....)))))) ......... .......... ...(((((.(( ((.....(((
ucuucacgca gaaagcgccu agccauggcg uuaguaugag ugucguacag ccuccaggcc
(...(((.((. ..(((((((. ......)))) )).....)).)) )....)))) )))))))..
```

Δ10 (21-30)

```
gaccugcccc uaauaggggc caugaaucac uccccuguga ggaacuacug ucuucacgca
.....((((( .....))))) .......... ...(((((.(( ((.....((( (...(((.((
gaaagcgccu agccauggcg uuaguaugag ugucguacag ccuccaggcc
...(((((. ......)))) )).....)).) )).....)))) )))))))..
```

Δ15 (21-35)

```
gaccugcccc uaauaggggc aucacucccc ugugaggaac uacugucuuc acgcagaaag
((..(((((( .....)))))) )))).....(( ((.(((((... ..(((((...( ((.((...((
cgccuagcca uggcguuagu augagugucg uacagccucc aggcc
((((...... .))))))... .)).)))... .))))))))) ))).. 
```

Δ20 (21-40)

```
gaccugcccc uaauaggggc gccccuguga ggaacuacug ucuucacgca gaaagcgccu
.....((((( .....))))) ...(((((.(( ((.....((( (...(((.(( ...(((((.
agccauggcg uuaguaugag ugucguacag ccuccaggcc
......))))) )....)).)) )....)))) )))))))..
```

SL (26-37)

```
gaccugcccc uaauaggggc gacacgggga aaacccccac uccccuguga ggaacuacug
....(((((( .....)))))) )....((((. ....)))).. ...((((.(( ((.....(((
ucuucacgca gaaagcgccu agccauggcg uuaguaugag ugucguacag ccuccaggcc
(...(((.(( ...(((((( . ......)))) ))....)).) )).....)))) ))))))))..
```

C (31-40)

```
gaccugcccc uaauaggggc gacacuccgc guacuuagug uccccuguga ggaacuacug
.....((((( .....))))) ((((((.... ......)))) )).(((((.(( ((.....(((
ucuucacgca gaaagcgccu agccauggcg uuaguaugag ugucguacag ccuccaggcc
(...(((.(( ...(((((( . ......)))) ))....)).) )).....)))) ))))))))..
```

pA5 (25-29)

```
 gaccugcccc uaauaggggc gacaaaaaac caugaaucac uccccuguga ggaacuacug
....(((((( .....)))))) )......... .......... ...((((.(( ((.....(((
ucuucacgca gaaagcgccu agccauggcg uuaguaugag ugucguacag ccuccaggcc
(...(((.(( ...(((((( . ......)))) ))....)).) )).....)))) ))))))))..
```

pA10 (21-30)

```
gaccugcccc uaauaggggc aaaaaaaaaa caugaaucac uccccuguga ggaacuacug
....(((((( .....)))))) )......... .......... ...((((.(( ((.....(((
ucuucacgca gaaagcgccu agccauggcg uuaguaugag ugucguacag ccuccaggcc
(...(((.(( ...(((((( . ......)))) ))....)).) )).....)))) ))))))))..
```

ISL

```
gaccugcccc uaauaggggc gacacuccgc cauggaucgc uuuccuguga ggaacuacug
.....((((( .....))))) (((((((((( (((((..((( ((((.((((( (((.(....)
ucuucacgca gaaagcgccu agccauggcg uuaguaugag ugucguacag ccuccaggcc
)))))))).. )))))))... ..))))))))) .......))) )))).....( ((.....))).
```

C.5. SHAPE Analysis of 5' UTR Fragments

Besides the 389 nt fragment, also the first 120 nt of the HCV 5' UTR, from the wild type, and the Δ20 mutant were assessed by SHAPE. It could be observed that the band pattern of the truncated variants was very similar to the full-length IRES (**fig. C.4**, **fig. 5.23**). Also, the binding of miR-122 was clearly visible in the wild type, whereas no change was detected in the Δ20 mutant.
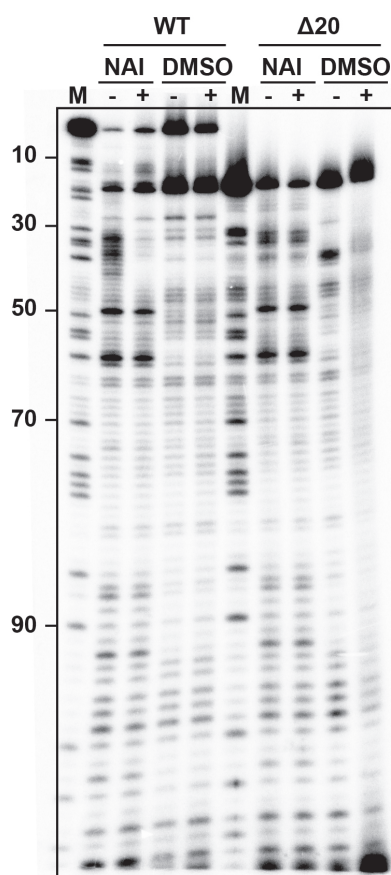
Figure C.4.: SHAPE analysis of the 120 nt wild-type and 100 nt Δ20 fragments. Auto-radiography image of the SHAPE results obtained for the WT and Δ20 sequences at 6.6 mM MgCl$_2$. The marker (M) shows all A residues. NAI indicates addition of the electrophile, and DMSO represents the cotrol reactions. "-" stands for the addition of miR-122-3p as non-binding control. Lanes marked with a "+" show reactions with the binding miR-122-5p strand.

In conclusion, the 120 nt fragment seemed to adopt a similar conformation as the 389 nt RNA. Therefore, most of the observed conformers in **fig. 5.19** can be assumed to be based upon local structures in this region.

C.6. Interaction of HCV Non-structural Proteins to the HCV 5' UTR and RISC Components

In preliminary experiments, it was investigated, whether non-structural proteins show any affinity for the 5' UTR. It was previously reported that NS3 can bind to SLIII of the HCV IRES, and displace the La protein, in order to prime the genome for RNA replication[68]. For the 5' terminal portion it is not known, whether HCV non-structural proteins can bind to modulate translation or replication. Thus, filter-binding assays were performed with purified HCV proteins. A significant enrichment could be achieved with NS3, while the helicase domain alone was not able to retain the radioactively labeled 120 nt fragment. Interestingly, NS5B in its full length variant showed a modest but clear enrichment for the HCV IRES RNA (**fig. C.5**A). These results were validated using electro-mobility shift assays. Incubation of labeled RNA with RRL and also with NS5B yielded a shift band, while the BSA control did not (**fig. C.5**B). Addition of NS3 lead to retention of most radioactive signal in the pocket of the gel (not shown). The normalized intensity suggested that around 5-10% of input RNA are bound to NS5B under the used conditions. To support a role of non-structural proteins in RNP remodeling to perform the switch from translation to replication, putative interactions of the viral proteins with components of the RISC were explored. To date, only indirect links to AGO-containing complexes have been established. To assess the physical interactions between the HCV proteins of interest and the RISC, co-immunoprecipitation assays were performed. For this purpose, the NS3-NS5B polyprotein was overexpressed in Huh7 "Lunet" cells (expressing T7 polymerase), and AGO2, NS3 or 5A were pulled down with specific antibodies. The material was analyzed by western blot to identify host and viral interaction partners. As a control, the interaction of NS3 and 5A, and AGO2 with DDX6 was tested. As reported, NS3 and 5A strongly interact and precipitating NS5A shows a considerable amount of pulled down NS3. Of note, NS3 was readily detected after NS5A pull-down(**fig. C.5**D), in contrast, an antibody against NS3 could not co-immunopreciptate NS5A (picrefEMSAE). Since the epitope of the used antibody lies in the helicase domain, is might be deduced that the NS5A interaction site is also located there. A small fraction of NS3 ($\sim$3-5% of input), but not NS5A or β-Actin was co-immunoprecipitated with AGO2.

In summary, NS3 can bind the 5' UTR of HCV, and shows affinity for the RISC, which make the protein a possible candidate to perform RNP remodeling. Additionally, binding of NS5B to the first 120 nt was noted, while association with AGO2 has yet to
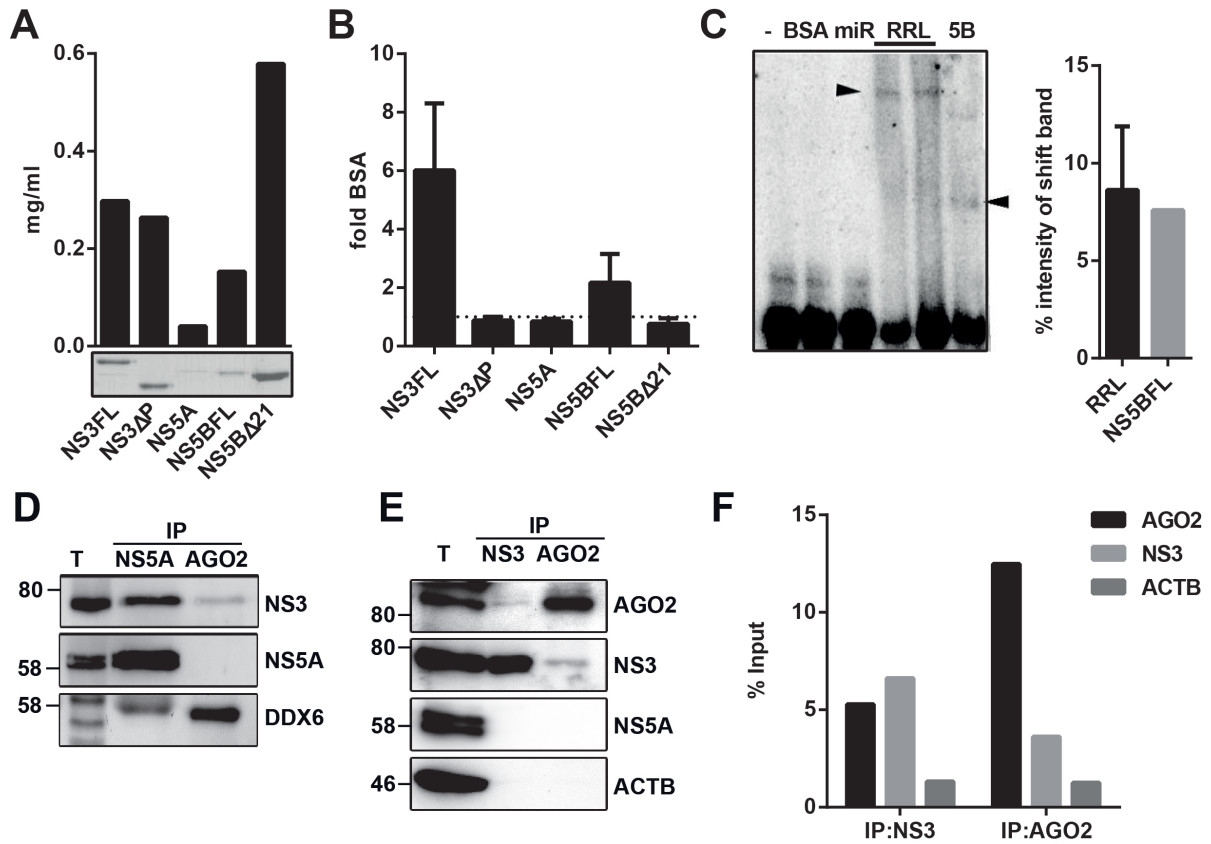
Figure C.5.: Determination of domain I and RISC binding viral proteins. A |
Quantification and assessment of purity of E. coli expressed NS-proteins. **B |** Filter binding
assay performed with 400 ng of purified NS-proteins and 1 fmol of 3'-labeled RNA. BSA was
used as baseline control. Only NS3 and NS5BFL can bind to the 5' 120 nt of HCV. **C |**
Validation of the filter binding assay by electric mobility shift assay. Translation competent
rabbit reticulocyte lysate (RRL) was used as positive control. **D |** Western blot of nonstructural
proteins co-immunoprecipitated with AGO2 after overexpression in "Lunet" T7 cells. T: total
lysate (10%). The asterisk indicates the heavy chain of the mouse antibody. Some aggregation
was visible in the pocket of the T lane for the DDX6 panel. **E |** Pull-down of viral and cellular
proteins with NS3 and AGO2. The AGO2:NS3 interaction was verified by western blotting,
Actin was used as control. **F |** Quantification of pull-down efficiency. Actin was used as
negative control.

be tested.

C.7. Primers

Table C.2.: Cloning of His-tagged NS proteins

Label	Sequence
SIN3H6	GCGGCCGCTC ATCATCACCA TCACCATTCG CGACCCATCA CTGCTTATGC
AIN3H6	GGTCGCGAAT GGTGATGGTG ATGATGAGCG GCCGCACCAC CGCGGAGACG
SIN4BH6	CATTTAAATC ATCATCACCA TCACCATATT AATATGCAGG CTTCATGG
AIN4BH6	ATTAATATGG TGATGGTGAT GATGATTTAA ATGAGCGGGT TGTATGTC
AIN5AH6	CAGGCCGGCC ATGGTGATGG TGATGATGCT TAAGACCGCT CGAGGGGGGC
SIN5AH6	TCTTAAGCAT CATCACCATC ACCATGGCCG GCCTGATGCA GGCTCGTCCA
SIN5BH6	GATCGCCATC ATCACCATCA CCATGGTACC GCCTTCACGG AG-GCC
AIN5BH6	GGTACCATGG TGATGGTGAT GATGGCGATC GCTCAGGTTC CGCTCGT

Table C.3.: Cloning of NS3 variants

Label	Sequence
SOUTQ460H	ACCCCCCGGG TCAGTGACAA CC
AINQ460H	CCCGCGGCGG TGACTGCGTG AGACAGCGTC TTGTGGGA
AOUTQ460H	TCGATAAGCT TTAATGCGGT AGT
SINQ460H	CACGCAGTCA CCGCCGCGGG CGCACAGGTA GAGGAAGA
A2ANS3P	CGCTTAATTA ATCAGGGAGA CCTTGTAACA ACGTCG

Table C.4.: Primers for *in vitro* assay templates

Label	Sequence
T7S2A9191	
T7S2A9415	TAATACGACT CACTATAGGG AGCTAACTGT TCCTT
T7S2A9507	
T7AHCV3(-)	TAATACGACT CACTATAGGT GCACGGTCTA CGAGA
A2A3(+)wt	ACATGATCTG CAGAGAGACC AG
A2A3(+)C	GCATGATCTG CAGAGAGACC AG
A2A3(+)3C	GGGACATGAT CTGCAGAGAG ACCAG
A2A3(+)3(-)	ACCUGCATGATCTG CAGAGAGACC AG
S2A3(-)	GACCTGCCCC TAATAGGGGC G
T7S1B9181	TAATACGACT CACTATAGGG CAGTAAGGAC CAAGCTCAAA C
S1B3(-)	GCCAGCCCCT GATGGGGCGA C
A1B3(+)UGU	ACTGGCCTCTCTGCAGATCATGT
A1B3(+)AGU	ACTGGCCTCTCTGCAGATCAAGT

Table C.5.: Oligos for cloning of miR-activity reporter.

Label	Sequence
S_5B_miR_3_Ban-Not	GCACCGCCGC AGATACTACC TGACCAGAGA CC-CAACCACT CCACTGC
A_5B_miR_3_Ban-Not	GGCCGCAGTG GAGTGGTTGG GTCTCTGGTC AG-GTAGTATC TGCGGCG
S_5B_miR_4_Ban-Not	GCACCACTCG CCCGGGCTGC CTGGGAAACA GTTA-GACACT CCCCTGC
A_5B_miR_4_Ban-Not	GGCCGCAGGG GAGTGTCTAA CTGTTTCCCA GGCAGCCCGG GCGAGTG
S_5B_miR_5_Ban-Not	GCACCTCAAT TGGGCGGTGA AGACCAAGCT CAAACTCACT CCATTGC
A_5B_miR_5_Ban-Not	GGCCGCAATG GAGTGAGTTT GAGCTTGGTC TTCACCGCCC AATTGAG
S_5B_miR_6_Ban-Not	GCACCCCCGC TCGGTAGAGC GGTACCCACT AG-GTACACTC CATAGGC
A_5B_miR_6_Ban-Not	GGCCGCCTAT GGAGTGTACC TAGTGGGTAC CGCTCTACCG AGCGGGG
S_5B_miR_3_Ban-Ban	GCACCGCCGC AGATACTACC TGACCAGAGA CC-CAACCACT CCACTG
A_5B_miR_3_Ban-Ban	GTGCCAGTGG AGTGGTTGGG TCTCTGGTCA GGTAGTATCT GCGGCG
S_5B_miR_4_Ban-Ban	GCACCACTCG CCCGGGCTGC CTGGGAAACA GTTA-GACACT CCCCTG
A_5B_miR_4_Ban-Ban	GTGCCAGGGG AGTGTCTAAC TGTTTCCCAG GCAGCCCGGG CGAGTG
S_5B_miR_5_Ban-Ban	GCACCTCAAT TGGGCGGTGA AGACCAAGCT CAAACTCACT CCATTG
A_5B_miR_5_Ban-Ban	GTGCCAATGG AGTGAGTTTG AGCTTGGTCT TCAC-CGCCCA ATTGAG
S_5B_miR_6_Ban-Ban	GCACCCCCGC TCGGTAGAGC GGTACCCACT AG-GTACACTC CATAGG
A_5B_miR_6_Ban-Ban	GTGCCCTATG GAGTGTACCT AGTGGGTACC GCTC-TACCGA GCGGGG

Table C.6.: Oligos for cloning of miR-activity reporter (continued)

Label	Sequence
S_5B_miR_3_Xba-Ban	CTAGAGCCGC AGATACTACC TGACCAGAGA CC-CAACCACT CCACTG
A_5B_miR_3_Xba-Ban	GTGCCAGTGG AGTGGTTGGG TCTCTGGTCA GGTAGTATCT GCGGCT
S_5B_miR_4_Xba-Ban	CTAGAACTCG CCCGGGCTGC CTGGGAAACA GTTA-GACACT CCCCTG
A_5B_miR_4_Xba-Ban	GTGCCAGGGG AGTGTCTAAC TGTTTCCCAG GCAGCCCGGG CGAGTT
S_5B_miR_5_Xba-Ban	CTAGATCAAT TGGGCGGTGA AGACCAAGCT CAAACTCACT CCATTG
A_5B_miR_5_Xba-Ban	GTGCCAATGG AGTGAGTTTG AGCTTGGTCT TCAC-CGCCCA ATTGAT
S_5B_miR_6_Xba-Ban	CTAGACCCGC TCGGTAGAGC GGTACCCACT AG-GTACACTC CATAGG
A_5B_miR_6_Xba-Ban	GTGCCCTATG GAGTGTACCT AGTGGGTACC GCTC-TACCGA GCGGGT

Table C.7.: Primers for miR-binding site mutations

Label	Sequence
S_U26/41A	CCCTAATAGG GGCGACACAC CGCCATGAAT CACACCCCTG TGAGGAACTA C
A_U26/41A	GTAGTTCCTC ACAGGGGTGT GATTCATGGC GGTGTGTCGC CCCTATTAGG G
S_U8763A	ACCCAACCAC ACCACUCGCC CGGG
A_U8763A	CCCGGGCGAG UGGUGUGGUU GGGU
S_U8800A	AAACAGUUAG ACACACCCCU AUCA
A_U8800A	UGAUAGGGGU GUGUCUAACU GUUU
S_U9204A	GCUCAAACUC ACACCAUUGC CGGA
A_U9204A	UCCGGCAAUG GUGUGAGUUU GAGC
S_U9391A	CUAGGUACAC ACCAUAGCUA ACUG
A_U9391A	CAGUUAGCUA UGGUGUGUAC CUAG

Table C.8.: Primers for SHAPE RT

Label	Sequence
A_105	CGACACTCAT ACTAACGCCA T
A_120	GGGCCTGGAG GCTGTACGAC
A_150	CCGGTGTACT CACCGGTTCC
A_160	CACCGGUUCCGCAGACCACUA

Table C.9.: Primers for cloning of IVTsc templates

Label	Sequence
pUC-S/2A/1-T7GG	CATAAAGCTT TAATACGACT CACTATAGGA CCTGCCCCTA ATAGGGGCGA CAC
pUC-S/2A/41-T7GG	CATAAAGCTT TAATACGACT CACTATAGGC CCTGTGAGG AACTACTGTC TTCA
pUC-A/2A/105	TAATCCCGGG CGACACTCAT ACTAACGCCA TGGCT
pUC-A/2A/120	TAATCCCGGG CCTGGAGGCT GTACGACACT CAT
pUC-S/2A/1-T7GG D20	CATCAAGCTT TAATACGACT CACTATAGGA CCTGCCCCTA ATAGGGGCTC CC
pUC-S/2A/3'120-T7GG (-)	CATCAAGCTT TAATACGACT CACTATAGGC CTGGAGGCTG TACGACACTC AT
pUC-S/2A/3'105-T7GG (-)	CATCAAGCTT TAATACGACT CACTATAGG CGACACTCAT ACTAACGCCA TGGCT
pUC-A/2A/3'(-)	TAATCCCGGG ACCTGCCCCT AATAGGGGCG ACAC

Table C.10.: Cloning of double IRES replicon

Label	Sequence
ARLUCAflII	CCTATTAGGG GCAGGTCCTT AAGTAACGTT ACTATTGTTC ATTTTTGAGA ACTCGC
SHIAflII	GCGAGTTCTC AAAAATGAAC AATAGTAACG TTACTTAAGG ACCTGCCCCT AATAGG
pA5 AflII	CTGACTCTTA AGGACCTGCC CCTAATAGGG GCGACAAAAA ACCATGAATC ACACCCCTGT
pA10 AflII	CTGACTCTTA AGCTGCCCCT AATAGGGGCA AAAAAAAAC ATGAATCACA CCCCTGTGAG
D10 AflII	CTGACTCTTA AGGACCTGCC CCTAATAGGG GCCATGAATC ACACCCCTGT GAGG
D15 AflII	CTGACTCTTA AGGACCTGCC CCTAATAGGG GCATCACACC CCTGTGAGGA ACTACTGTC
SL AflII	CTGACTCTTA AGGACCTGCC CCTAATAGGG GCGACACGGG GAAAACCCCC ACACCCCTGT
C AflII	CTGACTCTTA AGGACCTGCC CCTAATAGGG GCGACACACC GCGTACTTAG TGTCCCCTGT
M25 AflII	CTGACTCTTA AGGACCTGCC CCTAATAGGG GCGACTGAGG CGGTACAATG CGAGGGATGT
D20 AflII	CTGACTCTTA AGGACCTGCC CCTAATAGGG GCTCCCCTGT GAGGAACTAC TGTCTTCACG
ISL AflII	CTGACTCTTA AGGACCTGCC CCTAATAGGG GCGACACACC GCCATGGATC GCTTTCCTGT

Danksagung

Ich bedanke mich bei Prof. Dr. Ralf Bartenschlager, für die Möglichkeit diese Arbeit in seinem Institut verfassen zu können und seine Bereitschaft, als Prüfer zu fungieren.

Ganz besonders gilt mein Dank PD Dr. Volker Lohmann, für seinen motivierten Einsatz als Betreuer meiner Doktorarbeit. Besonders seine ständige Verfügbarkeit für Fragen, Diskussionen, Ideen und Hilfe während der gesamten Zeit, haben mir die Arbeit wesentlich erleichtert.

Außerdem danke ich der gesamten AGL für die tolle Atmosphäre innerhalb der Arbeitsgruppe, und die vielfältigen Aktivitäten abseits der Arbeit. Speziell sollen hier die Teilnehmer der unvergesslichen Fleischabende, Dr. Christian Harak, Max Meyrath und Rahel Klein, Erwähnung finden.

Bedanken möchte ich mich auch bei Christian Orlik, der mein Projekt im Rahmen seiner Masterarbeit tatkräftig unterstützt hat.

Weiterhin bedanke ich mich herzlich bei PD Dr. Barbara Müller, Dr. Dirk Grimm und Prof. Dr. Thomas Söllner für Ihre Teilnahme und hilfreichen Kommentaren bei meinen TAC Meetings.

Dank geht ebenso an alle Mitglieder der Arbeitsgruppen Bartenschlager, Ruggieri und Binder, die mir stets hilfsbereit und kollegial zur Seite standen und so für ein großartiges Arbeitsklima sorgten.

Nicht zuletzt danke ich meinen Eltern, die mir während der gesamten Doktorarbeit jede nur vorstellbare Unterstützung gaben, wann immer sie benötigt wurde.